DRIVER ADAPTATION TO CHANGES IN AUTOMOBILE HANDLING PROPERTIES

A DISSERTATION
SUBMITTED TO THE DEPARTMENT OF
MECHANICAL ENGINEERING
AND THE COMMITTEE ON GRADUATE STUDIES
OF STANFORD UNIVERSITY
IN PARTIAL FULFILLMENT OF THE REQUIREMENTS
FOR THE DEGREE OF
DOCTOR OF PHILOSOPHY

Holly Elyse Butterfield Russell
August 2015

This dissertation is online at: http://purl.stanford.edu/yk397hf0685

I certify that I have read this dissertation and that, in my opinion, it is fully adequate in scope and quality as a dissertation for the degree of Doctor of Philosophy.

J Gerdes, Primary Adviser

I certify that I have read this dissertation and that, in my opinion, it is fully adequate in scope and quality as a dissertation for the degree of Doctor of Philosophy.

Allison Okamura

I certify that I have read this dissertation and that, in my opinion, it is fully adequate in scope and quality as a dissertation for the degree of Doctor of Philosophy.

Stephen Rock

Approved for the Stanford University Committee on Graduate Studies.

Patricia J. Gumport, Vice Provost for Graduate Education

This signature page was generated electronically upon submission of this dissertation in electronic format. An original signed hard copy of the signature page is on file in University Archives.

Abstract

Automobile drivers frequently encounter changes in vehicle handling properties that require them to adjust their steering control actions. These changes may be benign, such as slightly different steering ratios in different cars, or potentially life-threatening, such as suddenly encountering a patch of black ice on the roadway. Understanding how drivers adapt to such handling changes is important for informing the design of new driver assistance systems and training methods. Although adaptation has been studied extensively in the laboratory for applications such as arm reaching and walking, there are still many unanswered questions about the adaptation process in the context of driving.

This dissertation addresses the need to understand how drivers adapt to handling changes by designing and implementing a novel user study with an experimental vehicle. Drivers complete several trials of a lane change task while the vehicle handling properties are modified in one of four ways that represent scenarios similar either to common laboratory experiments from arm reaching studies or to real-world situations specific to driving. The specific handling changes are (1) scaling the steering ratio, (2) reversing the steering direction, (3) scaling the steering wheel torque, and (4) simulating low friction vehicle dynamics. To enable the latter type of handling change, a new approach to handling modification has been developed using online simulation of the dynamics and tire forces of a reference vehicle model. The resulting control scheme provides a method of emulating a range of planar vehicle dynamics, in particular those of a vehicle traveling on an icy road. The results of user studies with the four handling modifications demonstrate that adaptation exists in automobile steering control tasks. The studies provide evidence that drivers adapt their steering control based on steering wheel angle, not on steering wheel torque. Finally, individual driving style influences the degree of adaptation necessary when encountering a low friction surface.

Acknowledgments

There have been so many people over the years who have influenced my life, even through small conversations and chance interactions, that I couldn't possibly list everyone here. What I know for sure is I could not have done this alone and I am so grateful to the many, many people who have helped me get to this point.

First, thank you to my Ph.D. advisor, Chris Gerdes. I started my time in his group knowing literally nothing about cars, but he saw enough curiosity and dedication in me to welcome me into the lab and put me straight into a project developing the steer-by-wire controller for our X1 vehicle. Over the years, Chris has provided a great deal of technical guidance and has also allowed me the freedom to figure things out on my own. Although at times this freedom was a bit scary, I really value the skills it forced me to develop. Chris has helped me build confidence in my technical and leadership abilities and now I really feel like I am capable of doing anything I want to. And a thank you to Chris cannot neglect my appreciation for all the special experiences he provided me throughout my time in the lab: monthly research trips to the Thunderhill race track, a trip to England to interact with the Williams F1 racing team, camping at Laguna Seca, race car driver training, and numerous opportunities to talk with the media.

The members of my reading committee, Allison Okamura and Steve Rock, have been great resources throughout my Ph.D. Allison taught me all about adaptation and was extremely enthusiastic about collaborating with our group. She helped shape the driver adaptation studies and provided valuable insights into what scientific statements we could make about the results. I really appreciate her attention to detail, in particular as she helped me develop much better figures to communicate my research

results. Steve taught several of my controls courses and gave me a solid foundation in control systems design. He was always willing to talk with me about my research and played a key role in challenging my ideas and making me describe my work clearly and rigorously.

I must thank all of the Dynamic Design Lab (DDL) members, past and present, for being some of the best colleagues I could have asked for. When I joined the lab in 2009, I immediately had a great set of labmates who welcomed me into the lab and helped me jump into the world of vehicle dynamics: Carrie Bobier, Craig Beal, Rami Hindiyeh, Adam Jungkunz, Mick Kritayakirana, Shad Laws, Hsien-Hsin Liao, Hyungchai Park, Nikhil Ravi, and Kirstin Talvala. I'm especially grateful to Carrie and Craig for giving me a lot of freedom to figure out how to make steer-by-wire work on X1, the car they designed and built from the ground up. You two laid the groundwork for the strong X1 team that today boasts the most diverse and exciting set of research of any of our testbeds (but maybe I'm biased). The students who joined the lab after me have always been supportive and enthusiastic about the challenging work we do, while making the lab a genuinely fun place to be: Avinash Balachandran, Matt Brown, Steve Erlien, Joe Funke, Tushar Goel, Jon Goh, Nitin Kapania, John Kegelman, Marcial Hernandez, Vincent Laurense, Shannon McClintock, Lucio Mondavi, John Subosits, Paul Theodosis, Sarah Thornton, and Vivian Zhang. And some of the most important people in the lab are our administrative staff, without whom nothing in the lab would run: Larry Cathey, Erina DuBois, Adele Tanaka, Jo Yuan, and previously Elizabeth Pearson and Jennifer Rahn.

The awesome researchers who helped me implement the user studies in this dissertation deserve an extra special thanks. Lene Harbott and Ilana Nisky spent many hours meeting with me to figure out how we could test adaptation in the car, setting up and running experiments, analyzing data, and teaching me how to do statistical analysis. Selina Pan joined us for the later studies, and jumped right in with enthusiasm. User studies take a lot of time and effort, and I really appreciate their willingness to spend weekends with me in the parking lot.

I have been fortunate to meet many people at Stanford who supported me in all the non-technical aspects of the Ph.D. Beth Pruitt was my first advisor at Stanford,

and although I decided the research in her group wasn't a good fit for me, she actively encouraged me to find something I would enjoy and to finish my Ph.D. Sheri Sheppard provided several opportunities to gain perspective, including the ME Women's Group, the E311A women's perspectives in engineering seminar, and the E311B designing your life course. Jennifer Raymond and Miriam Goodman sponsored the Empowering Emerging Scientists course that helped me create a plan of action for improving my work life. My group from that class, Sumant Sharma and Rhiannon Thomas, provided a consistent place to be heard and supported through the difficulties of the Ph.D. I was part of the first cohort of students in Stanford's Graduate Voice and Influence Program, which built my confidence and interpersonal skills and introduced me to many wonderful students and postdocs from all over the university. All of these people encouraged me and kept me going when I found the Ph.D. difficult.

One of my favorite activities outside of research has been mentoring the FIRST robotics team at Castilleja School. This team is full of amazing girls who are bursting with enthusiasm for learning new things. Anytime I was having a rough day, I could always count on one of the students to cheer me up by giving me the chance to help them figure out how to make their robot work. Thank you for letting me be a part of your lives these past six years.

I have been truly blessed to have a strong "crew" of friends in graduate school: Justin Bischoff, Roland Burton, Eleanor Crane, Sloan Devlin, Jordan Drewitt, Alex Egeler, Emily Egeler, Alex Haas, Sarah Houts, Laurent Lessard, Meaghan Kimball, Peter Kimball, Kiran Murthy, Matt Napoli, "Soccer" Karen Schuyler, Kelly Shea, Dan Sheinfeld, Brendan Tracey, "Volleyball" Karin Vroom, and Jonathan Vroom. These people have made the rest of life a lot of fun, including puzzle hunts, Pizza and What Have You, AC Durand soccer, epic Rock Band sessions, spring break trips, Ladies Craft Night, Stanford football, and so much more. Several of them went through the Ph.D. before me and provided hope that I too could do it. I'm sure I'm forgetting someone, and there's always room for more people in the crew, so thank you to all of you!

My family has always nurtured my love of learning and my silliness. They also sometimes know me better than I know myself. My mom, Laurie Ellison, was the first

person to suggest to me that maybe I would like engineering, and later that maybe I should consider going to graduate school. While my initial response to both of those suggestions was "you're crazy, Mom", it turns out she was totally right. Thank you to my mom and stepdad, Rick Ellison, for encouraging me to keep going when I wanted to quit and for going out of your way to help me with whatever I needed. My dad, Dave Butterfield, gave me my love of sports and showed me a model of perseverance and personal reinvention. I am so proud of my sister, Heidi Butterfield, and grateful for the friendship we have developed as adults. My extended family, both the Gliddens and the Butterfields, are just great people and a lot of fun to be around. Plus they didn't ask me *too* many times when I was going to be done with my Ph.D. My second family, the Russells, immediately welcomed me when I started dating their son and seamlessly integrated me into the family. I have valued my many trips to Colorado to spend time with Kelly, Carolyn, David, and Lauren, especially the time we have spent cheering for the Denver Broncos, playing lots of board games, and goofing off on Christmas morning.

And finally, to my dear husband Stephen, thank you for your constant support and love. The past 7+ years with you have been the best of my life. You are always willing to talk through whatever is on my mind, sharing good advice and giving me space to work things through. You have been my travel companion on many buddy trips, my partner in crime for silly adventures, and my fiercest supporter. With you by my side, I know I can face anything. I just love you and stuff.

Contents

Abstract **iv**

Acknowledgments **v**

Contents **ix**

List of Tables **xiv**

List of Figures **xvi**

1 Introduction **1**

1.1 Human Sensorimotor Learning 3

1.1.1 Types of Adaptation Studies 5

1.1.2 Metrics in Arm Reaching Studies 6

1.1.3 Key Adaptation Results 8

1.2 Automobile Studies Related to Adaptation 10

1.2.1 Experimental and Driving Simulator Studies 11

1.2.2 Driver-Vehicle Modeling 12

1.2.3 Key Driving Study Results 15

1.3 Vehicle Handling Modification 17

1.3.1 Handling Changes of Interest 17

1.3.2 Variable Dynamic Testbeds for Handling Modification 19

1.3.3 Key Handling Modification Results 21

1.4 Dissertation Contributions 23

1.4.1 User Study Protocol 23
1.4.2 Handling Modification Method 24
1.4.3 Experimental Evidence for Driver Adaptation 24
1.5 Dissertation Outline 26

2 Driver Adaptation User Study Design **28**
2.1 Study Overview 29
2.2 X1 Experimental Vehicle 31
2.2.1 Hardware Description 31
2.2.2 Software and Controls 33
2.2.3 Data Collection 33
2.3 Driving Task 33
2.3.1 Steering Wheel Torque 34
2.3.2 Cruise Control 38
2.3.3 Converting East-North Position to X-Y Coordinates 40
2.3.4 Signal Light Trigger 41
2.3.5 Safe Stop 44
2.4 Return to Start 45
2.4.1 Map Generation 45
2.4.2 Map Matching 47
2.4.3 Path-Following Steering Controller 47
2.4.4 Speed Limit 49
2.5 Choice of Metrics 50
2.5.1 Steering Wheel Reversal Rate 52
2.5.2 RMS Steering Velocity 54
2.5.3 Time to Steering Angle Peak 55
2.5.4 RMS Yaw Jerk 57

3 Adaptation to Steering Ratio Changes **58**
3.1 User Study #1: Steering Ratio Scaling 59
3.1.1 Study Participants 61
3.1.2 Sample Participant Data 62

3.1.3 Group Results 64
3.1.4 Discussion 69
3.2 User Study #2: Steering Direction Reversal 71
3.2.1 Study Participants 71
3.2.2 Sample Participant Data 72
3.2.3 Group Results 76
3.2.4 Discussion 80
3.3 General Discussion 81

4 Adaptation to Steering Torque Increase **84**
4.1 Study Participants 86
4.2 Sample Participant Data 86
4.3 Group Results 89
4.4 Discussion 91

5 Handling Emulation Controller Development **95**
5.1 Control Strategy Overview 96
5.2 Modeling Vehicle Dynamics and Tire Forces 99
5.2.1 Dynamics of the Reference Model 99
5.2.2 Dynamics of the Controlled Vehicle 103
5.3 Emulating Vehicle Dynamics Using Tire Forces 105
5.3.1 Choosing Tire Forces 105
5.3.2 Stability of the Error Dynamics 107
5.3.3 Discussion 109
5.4 Application to Low Friction Emulation 110
5.4.1 Converting Desired Force to Actuator Commands 113
5.4.2 Feedback Gain Selection 115
5.4.3 Incorporating Actuator Range Limitations 115
5.4.4 Unmodeled Roll Dynamics 117
5.5 Low Friction Emulation Experimental Results 118
5.5.1 Experimental Setup 118
5.5.2 $\mu = 0.1$ – Slalom Maneuver 119

5.5.3 $\mu = 0.3$ – Steering Actuator Limitation . . . 121
5.5.4 $\mu = 0.4$ – Step Inputs . . . 123
5.6 Future Research Directions . . . 123
5.7 Conclusion . . . 125

6 Adaptation to Low Friction Dynamics 127
6.1 Study Participants . . . 128
6.2 Sample Participant Data . . . 129
6.3 Dividing Participants into Groups . . . 132
6.4 Group Results . . . 136
6.5 Discussion . . . 140
6.6 Comparison with Torque Increase Study . . . 144
6.7 Future Research Directions . . . 146

7 Conclusion 149
7.1 Summary of Results . . . 149
7.2 Future Research Directions . . . 151
7.2.1 Expand the Scope of Handling Emulation . . . 151
7.2.2 Adaptation Studies with Physiological Measurements . . . 152
7.2.3 Generalization of Driver Adaptation . . . 152
7.2.4 Advanced Study of Adaptation to Handling Changes . . . 153

A Steering Control for the X1 Research Vehicle 154
A.1 Steering System Model . . . 154
A.1.1 Parameter Identification . . . 156
A.2 Controller Implementation . . . 158
A.3 Four-Wheel Steering Considerations . . . 162
A.3.1 Speed-Varying 4WS Algorithm . . . 162
A.3.2 Ackermann Steering Geometry for 4WS . . . 163

B Statistical Analysis Methods 166
B.1 Fundamental Concepts . . . 166

B.2 Probability Distributions 167
B.2.1 The Normal Distribution 167
B.2.2 The t Distribution 169
B.2.3 The F Distribution 170
B.3 Hypothesis Testing 171
B.3.1 The Two-Sample t-Test 173
B.3.2 Multiple Comparison Testing 173
B.4 Analysis of Variance 174
B.4.1 One-Factor ANOVA 175
B.4.2 Two-Factor ANOVA 176
B.4.3 One-Factor Repeated Measures ANOVA 178
B.4.4 Sphericity Corrections 180

C Handling Emulation with Mass and Inertia Changes **182**

D Statistical Results for Driver Adaptation Studies **185**

List of References **196**

List of Tables

2.1 Experimental vehicle parameters 32

3.1 Summary of repeated measures ANOVA results for Study #1 68
3.2 Summary of repeated measures ANOVA results for Study #2 76

4.1 Summary of repeated measures ANOVA results for Study #3 91

5.1 Feedback gains 115

6.1 Summary of repeated measures ANOVA results for Study #4 137

A.1 Identified steering system parameters 158

B.1 One-factor ANOVA table 176
B.2 Two-factor ANOVA table 179
B.3 One-factor repeated measures ANOVA table 181

D.1 Study #1: One-factor repeated measures ANOVA tables 186
D.2 Study #2: One-factor repeated measures ANOVA tables 187
D.3 Study #3: One-factor repeated measures ANOVA tables 188
D.4 Study #3: Two-factor ANOVA tables 189
D.5 Study #4: One-factor repeated measures ANOVA tables 190
D.6 Study #4: Two-factor ANOVA tables 191
D.7 Study #4: One-factor repeated measures ANOVA tables, Group 1 . . 192
D.8 Study #4: One-factor repeated measures ANOVA tables, Group 2 . . 193
D.9 Study #1: Results of pairwise comparisons 194

D.10 Study #2: Results of pairwise comparisons 194
D.11 Study #3: Results of pairwise comparisons 195
D.12 Study #4: Results of pairwise comparisons, Group 1 195

List of Figures

2.1 The driver adaptation study test course 29
2.2 Overview of the user study protocol 30
2.3 The X1 experimental vehicle 31
2.4 Linear spring model of steering torque for various steering ratios . . . 36
2.5 Block diagram of the full steering feel emulator 37
2.6 Weighting function for power assist in the full steering feel emulator . 38
2.7 Cruise control performance 39
2.8 Cone numbers used to compute X-Y coordinates 40
2.9 Comparison of E-N coordinates with X-Y coordinates 42
2.10 The course as seen by the driver at the end of the straight 43
2.11 Map of course with signal light active and inactive regions 43
2.12 Safe stop schematic 44
2.13 Map generated with the Quill software tool 46
2.14 Block diagram for the path-following steering controller 48
2.15 Example data for speed limit controller 51
2.16 Example of steering wheel reversal rate 53
2.17 Example of distance from signal light trigger to next local maximum steering angle 56

3.1 Yaw rate gain as a function of steering ratio and vehicle speed 60
3.2 Adaptation protocol for steering ratio scaling study 61
3.3 Sample data for steering ratio scaling study 63
3.4 Learning curves for steering ratio scaling study 65

3.5 Statistical significance for steering ratio scaling study 67
3.6 Adaptation protocol for steering direction reversal study 72
3.7 Sample data for steering direction reversal study, participant 1 73
3.8 Sample data for steering direction reversal study, participant 2 74
3.9 Learning curves for steering direction reversal study 77
3.10 Statistical significance for steering direction reversal study 78

4.1 Adaptation protocol for steering torque increase study 85
4.2 Sample data for steering torque increase study, participant 1 87
4.3 Sample data for steering torque increase study, participant 2 88
4.4 Learning curves for steering torque increase study 90
4.5 Statistical significance for steering torque increase study 92

5.1 Conceptual block diagram of the handling emulation system 97
5.2 The four-wheel planar vehicle model 99
5.3 Illustration of the coupled brush tire model 103
5.4 The 4WS bicycle model 104
5.5 Comparison of tire force curves for high and low friction surfaces . . . 111
5.6 Comparison between sliding and steering 112
5.7 Experimental maneuver with $\mu = 0.1$ 120
5.8 Experimental maneuver with $\mu = 0.3$ 122
5.9 Experimental maneuver with $\mu = 0.4$ 124

6.1 Adaptation protocol for low friction study 128
6.2 Sample data for low friction study, participant 1 130
6.3 Sample data for low friction study, participant 2 131
6.4 Classification of participants by maximum lateral acceleration 134
6.5 Metrics grouped by driving style for low friction study 135
6.6 Learning curves for low friction study, Group 1 138
6.7 Statistical significance for low friction study, Group 1 139
6.8 Learning curves for low friction study, Group 2 141
6.9 Statistical significance for low friction study, Group 2 142

6.10 Metrics grouped by driving style for torque study 145

A.1 Illustration of the components of aligning moment 155
A.2 Input and output steer angles for ETFE 156
A.3 ETFE for front left wheel 157
A.4 Identification of Coulomb friction torque for front left wheel 158
A.5 Block diagram of steering controller for each wheel 159
A.6 Steer angle tracking for front left wheel 161
A.7 Scaling factor for rear steer angle as a function of vehicle speed 163
A.8 Example of Ackermann geometry for 4WS 165

B.1 The normal probability density function 168
B.2 The t probability density function 170
B.3 The F probability density function 172

Chapter 1

Introduction

Steering an automobile is a familiar task for most adults in the United States – it is something that many people do every day. Drivers are so accustomed to performing this task that it is rarely necessary for them to explicitly consider the mechanism behind how their steering inputs result in particular vehicle motions. They instead rely on an internal mental model of this mapping, enabling them to focus on higher-level control such as navigating a desired path. However, the actual relationship between steering wheel inputs and vehicle dynamics can change for a variety of reasons, requiring drivers to adapt their internal model in order to safely steer the vehicle along the road. Changes in the mapping from steering wheel inputs to vehicle dynamics are caused by failures in the automobile itself, interaction with the environment, and fundamental vehicle dynamics principles. For example, as the vehicle's speed increases, its rotational velocity becomes more sensitive to steering inputs [42] so that motions that are benign at low speed have the potential to cause problems at higher speeds. When the road conditions are poor due to ice or snow, the vehicle dynamics become highly nonlinear and possibly even unstable [105]. A failure in the power steering system increases the amount of torque the driver must apply to steer the vehicle [48]. Understanding the process of adaptation to these handling changes has implications for advanced driver assistance systems, handover of control from an automated vehicle to a human driver, and extending models of human motor control from neuroscience to the important real-world context of driving.

Adaptation is a term that has different meanings for different communities of researchers and it is therefore important to understand what it means in these contexts. Automotive control researchers have accounted for the ability of drivers to adapt to handling changes by formulating the driver-vehicle system in terms of an adaptive controller [76, 93], which has been defined by Åström and Wittenmark as "a controller with adjustable parameters and a mechanism for adjusting the parameters" [1]. From a control systems perspective, it is reasonable to describe driver adaptation to handling changes as modification of parameters in an internal controller that maps steering inputs to resulting vehicle dynamics. In the neuroscience community, adaptation refers to a specific form of error-based sensorimotor learning. Researchers have studied the adaptation process for movements including directed arm reaches [64, 124], eye saccades [24, 102], and walking [25, 100], and over the past four decades they have developed an understanding of the hallmarks of adaptation and the brain processes involved. It is unknown whether the adaptation process is the same for the task of steering a vehicle as it is for these other well-studied activities. Arm reaching studies isolate the kinematics and dynamics of the arm from the rest of the body by keeping the torso and shoulder rigid while participants are seated [64, 124]. Although steering a vehicle also involves moving the arms, steering motions result in vehicle dynamics that are experienced by the entire body, so it is impossible to isolate the arms. In addition, the task of steering a vehicle through a course is more complex than point-to-point arm reaching motions, thus it may be more difficult to observe adaptation in the driving environment.

This dissertation contributes to the understanding of driver adaptation to handling changes by developing a user study protocol for studying adaptation in an experimental vehicle and applying the protocol to four different handling changes related to steering. The results of the studies show that drivers adapt to a change in steering ratio in a manner consistent with the sensorimotor learning literature, while a change in steering torque is compensated without adaptation. Studies on steering wheel direction reversal and low friction conditions demonstrate that the approaches taken by different drivers significantly affect the adaptation process for these handling

changes. These results indicate that automobile steering is an application where sensorimotor adaptation can be readily observed with both similarities to and differences from existing knowledge about the adaptation process.

The remainder of this chapter provides background on human sensorimotor learning, automobile studies related to adaptation, and methods of vehicle handling modification, concluding with a discussion of the dissertation contributions and an outline of the dissertation.

1.1 Human Sensorimotor Learning

The motor control system of the human body is responsible for all the movements we make in everyday life. The motor system enables everything from basic tasks such as walking and picking up a glass of water to complex skills such as playing the piano and hitting a golf ball. The motor system comprises a number of brain structures that play different roles in the acquisition of new skills and refinement or adaptation of old skills to new situations. Sensorimotor learning is a particular form of motor system learning where motion is guided by some type of sensory perception and performance improves over time with repeated practice. The performance improvement in sensorimotor learning is due to several different brain structures and learning processes. According to Krakauer and Mazzoni [63] and Wolpert et al. [144], the main components are **adaptation** or **error-based learning**, a form of learning where the motor system returns to previous levels of performance after a modification in the operating environment [27]; **skill** or **reinforcement learning**, which results in performance improvement (unlike adaptation, where performance can at best return to its baseline level); and **use-dependent plasticity**, where the mere repetition of certain movements serves as a form of training. Another way of thinking about the distinction between the first two learning modes is that adaptation modifies an existing motor control policy while skill learning creates an entirely new motor control policy [133].

To understand the distinction between these three components of motor learning, consider the process of learning to play the piano. An example of use-dependent

learning is practicing a sequence of notes on an electric keyboard with the volume muted, so the pianist learns the motions required for the song, but does not form a mapping between those motions and the sounds they will produce with the volume on. Learning a new song while hearing the sounds produced by the motions of the fingers is an example of skill learning, where performance is improved over time based on a "reward" signal [144]; in this case the reward signal is playing the correct notes with appropriate dynamics and tempo to produce music that sounds pleasing to the ear. Once the song has been learned, if the pianist must now play it while wearing weights on her wrists, adaptation is the process of recovering the ability to play the song as well as she did without the weights.

Adaptation is the focus of this dissertation because the goal is to understand the learning behavior of people who already know how to drive a car but experience changes in the relationship between steering inputs and vehicle dynamics. Adaptation is defined as motor learning driven by sensory prediction errors [125] to return task performance to pre-perturbation levels [63, 124] after some kind of change in the operating environment [27]. This type of learning uses a sensory prediction error signal to improve an **internal model** of the kinematics and dynamics of the motor system on a trial-by-trial basis [58, 124]. On each trial of a given task, the brain adjusts its planned (feedforward) command signal based on prediction error from the previous trial. Evidence that adaptation has occurred starts with the reduction of performance error over the course of some number of trials [27, 51, 62, 64, 67, 87, 124].

Further evidence for adaptation is demonstrated by **aftereffects**. Suppose the introduction of a perturbation to the operating environment causes a positive performance error. An aftereffect exists when the removal of the perturbation results in a negative performance error. Some researchers state that an aftereffect is the criterion that indicates adaptation has occurred and the internal model has indeed changed based on the perturbation [86]; others do not require the presence of an aftereffect [19, 38]. To summarize these assertions, if an aftereffect is present, then adaptation has certainly occurred, but if there is no aftereffect, there still may have been adaptation. Put another way, an aftereffect is a sufficient but not necessary criterion for adaptation.

1.1.1 Types of Adaptation Studies

Early studies of adaptation focused on understanding adaptation to visual field distortions caused by wearing prism glasses. In a seminal study by Helmholtz in 1866, participants wore prism glasses that laterally displaced the visual field [139]. When participants reached their arms toward a target, they showed lateral errors approximately equal to the visual field displacement, which decreased over repeated trials as they learned to compensate for the visual perturbation. Upon removing the prism glasses, the participants initially showed errors in reaching movements in the opposite direction to what was observed while wearing the glasses – an example of an aftereffect. A similar study by Held and Freedman using a rotary prism showed that when participants actively moved their arms, they adapted to the prism, but when the participants' arms were passively moved for them, no adaptation occurred [49]. The authors took this as evidence that in the passive case the normal connection between visual perception and motor output was not present. In other words, the participants did not experience any change in their internal models when their arms were moved passively.

An application that has been studied frequently over the past thirty years focuses on adaptation to changes in operating environment for the arm reaching to a target. In a typical arm reaching experiment, the participant grasps an indicator or a robotic manipulator with the hand while the arm is constrained in some way to limit its degrees of freedom. The participant is presented with a target location and rapidly moves the hand to the target, either stopping at the target (reaching) or hitting the target location and returning to the starting position (slicing) [121]. The participant's arm is obscured from view, and performance is based on the motion of a cursor on a screen linked to the motion of the manipulator. Depending on the goal of the study, the participant may or may not be given visual feedback of the cursor position [64].

Arm reaching studies initially focused on understanding the basic properties of arm motion control. Morasso showed that in arm reaching experiments, the hand trajectory demonstrated consistent motion consisting of approximately straight line paths and peaked tangential velocity curves for all motions, while the joint space

patterns were different for different movements [99]. Abend et al. extended this study to find that subjects tried to approximate curved paths with sequences of nearly straight segments and that the hand velocity exhibited multiple peaks when following a curved path [2]. Atkeson and Hollerbach showed that the peaked tangential velocity curves were consistent for unrestrained arm motions between targets through 3-D space, even when the hand paths were curved [7].

To expand this understanding of arm motion, researchers have conducted adaptation experiments with perturbations in kinematics, dynamics, and isometric reaching. The **kinematics** of the arm have been perturbed by visuomotor rotation, which consists of scaling [18, 19, 64], rotating [62, 64, 87, 121, 132, 133], or reversing [23, 133, 142] the relationship between the motion of the hand and the motion of the visual cursor. The **dynamics** of the arm have been modified by forces applied by the manipulator to the hand [27, 43, 124], by rotating the room to induce Coriolis forces on the arm [67], and by applying an inertial mass to the arm [62, 118]. Researchers have also studied adaptation in **isometric reaching** [51, 116, 147], where the screen cursor is controlled by the force applied by the participant on the manipulator while the arm is stationary and the cursor motion simulates the dynamics of the arm.

1.1.2 Metrics in Arm Reaching Studies

Researchers studying adaptation in arm reaching have defined several metrics to quantify the adaptation process observed in their studies. One common set of metrics concerns different types of error in completing the task. Angular error at peak hand velocity was used in a number of studies [51, 62, 64, 72, 87, 116, 118, 121, 132, 133], with decreasing angular error over trials indicating evidence of adaptation. A similar measure was used by Lackner and DiZio to quantify endpoint error in terms of lateral rather than angular deviation [67]. Gordon et al. [44] and Scheidt and Ghez [121] measured the error in extent, referring to overshooting the target position. Nisky et al. defined a measure of deviation from a straight line as an error metric [101]. Conditt et al. devised a figural distance metric to quantify the difference between path

shapes for complex two-dimensional paths [27].

Another set of metrics relates to the kinematics of the hand and the arm joints. The metrics for hand kinematics include trajectory in the horizontal plane [38, 39, 47, 67, 99, 101, 118, 121, 124, 145]; hand path curvature [2, 38, 39, 47, 121, 145]; tangential velocity [2, 39, 44, 47, 64, 67, 99, 101, 118, 124]; and tangential acceleration [44, 101]. Kinematic measures of the elbow and shoulder joints include joint angles [2, 38, 99, 118], joint angular velocities [2, 99], and joint angular accelerations [99]. Sainburg et al. also measured joint torques to enable analysis of the arm dynamics [118].

Researchers have also created normalized metrics to quantify the amount and time scale of adaptation. In a study of throwing an object while wearing prism glasses, Martin et al. used what they termed the adaptation coefficient, or the time constant of decay of an exponential curve fit to the lateral displacement of the throws from the target [86]. Krakauer et al. defined normalized adaptation percentage measures for scaling and rotation perturbations using peak hand tangential velocity and angular error, respectively [64]. Shadmehr and Mussa-Ivaldi defined a correlation coefficient between two trajectories as a way of quantifying amount of adaptation [124].

Measurements of the elapsed time during reaching movements have been used by several researchers to supplement kinematic variables [38, 44, 47, 51]. Nisky et al. used the product of endpoint error and movement time to emphasize the importance of both speed and accuracy in surgical performance [101]. Telgen et al. used reaction time (rather than movement duration) to examine the relationship between time and accuracy [133].

While these metrics are well suited to studies of adaptation during arm reaching, they are not directly applicable to adaptation to steering changes in an automobile. However, the underlying concepts can be used to devise relevant metrics for the experiments of interest to this dissertation. In general, it can be useful to understand the role of kinematic variables, time, and some kind of error. The kinematic variables in a vehicle steering study include steering wheel motion (position, velocity, and acceleration) and the lateral, longitudinal, and rotational components of position, velocity, and acceleration of the entire vehicle. The metrics used to analyze the

results of the experiments in this dissertation are described in detail in Chapter 2.

1.1.3 Key Adaptation Results

A common paradigm for studying adaptation and testing for aftereffects involves dividing the experiment into three blocks of discrete trials: pre-test, training, and post-test [19, 29]. The pre-test or baseline block establishes the user's performance on the metrics of interest as the basis of comparison for later blocks. During the training block, the motor system is perturbed in some way to test for adaptation, which only occurs if the perturbation causes performance error; if there is no performance error, then no adaptation is required. If the metric returns to the baseline value, the participant has fully adapted to the perturbation; if the metric only recovers part of the way to baseline, the participant has partially adapted [101]. The perturbation is removed for the post-test block, which therefore has the same effects on the motor system as the pre-test block. An aftereffect is present if the performance deviates from baseline at the beginning of the post-test, strengthening the case that the participant's internal model of the process has truly changed due to the perturbation. The rate of **washout** of the aftereffect is the number of trials it takes for the performance to return to baseline level again. More complicated sequences of trials have been used to test subtle effects such as interference of two different perturbations [51, 62, 130] and the influence of explicit strategy on adaptation [87, 132]. The simple pre-test/training/post-test paradigm is a good place to start for studying adaptation in new experimental contexts such as steering an automobile. The most basic hypothesis for steering studies is that drivers adapt to handling changes as evidenced by a return to baseline performance after initial errors due to the handling perturbations.

The learning curves observed in adaptation experiments typically have a roughly exponential decay [62, 64, 67, 86]. Some researchers fit single [67, 86, 132] or double [62, 64, 116] exponential functions to the observed data in order to quantify the rates of learning and forgetting the perturbations. Recent studies have focused on creating mathematical models that accurately predict the results of adaptation experiments using discrete-time linear time invariant systems [22, 72, 130, 132], with a goal of

better understanding the processes occurring in the brain during adaptation. The double exponential curve is well described by dual-rate dynamic systems models [72, 130] that include slow and fast processes. These results do not prove that single or double exponential decay is required for learning curves to represent adaptation, but rather suggest possible underlying models for the brain processes involved in adaptation. If adaptation to handling changes related to steering a vehicle results in single or double exponential learning curves, this supports the hypothesis that the relevant brain processes are related to those involved in adaptation of the arm.

An important theme of the adaptation literature for arm reaching has been comparing the effects of different types of perturbations to the motor system. Krakauer et al. demonstrated that participants exposed concurrently to both a visuomotor rotation (kinematic perturbation) and altered arm inertia (dynamic perturbation) experienced the same rate of adaptation as participants who only experienced one of these perturbations [62]. The authors took this as evidence that the motor system learns kinematics and dynamics separately. In another study that focused solely on visuomotor rotation, Krakauer et al. demonstrated different rates of learning and amounts of generalization of the learning to untrained distances and directions for two perturbations: scaling the cursor gain and rotating the cursor reference frame [64]. They hypothesized that the brain in fact processes extent and directional errors separately. Whether these differences in response to different types of perturbations exist for other applications besides arm reaching is an open question. The relevant hypothesis for steering an automobile is that drivers adapt differently to different types of handling condition perturbations.

Another key idea in the adaptation literature is the internal model concept, which says that the brain forms an inverse dynamics model of the process of interest and that this model must change when the system is perturbed [58, 146]. In the mathematical models described above, motor control is a closed loop process that includes both **feedforward** and **feedback** motor commands. Adaptation changes the feedforward component as the kinematics or dynamics of the system are perturbed [22, 146]. Feedforward is particularly relevant in motor control because the sensorimotor system has relatively long inherent time delays in feedback that preclude accurate motions

based on feedback alone [58, 125, 144]. It is common in arm reaching studies to use fast (0.5–1.5 second) "ballistic" motions of the arm in order to isolate the effects of this change in feedforward as much as possible before the feedback control can influence the motion [64, 101, 121]; in one study with complex movements that lasted about 2 seconds Conditt et al. observed aftereffects over the duration of the movements, indicating that feedforward was important throughout the motions [27]. The relationship between adaptation and feedforward control in motor learning is important in steering an automobile, where drivers use feedforward internal models to choose steering actions to follow a path [93]. A related hypothesis for studying adaptation is that drivers adapt their internal vehicle dynamics models like they do their internal models of arm motion.

In summary, adaptation has been well studied in the context of arm reaching, and researchers have learned a great deal about how people adapt to kinematic and dynamic changes to their arms. It is reasonable to hypothesize that these findings will extend to other tasks such as steering an automobile, but there are several open questions as described above. Fundamentally, can adaptation as it is understood in the motor learning community be observed in the driving context? If so, is the adaptation process consistent with what has been observed in arm reaching studies? Finally, what results are unique to steering an automobile?

1.2 Automobile Studies Related to Adaptation

Most studies of adaptation have examined tasks that were highly constrained in the possible motions that participants could make, and therefore have not fully represented the broad range of activities where motor learning is relevant. This has led researchers such as Wolpert et al. [144] to suggest that studies be undertaken on more realistic tasks such as driving in order to determine how well the theories of motor learning extend to more complex situations.

Studies of other real-world tasks besides driving have provided preliminary evidence that the understanding of adaptation from arm reaching studies extends to other activities. For example, Nisky et al. demonstrated partial adaptation of novice

users to the dynamics of a surgical robot manipulator commonly used in minimally invasive surgery [101]. They showed that the dynamics of the manipulator influenced the performance of both expert and novice users, suggesting that careful consideration of motor learning effects in surgical robot design could lead to improvements in robotic surgery.

Driving is considered to be a particularly rich application for the study of adaptation. For instance, Wessel cites failure in an automobile's power steering system as an example of an unanticipated event that requires fast behavioral adaptation [143]. In a review article on the role of working memory in motor skill acquisition, Seidler et al. describe certain aspects of learning to drive a new car (steering ratio, accelerator pedal sensitivity, etc.) as examples of sensorimotor adaptation [123]. The remainder of this section focuses on studies that have been conducted to understand motor learning in the automobile and the implications of driver-vehicle modeling for adaptation.

1.2.1 Experimental and Driving Simulator Studies

While motor learning researchers have referred to driving as a complex task in which adaptation is surely present [123, 143], focused studies of adaptation in driving or steering tasks have been limited. This section reviews some examples of driving simulator and experimental studies that suggest that motor learning, in particular adaptation, is important in steering tasks.

Several researchers have demonstrated learning effects in driving simulator studies. Schmidt et al. showed improvement in performance in simulated lane change maneuvers over time with lanekeeping assistance technology [122]; the results showed clear learning curves over time for three types of lanekeeping systems. Pick and Cole showed a learning effect for a lane change maneuver in path tracking performance and in the amount of arm muscle co-contraction required to steer the vehicle when the steering torque was changed [110]. Marchal-Crespo et al. studied performance in simulated wheelchair driving controlled by a steering wheel, showing that users improved path tracking performance over time and retained their performance better

when assisted by haptic steering wheel guidance [84]. These studies all demonstrated learning in the context of driving without specifically focusing on adaptation. In contrast, Cunningham et al. did a simulator study to examine the effects of temporal visuomotor adaptation, finding that drivers adapted to varying the time delay between steering inputs and vehicle motion, with a clear aftereffect for one delay length [29].

Few researchers have conducted studies relevant to adaptation in true driving scenarios. McRuer and colleagues performed a series of experimental studies in the 1970s to determine desirable vehicle dynamic characteristics by examining the closed loop driver-vehicle system [60, 91, 94]. They showed that drivers are robust to changes in steering ratio while regulating vehicle position in a straight lane, maintaining a roughly constant driver-vehicle system bandwidth [91]. This suggests that the drivers adapted to the modified steering ratio, but the steering task was designed to require primarily feedback control, so there was no direct evidence for a changing internal model in terms of feedforward steering control. In a recent study, Benderius and Markkula analyzed a large set of recorded driving data and determined that most steering motions could be well fit by bell-shaped velocity profiles, just like the hand velocities in arm reaches [11]. Benderius hypothesized that steering can be thought of as a reaching movement rather than a tracking task [10]. Taken a bit further, this suggests that drivers can adapt to changes in steering system dynamics in a similar way to adaptation in arm reaching.

1.2.2 Driver-Vehicle Modeling

Modeling the steering behavior of the driver in addition to the vehicle dynamics has been a topic of research interest for decades. MacAdam [78], Plöchl and Edelmann [112], and Benderius [10] have written detailed reviews of the history of driver-vehicle models. These models vary greatly in complexity and focus depending on the application, but they all represent the driver as a component in a closed loop control system. The elements of these models that are particularly relevant to adaptation to handling changes involve control of lateral vehicle motion through steering.

Fundamentally, steering a vehicle consists of a combination of feedback and feedforward control. A model structure that contains the key elements of interest to this dissertation was proposed by McRuer et al. in 1977 with three main driver control blocks: a feedback term with loops to control heading angle and lateral position; a feedforward term based on preview of the desired path, called pursuit control; and a second feedforward term representing a set of discrete motions corresponding to particular maneuvers such as lane changes, which McRuer called precognitive control [93]. The feedforward terms are essentially open-loop commands based on the driver's inherent understanding of the mapping between steering motions and the resulting vehicle dynamics, while feedback is necessary to correct for errors in the open-loop commands and to compensate for disturbances to the system.

Over several years, McRuer et al. formulated a well-known model of compensatory steering control called the crossover model to describe the ability of drivers to control vehicles with a range of steering system properties [91, 92, 93, 94, 96] (which was also used to describe aircraft pilots [95]). This model represents the combined driver-vehicle system with the following quasi-linear transfer function in the vicinity of the crossover frequency ω_c, with τ representing a time delay.

$$Y(s)G(s) = \omega_c \frac{e^{-s\tau}}{s} \tag{1.1}$$

This model predicts that any changes in the vehicle dynamics transfer function $G(s)$ will be balanced by changes in the driver behavior $Y(s)$ in order to maintain a constant product of the two. McRuer and Klein's 1976 study demonstrated that this was in fact the case for a range of steering ratios for a straight-line position regulation task (a task for which only feedback steering control was necessary) [91]. Donges formulated a model with similar components to those described by McRuer et al., adding feedback on path curvature to the feedback loops for heading angle and lateral position [32]; this model also demonstrated features of the crossover model. Feedback control is clearly necessary to keep the vehicle on the road and following the desired path, but it does not indicate anything about adaptation or learning – this is the domain of feedforward control.

The first feedforward model element is preview, or the concept that in order to control the vehicle, drivers must look some preview distance L_p ahead of its current position. The idea of preview or lookahead was described in the 1960s by Sheridan with driving as one example [127]. Since then, preview has been included in numerous driver-vehicle models, including those by Donges [32], MacAdam [75, 77], McRuer et al. [93], Pick and Cole [111], Sharp et al. [126], and Ungoren and Peng [137]. To quantify preview, Kondo and Ajimine measured the distance from the driver to the lookahead point or sight point on the ground and demonstrated that this distance grows approximately linearly with vehicle speed [61]. Other researchers have normalized this as preview time, $T_p = \frac{L_p}{V}$ (where V is the vehicle longitudinal velocity), which has been reported as between 0.5 and 2.0 seconds for average drivers [126, 137]. The presence of preview means that the driver begins to steer prior to entering a curve in anticipation of the resulting vehicle dynamics. Preview is therefore a type of feedforward control, which adaptation researchers study to find evidence of changing internal models of arm dynamics.

The second feedforward block from the model proposed by McRuer et al. [93] (precognitive control) has been described as the internal vehicle model concept, which has been used in driver models to capture the idea that drivers possess an implicit model of the vehicle dynamics that they use to choose control inputs [77, 78]. Internal vehicle dynamics models have been represented in the literature with neural networks [46, 79], fuzzy logic control [55], and model predictive control [59]. If drivers do in fact have an internal model of the vehicle dynamics, their steering performance should change when the handling properties of the vehicle change, since this means the internal model must be updated to match the new vehicle properties. Therefore, demonstration of adaptation to handling changes would support the internal vehicle model concept, though studies along these lines have so far been limited.

Several researchers have noted that another important factor in steering control not represented above is the neuromuscular dynamics of the arms. In 1971 Magdaleno and McRuer proposed an overall model of the general human-machine system (not specific to the automobile), including neuromuscular dynamics with various physiological time delays [83, 90]. A simple model of the driver's neuromuscular dynamics

as a second order system was used by Hess and Modjtahedzadeh to represent high frequency driver steering inputs [50, 97]. Modeling the neuromuscular dynamics of the arms with varying complexity has been of particular interest recently to Cole and colleagues, with models including features such as muscle co-contraction, stretch reflex, and arm inertia [26, 109, 110, 111]. A key part of steering is therefore a motor control process, so it is reasonable to hypothesize that motor adaptation effects are present in certain steering control scenarios.

1.2.3 Key Driving Study Results

The results of the driving studies and the elements of the driver-vehicle models discussed above suggest that steering an automobile is a task where motor adaptation should be readily observed. Drivers use a combination of feedforward and feedback control to steer vehicles [32, 93], a control strategy that also exists for arm reaching motions [125]. The importance of feedforward control in steering tasks suggests that there is a fundamental relationship between steering and arm reaching. Benderius and Markkula demonstrated that many feedforward steering motions follow bell-shaped speed profiles like arm reaches do [11] and hypothesized that steering is a type of reaching task [10].

Several studies have demonstrated that drivers can adjust to changing environments, although without specifically considering adaptation in the context of motor control. McRuer et al. showed that drivers are robust to changes in steering ratio when performing lane regulation tasks [91]. Based on experimental data from different vehicle configurations, Weir and DiMarco proposed boundaries of satisfactory vehicle response within which drivers can safely control the vehicle [141], suggesting that drivers are robust to a range of handling properties. One study that did directly investigate adaptation was performed by Cunningham et al. by varying the length of time delay from steering inputs to vehicle motion in a driving simulator [29], a type of adaptation they referred to as temporal visuomotor adaptation. They demonstrated this adaptation through improvement in path completion and tracking performance over the course of training with the delayed steering input. Although this result is an

interesting application of adaptation in the context of steering a car, time delay in the steering system is not a handling change that would be encountered in typical driving situations. Taken together, these studies suggest that drivers should be able to adapt to vehicle handling changes in a manner consistent with adaptation to visuomotor rotation in arm reaching, a hypothesis that requires further investigation.

Driver-vehicle models assume that drivers have an inherent understanding of the vehicle dynamics. The internal vehicle dynamics model concept has been proposed as one way to represent this understanding. It is challenging to directly test for the presence of such models in drivers, but the results of recent studies support their existence. The preview optimal artificial neural network approach used by Guo et al. to describe the internal model resulted in similar control inputs and vehicle trajectories to those generated by human drivers in a simulator study, suggesting that drivers do in fact use internal models [46]. Keen and Cole proposed a driver-vehicle model using multiple internal vehicle dynamics models, each covering a portion of the entire nonlinear dynamic operating range of the vehicle, to explain variations in driver skill [59]. Pick and Cole performed two simulator studies of lane change maneuvers that showed that path following performance did not change when the steering torque was modified, but performance worsened when the steering ratio was changed [110, 111]. This result supports the hypothesis that drivers base their steering control on an internal model of the relationship between steering wheel angle and lateral/yaw dynamics, rather than between steering torque and lateral/yaw dynamics. However, the basis of the internal vehicle dynamics models and how they change has not been settled.

Given that drivers use feedforward control, regularly adapt to the demands of changing environments, and seem to have an underlying internal model of the vehicle dynamics, steering a vehicle is a task that is well matched to the study of motor adaptation. A key hypothesis that links the adaptation literature and prior research on driver-vehicle interaction is that there should be empirical evidence for a changing internal model of the mapping from steering control to vehicle dynamics for a range of handling conditions.

1.3 Vehicle Handling Modification

To enable studies of how drivers adapt to handling changes, it is important to understand what handling encompasses. At a fundamental level, handling can be described as the interaction between the vehicle, the driver, and the environment [12]. The main components that determine the handling of the overall system are the vehicle's dynamic response to prescribed control inputs (e.g. steady state cornering or sinusoidal steering) [119], the combined driver-vehicle performance as measured through closed-loop task performance (e.g. navigation of specific courses) [13, 119], and the control and mental effort required of the driver to achieve the given performance [13, 141]. The first two components are closely related to the directional stability – and therefore the safety – of the vehicle [119]. The specific vehicle dynamic properties that have the strongest effects on perceived handling quality are related to lateral and yaw dynamics [13, 141]; these include both steady state characteristics such as steady state gain from steering angle to yaw rate and transient characteristics such as yaw time constant [119, 141]. Subjective measures of driver rating have been widely used to quantify the effort required by the driver and confirm the importance of specific vehicle dynamics properties [13, 28, 113, 141]. Common test maneuvers used to quantify handling performance include single lane change [13, 37, 113, 119], double lane change [37, 119], braking during cornering [13, 119], and obstacle avoidance maneuvers [82, 119]. This basic understanding of handling informs the following discussion of the handling changes that are of interest to this dissertation and methods of modifying the handling characteristics of a vehicle.

1.3.1 Handling Changes of Interest

There are four handling changes of particular interest in the study of driver adaptation. In keeping with the observation above that lateral and yaw dynamics are the most important elements of handling, all of the handling changes in this dissertation involve the steering system, which directly influences lateral and yaw dynamics.

The first handling change is scaling the steering ratio of the vehicle, or the relationship between the steering wheel angle and the road wheel angle. This change is related both to fundamental handling measures and to perturbations in visuomotor adaptation studies. Steering ratio directly affects the steady state yaw rate gain and yaw time constant, which are key handling measures [141]. Driving the car at a constant speed while changing the steering ratio provides a method of simulating the change in yaw rate gain that occurs as vehicle speed changes. Driver response to steering ratio changes has been explored by McRuer et al. [91], Pick and Cole [111], and Shoemaker et al. [128]. In the context of arm reaching adaptation studies, scaling the steering ratio is similar to scaling the cursor gain in visuomotor studies [18, 19, 64], so a study of driver adaptation to steering ratio changes provides a clear link to the existing adaptation literature.

The second handling change is reversing the direction of the steering wheel so that the driver must turn the steering wheel left for the road wheels to turn right, and vice versa. This is designed to be similar either to visuomotor rotation [64] or to mirror reversal [133] in arm reaching studies. Although this is not a handling change that drivers would experience outside the research environment, it is interesting because of its link to these existing adaptation studies and the contrast it provides to scaling the steering ratio.

The third handling change is scaling the torque felt by the driver on the steering wheel. Some researchers have demonstrated that the presence of steering torque improves driver performance and control. In a simulator study, Liu and Chang showed that steering torque improved steering performance following a skid [74]. Toffin et al. showed that modification of steering torque resulted in minimal changes to driver steering behavior for realistic torque levels [135], suggesting that drivers are robust to such changes. Pick and Cole showed that drivers modified the co-contraction of their arm muscles in response to changes in steering torque [110], while path-following performance was unaffected; they also demonstrated a learning effect of decreasing level of co-contraction as drivers gained experience with each steering torque level, although this was not classified as adaptation in the sense it is used in this dissertation. These studies suggest that, while the presence of steering torque is important for

vehicle steering control, drivers are robust to its magnitude.

The final handling change is emulating the dynamics that the vehicle would experience if it were traveling on a low friction road. This includes snowy, icy, and wet roads where the tires have less grip than they do in dry conditions and therefore less capability to generate force to turn the vehicle. This makes the vehicle more difficult to control and contributes to a large number of collisions; for instance, between 2005 and 2007 approximately 26,000 crashes in the United States were directly attributed to slick road conditions, while another 684,000 crashes were caused by driver decision errors including driving too fast for the road conditions [129]. To meet this challenge, manufacturers have implemented driver assistance systems such as electronic stability control (ESC) for these conditions [73]. Although these systems have helped to decrease the number of accidents [34], over-reliance on them by drivers may lead to deterioration in driving skill [20]; drivers who have never experienced limit handling driving situations cannot be expected to know how to safely control their vehicles if they do encounter such situations. Low friction road conditions clearly present a challenge to drivers; understanding how drivers adapt to these conditions can help inform the discussion about the role and proper design of driver assistance systems.

1.3.2 Variable Dynamic Testbeds for Handling Modification

Achieving all four of the desired handling changes described above requires a vehicle that can control the steering wheel torque, the steering ratio and direction, and the lateral and yaw dynamics in specific ways. A useful approach to designing such a vehicle is the idea of a variable dynamic testbed. This approach has been used since at least the 1970s for evaluation of the effects of mechanical changes on vehicle handling, emulation of a range of vehicle handling characteristics, assessment of human response to vehicle dynamics, and exploration of new control algorithms using a suite of actuators. Bergmiller [15] provides a detailed review of the history of such vehicles.

Much of the early design of flexible vehicles to enable modification of vehicle dynamics was conducted by automotive manufacturers. General Motors modified a production vehicle into a “Variable Response Vehicle” with electrohydraulic steering

on all four wheels to study vehicle handling characteristics [88]. Nissan's "In-Vehicle Simulator" was a custom vehicle with active suspension, four-wheel steering, all-wheel drive, and the ability to modify the wheelbase and weight distribution, all in order to enable research into human responses to vehicle dynamics [6]. The "Porsche Experimental Prototype" had a modular design with a modular hull and a flexible engine compartment that could drive either axle, with the goal of investigating vehicle dynamics and aerodynamics [103].

Several academic researchers modified production vehicles to add additional actuation capabilities for handling research. One of the first variable vehicle testbeds developed in an academic setting was the "Variable Characteristic Car" from Melbourne University in 1980, which used electrohydraulic actuators to control front steering angle and steering wheel torque with the goal of studying a range of handling characteristics [33]. In a project with the National Highway Traffic Safety Administration (NHTSA) during the 1990s, researchers at California Institute of Technology developed a "Variable Dynamics Testbed Vehicle" with four-wheel steering and active suspension in order to emulate the dynamics of a range of other vehicles in a single testbed [69, 70, 71]. Chalmers University developed the "SIRIUS 2001" vehicle in conjunction with Volvo, adding four-wheel steering and brake-by-wire to enable study of electronics and communication protocols [54].

Recently, academic institutions have developed several custom vehicles to test a range of control algorithms, among them handling modification techniques. Stanford University students in the Dynamic Design Laboratory have built two custom by-wire vehicles since the early 2000s, known as "P1" [68] and "X1" [16]. P1 was designed with front independent steer-by-wire and rear independent electric drive. X1[1] (used for the experiments in this dissertation) was designed to be modular to allow incorporation of new actuation schemes and currently includes four-wheel independent steer-by-wire, rear electric drive, four-wheel independent electrohydraulic braking, and a steering wheel force feedback motor. At TU Braunschweig, the experimental testbed "MOBILE" was developed with steer-by-wire, electric drive, and electromechanical braking

[1]The author designed the steer-by-wire controller (Appendix A) and contributed suspension hardware and basic software to this experimental vehicle.

on all four wheels; the purpose of this vehicle is to test a variety of electronics and vehicle control applications [14]. Researchers at Universität Paderborn developed a lightweight go-kart sized vehicle called "Chamäleon", with electric motors on each wheel to control steering, drive, and suspension actuation and a joystick for steering control [65].

1.3.3 Key Handling Modification Results

One line of vehicle handling modification research has explored ways of modifying specific vehicle parameters of interest through active steering control. Yih and Gerdes used full state feedback and steer-by-wire to modify the effective front tire cornering stiffness and to compensate for variable vehicle loading, demonstrating the control scheme in experiment with a modified Corvette [149]. Yamaguchi and Murakami took this approach further by estimating the tire cornering stiffnesses and modifying the front cornering stiffness when its variation from its nominal value exceeded a threshold, with experimental results validating the approach on a golf cart-like electric vehicle [148]. Brown et al. followed a similar control methodology to Yih and Gerdes by using the front steer-by-wire and rear differential drive capabilities of the P1 vehicle at Stanford University to emulate a range of vehicle handling properties, including weight distribution, overall mass, and front and rear tire cornering stiffness [21]. The authors explored the limitations of using this method for a wide range of emulated vehicle parameters and concluded that low-speed sideslip behavior is difficult to emulate.

Another body of research has used four-wheel steering (4WS) to control lateral and yaw dynamics to achieve desired handling characteristics. An early result from Sano et al. showed that designing the ratio of rear steer angle to front steer angle as a function of speed could provide maneuverability at low speed and stability at high speed and explored the design parameters used to properly choose this ratio [120]. Horiuchi et al. leveraged a feedforward-feedback structure to achieve desired lateral acceleration and yaw rate responses based on a linear reference model, and confirmed the feasibility of their approach in experiment [52]. Ro et al. demonstrated improved directional

stability in simulation using a sliding-mode 4WS controller, including robustness to wind disturbances and parameter uncertainty [114]. Marino and Scalzi designed a controller that decoupled body sideslip angle and yaw rate to allow for a wider range of possible emergency maneuvers, such as a zero yaw rate maneuver in a highly dynamic "moose test," which improved vehicle performance in simulation compared to using front steering alone [85].

Leveraging the capabilities of variable dynamic testbeds, other researchers have demonstrated different methods of emulating the dynamics of different vehicles on a single testbed. Lee used the Variable Dynamics Testbed Vehicle (VDTV) to emulate the lateral dynamics of a variety of vehicle types as part of a NHTSA project to study how vehicle handling characteristics influence crash avoidance [69, 70, 71]. The VDTV used a model-following control approach with yaw rate, lateral acceleration, and/or sideslip angle feedback, using linear tire models. More recently, Akar and Kalkkuhl proposed a lateral dynamics emulation scheme that tracked the sideslip angle and yaw rate of a linear reference model using sliding mode control for four-wheel steering, which also demonstrated robustness to some vehicle parameter uncertainty in simulation [4].

None of the approaches discussed above have demonstrated the ability to emulate low friction vehicle dynamics, a handling condition that is of particular interest for driver adaptation. One way of doing this is the commercial SKIDCAR system [31], which modifies the mechanical properties of the vehicle by supporting much of its mass on a frame with caster wheels to reduce the normal force on the tires. This limits the available tire force in order to emulate the dynamics that would occur on a low friction surface, allowing drivers to experience driving at the limits of handling (see for example the study by Gregersen on the efficacy of skid training for new drivers in Sweden [45]). Although the SKIDCAR system is useful for driver training, for the application of studying how drivers adapt to handling changes it is desirable to use a single testbed that is capable of creating all four handling changes. Additionally, since the SKIDCAR allows the tires to truly reach their handling limits, the ability to stop the vehicle is reduced. From an experimental safety standpoint, a testbed with a low friction emulation algorithm can enable the studies of interest while maintaining

the ability to safely bring the vehicle to a stop when needed. A main result of this dissertation is the development and experimental demonstration of such a low friction emulation algorithm on the X1 research testbed.

1.4 Dissertation Contributions

The literature reviewed above raises important questions about adaptation in the context of steering an automobile. Can motor adaptation be observed in a vehicle steering task? Is there evidence that drivers change their internal models of the mapping from steering inputs to vehicle dynamics when the handling properties change? How can a range of handling changes be created in a controlled manner on an experimental testbed? To address these questions, this dissertation develops a protocol for driver adaptation studies, designs a flexible method of handling modification that can be applied to low friction emulation, and conducts user studies of four different handling changes. The specific contributions of the dissertation are described in more detail below.

1.4.1 A user study protocol for an experimental vehicle to test how drivers adapt to changes in vehicle handling related to steering

The user study protocol was designed to enable the study of several handling changes, some of which are similar to the types of perturbations used in arm reaching studies, and some of which are more relevant to real-world driving scenarios. Since the focus is on how drivers change their steering control in the face of these handling changes, the protocol isolates steering from longitudinal control. During the steering task, a simple lane change with randomized direction, the user controls the steering while the vehicle speed is regulated by cruise control. Between trials, the vehicle steers itself along a path to return to the start of the course, with the driver controlling the speed so that the learning of the perturbation to the steering system is confined to the discrete steering task trials. The sequence of trials is similar to many motor learning

studies, with a few trials at baseline handling condition, followed by several trials with perturbed handling, and finally returning to the baseline condition to test for aftereffects. As described in Section 1.1.2, the metrics typically used in arm reaching studies do not directly map to metrics that are useful to analyze adaptation to steering changes; the metrics chosen for this study protocol are steering wheel reversal rate, RMS steering speed, time to local maximum steering angle, and RMS yaw jerk, which are described in detail in Section 2.5.

1.4.2 A method of vehicle handling modification to enable emulation of low friction vehicle dynamics via four-wheel steering (4WS)

This method uses a model-following approach to track the planar dynamics of a reference model with the desired handling properties. Since the reference model is simulated online, the reference model tire forces are available in real time to the handling emulation controller. The controller combines feedforward of the reference model tire forces with linear and nonlinear feedback of state errors. The four-wheel steer-by-wire system of the experimental vehicle controls lateral and yaw dynamics, while the longitudinal dynamics are controlled through the electric drive motor and the electrohydraulic braking system. By accounting directly for the tire forces, it is straightforward to show stability of the error dynamics. The handling emulation method is applied to the problem of emulating the dynamics of a reference model whose tires are on a low friction surface such as ice. The performance of the controller for this application is demonstrated experimentally for several friction coefficients.

1.4.3 Experimental evidence that drivers adapt to steering changes

The user study protocol was applied to the four handling changes described in Section 1.3.1: steering ratio reduction, steering direction reversal, steering torque increase, and low friction dynamics. In all studies except the steering torque increase, there

was evidence that drivers adapted to the handling changes over the course of just ten trials. These real-world studies extend the understanding of motor learning from the well-studied activities of eye saccades and arm reaches to the complex activity of steering a vehicle. In addition to this important result, these studies provide two key insights specific to steering a vehicle:

Drivers are sensitive to steering ratio and robust to steering torque

Drivers in the steering ratio reduction study clearly adapted to the handling change, as evidenced by large changes in the behavioral metrics when the steering ratio was perturbed that gradually returned to baseline levels, while drivers in the steering torque increase study showed very little change in behavior when the torque was increased. This suggests that drivers use the relationship between steering wheel **angle** and vehicle dynamics as a basis for control, rather than the relationship between steering wheel **torque** and vehicle dynamics. This idea has been proposed by Pick and Cole based on driving simulator studies [110, 111], and the results of these two adaptation experiments support this understanding of how drivers formulate their control actions.

Driving style affects the adaptation process

In the low friction dynamics user study, two groups of participants emerged who experienced different vehicle dynamics from each other. The reference dynamics for the low friction emulation controller used in this study depend on the driver's steering inputs, with more aggressive inputs tending to make the vehicle feel less controllable as the reference dynamics approach the limits of handling. Some drivers made small, smooth steering inputs to make the lane change, staying away from the handling limits of the reference model; these drivers therefore did not experience a large change in handling dynamics to which they would need to adapt. In contrast, the second group of participants made more aggressive steering actions that resulted in significant changes to the vehicle's handling; these participants adapted to the handling change they experienced. So unlike the other user studies in this dissertation, where all

participants experienced the same perturbations, this study highlights an interesting feature of driving: there are different ways to steer a vehicle through a course and individual driving style greatly affects the development of handling dynamics.

1.5 Dissertation Outline

Chapter 2 describes the development of the driving user study protocol, beginning with an overview of the experiment. This is followed by a review of the technical capabilities of the X1 research vehicle, which informs the details of the study design. Further details on the lane change task phase of the study include two methods of modifying steering wheel torque, a custom cruise control algorithm, GPS-based triggering of signal lights to indicate desired lane change direction, and a GPS-based safe stop controller for safety in the event that the car goes off the course. Next, the elements of the automated return to start phase is described, including map generation, the path-following steering algorithm, and a speed limit controller. Finally, the four metrics used for studying driver adaptation are explained to provide background for the user study results.

Chapter 3 presents the results of the first two user studies, which were designed to parallel the two visual cursor kinematics perturbations studied by Krakauer et al. in arm reaching studies [64]. These two vehicle studies involve modifications to the steering ratio of the vehicle: in the first, the steering ratio is scaled down to make the steering very sensitive to driver steering wheel inputs; in the second, the steering wheel direction is reversed so that steering wheel inputs to the left result in vehicle motion to the right, and vice versa. Results of these studies using the protocol developed in Chapter 2 demonstrate adaptation in the automobile environment and raise questions about how drivers adapt to more realistic handling changes.

Chapter 4 presents results from a user study for one of these realistic handling changes, an increase in steering wheel torque to simulate a power steering failure. Unlike in the first two studies, participants do not show significant changes in steering behavior due to the modified steering torque. This handling change therefore does not require adaptation, and participants likely compensate for the change by stiffening

their arms.

To enable the study of the final handling change, **Chapter 5** details the development of a novel handling emulation controller that uses four-wheel steering to track the planar dynamics of a reference vehicle model that is simulated in real time on the experimental vehicle. Tire forces on the experimental vehicle are chosen to generate fast, stable error dynamics. The handling emulation controller, which in general can track any planar reference model within the physical limits of the car, is applied to the specific case of emulating the dynamics of a vehicle traveling on a low friction surface such as ice. The limitation of rear steering angle is addressed in the formulation of the controller, ensuring consistent behavior of the vehicle. Experimental results for this application confirm that the controller successfully tracks the dynamics of reference models with a range of friction coefficients.

With the results from the final user study, **Chapter 6** demonstrates driver adaptation to the low friction handling condition. The degree of handling change experienced is not consistent among participants, but rather depends on different driving styles. This leads to clear differences in the adaptation process between two groups of participants who take different approaches to the lane change task.

Chapter 7 summarizes the results and proposes extensions of the work in this dissertation to improve understanding of driver adaptation to handling changes. Expanding the scope of the handling emulation controller to consider additional handling changes would be beneficial in car design and could allow drivers to tune the handling of their vehicles to personalize their driving experience. Studies of adaptation to the handling changes considered in this dissertation should be repeated and expanded, specifically by adding physiological measurements including brain activity to give a more complete picture of adaptation processes, and by modifying the experimental protocol to explore how adaptation generalizes to untrained conditions. Finally, adaptation studies in the automobile could be expanded to include both longitudinal control and steering in the study of several handling changes and to further investigate the issue of handover of control from an automated vehicle to a human driver.

Chapter 2

Driver Adaptation User Study Design

Based on the background literature on human motor learning, it is clear that there are specific processes that take place in the brain when someone learns a new task or when something about the task environment changes. From the wealth of studies that have demonstrated motor learning, there is a good deal of understanding of how certain types of learning take place. However, most of these studies have been conducted in laboratory environments on constrained tasks that bear little resemblance to the types of activities that people encounter in daily life that may provide opportunities for motor learning. When faced with these real-world environments, do people undergo the same learning process as measured in the laboratory?

The hypothesis of this dissertation is that drivers do in fact undergo similar learning processes when they experience changes in vehicle handling. Handling is concerned with the way the vehicle dynamics respond to inputs from the driver under various conditions, particularly in the lateral direction. For instance, a driver might perceive a vehicle as responsive if it turns suddenly in response to a sharp steering wheel change, while it might feel laggy if the turning rate takes longer to develop. Handling can change for many reasons, including suddenly encountering a patch of ice, power steering failure, and increasing the weight on the rear of the vehicle by putting a large load in the trunk.

This chapter develops a protocol for user studies to test the hypothesis for a variety of modifications to the vehicle handling. The study protocol is implemented on an

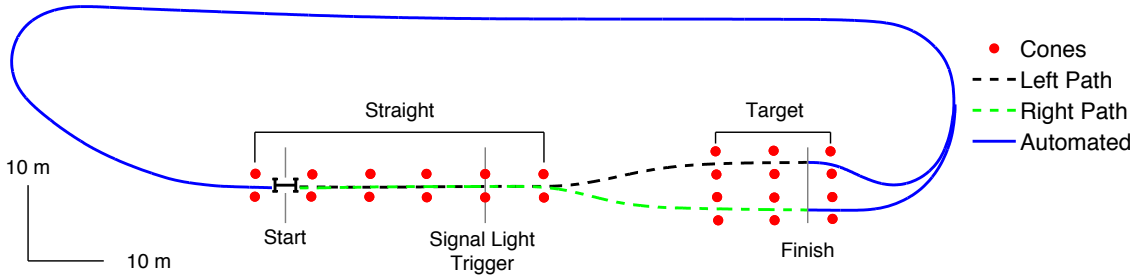

Figure 2.1: The driver adaptation study test course.

experimental by-wire vehicle for four types of modifications, the results of which are discussed in later chapters.

2.1 Study Overview

The study uses a simple lane change task to investigate how drivers adapt to sudden changes in vehicle handling. The test course for the study is pictured in Fig. 2.1, with lanes demarcated by traffic cones. The task requires the driver to steer the vehicle down the center lane of the course as it automatically accelerates to a speed of 8 m/s, make a single lane change right or left, and come to a stop into one of two target gates. The direction of the lane change is indicated by a signal light in the driver's direct line of sight and is triggered just prior to the end of the straight center lane. After stopping in the target gate, the vehicle automatically steers back to the start of the course while the driver controls the vehicle speed for safety. This semi-automated return to start phase of the experiment is necessary to reset the vehicle at the beginning of the course and also simulates the experience of being in an automated vehicle that does not require steering input from the driver.

The steering task is the phase of the experiment where the hypothesis is tested. The speed is controlled automatically to facilitate comparisons between drivers and to enable the driver to focus solely on steering to complete the lane change task. During this phase, the vehicle handling is modified according to the desired experimental protocol, pictured in the top panel of Fig. 2.2. The first four trials are performed under

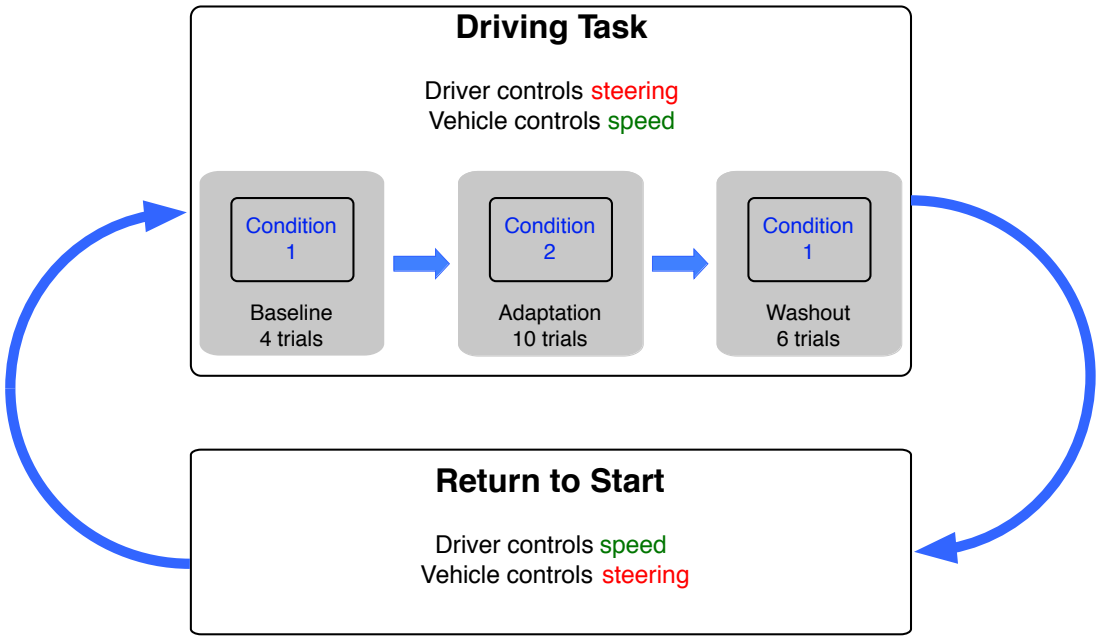

Figure 2.2: Overview of the user study protocol.

baseline handling conditions. Next, a perturbation is made to the vehicle handling, applied consistently for ten adaptation trials. Finally, during the washout block of six trials, the handling is returned to the baseline condition to test for aftereffects in the driver's motor control.

There are several options for the handling modification, and four of them are addressed in this dissertation. These are (1) scaling the steering ratio, (2) reversing the direction of steering wheel control, (3) increasing the torque felt at the steering wheel, and (4) emulating the behavior of a vehicle traveling on an icy road. More details on the design of these specific modifications are found in subsequent chapters along with the experimental results.

The remainder of this chapter describes the engineering implementation of the experiment, including details on the experimental vehicle, the driving task phase, and the return to start phase. The chapter concludes with a discussion of the metrics used to analyze adaptation during vehicle handling changes.

Figure 2.3: The X1 experimental vehicle.

2.2 X1 Experimental Vehicle

The X1 experimental vehicle (Fig. 2.3), designed and built entirely by students at Stanford University, is used for all experiments in this dissertation. This vehicle is used for a wide range of experiments in vehicle dynamics and control, including shared control between the driver and the vehicle for obstacle avoidance [35], emulation of the dynamics of a vehicle traveling on an icy surface [117], and designing appropriate steering wheel torque feedback to create a realistic steering feel [8]. Table 2.1 lists the values of the physical parameters of X1 that are relevant to this work.

2.2.1 Hardware Description

The drivetrain consists of a 75 kW brushless permanent magnet motor with 240 Nm of peak torque (UQM Technologies, Inc., Frederick, CO) and an open differential with 7:1 gear reduction (Strange Engineering, Morton Grove, IL). The motor is powered by

Table 2.1: Experimental vehicle parameters

Parameter	Symbol	Value	Units
Mass	m	1973	kg
Yaw moment of inertia	I_z	2000	$kg \cdot m^2$
Distance from CG to front axle	a	1.54	m
Distance from CG to rear axle	b	1.21	m
Front cornering stiffness	$C_{\alpha f}$	140	$kN \cdot rad^{-1}$
Rear cornering stiffness	$C_{\alpha r}$	170	$kN \cdot rad^{-1}$
Maximum front steer angle	$\delta_{f,max}$	18	deg
Maximum rear steer angle	$\delta_{r,max}$	14	deg

a pack of 28 deep-cycle lead-acid batteries (Optima Batteries, Inc., Milwaukee, WI) with a nominal pack voltage of 336 V. The vehicle is equipped with a dual braking system consisting of two brake calipers on each wheel, one for manual braking and one for electronically controlled braking. The manual brakes use a standard configuration of hydraulic components. With the electronic brakes (TNO, Delft, Netherlands), the brake pressure on each wheel can be controlled independently through a hydraulic pump. The maximum pressure for each wheel is 120 bar and the brake pressure has a rise time of about 100 ms.

The steering is controlled with independent steer-by-wire systems on all four wheels, each consisting of a DC motor (Magmotor, West Boylston, MA), a harmonic drive with gear reduction of 160:1 (Harmonic Drive LLC, Peabody, MA), a motor controller that communicates via CAN (ADVANCED Motion Controls, Camarillo, CA), and a custom steering linkage. A pack of 4 lead-acid batteries (EnerSys, Reading, PA) with a nominal pack voltage of 48 V provides power for the steering motors. The front wheels are capable of steering to $\pm 18°$, while the rear wheels can steer to $\pm 14°$. The suspension is designed to minimize the effect of longitudinal forces on the measured steering torque at the tie rod, which aids in estimation of tire-road friction values for stability control [17]. A custom-built adjustable steering wheel assembly provides haptic feedback to the driver using a DC motor (Magmotor) and a harmonic drive (Harmonic Drive LLC), providing maximum steering wheel torque of 6 Nm.

Vehicle localization and state measurement is performed with a system that tightly

integrates an inertial measurement unit (IMU) and a Global Navigational Satellite Systems (GNSS) receiver (NovAtel, Inc., Calgary, Alberta, Canada). The system provides position, velocity, acceleration, and rotational rate information at 100 Hz. The satellite measurements are augmented with differential global positioning system (dGPS) corrections from OmniStar (Houston, TX) and a local base station to provide overall position accuracy within 2 cm.

2.2.2 Software and Controls

The vehicle has a single control computer to handle all basic vehicle sensing and control, the MicroAutoBox II 1401/1511/1512 (dSPACE GmbH, Paderborn, Germany). Control software is designed using Simulink (version R2011a, MathWorks, Natick MA) and operates at 500 Hz (0.002 s sample period). The low-level controller for the steer-by-wire system is discussed in Appendix A; controllers for other subsystems were also developed by Stanford University students.

2.2.3 Data Collection

Program execution and data recording are controlled through ControlDesk software (version 7.1, dSPACE GmbH). Over 200 signals are recorded at each execution time step, of which approximately 50 are relevant to the driver adaptation studies and handling emulation controller. Data recorded in ControlDesk are exported to MATLAB (version R2011a, MathWorks) for analysis.

2.3 Driving Task

As described above, the driving task consists of a single lane change at a prescribed speed. The task starts with the vehicle stationary at the beginning of the course (Fig. 2.1, Start line). The experimenter, sitting in the passenger seat, pushes a button to activate the cruise control system, which accelerates the vehicle up to a maximum speed of about 8 m/s and holds at that speed. As the vehicle accelerates, the driver steers it straight down a 10 ft wide lane bordered by pairs of cones. When the vehicle

approaches the end of the straight segment, one of two signal lights on the vehicle's front bumper illuminates to indicate which direction the driver should steer. Based on which light is active, the driver steers into the left or right gate, each of which is 10 ft wide and demarcated by pairs of cones. As soon as the driver has completed the steering action, he presses the brake to bring the car to a stop before the last pair of cones in the target gate. The lateral (steering) and longitudinal (acceleration and braking) control of the vehicle are separated during the task to standardize the experiment between drivers and to ensure that drivers are primarily focused on the steering task rather than on maintaining vehicle speed. The subsystems that make up the driving task are described in more detail below.

2.3.1 Steering Wheel Torque

In a conventional steering vehicle, the driver feels torque at the steering wheel (handwheel) that communicates information about the tire forces that the vehicle is experiencing. For a steer-by-wire vehicle such as X1, there is no mechanical connection between the handwheel and the road wheels. This means that there is also no direct application of steering torque related to the tire forces, so for driver safety and comfort it is necessary to create an artificial steering feel. In general, with a force feedback steering system, the handwheel torque τ_{hw} can be modeled as the sum of the torque applied by the motor τ_{motor} and the torque due to the steering system dynamics. A simple version of this model is

$$\tau_{\text{hw}} = \tau_{\text{motor}} + J\ddot{\delta}_{\text{hw}} + b\dot{\delta}_{\text{hw}}, \tag{2.1}$$

where δ_{hw} is the handwheel angle, J is the steering system inertia, and b is the steering system damping. The designer is free to choose the motor torque to provide the desired steering feel; two different motor torque models are used for the studies presented here: the linear spring model and the full steering feel emulator.

Linear Spring Model

For the first two user studies (Chapter 3), the motor torque is a simple linear function of handwheel angle within the road wheel angle limits $\pm\delta_{\mathrm{f,max}}$ and a much stiffer affine function of steering wheel angle outside these limits to simulate steering stops. The handwheel torque is modified along with the steering ratio so that there is a constant torque for a given road wheel angle, although this will correspond to a different handwheel angle depending on the steering ratio. The maximum handwheel angle $\delta_{\mathrm{hw,max}}$ is found from

$$\delta_{\mathrm{hw,max}} = |\delta_{\mathrm{f,max}} K_{\mathrm{sr}}|, \tag{2.2}$$

where K_{sr} is the steering ratio and the absolute value provides the correct steering wheel torque for negative steering ratios. Given this limit, the torque command is found from the following.

$$\tau_{\mathrm{motor}} = \begin{cases} -\dfrac{1.125\pi}{\delta_{\mathrm{hw,max}}}\delta_{\mathrm{hw}}, & |\delta_{\mathrm{hw}}| \leq \delta_{\mathrm{hw,max}} \\ -1.125\pi \operatorname{sgn}(\delta_{\mathrm{hw}}) - 100(\delta_{\mathrm{hw}} - \delta_{\mathrm{hw,max}} \operatorname{sgn}(\delta_{\mathrm{hw}})), & |\delta_{\mathrm{hw}}| > \delta_{\mathrm{hw,max}} \end{cases} \tag{2.3}$$

The torque command is then limited to a maximum value of 6 Nm to stay within the limits of the force feedback steering system hardware. The relationship between handwheel motor torque and handwheel angle for a range of steering ratios is plotted in Fig. 2.4. Note that negative steering ratios are not plotted, but these would be identical to the positive steering ratios in the figure. For example, the curve for -15:1 steering ratio would lie directly on top of the 15:1 steering ratio curve.

When a vehicle is traveling at low speed and experiencing moderate levels of lateral acceleration, as is the case for this user study protocol, the primary source of steering torque feedback is jacking torque, which comes from vertical tire forces. Jacking torque is well approximated by a linear spring model [8, 53], so this implementation is a reasonable approximation to the steering torque that would be experienced in a typical passenger vehicle.

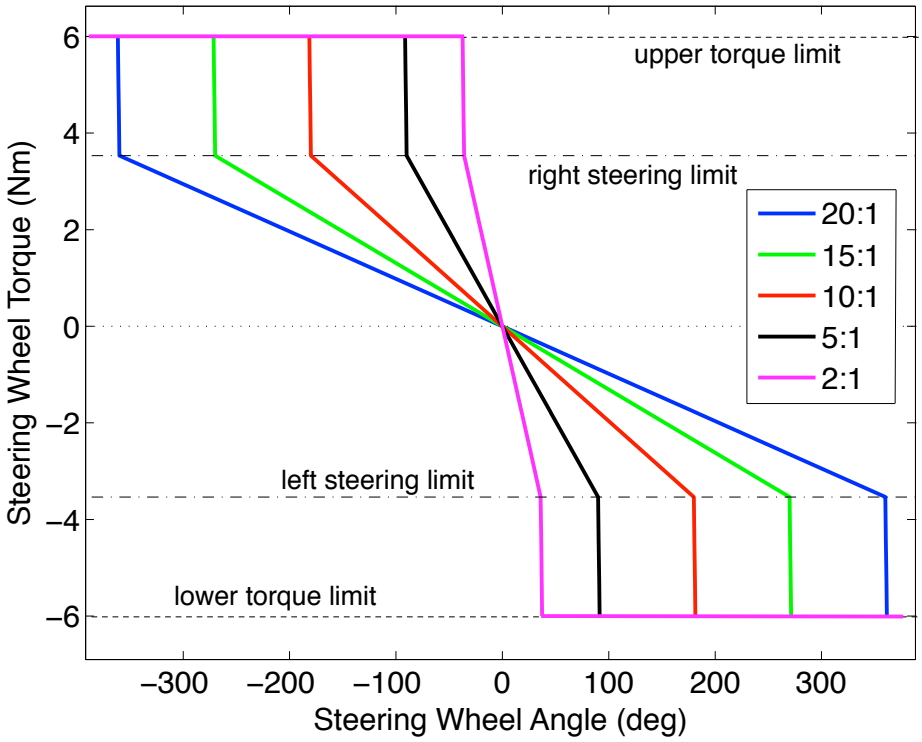

Figure 2.4: Linear spring model of steering torque for various steering ratios. The relationship between steering wheel torque and road wheel angle is held constant. Identical curves exist for negative steering ratios.

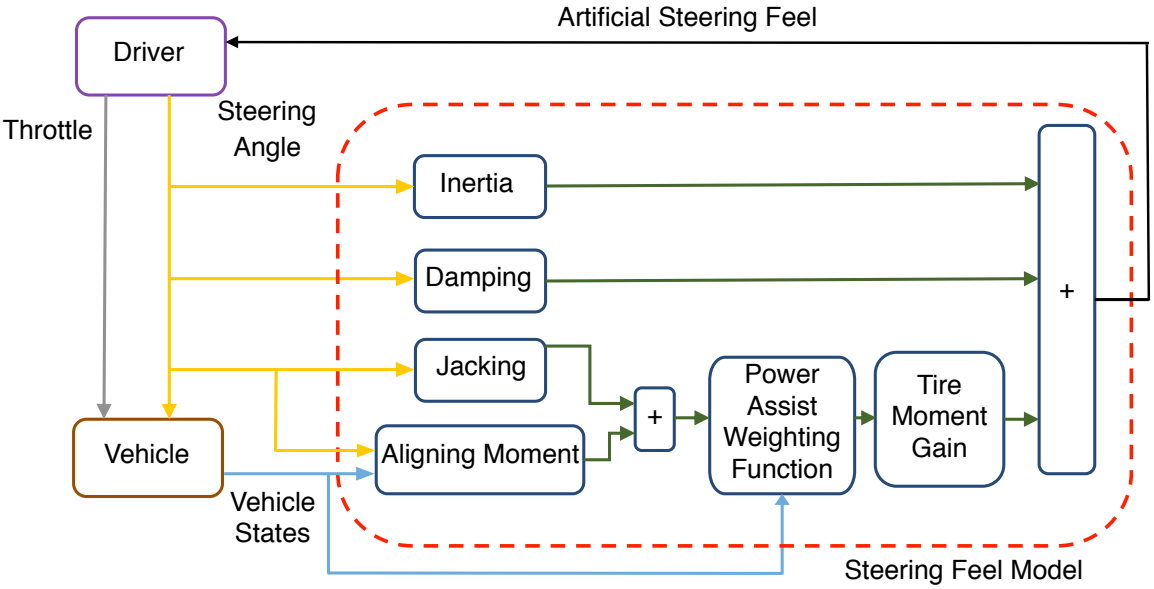

Figure 2.5: Block diagram of the full steering feel emulator.

Full Steering Feel Emulator

For the final two user studies (Chapters 4 and 6), the handwheel torque uses a more complex model that mimics the torque that would normally be observed in a conventional steering car. The motor torque for the full emulator is given by

$$\tau_{\text{motor}} = \tau_{\text{inertia}} + \tau_{\text{damping}} + K\tau_{\text{assisted}}, \tag{2.4}$$

where τ_{inertia} and τ_{damping} are used to modify the effective inertia and damping experienced at the handwheel, the total assisted tire moment τ_{assisted} models the combination of tire aligning moment τ_{aligning}, tire jacking torque τ_{jacking}, and power assist, and K is a gain that controls how much of the total assisted tire moment is transmitted to the handwheel. The assisted tire moment is modeled with the following equation, where W is a power assist weighting function that depends on the front tire slip angle α and the lower limit parameter γ, as depicted in Fig. 2.6.

$$\tau_{\text{assisted}} = W(\alpha, \gamma)\left(\tau_{\text{jacking}} + \tau_{\text{aligning}}\right) \tag{2.5}$$

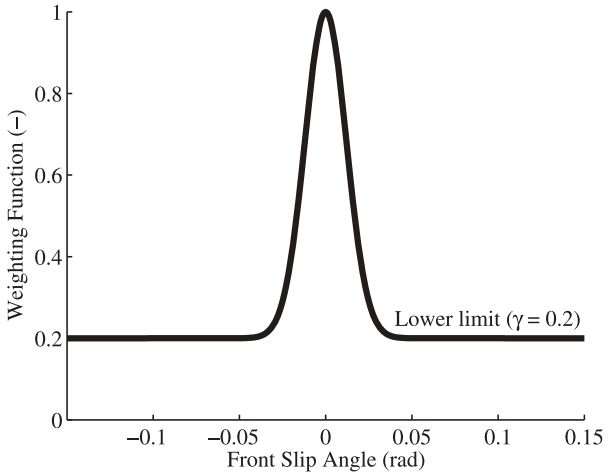

Figure 2.6: Weighting function for power assist in the full steering feel emulator (from Balachandran and Gerdes [8]).

For the steering torque study presented in Chapter 4 and the low friction study in Chapter 6, the weighting function lower limit and the assisted tire moment gain are modified to create the desired steering feel.

2.3.2 Cruise Control

To keep the conditions of the experiment consistent across all participants and to focus the driver's attention on the steering task, a cruise control algorithm regulates the vehicle's longitudinal speed. When the cruise control button is pressed, the set speed $U_{\mathrm{x,set}}$ is gradually increased from 0 to 8 m/s using a two-pole 0.5 Hz discrete low pass filter, $L_2(z)$.

$$L_2(z) = \frac{3.948 \times 10^{-5}}{z^2 - 1.987z + 0.9875} \tag{2.6}$$

$$U_{\mathrm{x,set}} = 8L_2(z) \tag{2.7}$$

Given the set speed, electric drive motor torque τ_m, actual speed U_{x}, and proportional feedback gain $K_{\mathrm{cruise}} = 35\ \mathrm{N \cdot s}$, the control algorithm is a simple proportional

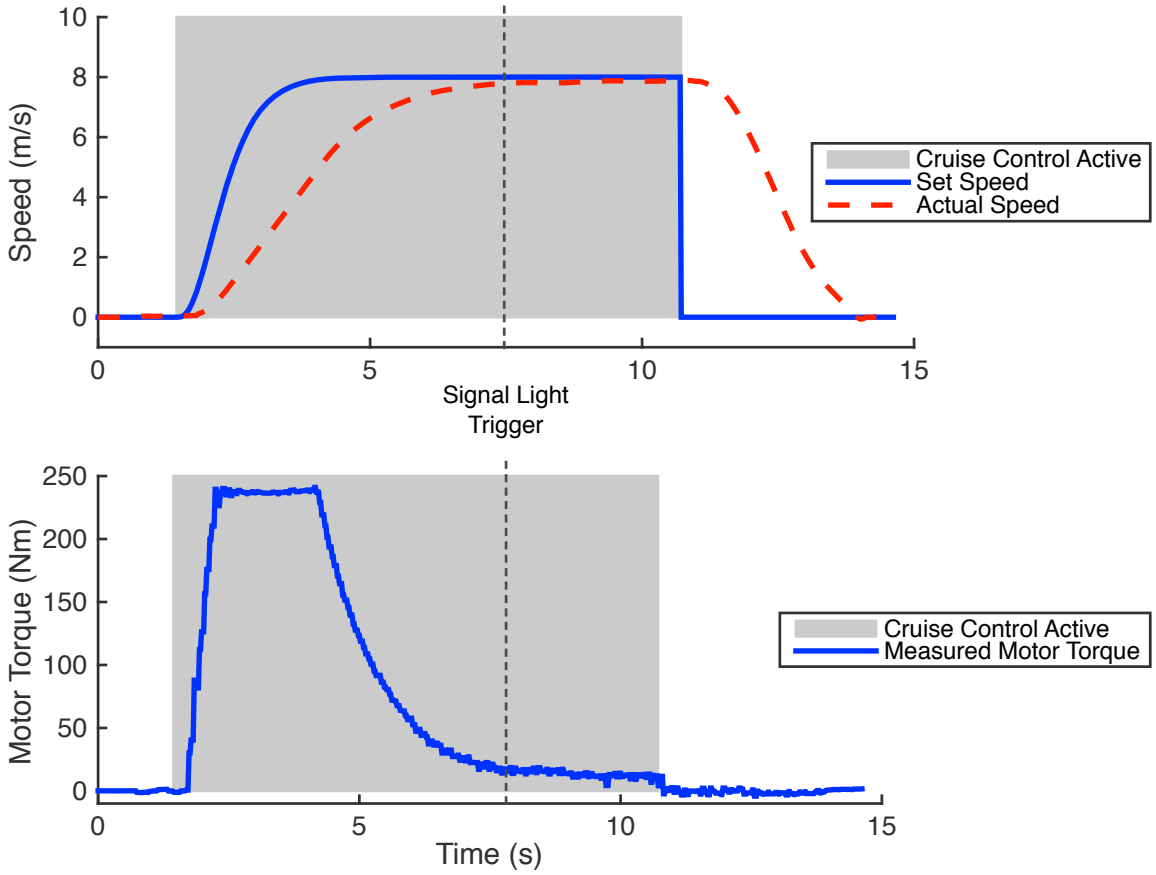

Figure 2.7: Cruise control performance. The cruise control algorithm is active in the shaded region, accelerating the vehicle to 8 m/s (top). The drive motor torque also gradually ramps up to its limit and then follows a proportional control law to track the set speed (bottom).

controller.

$$\tau_{\mathrm{m}} = K_{\mathrm{cruise}} \left(U_{\mathrm{x,set}} - U_{\mathrm{x}} \right) \tag{2.8}$$

The operation of the cruise control algorithm for a sample trial is depicted in Fig. 2.7. The vehicle speed U_{x} is slightly less than the desired 8 m/s because the control algorithm does not take into account losses such as aerodynamic drag and tire rolling resistance. However, the performance of the cruise control is consistent across trials, so all drivers experience the same behavior for each trial.

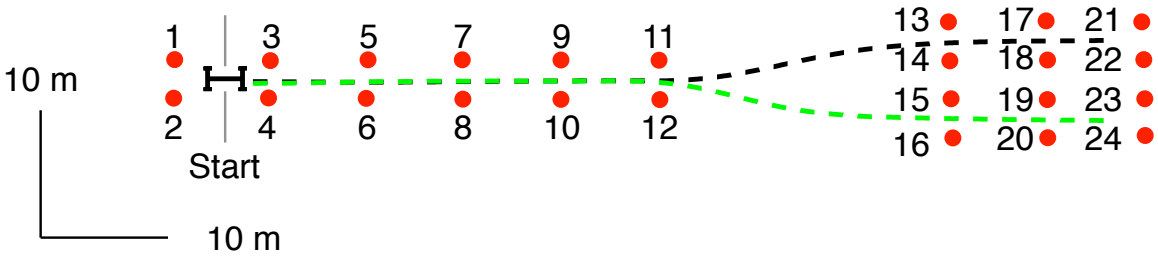

Figure 2.8: Cone numbers used to compute X-Y coordinates. This is a zoomed-in view of the course layout from Fig. 2.1.

There is a short delay between activating the cruise control and beginning to apply drive torque because communication with the drive motor occurs every 50 ms. Since the set speed smoothly increases over the course of about 1 second, the drive motor torque at first ramps from zero to its maximum value of 240 Nm, then saturates for a couple seconds. The torque gradually reduces to a steady-state value at around 9 seconds, then the driver steps on the brake at about 11 seconds to disable the cruise control and bring the car to a stop at 14 seconds.

2.3.3 Converting East-North Position to X-Y Coordinates

The east and north coordinates of the vehicle center of gravity are measured by the on-board GPS system with origin at a fixed reference location near the testing site. For several components of the experiment, it is useful to operate in a different set of coordinates, with the origin centered between the first pair of cones on the straight, X lying along the straight in the direction of travel, and Y at 90° counterclockwise from X (to the left as viewed from the driver's perspective).

The cones demarcating the path are numbered from start to end as depicted in Fig. 2.8. For any coordinate pair (E,N), the conversion to (X,Y) is achieved by the following algorithm. First, the new origin is placed at the midpoint of cones 1 and 2. The position of a point (E,N) is translated to this origin by subtracting the origin position (E_0,N_0), which is defined by the following equation, where $E(i)$ and $N(i)$

are the east and north coordinates of cone i.

$$\begin{aligned} E_0 &= \frac{1}{2}(E(1) + E(2)) \\ N_0 &= \frac{1}{2}(N(1) + N(2)) \end{aligned} \tag{2.9}$$

Next, the angle of the path counterclockwise from east is computed from the positions of the first and last cones along the left side of the center lane.

$$\theta = \tan^{-1}\left(\frac{N(22) - N(1)}{E(22) - E(1)}\right) \tag{2.10}$$

Finally, the X and Y coordinates for each point are computed by applying the rotation matrix R to the translated (E,N) point.

$$\begin{bmatrix} X \\ Y \end{bmatrix} = \begin{bmatrix} \cos\theta & \sin\theta \\ -\sin\theta & \cos\theta \end{bmatrix} \begin{bmatrix} E - E_0 \\ N - N_0 \end{bmatrix} = R \begin{bmatrix} E - E_0 \\ N - N_0 \end{bmatrix} \tag{2.11}$$

This transformation is applied to measured cone positions prior to the experiment to create a map of the steering task area. Fig. 2.9 compares the course in both sets of coordinates. During the experiment, measurements of the (E,N) position of the vehicle's center of gravity are transformed into (X,Y) coordinates in real time to enable the functionality of the signal light trigger and the safe stop, discussed below.

2.3.4 Signal Light Trigger

The signal lights (Fig. 2.10) are attached to the front bumper of the experimental vehicle, directly in the driver's view along the path. Both lights are off while the vehicle accelerates down the straight segment of the course. As the vehicle comes to the end of the straight, one of the lights illuminates to indicate which lane the driver should change into. The condition for activating the signal lights is that the vehicle center of gravity is within a certain range of X values, as pictured in Fig. 2.11 (light on in shaded region).

The lane change direction for each trial is predetermined by generating a vector of

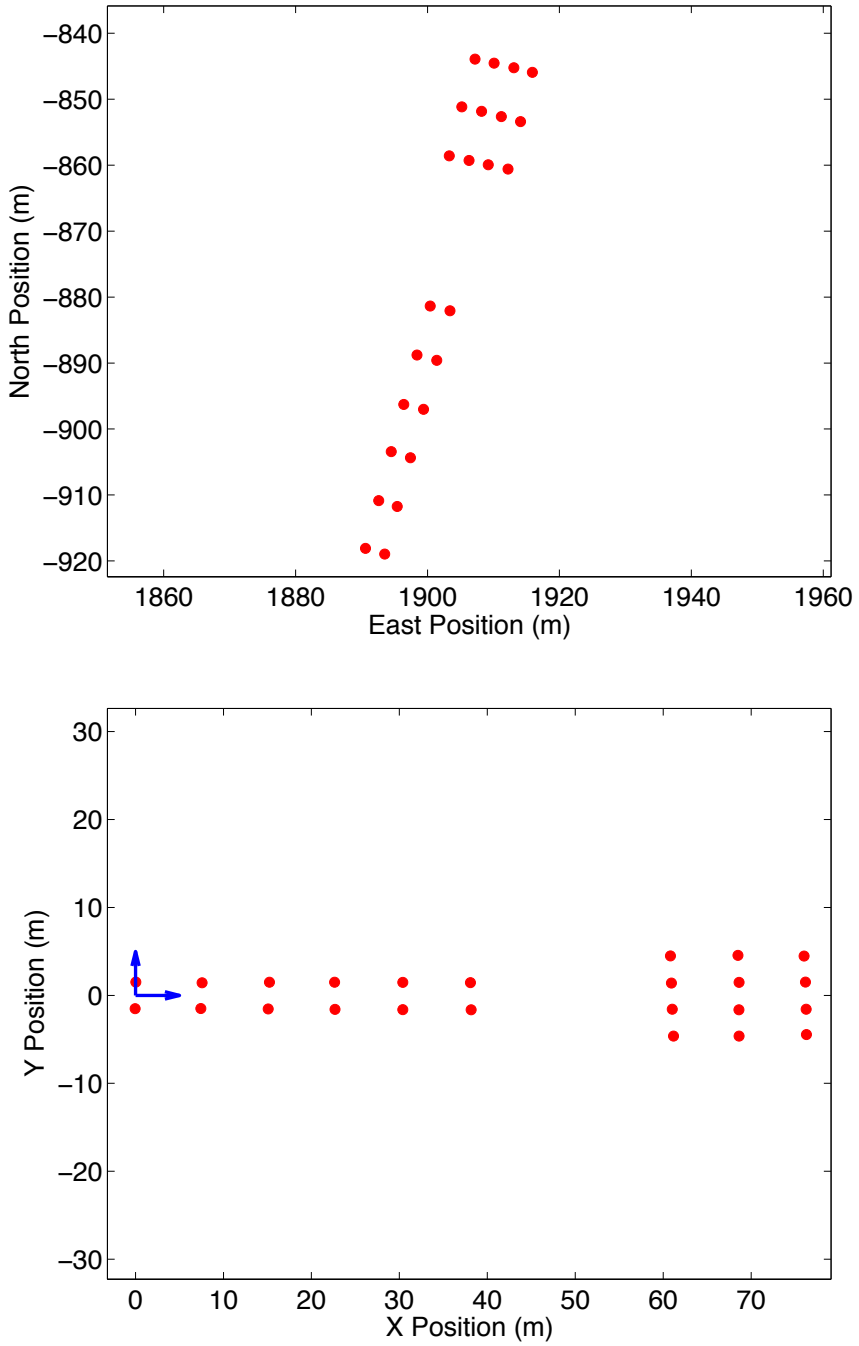

Figure 2.9: Comparison of E-N coordinates (top) with X-Y coordinates (bottom) of the user study course.

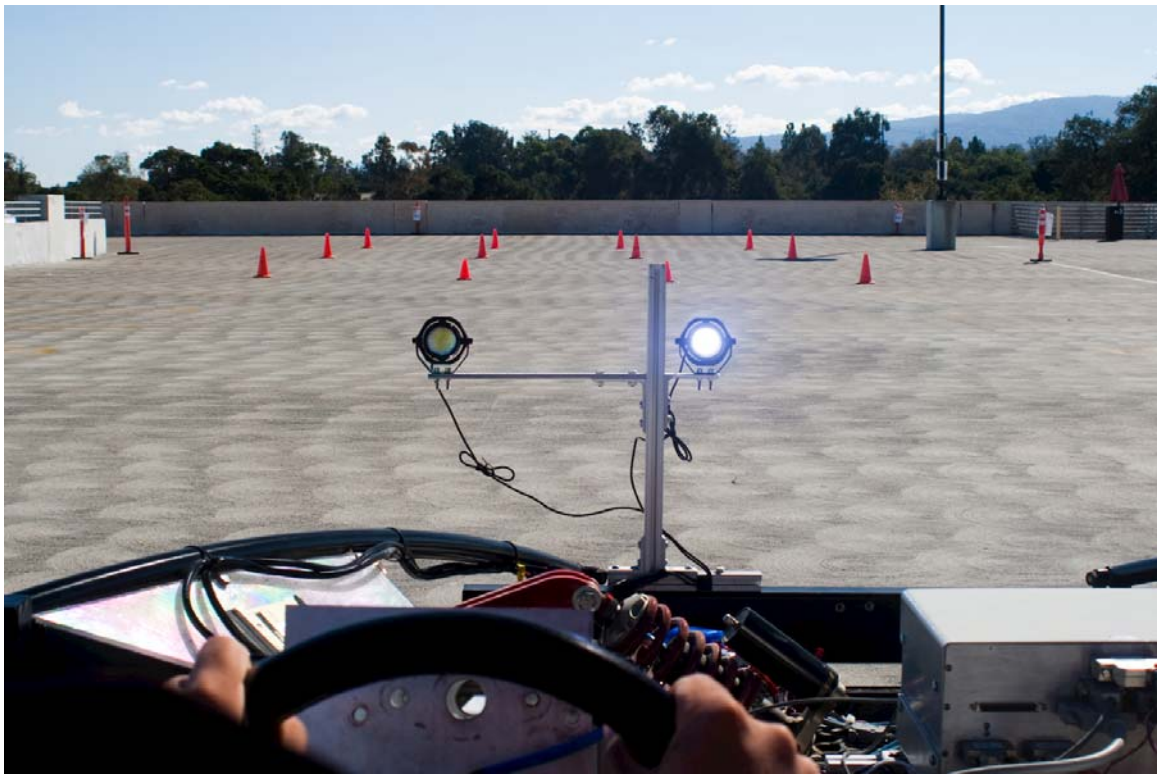

Figure 2.10: The course as seen by the driver at the end of the straight. The right signal light is illuminated, indicating that the driver should steer into the right lane.

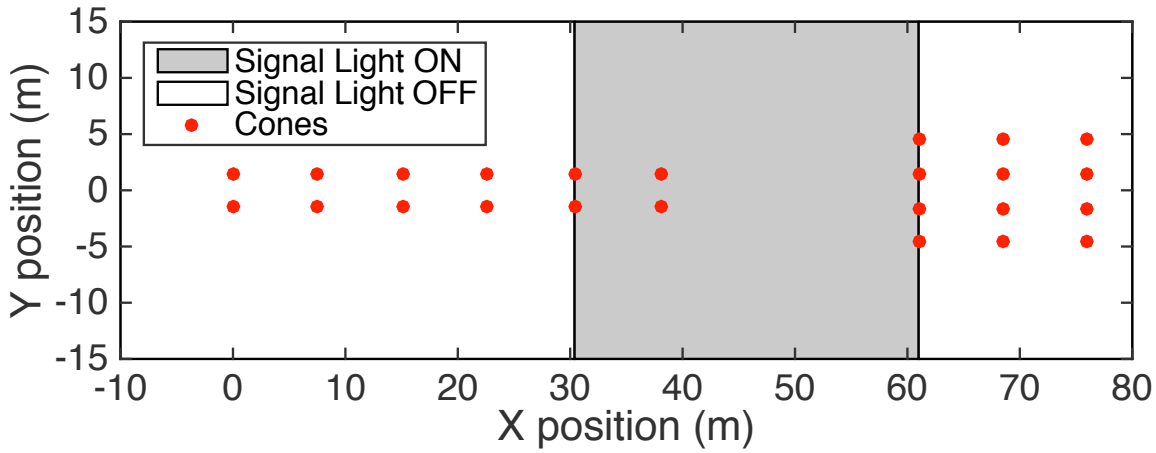

Figure 2.11: Map of course with signal light active and inactive regions.

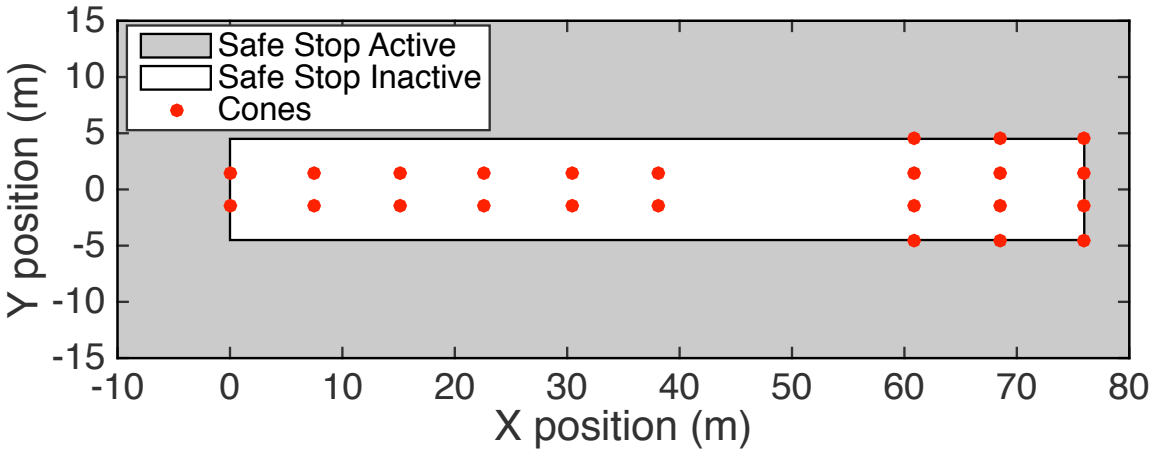

Figure 2.12: Safe stop schematic. If the vehicle center of gravity leaves the white region, the safe stop controller engages to bring the vehicle to a complete stop.

twenty discrete random variables in the set $\{-1, 1\}$, with -1 corresponding to a right turn and 1 corresponding to a left turn. The vector of random variables is adjusted by hand to ensure that there are an equal number of trials in each direction.

2.3.5 Safe Stop

During the experiment, the driver will experience unfamiliar vehicle handling characteristics and can possibly drive off the course as a result. Since the course is set up in a parking lot, there are obstacles (walls, light poles, barriers) that could be dangerous in the event that the vehicle goes outside the traffic cones demarcating the course. When this occurs, it may take some time for the driver to apply the brakes, which could be too late to prevent a collision. To keep the driver and the vehicle safe from collisions, a safe stop controller brings the vehicle to a complete stop in this case.

A safe box is defined in terms of the X-Y coordinates of the course, as depicted in Fig. 2.12. If the vehicle's center of gravity ever leaves this box, the electronic brake system engages until the vehicle is fully stopped and the experimenter manually switches off the safe stop controller. When the safe stop engages, the total brake pressure is computed with the following equation, where K_p is the speed to pressure gain (15 bar/(m/s)) and $p_{\min}$ is the minimum pressure (10 bar). The total pressure

is then split equally between the four wheels so that the brake pressure command for each wheel is $\frac{p}{4}$.

$$p = K_p U_x + p_{\min} \tag{2.12}$$

If the safe stop ever engages, a software latch ensures that it continues to apply brake pressure until the experimenter triggers a hardware switch. This prevents a situation where the brakes apply briefly and then disengage. The safe stop is rarely necessary, but in the few instances that it is needed, it reacts faster than the driver or the experimenter could.

2.4 Return to Start

After the driver completes the lane change and brings the vehicle to a stop, the path-following controller is activated to steer the vehicle back to the start of the course. During this phase of the experiment, the driver controls the speed of the vehicle with the accelerator and brake pedals, while the steering is controlled automatically to track a reference path. This phase is important for two reasons. First, since the driver does not control the steering during this phase, any adaptation to the handling perturbation is confined to the lane change task and can be analyzed consistently between participants. Second, the semi-automated nature of this phase mimics a self-driving car, and thus the experiment addresses a scenario in which a human driver takes over steering control from an autonomous vehicle.

2.4.1 Map Generation

The reference path is designed using a MATLAB program called Quill (Fig. 2.13) that was developed at Stanford University. The path consists of a set of simple path elements that have curvature described by simple primitives: straight segments (no curvature), arcs (constant curvature), and clothoids (linearly varying curvature). Each straight segment is followed by an associated set of turn elements – an entry

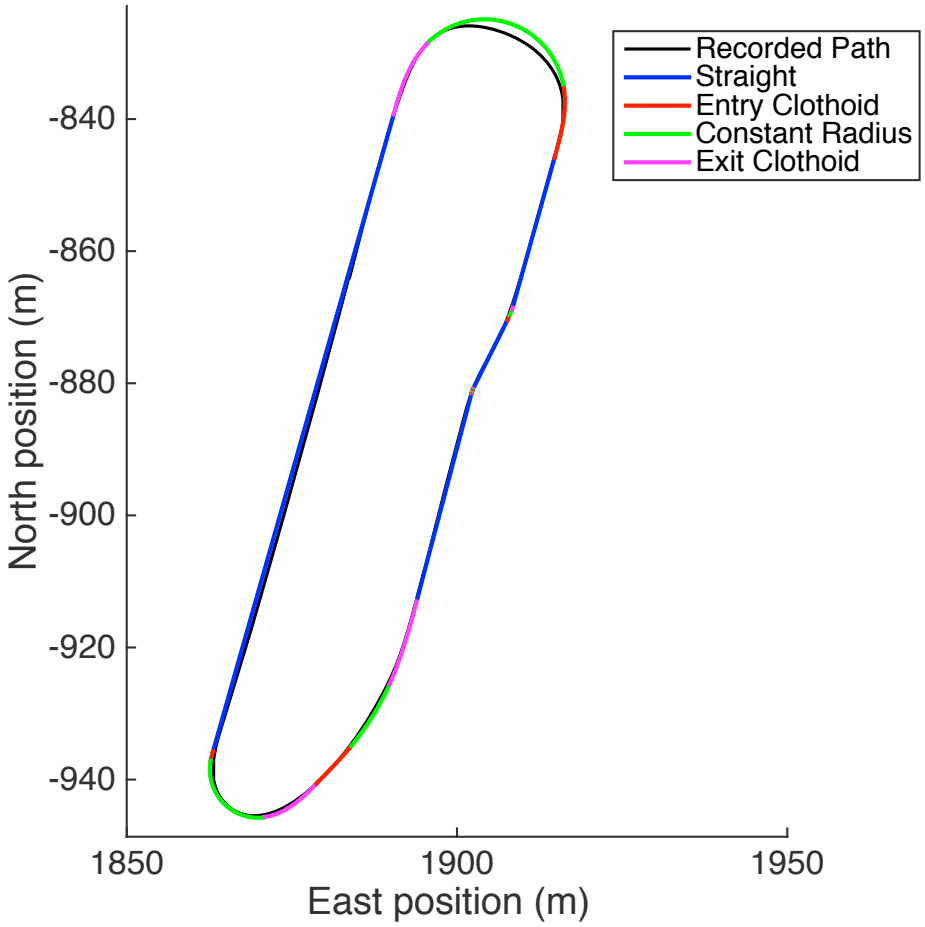

Figure 2.13: Map generated with the Quill software tool. Straight segments are drawn in blue, constant radius arcs in green, entry and exit clothoids in red and magenta, respectively.

clothoid (linearly increasing curvature), an arc, and an exit clothoid (linearly decreasing curvature). The equations for east position, north position, and heading angle for each type of segment are summarized in [134]. The path is stored in an efficient map structure consisting of a small number of path segments with a few associated parameters, rather than as a large number of individual (E,N) or (X,Y) coordinates.

To create a reference map, first the east and north coordinates of the desired path are measured with the on-board GPS system while driving the vehicle through the course. The path is created in Quill by adding enough straight segments to adequately represent the straights on the measured path, then turns are added automatically. The parameters of the turn segments are adjusted until the calculated path is close enough to the measured path. Adjusting turn parameters entails changing the length of the clothoid segments with respect to the constant radius arc segment. Finally, the map data are exported to a CSV file consisting of map segments and parameters including segment length, east and north position, heading angle, and segment curvature.

2.4.2 Map Matching

This step uses a Newton-Raphson method to identify the distance along the path s corresponding to the vehicle's current position. This is an iterative method that is initialized with the results from the previous time step. The algorithm estimates the closest point on the path to the current vehicle position by guessing the east and north positions, the heading angle, and the path curvature in an iterative manner. After the closest path point has been identified, the algorithm computes the lateral error e, the heading error $\Delta\psi$, and the curvature κ of the current path segment. These values are used in the path-following steering controller to keep the vehicle on the desired path.

2.4.3 Path-Following Steering Controller

The path-following steering controller uses feedforward steering on both the front and rear wheels to approximately follow a path with the given curvature, and lanekeeping feedback on the front wheels only to ensure acceptable path tracking. The controller

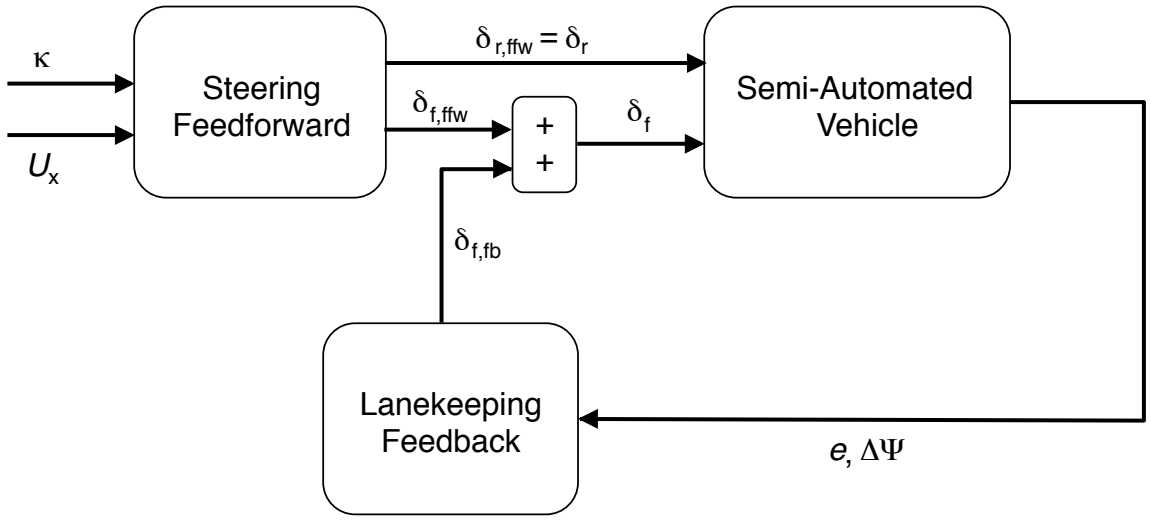

Figure 2.14: Block diagram for the path-following steering controller, adapted from Kapania and Gerdes [56].

is based on the work by Kapania and Gerdes [56] and by Kritayakirana and Gerdes [66], and is summarized in Fig. 2.14. The steering angles are given by a combination of feedforward and feedback on the front wheels, and feedforward only on the rear wheels.

$$\begin{aligned} \delta_{\mathrm{f}} &= \delta_{\mathrm{f,ffw}} + \delta_{\mathrm{f,fb}} \\ \delta_{\mathrm{r}} &= \delta_{\mathrm{r,ffw}} \end{aligned} \tag{2.13}$$

The feedforward front and rear steer angles necessary to track a path with a given curvature κ at vehicle speed U_{x} are computed from the steering geometry, assuming small angles; L is the vehicle length and $\alpha_{\mathrm{f,ffw}}$ and $\alpha_{\mathrm{r,ffw}}$ are the feedforward front and rear tire slip angles, respectively.

$$\begin{aligned} \delta_{\mathrm{f,ffw}} &= \frac{L\kappa}{2} - \alpha_{\mathrm{f,ffw}} \\ \delta_{\mathrm{r,ffw}} &= -\frac{L\kappa}{2} - \alpha_{\mathrm{r,ffw}} \end{aligned} \tag{2.14}$$

The tire slip angles that produce the desired feedforward forces are found using a linear tire model with front and rear tire cornering stiffnesses C_{f} and C_{r}. The linear

tire model is appropriate for this work because the vehicle speed is low and the vehicle never approaches its handling limits (unlike in [56] and [66] which require nonlinear tire models).

$$\begin{aligned} \alpha_{\mathrm{f,ffw}} &= \frac{-F_{\mathrm{yf,ffw}}}{C_{\mathrm{f}}} \\ \alpha_{\mathrm{r,ffw}} &= \frac{-F_{\mathrm{yr,ffw}}}{C_{\mathrm{r}}} \end{aligned} \tag{2.15}$$

The feedforward lateral tire forces necessary to track a path with the given curvature are computed assuming steady-state cornering from the vehicle speed U_{x}, the path curvature κ, the mass m, the center of gravity to front axle distance a, and the center of gravity to rear axle distance b.

$$\begin{aligned} F_{\mathrm{yf,ffw}} &= \frac{mb}{L} U_{\mathrm{x}}^2 \kappa \\ F_{\mathrm{r,ffw}} &= \frac{ma}{L} U_{\mathrm{x}}^2 \kappa \end{aligned} \tag{2.16}$$

The lanekeeping feedback controller, based on the work of Rossetter and Gerdes [115], combines the current lateral error e and heading error $\Delta\psi$ into a single lookahead error e_{LA} projected a distance in front of the vehicle, x_{LA}. This lookahead error is then used in a simple proportional control law. For this study, $x_{\mathrm{LA}} = 5$ m and $K_{\mathrm{fb}} = 0.052$ rad/m.

$$\begin{aligned} e_{\mathrm{LA}} &= e + x_{\mathrm{LA}} \Delta\psi \\ \delta_{\mathrm{f,fb}} &= -K_{\mathrm{fb}} e_{\mathrm{LA}} \end{aligned} \tag{2.17}$$

In summary, the map matching algorithm computes the curvature of the desired path and the current lateral and heading errors, then the steering controller calculates feedforward and feedback steering angles to track the path.

2.4.4 Speed Limit

Since the driver controls the speed of the vehicle during the return to start phase, it is important to limit the speed for safety. Rather than enforcing a hard speed limit, the

acceleration of the vehicle is limited when its speed exceeds a threshold of $U_{\mathrm{x,max}} = 5$ m/s. The acceleration limit is implemented through the torque command to the drive motor, τ_{cmd}.

The algorithm is straightforward: if the vehicle speed is less than $U_{\mathrm{x,max}}$, allow the driver to command full motor torque (and thus maximum acceleration); if the speed exceeds $U_{\mathrm{x,max}}$, limit the torque to 10% of its full value (approximately 24 Nm). To prevent step changes in commanded torque and to reduce switching when the speed is near $U_{\mathrm{x,max}}$, a single-pole 0.5 Hz discrete low pass filter $L_1(z)$ is applied to the torque command signal.

$$\tau_{\mathrm{cmd}} = \begin{cases} \tau_{\mathrm{des}} & \text{if } U_{\mathrm{x}} \leq U_{\mathrm{x,max}} \\ \max(\tau_{\mathrm{des}}, 0.1\tau_{\mathrm{max}}) & \text{if } U_{\mathrm{x}} > U_{\mathrm{x,max}} \end{cases} \tag{2.18}$$

$$L_1(z) = \frac{6.283 \times 10^{-3}}{z - 0.9937} \tag{2.19}$$

$$\tau_{\mathrm{cmd,filt}} = L_1(z) \times \tau_{\mathrm{cmd}} \tag{2.20}$$

The performance of the speed limiter is shown in Fig. 2.15, where the commanded and measured drive motor torques are in the top panel and the measured vehicle speed is in the bottom panel. The filtered torque command is smoother than the driver command throughout. Taking the smoothing into account, the torque command follows the driver's intent throughout the maneuver, except when the speed exceeds 5 m/s. During those intervals, the command smoothly transitions to a maximum of 24 Nm, or 10% of the maximum drive motor torque.

2.5 Choice of Metrics

As described in Section 1.1.2, the extensive study of adaptation to changes in arm kinematics and dynamics has resulted in the development of several common metrics to quantify the adaptation process. These include task performance error in terms of angular or lateral error, measures of hand and arm kinematic variables, normalized adaptation percentage measures, and movement time. The exact metrics used

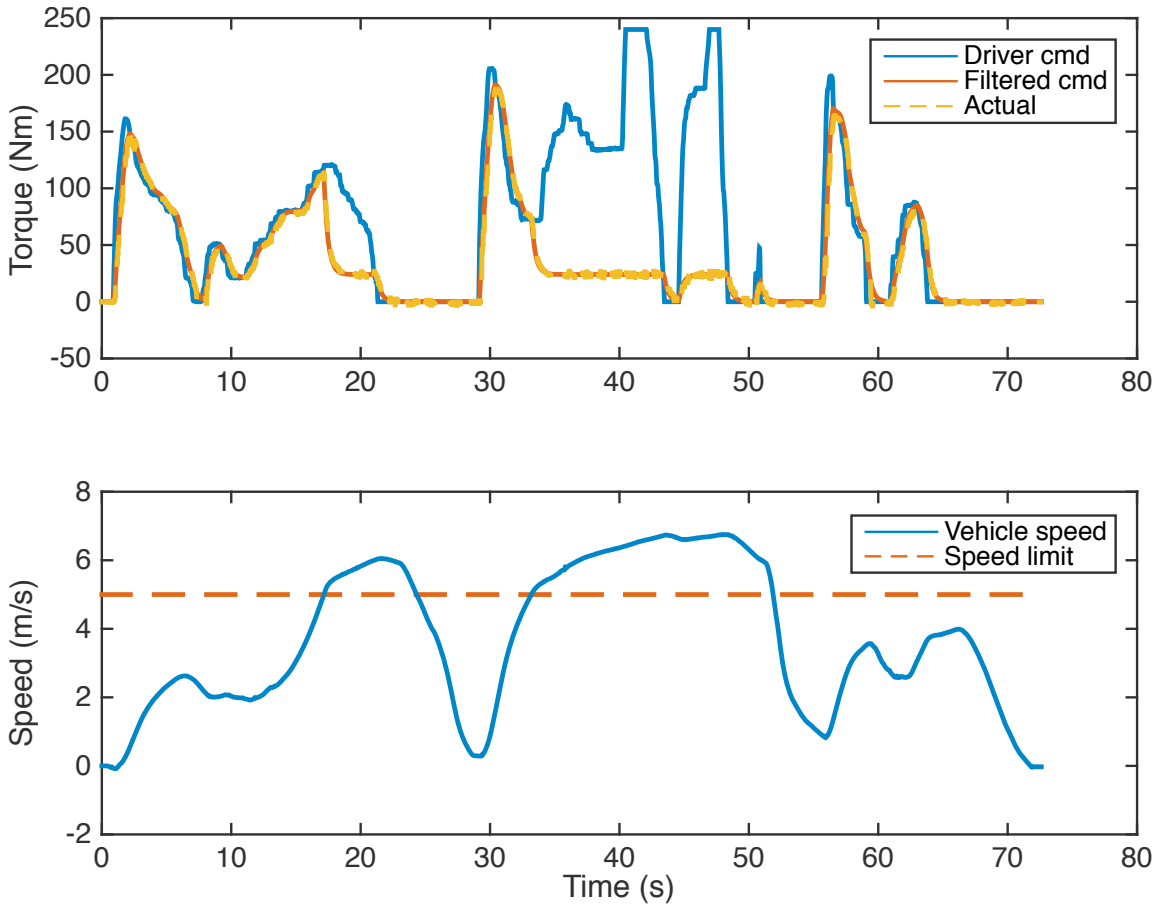

Figure 2.15: Example data for speed limit controller. The upper plot shows the demanded and actual drive motor torque; the lower plot shows the vehicle speed.

in arm reaching studies do not directly apply to automobile steering studies, but the underlying principles can inform the development of metrics suited to the experimental design. The metrics used for the studies in this dissertation are described in the remainder of this section.

2.5.1 Steering Wheel Reversal Rate

The first metric is related to the frequency characteristics of steering motions. Steering wheel reversal rate (SRR) has been used since at least the 1970s in the assessment of driver workload and task demands [80]. This metric measures the number of times the driver reverses the direction of the steering wheel through a small angle, divided by the total time for the maneuver. The size of the angle or gap necessary to count a direction reversal varies in the literature, with many studies reporting gap sizes between 0.5° and 10° [80]; for the studies in this dissertation, it is 0.5°. The SRR for an example trial is shown in Fig. 2.16.

SRR is a simple representation of the frequency of steering motions made by the driver. Although the information this metric provides about steering frequency is limited, several studies have found it useful for exploring driver workload. For example, increases in SRR have been shown to correlate with increases in difficulty of driving tasks [89]. Fairclough and Graham demonstrated that sleep-deprived drivers displayed reduced SRR and increased number of lane departures compared to a control group [36], which suggests that a moderate level of SRR is required during attentive driving. Owens et al. used a larger gap magnitude of 5° to assess driver distraction level, demonstrating that the SRR with this gap increased with higher levels of driver distraction [106]. A general conclusion from these studies is that SRR should be in a moderate range for safe steering control, neither too high (indicating high task demand or lack of attention) nor too low (indicating fatigue).

In addition to its correlation to task difficulty, this metric also relates to overshoot in steering behavior. Normal steering behavior includes some oscillations of the steering wheel to keep the vehicle in the lane in addition to the larger motions necessary to make a lane change. An increase in SRR indicates that the driver needs to make

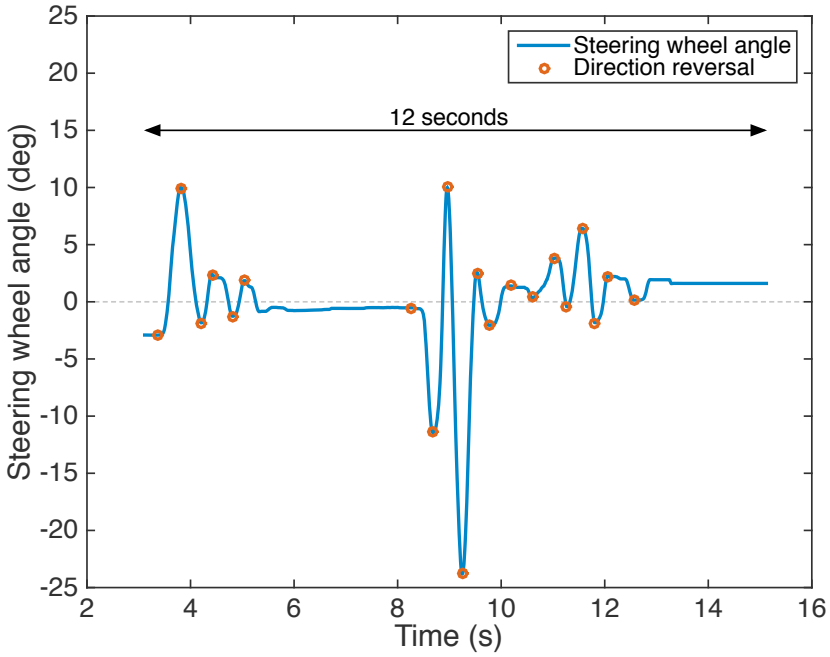

Figure 2.16: Example of steering wheel reversal rate. For this trial, there are 20 direction reversals in 12 seconds, resulting in an SRR of 1.66 s^{-1}.

more corrections to successfully navigate the lane change task. This means that the vehicle dynamics are not responding in the way the driver predicts with his internal model, so he must steer back in the other direction to compensate for the error. In this way, the SRR captures the feedback behavior of the driver. In the context of metrics used in arm reaching studies, SRR can be thought of as a measure of the frequency characteristics of the arm kinematics used to steer the vehicle.

2.5.2 RMS Steering Velocity

Another metric that relates to the kinematics of steering is the root mean square (RMS) steering velocity. Benderius and Markkula found that the steering velocity in most steering corrections followed bell-shaped profiles, much like tangential hand velocity in arm reaching movements [11]. RMS road wheel and steering wheel velocities have been used to compare driver performance with different lanekeeping systems for lane change tasks in a simulator study [122], with larger RMS velocities observed in emergency lane changes compared to normal lane changes. Maximum steering velocity is a similar metric that has been used as a measure of cognitive workload during distracted driving studies [106], suggesting that higher steering velocity is related to faster steering corrections that may be necessary with a higher workload.

For the studies in this dissertation, the steering velocity is defined as the derivative of the driver's desired front road wheel angle. This is found by dividing the steering wheel angle by the steering ratio, taking a first-order finite difference, and filtering the resulting signal with a zero-phase 10 Hz digital low-pass filter. The RMS value of this signal over the entire course of each trial is used as a measure of the average steering speed required to complete the lane change task. This definition is used instead of simply differentiating the measured front road wheel angle because in the low friction emulation study (Ch. 6), the front road wheel angle is controlled by a vehicle dynamics controller rather than directly by the driver, and therefore does not accurately reflect the driver's steering control input.

In the context of driver adaptation to handling changes, the RMS steering velocity also relates to the feedback signal of the human motor system. When the driver's

internal model of the vehicle dynamics is incorrect, the steering commands result in errors in path tracking that the driver must correct by steering differently. These steering corrections need to happen quickly to successfully complete the maneuver in the fixed course length. Increased RMS steering velocity is an indication of increased amount of feedback control to correct errors. As the driver's internal model improves due to adaptation, the need for feedback error correction declines and the RMS steering velocity decreases correspondingly.

2.5.3 Time to Steering Angle Peak

Some arm reaching studies have used measurements of movement duration to aid in characterizing the accuracy of arm movements [38, 44, 101, 133]. The lane change task used for this dissertation is fixed in duration since the course length and vehicle speed are fixed, so overall movement duration is not a useful metric. However, the timing of the steering motion used to complete the lane change is important and informative to the understanding of the adaptation process.

As the vehicle nears the end of the straight section of the course, one of the signal lights turns on to indicate the direction of the desired lane change. The time to steering angle peak metric computes the elapsed time between the onset of the signal light and the next local maximum steering wheel angle, as illustrated in Fig. 2.17. The first handwheel maximum after a steering wheel torque event was used by Switkes et al. to quantify driver response to steering wheel torque disturbances that might occur in an assistive lanekeeping system, and demonstrated that drivers respond more quickly to larger torque disturbances [131].

Compared with the baseline time to steering angle peak, a smaller time to steering angle peak indicates either that the driver does not have a correct internal model of the vehicle dynamics or that he is uncomfortable with the dynamics and makes the steering motion early to ensure successful completion of the lane change. Larger time to local maximum steering angle is related either to internal model error opposite to the first case or to increased comfort with the handling dynamics such that the lane change is performed relatively late. This metric is therefore related to feedforward

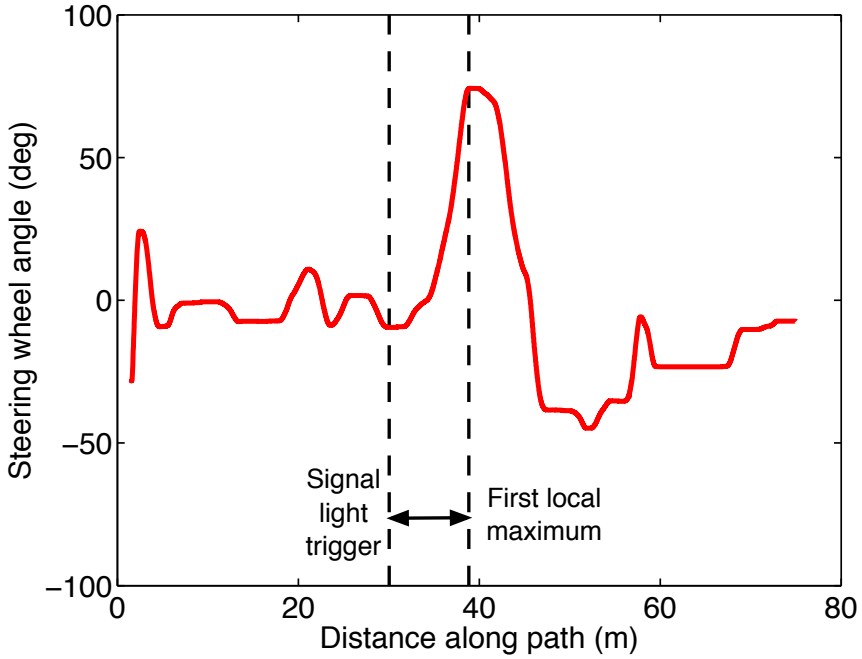

Figure 2.17: Example of distance from the signal light trigger position to the next local maximum steering angle. The elapsed time between these two points is the time to steering peak metric.

commands that the driver makes in order to try to steer along the desired trajectory.

2.5.4 RMS Yaw Jerk

The final metric is related to the kinematics of the vehicle rather than of the driver's arms. Yaw rate is defined as the rotation rate of the vehicle in the ground plane, and yaw jerk is the second derivative of yaw rate. Low values of yaw jerk are perceived as characteristic of smooth vehicle handling, and therefore reflect the ability of the driver to smoothly control the vehicle. Maximum yaw jerk was used by Schmidt et al. in a driving simulator comparison of lanekeeping assistance as a measure of the smoothness of the lanekeeping interventions [122].

Yaw jerk is computed by twice differentiating the measured yaw rate signal, followed each time by a zero-phase 10 Hz discrete low-pass filter. The RMS value of yaw jerk is used as a way of quantifying the smoothness of the entire maneuver. When RMS yaw jerk increases compared to baseline, this is an indication that the driver is making more sudden changes in steering inputs and is likely having a less comfortable driving experience. Using a measure of the vehicle kinematics in addition to metrics that quantify driver steering behavior reflects the important fact that the driver is in a moving vehicle and experiences its kinematics and dynamics with his body.

Chapter 3

Adaptation to Steering Ratio Changes

The user study protocol developed in Chapter 2 provides an experimental paradigm for testing adaptation to several different handling changes related to driver steering control. The first two experiments conducted with this protocol were designed to parallel a study by Krakauer et al. of visuomotor adaptation in the context of arm reaching [64]. This study demonstrated differences in the time scale and generalization of adaptation to two visuomotor transformations: (1) changing the scaling factor between hand motion and cursor motion and (2) rotating the reference axes of the cursor compared to the hand. Since the adaptation process was different for the two perturbations, the authors hypothesized that the brain processes errors in extent and direction separately.

What perturbations on the automobile are analogous to the two visuomotor transformations in this study? In arm reaching studies, the scaling or rotation of a visual cursor's motion has a direct effect on the way the user's input influences cursor motion. In a similar manner, changing the relationship between the steering wheel angle and the front road wheel angle directly affects how the driver's steering input influences the motion of the car. Scaling the gain on the cursor's motion is similar to changing the magnitude of the steering ratio, or how much the driver must turn the steering wheel in order to turn the road wheels through a given angle. Cursor

coordinate frame rotation is similar to reversing the direction of the steering wheel, so that the driver must turn the steering wheel to the left for the road wheels to turn right, and vice versa.

The hypothesis of this chapter is that the adaptation process for these two perturbations is similar to adaptation to cursor scaling and rotation in arm reaching studies. This means that upon application of the perturbation, there will exist a change in a metric followed by approximately exponential decay back toward the baseline level; upon removal of the perturbation, the metric will change in the opposite direction, indicating an aftereffect. Furthermore, since steering is a continuous task with many small corrections in order to keep the vehicle on course, it should be possible to observe adaptation over the course of just a few trials of the task, rather than several hundred trials as is typical for arm reaching studies. Finally, the adaptation process should be somewhat different between the two perturbations, just as gain scaling and coordinate frame rotation seem to be processed differently by the brain during arm reaching.

The remainder of this chapter details the experimental results from these two studies, steering ratio scaling and steering wheel direction reversal. The results show clear differences between the the adaptation processes for the two steering perturbations, which is consistent with the literature on arm reaching adaptation. Evidence from these studies that drivers require several seconds to change their internal models of the vehicle dynamics suggests that it is critical for automated vehicle designers to consider the period of motor adaptation when handing over control from an automated vehicle to a human driver.

3.1 User Study #1: Steering Ratio Scaling

The first study is designed to be similar to scaling the cursor gain in arm reaching studies [64, 138] by scaling the relationship between steering input and vehicle dynamics output via a steering ratio change. An automobile's steering ratio is the angle that the steering wheel must turn for every 1° that the road wheels turn. Modifying

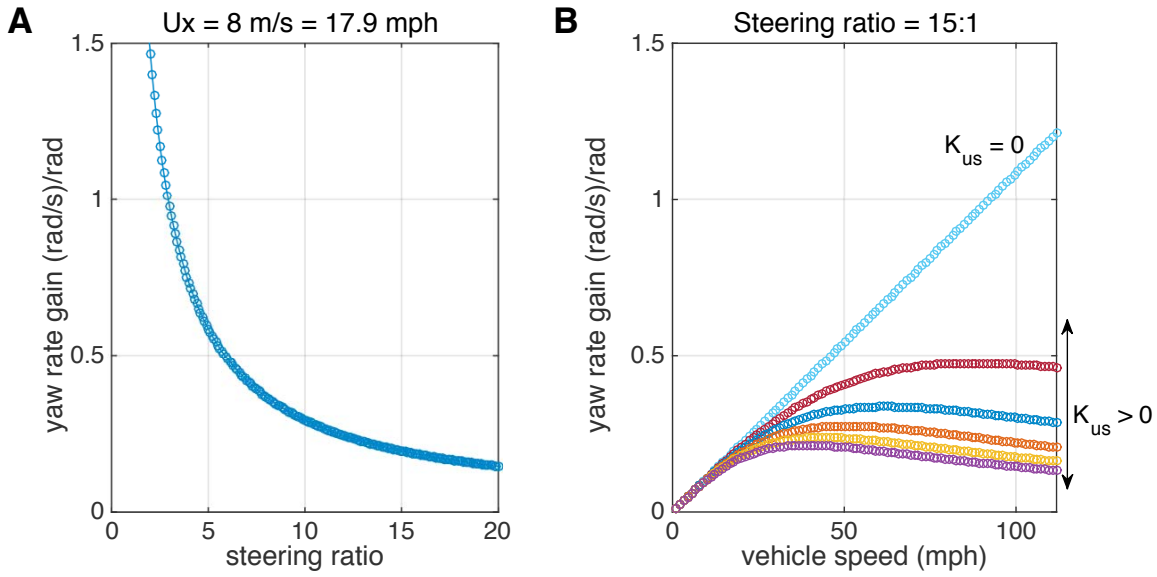

Figure 3.1: Yaw rate gain as a function of (A) steering ratio, with constant vehicle speed and fixed K_{us}, and (B) vehicle speed, with constant steering ratio and several values of K_{us}.

the steering ratio changes the mapping between steering wheel motion and the resulting vehicle yaw rate (rate of rotation). Steering ratio does not change over the course of normal driving, as most passenger vehicles have fixed steering ratios. However, the mapping from steering wheel angle to yaw rate also depends on the vehicle speed U_{x}, which varies greatly in everyday driving situations.

In steady state, the gain from steering wheel angle δ_{hw} to yaw rate r_{ss} is

$$\frac{r_{\text{ss}}}{\delta_{\text{hw}}} = \frac{U_{\text{x}}}{N\left(L + K_{\text{us}}U_{\text{x}}^2\right)}, \tag{3.1}$$

where L is the vehicle length, N is the steering ratio, and K_{us} is the understeer gradient of the vehicle, which describes the relationship between steering input and lateral acceleration in a steady turn and varies between vehicles. Fig. 3.1 demonstrates how the yaw rate gain varies with steering ratio (A) and with vehicle speed (B). As the figure shows, the yaw rate gain can be varied between 0 and 1.5 (rad/s)/rad both by changing the steering ratio and by changing the vehicle speed.

For this study, using the X1 experimental vehicle (Section 2.2), the steering ratio

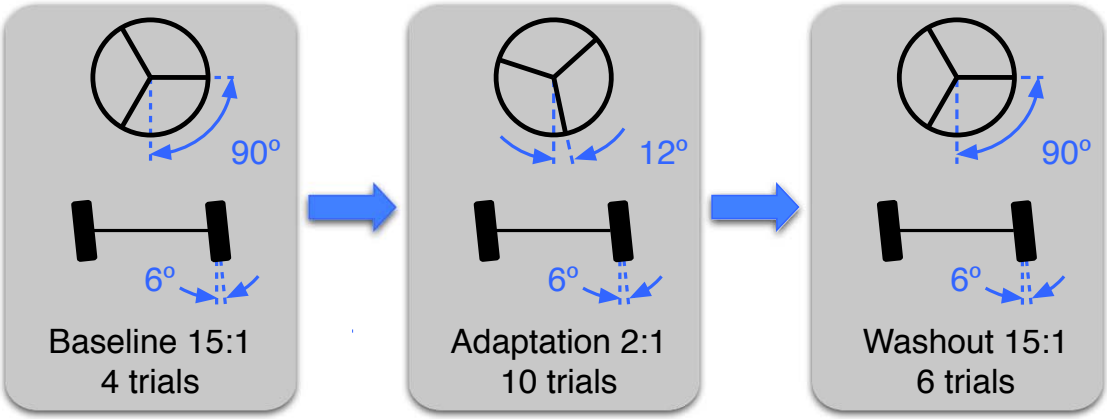

Figure 3.2: Adaptation protocol for steering ratio scaling study.

is changed from a baseline value of 15:1 to a much more sensitive 2:1 during the adaptation block, as depicted in Fig. 3.2. The magnitude of the corresponding change in yaw rate gain is comparable to taking a neutrally handling vehicle ($K_{\text{us}} = 0$) from low speed appropriate for parking lot navigation ($\approx$ 9 mph) to highway speed ($\approx$ 67 mph). In conjunction with modifying the steering ratio, the experiment also scales the steering wheel torque during the adaptation block to maintain a constant level of torque associated with a given *road wheel* angle, although the corresponding steering wheel angle depends on the steering ratio. The details of the linear spring model steering wheel torque used in this study are discussed in Section 2.3.1.

3.1.1 Study Participants

The steering ratio scaling study was conducted with ten participants ranging in age from 23 to 64 years, with a median of 29 years. Driving experience of the participants ranged from 4 to 48 years, with a median of 10.5 years. There were four men and six women. All participants were right-handed and without known neurological impairment. Participants only experienced the steering ratio handling change and did not participate in any other studies.

3.1.2 Sample Participant Data

Example data for a representative participant are shown in Fig. 3.3. The top panel shows the front road wheel angle versus distance along the path for each trial, while the bottom panel shows the corresponding paths taken by the vehicle. The road wheel angle and vehicle path traces are colored according to which experimental block they belong to. The road wheel angle traces are normalized for a left turn for ease of comparison, although all participants performed an equal number of left and right lane changes.

An interesting qualitative feature of the steering traces in Fig. 3.3A is the shape of the steering wheel motions. During the baseline block (Trials 1–4, green) the sample participant used simple steering profiles to make the lane change, making a smooth, large motion for the initial lane change followed by a smaller motion in the opposite direction to straighten the car relative to the target gate. These smooth motions were accompanied by a few small oscillations throughout the maneuver to maintain the desired vehicle trajectory. When the steering ratio was perturbed from 15:1 to 2:1 in the adaptation block (Trials 5–14, blue), the driver used dramatically different steering behavior to complete the task, initially using an increased number of high-magnitude steering oscillations during both the straight and the lane change segments of the course. During later trials in this block, the oscillations were reduced in number and magnitude, and the steering profiles more closely resembled the baseline steering profiles, suggesting that the participant adapted to the steering ratio change. On removal of the perturbation in the washout block (Trials 15–20, red), the steering profiles immediately looked like the profiles from the baseline block, with smooth steering motions and few oscillations.

Another notable feature of the steering traces is the timing of the local maximum steering angle following the triggering of the lane change direction signal light, denoted by the black triangles in Fig. 3.3A. During the last three trials of the baseline block, this timing was fairly consistent, suggesting that this was the driver's preferred steering timing for a lane change. In Trial 5, when the steering ratio was reduced, the peak steering angle occurred noticeably earlier since the reduced steering ratio

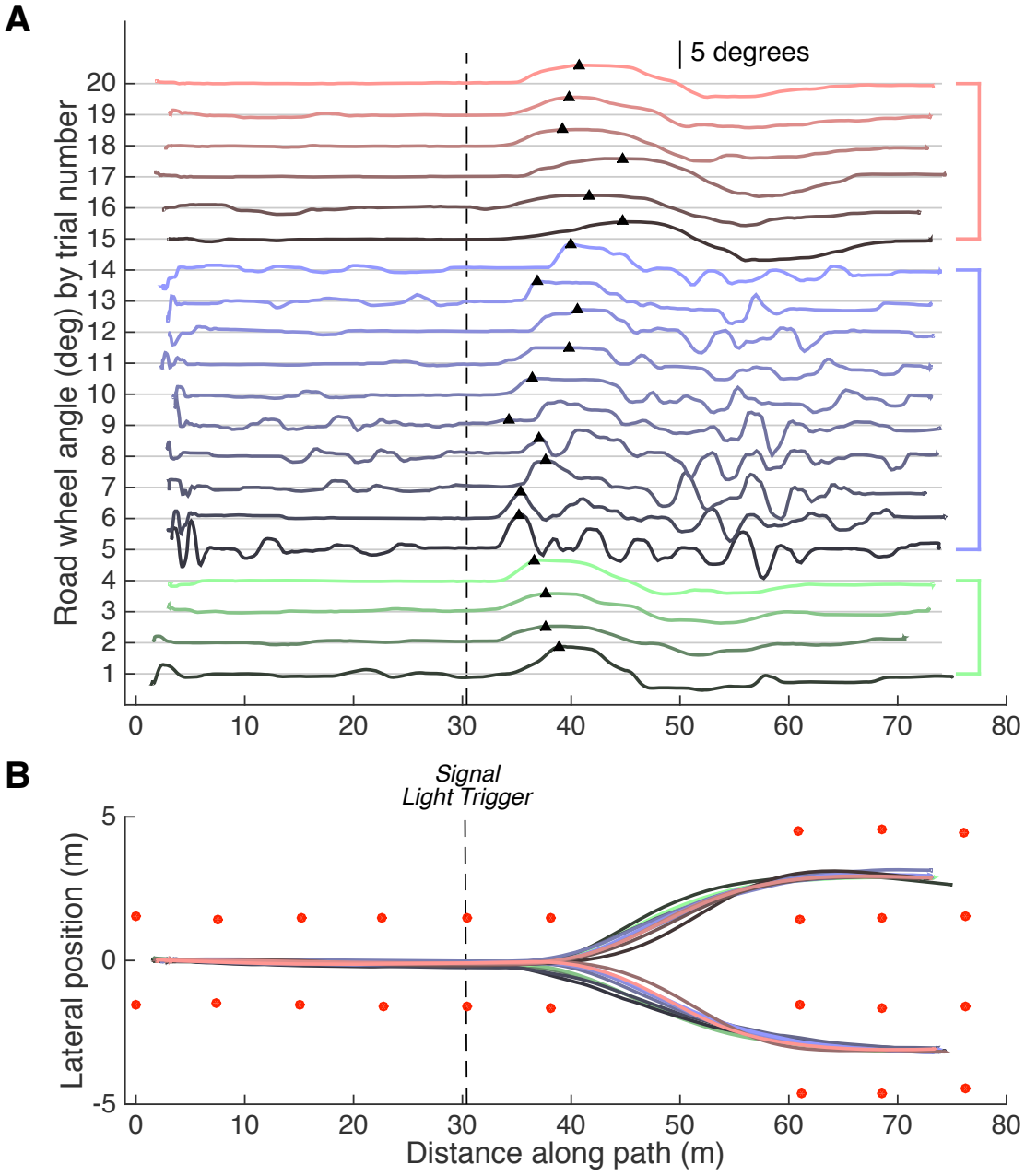

Figure 3.3: Sample data for User Study #1 (steering ratio scaling). (A) Road wheel angle traces as a function of distance along the path for each trial, with black triangles denoting the local maximum steering angle. (B) Paths taken by the vehicle, with the vertical axis not-to-scale with the horizontal for ease of visualization.

resulted in a faster vehicle response that required the driver to compensate. Over the course of the adaptation block, the peak gradually shifted later as the steering behavior more closely resembled baseline. When the steering ratio reverted to 15:1 in Trial 15, the peak occurred much later than the baseline value, then gradually returned to baseline over the rest of the washout block.

Despite the clear differences in steering behavior over the course of the experiment, Fig. 3.3B shows that all the paths taken by the vehicle were similar and the participant was able to successfully complete the lane change in all trials. It should be noted that the lane change task was lightly constrained, in that drivers could choose the timing of the steering motion for the lane change with some freedom; a number of different paths resulted in successful task completion. However, it is remarkable that the paths were so consistent given the obvious changes in steering inputs during the adaptation block.

These key features of the sample participant's steering data suggest that adaptation has occurred. To properly assess this claim, it is necessary to analyze the data of the entire participant population. The following section uses the metrics described in Section 2.5 to characterize the group performance.

3.1.3 Group Results

Average data for all ten participants are shown in Fig. 3.4 for the four metrics described in Section 2.5. Markers and lines denote the mean values across all ten participants for each trial, with colored regions indicating the 95% confidence intervals on the mean calculated using a t distribution.

The oscillatory behavior that was observed in Fig. 3.3A is quantified as the steering wheel reversal rate (SRR) in Fig. 3.4A. The SRR increased dramatically from baseline (green) when the steering ratio was perturbed in Trial 5 (adaptation, blue). The SRR then decreased over the course of the adaptation block, returning to the baseline level by Trial 14, resulting in a roughly exponentially shaped learning curve. In the washout block, the SRR was fairly constant and slightly smaller than baseline. The RMS steering velocity (Fig. 3.4B) and RMS yaw jerk (Fig. 3.4D) metrics both resulted in

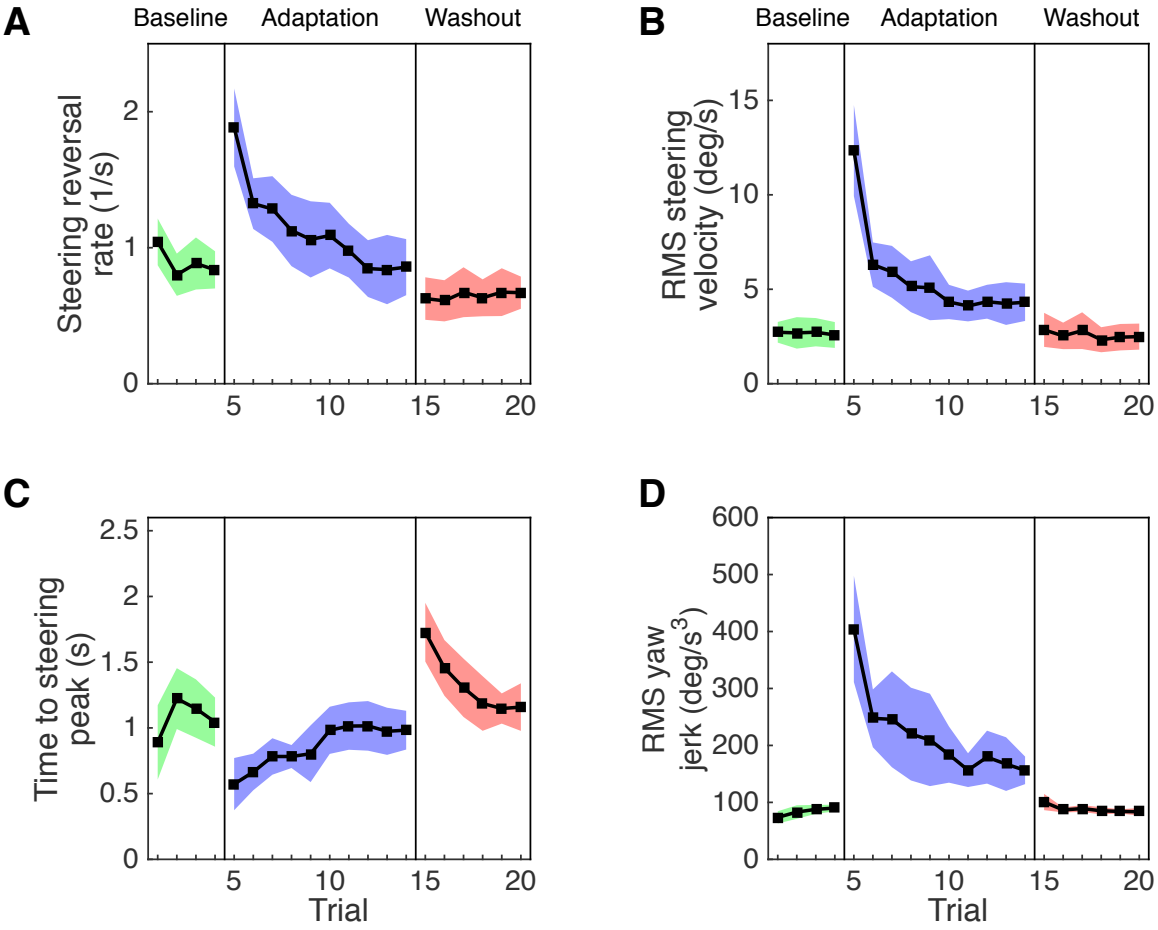

Figure 3.4: Learning curves for steering ratio scaling study ($n = 10$). (A) Steering reversal rate (SRR). (B) RMS steering velocity. (C) Time to steering angle peak. (D) RMS yaw jerk. The steering ratio was 15:1 for the baseline and washout blocks, 2:1 for the adaptation block. Colored regions show 95% confidence intervals from a t distribution.

learning curves shaped similarly to the SRR learning curve. By the end of adaptation, the metrics did not quite reach baseline, indicating that the participants partially adapted to the perturbation according to these metrics. These learning curves suggest that the drivers improved their models of how the vehicle dynamics would respond to their steering inputs as the adaptation block progressed, with gradual reductions in required steering effort and increased smoothness of vehicle motion.

The learning curve for the time to steering peak metric (Fig. 3.4C) is shaped differently from the curves for the first three metrics, since this metric decreased upon application of the perturbed steering ratio. The steering peak occurred earlier than baseline during the early adaptation trials, gradually returning to baseline as drivers learned the new steering ratio. When the steering ratio was returned to its original value for the washout block, there was a clear shift in steering peak timing to occur later than the baseline value – an example of an aftereffect since the metric changed in the opposite direction as it did upon initial application of the steering ratio perturbation.

These learning curves are informative and clearly point to the presence of adaptation. However, to make statements about adaptation, it is necessary to analyze statistical measures of significant differences between conditions. This is captured in Fig. 3.5, which displays data from the four metrics for a limited number of trials along with lines indicating statistically significant differences between trials. Bar height denotes the mean across all participants for a given trial, while error bars indicate 95% confidence intervals on the mean from a t distribution. For each metric, following a one-way repeated measures ANOVA, post-hoc tests were performed between all pairs of trials with p-values modified with Bonferroni corrections for multiple comparisons. The corrected p-values were considered significant at the $\alpha = 0.05$ level. Details on the statistical methods can be found in Appendix B. For this study, the repeated measures ANOVA showed significant differences among the means of all four metrics at the $\alpha = 0.05$ level. The ANOVA results are summarized in Table 3.1 and presented in full in Appendix D.

Steering reversal rate (Fig. 3.5A), RMS steering velocity (Fig. 3.5B), and RMS yaw jerk (Fig. 3.5D) all resulted in significant differences between the same pairs

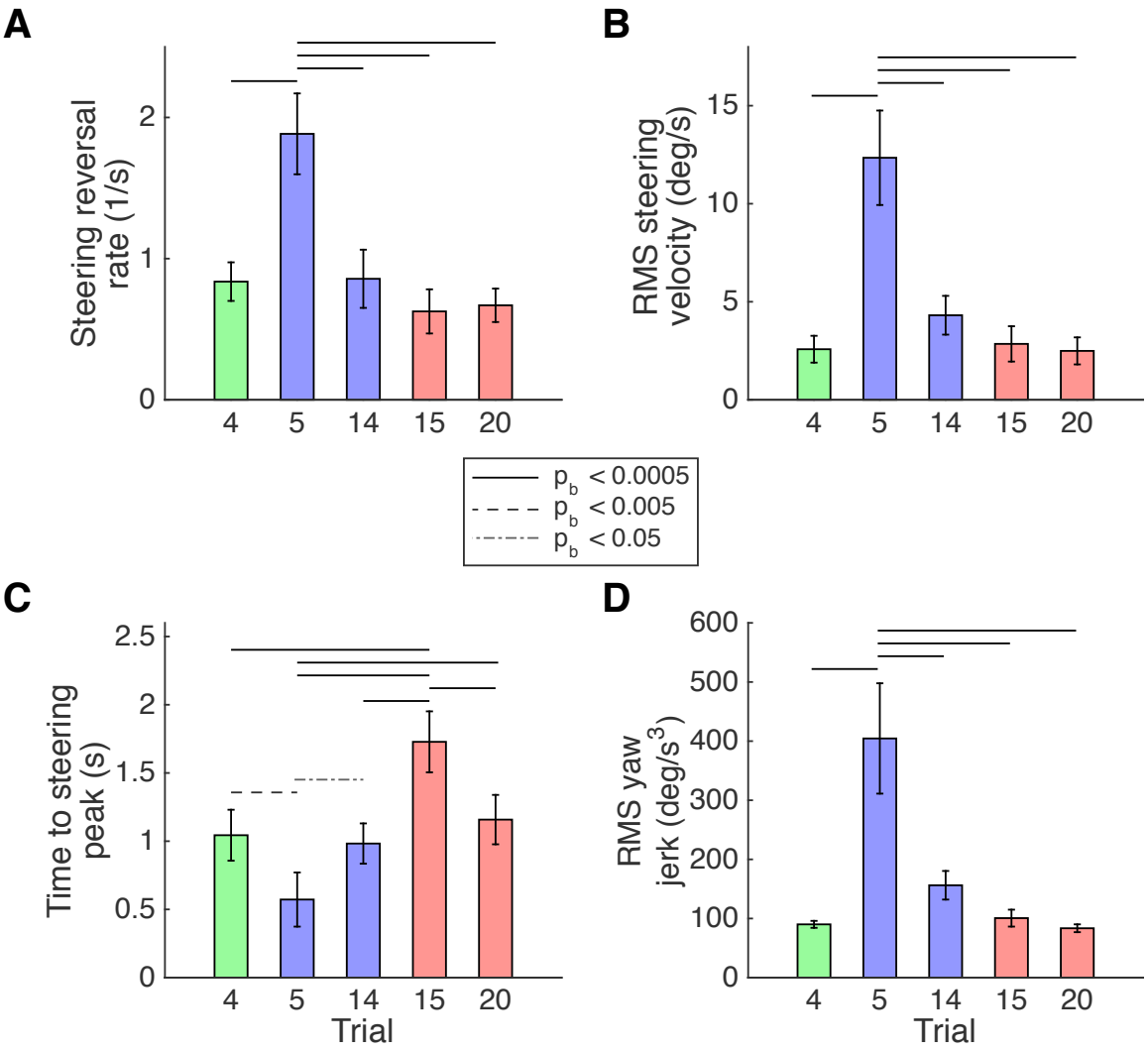

Figure 3.5: Statistical significance for steering ratio scaling study ($n = 10$). (A) Steering wheel reversal rate (SRR). (B) RMS steering velocity. (C) Time to steering angle peak. (D) RMS yaw jerk. In all panels, Trial 4 is the last trial of the baseline block (15:1), Trials 5 and 14 are the first and last trials of the adaptation block (2:1), and Trials 15 and 20 are the first and last trials of the washout block (15:1). Error bars indicate 95% confidence intervals from a t distribution; horizontal lines indicate significant Bonferroni-corrected p-values between trials.

Table 3.1: Summary of repeated measures ANOVA results for Study #1. For all metrics, the uncorrected $df_c = 4$ and $df_e = 36$. Values of df_c, df_e, and p_{gg} below have been adjusted with Greenhouse-Geisser ϵ corrections for sphericity. Significant p-values are denoted by boldface type.

Metric	ϵ	df_c	df_e	$F(df_c, df_e)$	p_{gg}
Steering reversal rate	0.64	2.54	22.87	52.62	**4.13e-9**
RMS steering velocity	0.32	1.29	11.63	74.97	**3.06e-6**
Time to steering peak	0.77	3.06	27.53	26.10	**3.90e-8**
RMS yaw jerk	0.29	1.17	10.53	55.30	**2.22e-5**

of trials. For these three metrics, the first adaptation trial was significantly different from all other trials ($p < 0.0005$ for Trial 5 compared to Trials 4, 14, 15, and 20), with no other significant differences. Introduction of the steering ratio perturbation caused noticeable changes with respect to baseline in performance on the metrics, indicating that some kind of error was introduced in the driver's control algorithm for steering the vehicle. The lack of statistically significant differences between Trials 4 and 14 (baseline and late adaptation) means that the performance returned to baseline by the end of the adaptation block and serves as evidence that adaptation occurred. Trials 15 and 20 (early and late washout) also showed no statistically significant difference from baseline, indicating that there is no evidence of an aftereffect for these three metrics.

However, the time to steering peak metric (Fig. 3.5C) resulted in a different set of significant differences between trials than the other metrics. Upon applying the reduced steering ratio in Trial 5, the steering peak occurred significantly earlier, then returned to baseline by Trial 14. As in the other metrics, this indicates that the drivers adapted to the steering ratio perturbation by the end of the adaptation block. The difference in this metric is that when the steering ratio was returned to 15:1 in Trial 15, the steering peak shifted significantly later than baseline ($p < 0.0005$). This is clear evidence of an aftereffect, since the removal of the perturbation resulted in an error in the opposite direction as the error induced by the application of the perturbation. This aftereffect was relatively short-lived, as the steering peak shifted back to baseline

by Trial 20. The presence of this aftereffect provides further evidence that the drivers changed their internal models used to plan appropriate steering actions to complete the lane changes.

3.1.4 Discussion

The original motivation for changing the steering ratio was to study a similar perturbation to the scaling of cursor gain in visuomotor rotation in arm reaching studies [18, 19, 64]. The data from the steering ratio modification study resulted in similar exponentially shaped learning curves to those presented for cursor gain scaling by Krakauer et al. [64]. The learning curves in the steering ratio study return to baseline somewhat faster than for cursor gain scaling (10 trials versus about 20 trials). This makes sense if each small steering correction is thought of as a learning opportunity during which some portion of the adaptation occurs. Additionally, each trial in the steering ratio study was about 15 seconds in duration, while the trials in Krakauer et al.'s study were only 1.25 seconds each. Although the two studies cannot be rigorously compared in a statistical sense, a striking feature of the learning curves in Fig. 3.4 is that the data show much less spread than the data points in the Krakauer et al. study. The fact that adaptation to the steering ratio change is so clear for the entire participant population is remarkable because of the complex mental processes involved in steering a car and because the drivers feel changes in vehicle dynamic response not just at the arms but also on their entire bodies.

The result of this study – that drivers adapt to steering ratio changes – aligns well with other studies investigating driver performance in the presence of changing steering ratio. McRuer et al. showed that drivers perform lane regulation tasks robustly to steering ratio changes ranging from 9:1 to 25:1 [91], applying the crossover model of the closed-loop driver-vehicle system to show that drivers modify their control inputs to maintain a constant system bandwidth. However, their study considered a regulation task that only required small steering corrections, rather than a dynamic maneuver like the lane change used here. They also did not explore the time course of adaptation, reporting average driver-vehicle transfer functions modeled from several

minutes' worth of data for each steering ratio. Nevertheless, this study has greatly informed the development of driver-vehicle models over the past few decades. The results of Study #1 extend the conclusions from McRuer et al.'s regulation task in demonstrating that, given enough time to adapt, drivers can control a vehicle with a very small steering ratio (2:1) in a dynamic lane change maneuver just as well as with a standard steering ratio of 15:1.

In a pair of simulator studies, Pick and Cole provided evidence that changes in steering ratio significantly affected the ability of drivers to follow a desired path in a double lane change [110, 111]. This led them to postulate that "drivers base their control on an understanding of the relationship between vehicle response and steering wheel angle rather than between vehicle response and steering torque" [111]. The results of Study #1 are consistent with this claim: since drivers required several trials to recover their baseline performance when the mapping from steering wheel angle to vehicle response was changed, they were in fact updating their internal model of the mapping from steering wheel angle to vehicle dynamics. Pick and Cole reported a larger degree of variability in vehicle paths due to steering ratio changes than was observed in Study #1. One reason for this difference is that Pick and Cole instructed drivers to follow the lane centerline as closely as possible, while in Study #1, participants were free to time the lane change according to their preference. In addition, the Pick and Cole study was performed at a vehicle speed of 38.9 m/s, giving drivers just over 1 second to complete each half of the double lane change; in Study #1 drivers had 2.8 seconds to complete the lane change at 8 m/s. The steering task for Pick and Cole's study therefore required faster steering inputs that amplified the effect of the yaw rate gain change due to steering ratio changes.

Driver adaptation to handling changes is also highly relevant to the issue of handover of control from an automated vehicle to a human driver. Proposed automated vehicles would require human operators to take over control in certain circumstances when the vehicles determine they are unable to safely pilot themselves [3, 9]. The exact process that would be involved in this handover of control has not been fully developed. The results of Study #1 show that drivers require a period of time to

adapt to the change in yaw rate gain that occurs with a large, sudden change in vehicle speed, a situation that could easily occur in a handover scenario. For example, suppose a driver has steered the vehicle through the city at low speed, then has given control to the vehicle to navigate the highway at high speed, so his internal model of the vehicle dynamics includes a low yaw rate gain. If the driver is suddenly required to take over steering control at highway speed, the results of Study #1 suggest that it will take several steering motions before he has adapted to the new vehicle dynamics. This means that over the course of several seconds, the driver is gradually adapting to the modified handling dynamics and therefore his steering performance is altered from baseline. During this time, he may be able to safely steer the vehicle, but until his steering performance returns to baseline with the new handling dynamics, his ability to respond to any unexpected events will be impaired. This study shows, therefore, that the motor control aspects of vehicle-to-driver handover must be considered in automated vehicle design.

3.2 User Study #2: Steering Direction Reversal

The second user study is designed to relate to the coordinate frame rotation in arm reaching studies. As illustrated in Fig. 3.6, the perturbation applied during the adaptation phase is to reverse the steering wheel direction so that a right turn of the steering wheel results in a left turn of the road wheels. In contrast to Study #1, the steering ratio magnitude stays constant throughout the experiment; the direction change is performed by changing the sign of the steering ratio for a resulting ratio of -15:1. The linear spring model used to scale the steering wheel torque in Study #1 is also applied in this study, with the direction of the steering wheel torque always serving to guide the steering wheel toward center.

3.2.1 Study Participants

The steering direction reversal study was conducted with eleven participants ranging in age from 22 to 43 years, with a median of 29 years. Driving experience of the

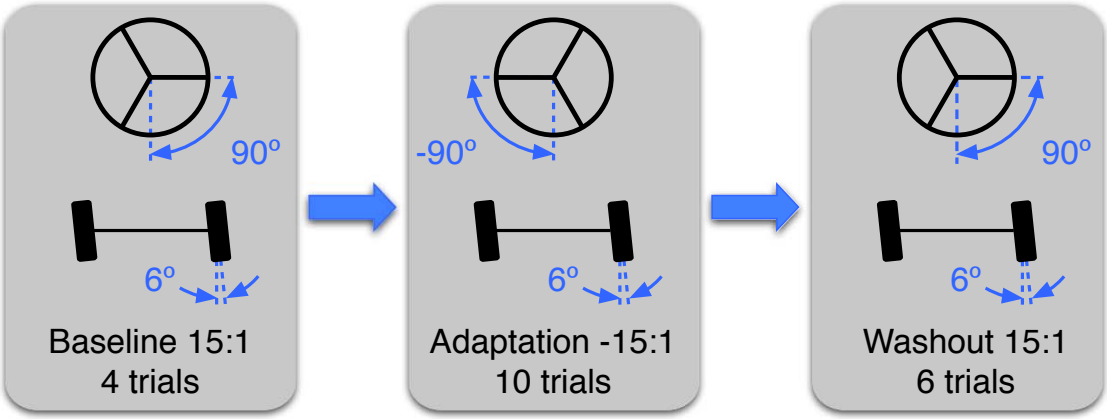

Figure 3.6: Adaptation protocol for steering direction reversal study.

participants ranged from 6 to 26 years, with a median of 13 years. There were ten men and one woman. Two participants were left-handed and the remainder were right-handed. All participants reported no neurological impairments. One additional participant was excluded from data analysis because of repeated failure to steer into the correct gate over the course of several trials, thereby failing to successfully complete the experiment. All participants experienced only the steering direction reversal and did not participate in any of the other user studies.

3.2.2 Sample Participant Data

Example data for two participants in this study are shown in Fig. 3.7 and Fig. 3.8. As in Study #1, both participants demonstrated smooth, simple steering motions in the baseline (green) and washout (red) blocks. However, the two participants displayed extremely different steering behaviors during the adaptation block.

The first sample participant used steering profiles with flattened peaks during the first two adaptation trials with the reversed steering direction (Fig. 3.8A), then quickly reverted to the dual-peaked steering profiles from baseline. This participant also made more steering corrections near the end of the lane change maneuver during the adaptation block as compared to the baseline and washout blocks, particularly in Trials 11, 12, and 14. The vehicle paths (Fig. 3.8B) were so consistent that to an

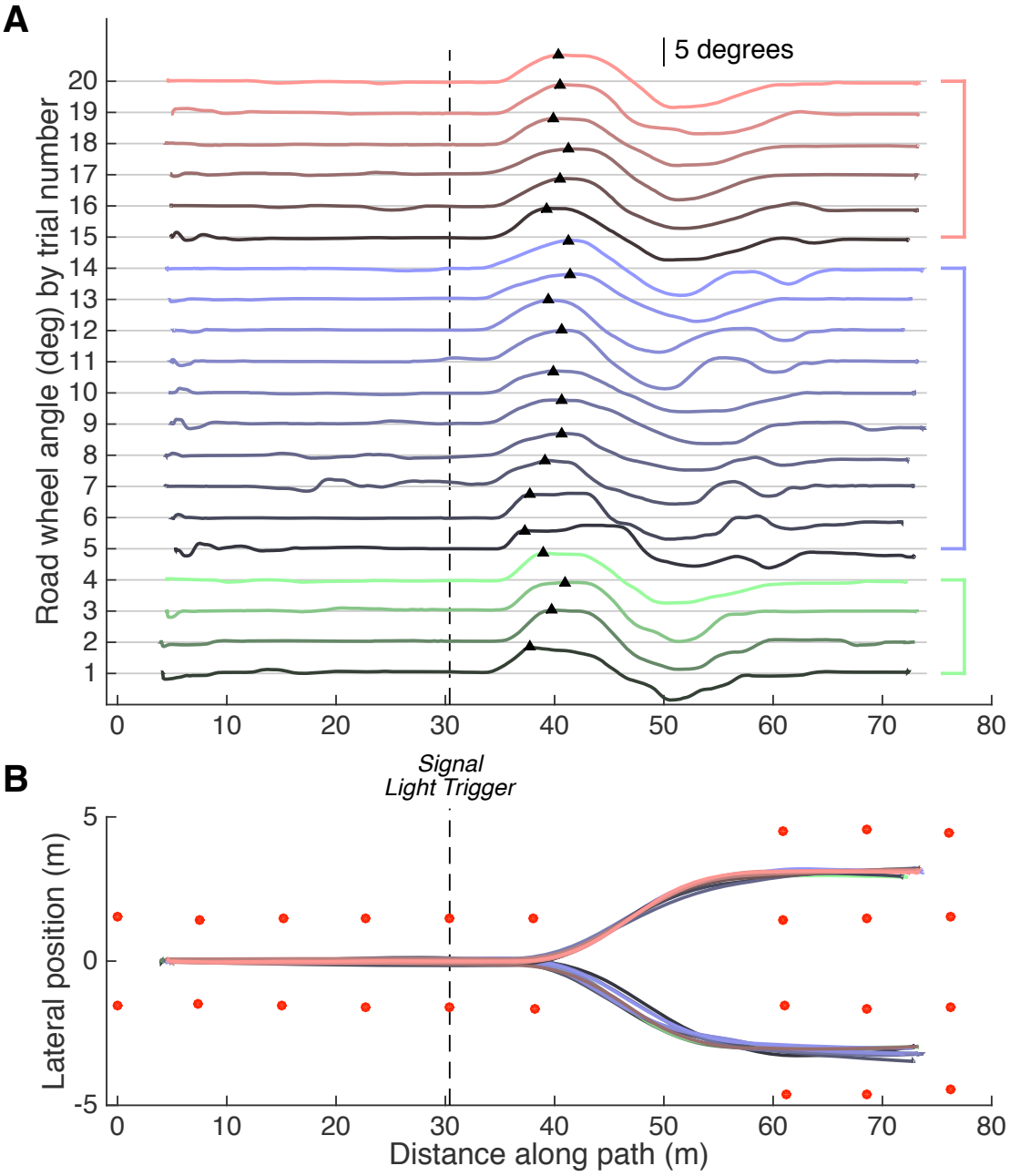

Figure 3.7: Sample data for User Study #2 (steering direction reversal), participant 1. (A) Road wheel angle traces as a function of distance along the path for each trial, with black triangles denoting the local maximum steering angle. (B) Paths taken by the vehicle, with the vertical axis not-to-scale with the horizontal for ease of visualization.

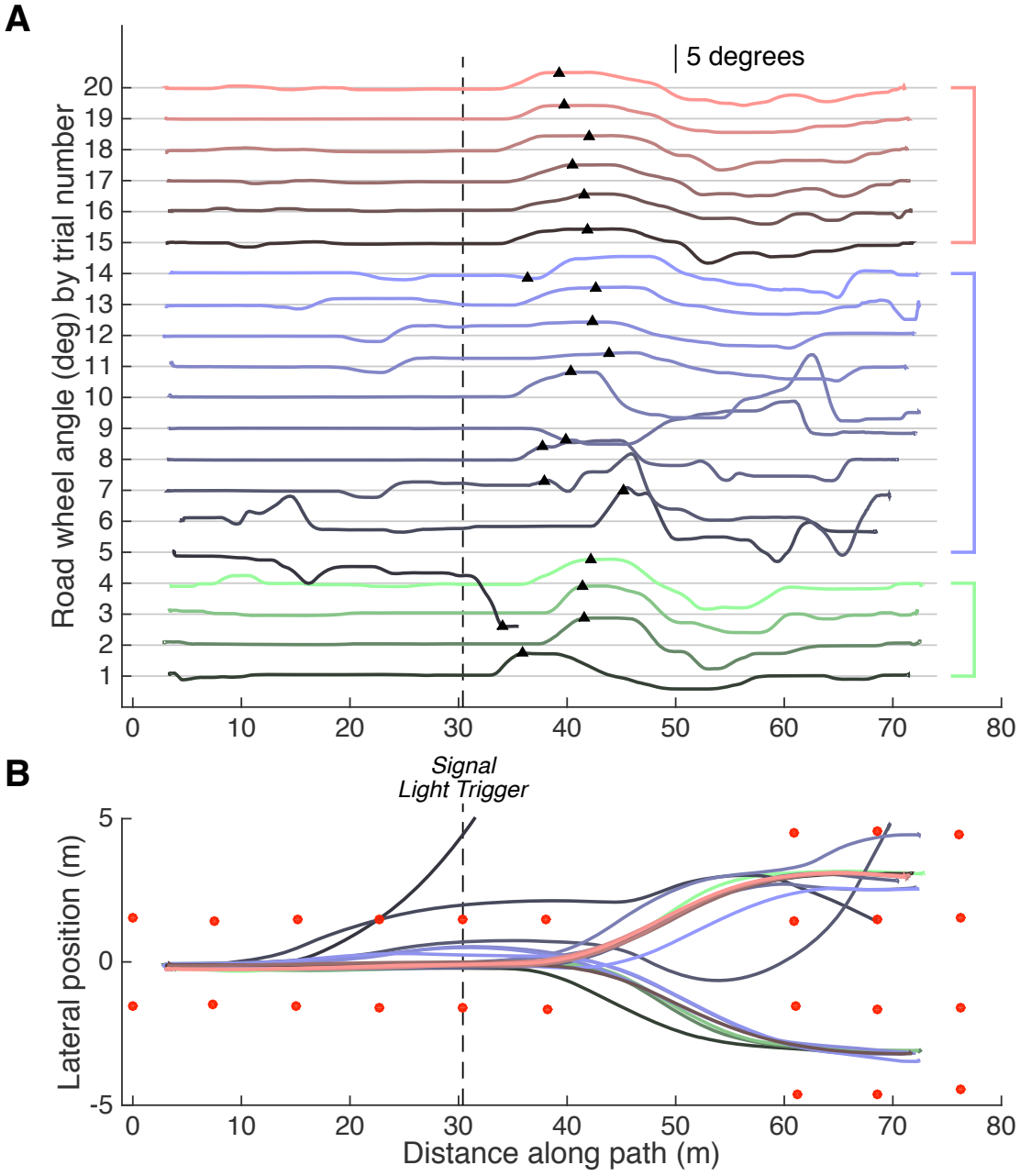

Figure 3.8: Sample data for User Study #2 (steering direction reversal), participant 2. (A) Road wheel angle traces as a function of distance along the path for each trial, with black triangles denoting the local maximum steering angle. (B) Paths taken by the vehicle, with the vertical axis not-to-scale with the horizontal for ease of visualization.

outside observer it would appear that no perturbation was made. Aside from these subtle changes during the adaptation block, this participant demonstrated consistent steering behavior throughout the experiment and was able to successfully complete the lane change on all trials.

In contrast, the second sample participant found the steering direction reversal extremely challenging and was unable to keep the vehicle within the traffic cones on several trials (Fig. 3.8B). As soon as the perturbation was applied in Trial 5, the participant steered off the course and the trial was aborted for safety. On subsequent trials, the participant was able to complete the lane change, but continued to struggle to steer the vehicle, hitting traffic cones several times, particularly on left turns. The steering angle traces in Fig. 3.8A reflect this steering control challenge. The steering profiles during the adaptation block remained different from the baseline profile throughout the block. Although the lane change performance improved over the adaptation block and the steering profiles became smoother and more consistent, the steering motions remain slower and lower magnitude than the baseline motions. Note that on Trial 9 the participant steered into the wrong target gate, which explains the inverted steering profile for that trial compared to the others. During the washout block, when the steering direction was returned to normal, both the steering profiles and the vehicle paths quickly returned to baseline performance, suggesting that no aftereffect was present and that there was no long-term effect on the driver's ability to control the vehicle in normal handling conditions.

The differences in performance between these two participants are representative of the overall group results. Most participants successfully completed all trials; two participants veered completely off the course in Trial 5, while two additional participants hit cones on one or more trials but completed all lane changes. Five participants steered into the wrong target gate for one trial; these data were still included in the group analysis.

Table 3.2: Summary of repeated measures ANOVA results for Study #2. For all metrics, the uncorrected $df_c = 4$ and $df_e = 40$. Values of df_c, df_e, and p_{gg} below have been adjusted with Greenhouse-Geisser ϵ corrections for sphericity. Significant p-values are denoted by boldface type.

Metric	ϵ	df_c	df_e	$F(df_c, df_e)$	p-value
Steering reversal rate	0.72	2.90	28.97	4.94	**0.015**
RMS steering velocity	0.28	1.13	11.32	10.69	**7.5e-3**
Time to steering peak	0.78	3.14	31.37	3.69	**0.022**
RMS yaw jerk	0.36	1.45	14.45	5.33	**0.037**

3.2.3 Group Results

Average data for all eleven participants are shown in Fig. 3.9 for the four metrics. As in Study #1, markers and lines denote the mean values across all participants for each trial, with colored regions indicating the 95% confidence intervals on the mean calculated using a t distribution.

Fig. 3.10 displays the results of statistical comparisons between trials for the four metrics, with pairwise post-hoc comparisons between each pair of trials in the figure following a one-way repeated measures ANOVA. All four metrics had significant differences in mean according to the ANOVA at the $\alpha = 0.05$ significance level, as tabulated in Table 3.2.

Steering reversal rate (SRR) increased when the steering direction was reversed (-15:1 ratio) in Trial 5, although not as drastically as it did in Study #1. It then decreased over the course of the adaptation block towards baseline, although based on Fig. 3.9A it did not fully recover the baseline level. During the washout period, when the steering direction was returned to normal (15:1 ratio), the SRR recovered fully to baseline. Interestingly, the results of the post-hoc tests demonstrated in Fig. 3.10A show that Trials 4 (baseline) and 14 (late adaptation) did not have a statistically significant difference in SRR. The only statistically significant differences were found between Trial 5 (first adaptation trial) and Trials 4 and 20 (late washout). Although differences in the mean SRR can clearly be discerned with the eye, due to the relatively

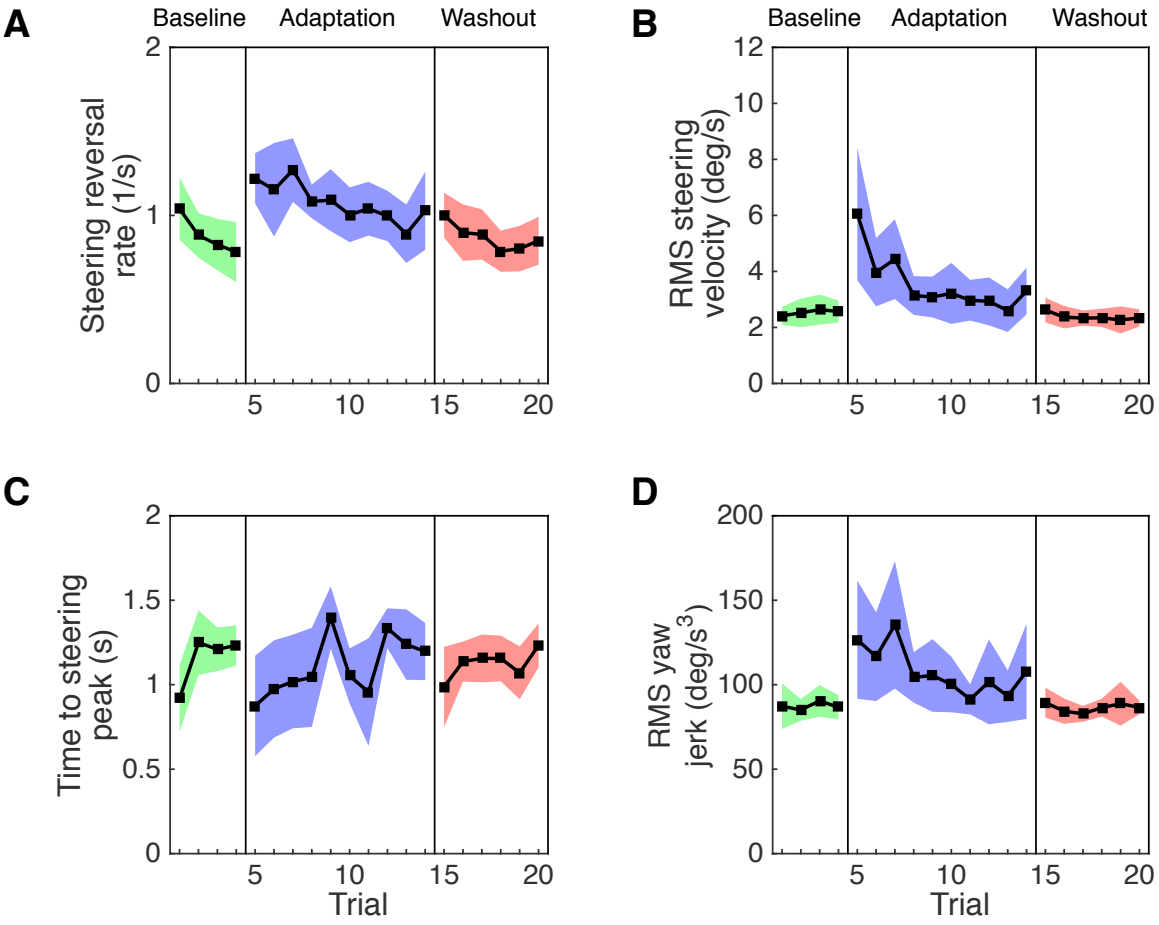

Figure 3.9: Learning curves for steering direction reversal study ($n = 11$). (A) Steering reversal rate (SRR). (B) RMS steering velocity. (C) Time to steering angle peak. (D) RMS yaw jerk. The steering ratio was 15:1 for the baseline and washout blocks, -15:1 for the adaptation block. Colored regions show 95% confidence intervals from a t distribution.

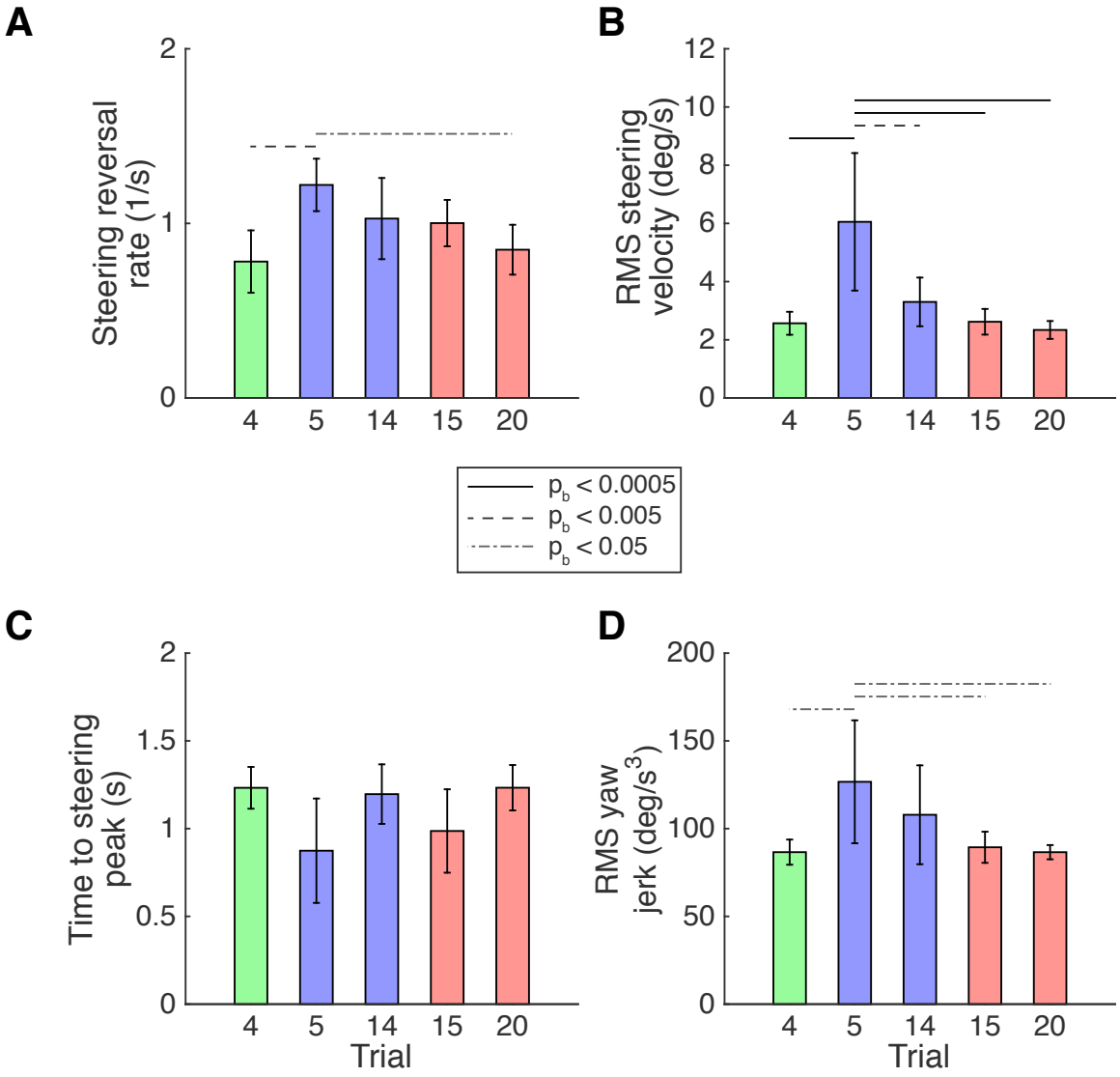

Figure 3.10: Statistical significance for steering direction reversal study ($n = 11$). (A) Steering wheel reversal rate (SRR). (B) RMS steering velocity. (C) Time to steering angle peak. (D) RMS yaw jerk. In all panels, Trial 4 is the last trial of the baseline block (15:1), Trials 5 and 14 are the first and last trials of the adaptation block (-15:1), and Trials 15 and 20 are the first and last trials of the washout block (15:1). Error bars indicate 95% confidence intervals from a t distribution; horizontal lines indicate significant Bonferroni-corrected p-values between trials.

large variance in the data there were no statistically significant differences.

The RMS steering velocity (Fig. 3.9B and Fig. 3.10B) showed a similar learning curve as in Study #1. The steering velocity increased significantly compared to baseline when the steering direction was reversed in Trial 5 and gradually decreased over the course of the adaptation block. The metric then stayed at baseline when the steering was returned to normal for the washout block, with only Trial 5 being significantly higher than all other trials. The learning curve was approximately exponentially shaped and the return to baseline suggests that adaptation to the reversed steering direction took place.

The time to steering peak metric (Fig. 3.9C) showed an interesting learning curve that was very different from the common exponential shape. The steering peak occurred earlier when the steering direction was perturbed, then trended back toward baseline for the first four adaptation trials. During subsequent trials with the direction reversal, the learning curve showed sudden large changes in steering peak timing, followed by a return to baseline timing during the last three trials of the block. However, none of the pairwise comparisons between trials in Fig. 3.10C resulted in statistically significant differences. The fact that the learning curve did not monotonically return to baseline, but instead oscillated before eventually returning, suggests that there was an additional mental process in addition to adaptation; for instance, the use of an explicit cognitive strategy. Although participants in Study #2 were not instructed to use any particular strategy to improve their performance, in post-study debriefing some participants described employing cognitive strategies such as mentally repeating a phrase like "steer left to turn right".

Finally, the RMS yaw jerk metric (Fig. 3.9D and Fig. 3.10D) resulted in an approximately exponential learning curve with no aftereffect. The variance on the yaw jerk increased greatly during the adaptation block, as demonstrated by the large confidence intervals in Fig. 3.9D. This reflects the differences observed in the sample participant steering traces and vehicle paths (Fig. 3.7 and Fig. 3.8), where the first participant showed smooth steering motions throughout the experiment, while the second participant repeatedly went outside the desired path with large steering corrections. The first participant's smooth steering motion resulted in smooth vehicle

kinematics and likely represented the lower end of the confidence intervals; the second participant likely contributed to the higher end of the confidence intervals.

3.2.4 Discussion

The results of this study suggest that drivers adapted to the reversed steering direction, but there is evidence of additional mental processes along with the adaptation. Some of the learning curves in Fig. 3.9 are different from those in Study #1 and what has typically been demonstrated in the motor learning literature. The RMS steering velocity and RMS yaw jerk resulted in approximately exponential learning curves, while the learning curve for the steering reversal rate had a roughly linear shape. In all three of these metrics, adaptation to the perturbation was observed in that the baseline performance was recovered by the end of the adaptation block. The approximately linear learning curve for SRR still demonstrates adaptation, but simply indicates that the process is better described by a linear function than an exponential. By contrast, the learning curve for time to steering peak was somewhat oscillatory, with large, sudden changes on several trials. Although there were no statistically significant differences between the trials of interest, this metric clearly demonstrated an interesting adaptation process that merits further exploration.

A reasonable explanation for the shape of the time to steering peak learning curve is that participants were using an explicit strategy to deal with the handling change. Some recent arm reaching studies have demonstrated that the use of an explicit strategy to counter a visuomotor rotation can be useful during the first few rotated trials, but continuing to use the explicit strategy while simultaneously adapting results in worse performance than either strategy alone or adaptation alone [87, 132]. For the steering direction reversal study, this could manifest as the observed non-monotonic learning curve, with the oscillations reflecting the competing contributions of the explicit strategy and the implicit adaptation process.

The handling change of direction reversal is fundamentally different from the steering ratio change, meaning that the internal model of the mapping from steering inputs to vehicle dynamics is modified in a different way. Rather than scaling how much

steering input is required, drivers must invert the sign of their steering input. This direction reversal also means that the lateral acceleration produced by the vehicle and felt at the body is in the opposite direction as the arm motion; in contrast, the lateral acceleration is always in the same direction as the arm motion for the steering ratio study. It is not surprising, therefore, that the learning curves for the two studies were different. Drivers adapted differently to the two steering perturbations, indicating that there are different mechanisms for adapting to steering magnitude and direction changes. In particular, the steering direction change study resulted in evidence of possible explicit strategy that was not present in the steering ratio scaling study.

3.3 General Discussion

The results of the studies presented in this chapter demonstrate that adaptation to vehicle handling changes can be observed for the case of steering ratio scaling and direction reversal. The particular handling changes examined in these two studies were designed to relate to prior arm reaching studies that provide evidence for the claim that gain scaling and coordinate frame rotation result in different brain processing for a visuomotor rotation task. The steering ratio scaling study resulted in approximately exponential learning curves that clearly showed adaptation over the course of ten trials of the steering task, with an aftereffect in the time to steering peak metric strengthening the case that the driver learned a new internal model of the vehicle dynamics when the steering ratio was changed. The steering direction reversal study showed similar learning curves for some metrics, but the time to steering peak metric was quite different, suggesting that this handling change was more challenging or involved another learning process.

Although these results are generally consistent with those of laboratory-based arm reaching studies, there are some key differences between the two paradigms. First, the elapsed time is very different: in the arm reaching studies, trials occurred at precise 1.25 second intervals, while in the vehicle handling change studies presented here, each trial took on the order of three minutes from start to finish, with approximately 14 seconds during the steering task. On a related note, the arm reaching studies showed

adaptation over the course of about twenty to sixty trials, while participants in Studies #1 and #2 adapted to the steering ratio change over just ten trials of the steering task. This is likely related to the fact that there was feedback of error during the trials, since the drivers needed to control the vehicle's position to successfully complete the lane change. Steering is a continuous learning opportunity, so every small steering correction can be viewed as a miniature trial during which the participants modified their internal models of the handling dynamics.

Second, in arm reaching studies, the dynamics and kinematics of the arm are isolated from the rest of the body. In the vehicle, although the handling change directly affects the motion that the arms need to make to steer the vehicle, the steering motion has consequences for the dynamics of the vehicle, which in turn affect the driver's entire body. This makes it all the more interesting that there are approximately exponential learning curves for the steering ratio scaling study, since the overall experience of the perturbation is much more complex than in the case of isolating the arm. The adaptation block showed exponential learning curves for all four metrics in Study #1, while the learning curves were shaped somewhat differently for Study #2 but nevertheless demonstrated adaptation. The third metric, elapsed time between signal light triggering and subsequent steering angle peak, also showed a clear aftereffect for Study #1, indicating that participants truly modified their internal models.

An interesting feature of these studies is that participants were instructed explicitly when and how the vehicle handling change would occur, an approach that is not typically used in arm reaching studies. That is, prior to Trial 5 they were told that either the steering ratio would become very sensitive or that they would have to steer in the opposite direction, and likewise were told prior to Trial 15 that the steering would return to its original condition. This notification was implemented for safety reasons since the steering perturbations were extreme and increased the likelihood that participants would drive off the course. Even with the opportunity to strategically plan their steering control motions based on their knowledge of the handling conditions, participants were not able to immediately change their internal models of the vehicle handling dynamics, resulting in significant changes to the metrics that

took several trials to return to baseline levels. This suggests that the motor learning that occurred during these studies could not be controlled by explicit strategy. It would be informative to carefully test this hypothesis in a future study.

The studies in this chapter have demonstrated that drivers adapt to changes in steering ratio over the course of several steering motions. This new result extends the understanding of motor adaptation beyond the well-studied paradigms of eye saccades and arm reaches into the far more complex arena of automobile control. An even more compelling question is whether drivers adapt in this same way to more realistic handling changes that they would be likely to encounter over the course of everyday driving. The next chapter presents the results of a study investigating one such handling change, where the steering wheel torque was increased to simulate a power steering failure.

Chapter 4

Adaptation to Steering Torque Increase

The two studies in Chapter 3 demonstrated that drivers adapt to changes in steering ratio over just ten trials of the lane change task. The process of adaptation to steering ratio scaling is analogous to arm reaching studies where the gain from arm motion to cursor motion is scaled. The link between steering direction reversal and visuomotor rotation in arm reaching studies is not as direct, since it appears that learning of the steering direction reversal is more complex and may involve a strategic component in addition to adaptation. These studies provided the first step in studying adaptation during steering tasks: evidence that adaptation exists in these situations and a link to the established body of literature in visuomotor adaptation.

The next step is to perform studies with handling changes that are more realistic and more likely to occur in everyday driving. To begin addressing this need, this chapter presents the results of User Study #3, which modifies the torque on the steering wheel without changing anything about how the vehicle dynamics respond to driver inputs. Steering torque has been demonstrated to be important for vehicle control [74, 135], but studies by Pick and Cole suggest that drivers are robust to changes in the magnitude of the torque [110, 111]. Study #3 tests whether drivers show behavioral adaptation to a steering torque increase.

A torque increase was chosen because it is representative of what happens when

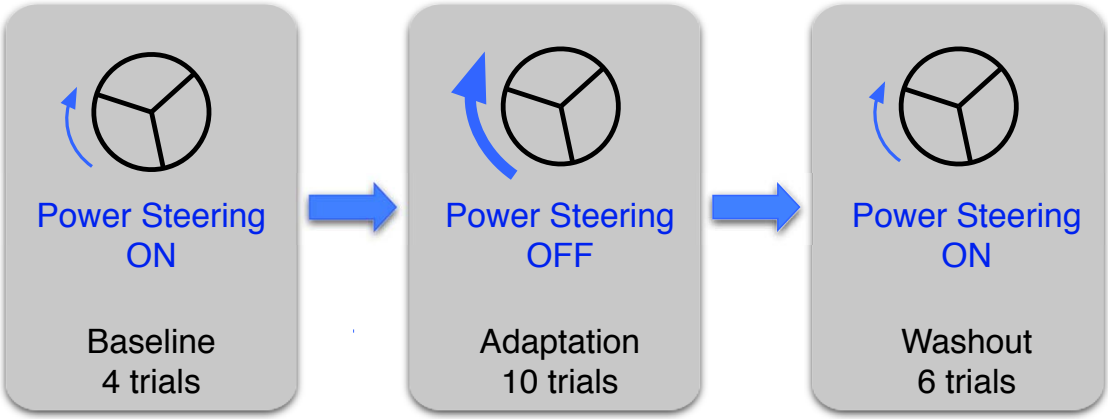

Figure 4.1: Adaptation protocol for steering torque increase study. Size of arrow in each block signifies the amount of torque resisting the driver's steering wheel motion.

a power steering system fails. Power steering, which augments the torque applied by the driver on the steering wheel, was first developed in the early 1900s, with hydraulic power steering systems dating back to 1928 [30]. Power steering is now a standard feature on most passenger vehicles. When a power steering system fails, it no longer provides assistive steering torque, so the driver must apply a greater amount of torque to move the steering wheel.

The experimental protocol for this study follows the same sequence of baseline, adaptation, and washout trials as the other studies, with the steering wheel torque perturbed during the adaptation block to simulate the power steering failure (Fig. 4.1). Since the experimental vehicle is steer-by-wire, the tire forces do not propagate to the steering wheel, so the steering torque is produced by an electric motor. The steering torque for this study is controlled according to the full steering feel emulator described in Section 2.3.1. This emulator uses a steering feel model that reproduces the approximate tire moments that the driver expects to feel through the steering wheel, in addition to simulating a power assist function [8]. The full emulator model enables steering feel tuning through just a few physically intuitive parameters. Eqs. 2.4 and 2.5, which describe the motor torque computed by the full emulator

model, are reproduced here for convenience.

$$\tau_{\text{motor}} = \tau_{\text{inertia}} + \tau_{\text{damping}} + K\tau_{\text{assisted}} \tag{4.1}$$

$$\tau_{\text{assisted}} = W(\alpha, \gamma)\,(\tau_{\text{jacking}} + \tau_{\text{aligning}}) \tag{4.2}$$

For this study, since the steering torque increase is designed to simulate a power steering failure, the perturbation in steering torque is implemented by changing the amount of power assist. The power assist is removed by changing the lower limit parameter γ of the weighting function W from 0.2 in the baseline block to 1 in the adaptation block, while the tire moment gain K is increased from 0.03 to 0.05. These changes result in a steering feel that is heavy and requires increased steering torque applied by the driver in order to complete the lane change maneuver.

4.1 Study Participants

Twelve people participated in this study, none of whom participated in any of the other three studies. Their ages ranged from 23 to 31 years, with a median age of 27 years. Driving experience ranged from 6 to 15 years with a median of 9 years. There were six men and six women; one participant was left-handed and the remainder were right-handed. No neurological impairments were reported.

4.2 Sample Participant Data

Steering angle traces and vehicle paths for two representative participants from Study #3 are depicted in Fig. 4.2 and Fig. 4.3. The two participants used different steering strategies, and both were fairly consistent throughout the experiment. Sample participant 1 (Fig. 4.2) made the lane change by quickly steering one way and holding the steer angle constant for several meters, then quickly steering in the opposite direction and holding a constant steer angle again, finally returning quickly to center. In contrast, sample participant 2 (Fig. 4.3) made slower steering motions, with smooth peaks rather than holding a constant steer angle; this participant also steered with

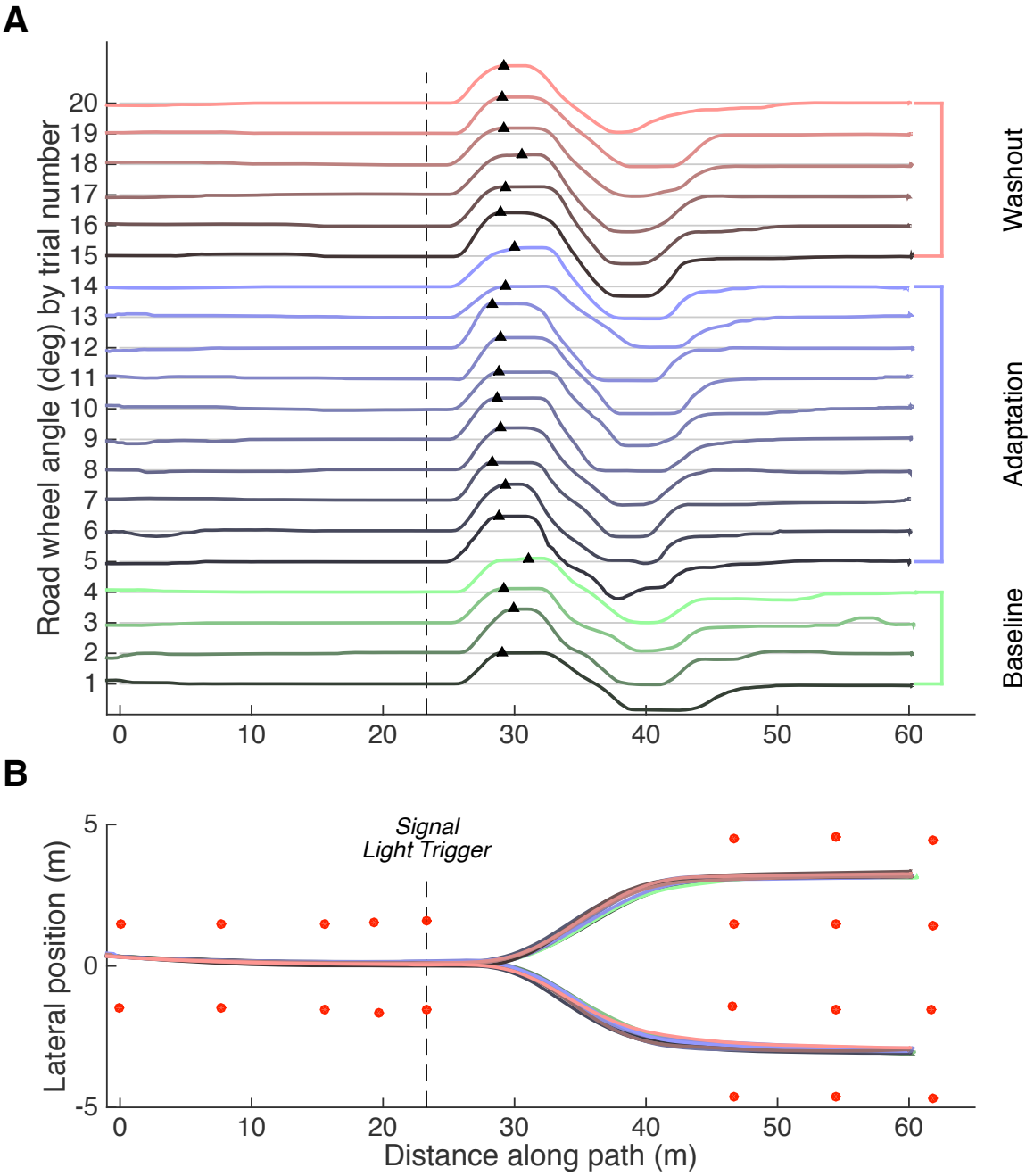

Figure 4.2: Sample data for User Study #3 (steering torque increase), participant 1. (A) Road wheel angle traces as a function of distance along the path for each trial, with black triangles denoting the local maximum steering angle. (B) Paths taken by the vehicle, with the vertical axis not-to-scale with the horizontal for ease of visualization.

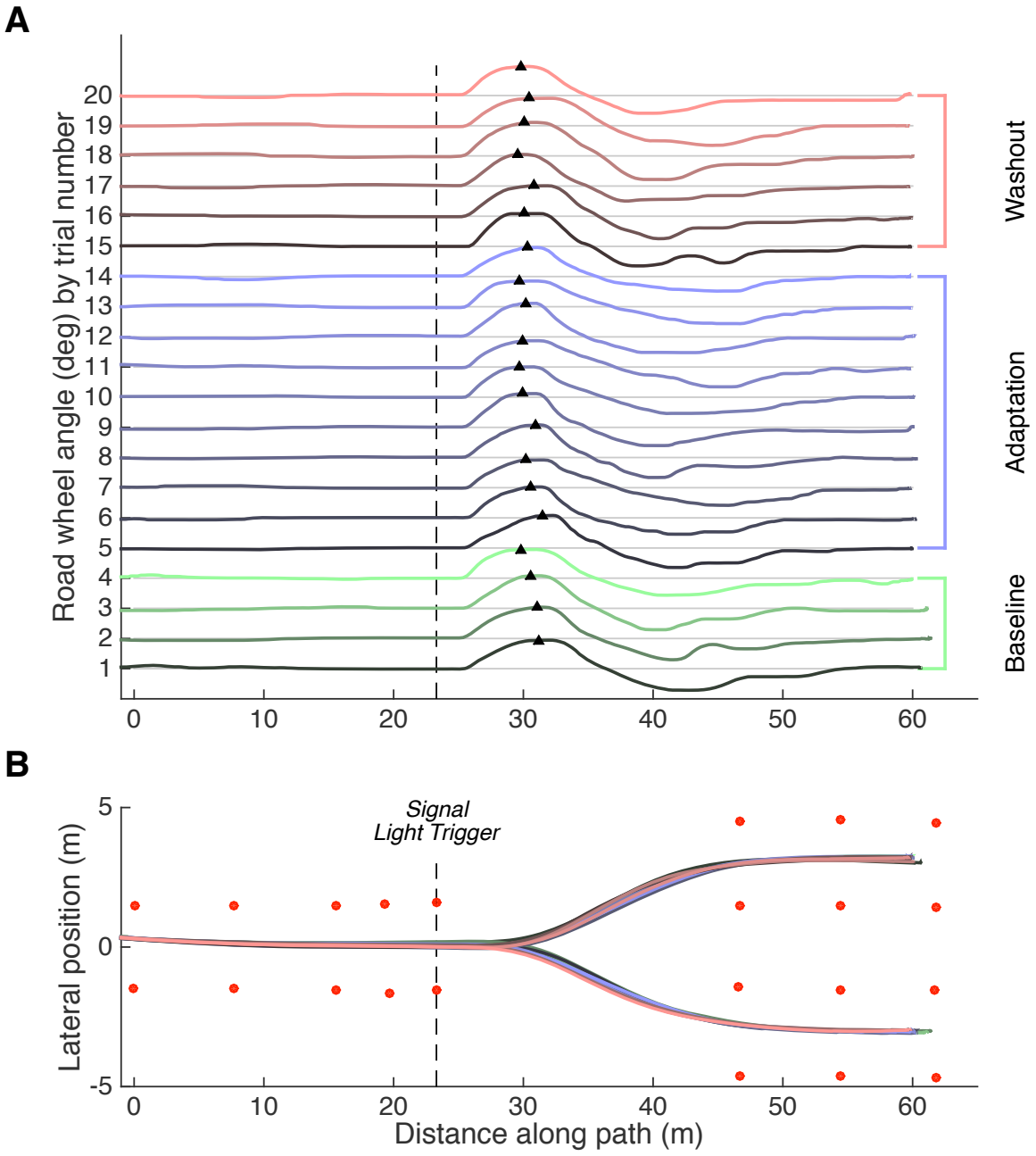

Figure 4.3: Sample data for User Study #3 (steering torque increase), participant 2. (A) Road wheel angle traces as a function of distance along the path for each trial, with black triangles denoting the local maximum steering angle. (B) Paths taken by the vehicle, with the vertical axis not-to-scale with the horizontal for ease of visualization.

lower magnitude than participant 1. Both participants maintained consistent steering profiles for all trials, with very slight changes upon perturbation of the steering wheel torque. Despite the different approaches to steering, the vehicle paths for both participants showed very little variability.

4.3 Group Results

The average values of the four metrics for Study #3 are shown in Fig. 4.4. Compared to the learning curves for the first two studies (Fig. 3.4 and 3.9), it is immediately apparent that none of the four metrics changed much upon the increase in steering torque. Steering reversal rate (Fig. 4.4A) and RMS steering velocity (Fig. 4.4B) remained nearly constant for the entire experiment. The time to steering peak (Fig. 4.4C) slightly increased on Trial 5 when the torque was increased, then immediately returned to baseline level for the remainder of the adaptation block. It then decreased slightly on Trial 15 when the power steering function was restored, again returning immediately to baseline level on the following trial. These changes were minor, however. The RMS yaw jerk (Fig. 4.4D) increased more noticeably on Trial 5, then gradually decayed with a linear trend over the course of the adaptation block. The increase in RMS yaw jerk was only about 10% of the baseline value, while for the steering ratio modification in Study #1 the RMS yaw jerk increased by about 400% when the steering ratio was decreased. This means that change in vehicle dynamics due to the steering torque increase was much less apparent to the driver than the change due to steering ratio scaling. The fact that these metrics showed minimal differences between experimental conditions suggest that drivers did not experience large changes to their internal models of the vehicle dynamics when the steering torque was perturbed.

The results of one-way repeated measures ANOVA on each of the metrics statistically confirm the behavior seen in the sample participant data traces. As Table 4.1 highlights, only the RMS yaw jerk had a statistically significant difference between trials. Therefore, post-hoc tests were performed only for this metric, using pairwise comparisons between trials and Bonferroni corrections on the p-values, with

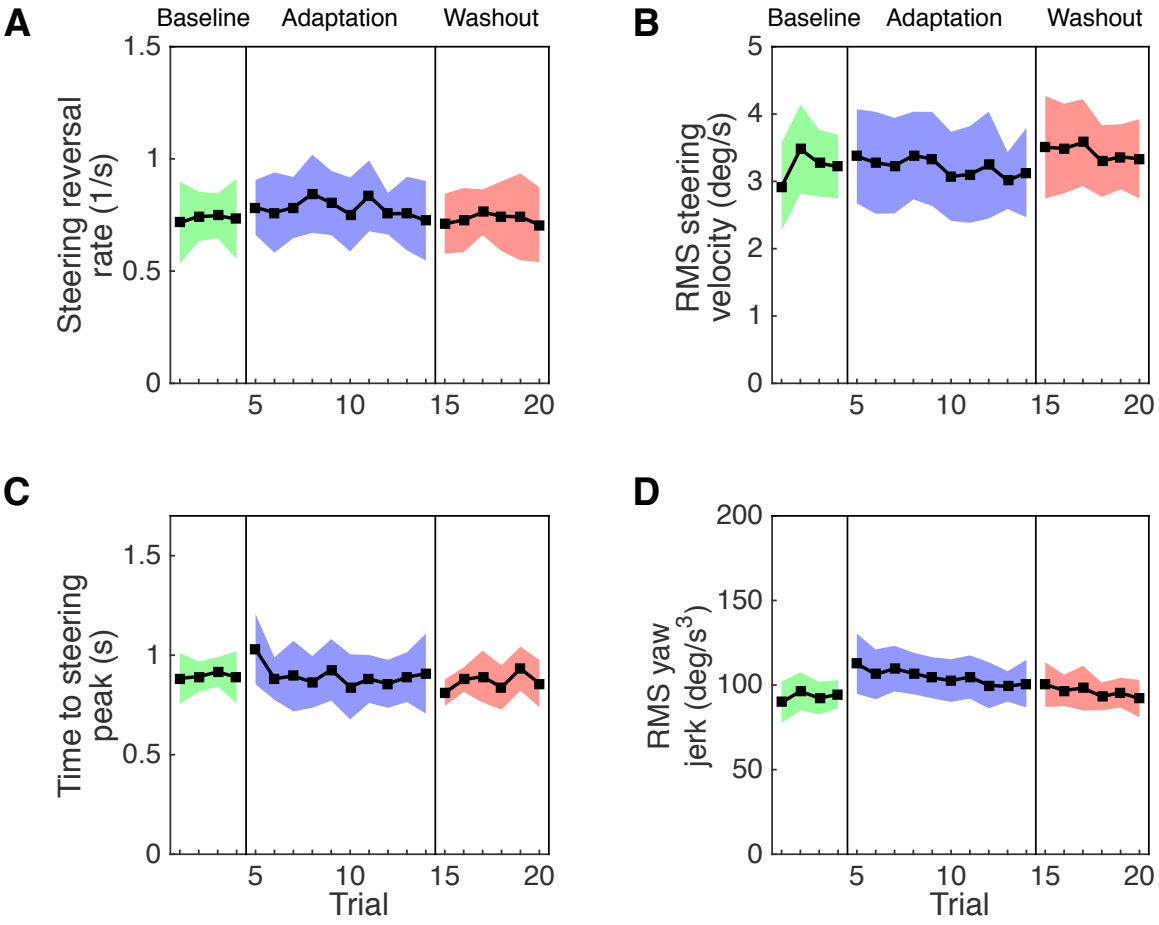

Figure 4.4: Learning curves for steering torque increase study ($n = 12$). (A) Steering reversal rate (SRR). (B) RMS steering velocity. (C) Time to steering angle peak. (D) RMS yaw jerk. The steering torque included power assist for the baseline and washout blocks, no power assist for the adaptation block. Colored regions show 95% confidence intervals from a t distribution.

Table 4.1: Summary of repeated measures ANOVA results for Study #3. For all metrics, the uncorrected $df_c = 4$ and $df_e = 44$. Values of df_c, df_e, and p_{gg} below have been adjusted with Greenhouse-Geisser ϵ corrections for sphericity. Statistically significant p-values at the $\alpha = 0.05$ level are denoted with boldface type.

Metric	ϵ	df_c	df_e	$F(df_c, df_e)$	p_{gg}
Steering reversal rate	0.75	3.00	32.94	0.58	0.564
RMS steering velocity	0.61	2.45	26.96	1.38	0.269
Time to steering peak	0.73	2.93	32.25	1.89	0.168
RMS yaw jerk	0.62	2.46	27.08	5.58	**0.009**

significance at the $\alpha = 0.05$ level. The results of the post-hoc tests are shown in Fig. 4.5. There were two significant differences in mean for the RMS yaw jerk: upon application of the increased steering torque in Trial 5, the RMS yaw jerk increased significantly compared to baseline (Trial 4), and RMS yaw jerk in Trial 5 was also significantly higher than in Trial 20, by which point it had completely returned to baseline level. Although the vehicle dynamics were therefore somewhat less smooth when the steering torque was increased, this had no significant effect on the steering inputs chosen by the drivers (Fig. 4.5A,B,C).

4.4 Discussion

In contrast to the results of Chapter 3, the group results presented in Fig. 4.4 and 4.5 clearly show that drivers did not change their steering behavior in response to increased steering torque. Since most passenger vehicles today are equipped with power steering, the majority of drivers never experience the greater amounts of steering torque needed for a manual steering car unless their power steering system fails. Regardless of this lack of experience, and although the adaptation block required on the order of twice as much steering torque to complete the lane change maneuver, the drivers in this study maintained the same timing and speed of their steering motions, suggesting that they were insensitive to the amount of torque required. The amount of steering torque that was required during the adaptation block was realistic for

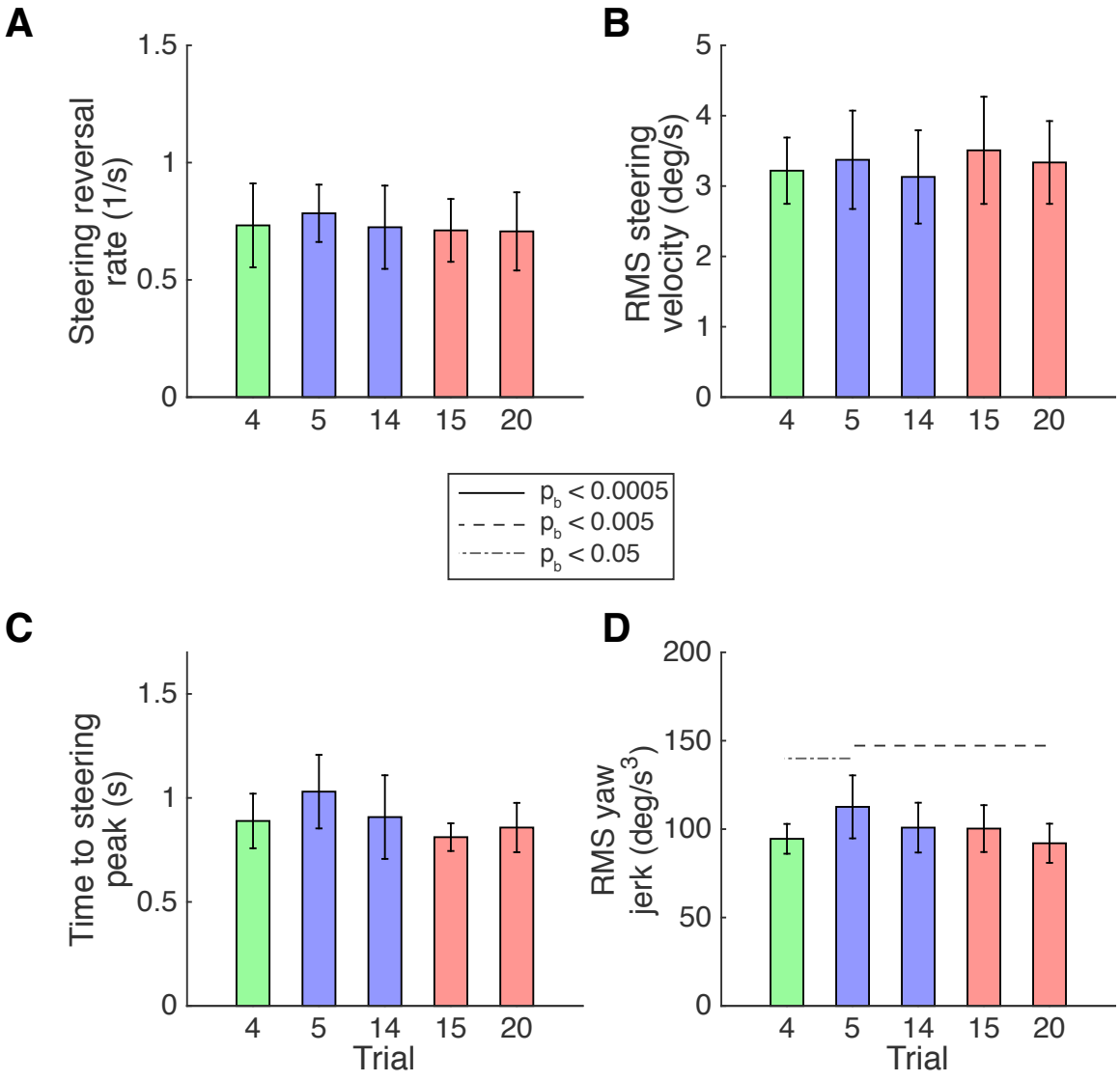

Figure 4.5: Statistical significance for steering torque increase study ($n = 12$). (A) Steering wheel reversal rate (SRR). (B) RMS steering velocity. (C) Time to steering angle peak. (D) RMS yaw jerk. In all panels, Trial 4 is the last trial of the baseline block (power assist ON), Trials 5 and 14 are the first and last trials of the adaptation block (power assist OFF), and Trials 15 and 20 are the first and last trials of the washout block (power assist ON). Error bars indicate 95% confidence intervals from a t distribution; horizontal lines indicate significant Bonferroni-corrected p-values between trials.

a system without power steering, since the torque levels were generated by tuning a steering feel emulator that was designed to replicate a range of realistic steering torque models.

The idea that drivers are robust to changes in the amount of steering torque has been promoted by Pick and Cole, who demonstrated in a simulator study that drivers maintained consistent path-following performance during a double lane change maneuver regardless of the amount of steering torque that was required [110]. They further asserted that it is likely that drivers use angle control rather than torque control to choose steering inputs. The results of the present study and Study #1 are consistent with this hypothesis, demonstrating clear adaptation of steering control behavior to the steering ratio modification but no significant change in steering behavior with increased steering torque.

But how do drivers compensate for the torque change? They are clearly able to maintain consistent path-following performance (Figs. 4.2–4.3) and consistent steering inputs, although the vehicle dynamics become somewhat less smooth when the steering torque is increased (Fig. 4.5D). A possible mechanism for this compensation is that drivers increase the co-contraction of their arms, meaning that they contract opposing sets of muscles at the same time, effectively stiffening their arms to overcome the torque at the steering wheel [109]. Pick and Cole proposed co-contraction as a method of increasing control bandwidth based on their measurements of muscle activation in their double lane change study [110]. In the motor learning literature, increasing arm stiffness is typically seen as a way to compensate for changes in the force on the hand without adapting the internal model of arm kinematics and dynamics [124]. This is exactly what the results of the steering torque study suggest: drivers did not change their steering inputs because their internal model of the mapping from steering motion to vehicle dynamics did not change. Therefore, they compensated for the steering torque increase through a different mechanism, and a promising hypothesis that could be measured explicitly in future studies is that they did this by stiffening their arms through increased muscle co-contraction. Although this study did not find any evidence of adaptation in terms of steering behavior, it is possible that the development of increased muscle co-contraction occurred as an adaptation

process within the first trial of increased steering torque. This co-contraction could therefore be an example of adaptation on a shorter time scale than the several trials that were necessary to adapt to the steering ratio change (Ch. 3).

This chapter has demonstrated that drivers compensate for changes in steering torque without changing the speed or timing of their steering motions. For this handling change, there was no adaptation observed through the steering metrics, suggesting that drivers are insensitive to the magnitude of steering torque, at least on the time scale of a lane change event. What happens when drivers encounter another realistic handling change: driving on a low friction surface? Do drivers adapt their steering control due to this change, or do they compensate for it in some other way, perhaps by stiffening their arms? The final user study will explore these questions in Chapter 6; but first, in order to enable a controlled experiment with low friction vehicle dynamics, the handling emulation controller will be developed in Chapter 5.

Chapter 5

Handling Emulation Controller Development

The user study results presented in the previous two chapters demonstrate that drivers adapt to certain changes in vehicle handling. The data for Studies #1 and #2 showed significant learning trends over the course of the adaptation block with full recovery of baseline performance. The approximately exponentially shaped learning curves are similar to the learning curves seen in other adaptation studies such as arm reaches under visuomotor rotation, suggesting that the same underlying brain processes in this well-studied paradigm may also influence adaptation in driving tasks.

These experiments used simple scaling and reversal modifications to the mapping between the steering wheel and the road wheels to change the vehicle handling. There are other types of vehicle handling modifications that require more complicated controllers. The modifications discussed in this chapter involve controlling the steering and longitudinal actuators so that the experimental vehicle displays specified handling characteristics. This chapter considers desired dynamics that differ from the experimental vehicle's natural dynamics in two ways: first, the reference dynamics could come from a vehicle with different physical parameters than the experimental vehicle; second, the reference dynamics could be from a model of a vehicle traveling on a surface with a different friction coefficient than the experimental vehicle experiences, such as a low friction surface like ice or snow.

The low friction case is particularly interesting for the user study paradigm described in this dissertation. Driving on a low friction surface such as ice is challenging for drivers, and understanding how they change their behavior to account for the nonlinear vehicle dynamics rarely encountered in good road conditions can contribute to a fuller picture of the adaptation process for handling changes. The handling emulation controller described in this chapter provides both a method of studying the learning process for this scenario and a tool for training drivers to become more comfortable with driving in low friction conditions. In addition, the controller enables other types of handling modifications that may be explored in future user studies.

This chapter presents a handling modification approach based on matching the tire force commands on the controlled vehicle with reference model tire forces. This control scheme can track a general planar reference model with lateral, yaw, and longitudinal dynamics and nonlinear, coupled tire forces. The essential problem is one of coordinating actuators to produce the right combination of lateral force, longitudinal force, and yaw moment to track the desired vehicle dynamics. The control strategy uses a feedforward-feedback structure with nonlinear compensation for centripetal acceleration errors. The handling modification control approach is demonstrated for the application of emulating the dynamics of a vehicle on a low friction surface such as an icy road. The idea of using a force-based handling emulation controller for this application was originally proposed by the author for lateral vehicle dynamics [117]. Additionally, the approach provides a straightforward way to track a reduced set of states when particular actuators limit the achievable tire forces.

5.1 Control Strategy Overview

The handling modification method is designed to run in real time on an experimental vehicle. The control strategy follows the block diagram depicted in Fig. 5.1 and can be divided into the following three steps:

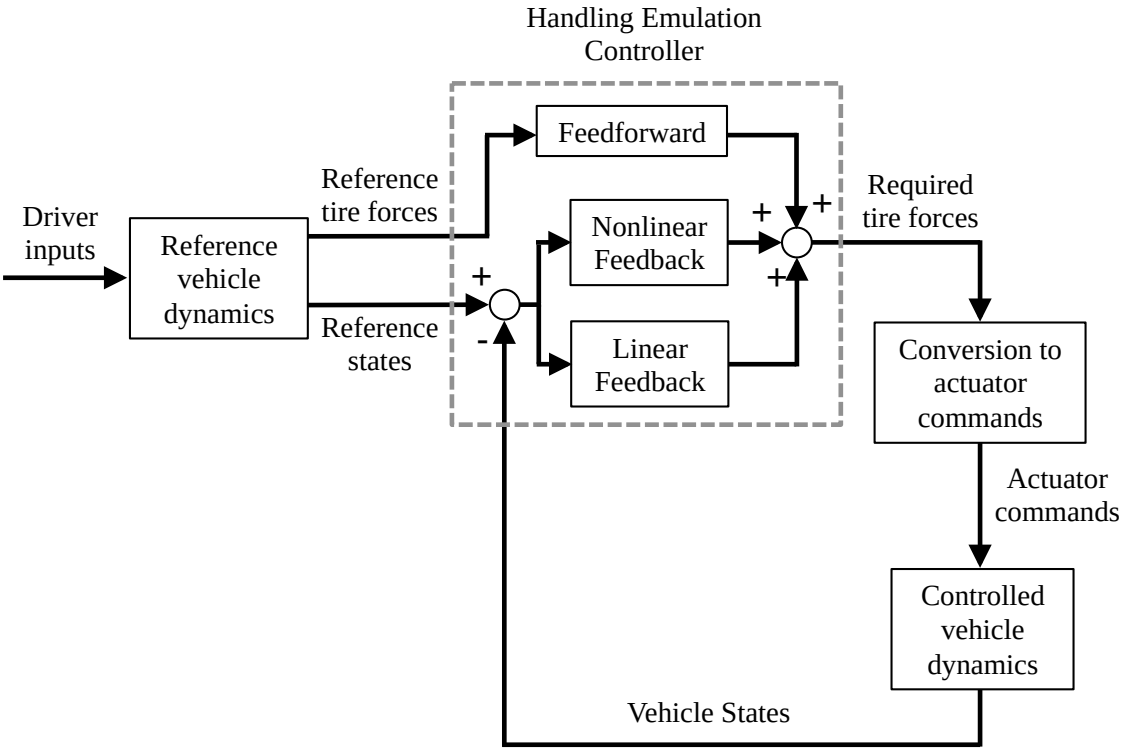

Figure 5.1: Conceptual block diagram of the handling emulation system.

Reference vehicle dynamics

Given driver command inputs (steering wheel angle and accelerator pedal position), a planar model of the reference dynamics is simulated along with the corresponding reference tire forces, which are computed using a nonlinear tire model. The reference dynamic states are the command input for the handling emulation controller.

Handling emulation controller

The controller computes the tire forces required for the vehicle to track the reference model dynamics. The control scheme consists of a combination of feedforward, nonlinear feedback, and linear feedback terms. The feedforward terms approximately match the reference tire forces; the nonlinear feedback terms compensate for centripetal acceleration error; and the linear feedback terms enforce system stability and state tracking.

Controlled vehicle dynamics

The required tire forces are converted into actuator commands (steer angles, drive torques, and brake forces) and applied to the controlled vehicle in order to track the dynamics of the reference model. This tire force-based approach is advantageous for a few reasons. First, the reference forces are already computed while generating the desired vehicle dynamics, so they can be used directly in the controller with no additional computation. Second, the reference tire forces constitute the majority of the controlled vehicle tire forces, with the feedback terms only serving to correct state tracking error and provide stability. This means that the feedforward terms drive the dynamics very close to the desired values, and good tracking can be enforced with smaller feedback gains than a controller using feedback alone would require. Finally, the controller structure allows the use of a straightforward method for proving closed-loop stability of the handling modification system.

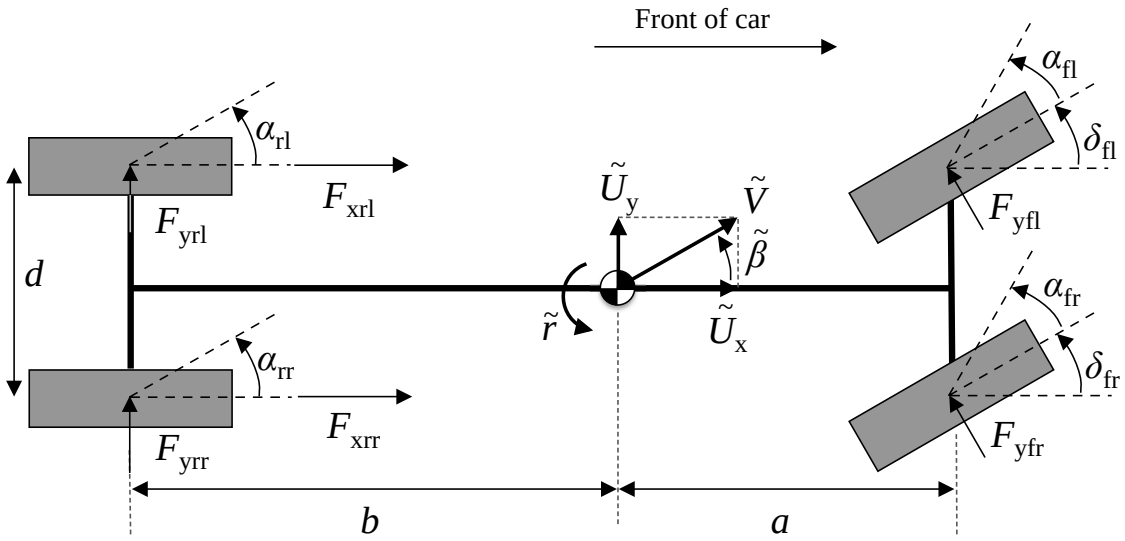

Figure 5.2: The four-wheel planar vehicle model, used to generate the reference model dynamics. The vehicle is rear-wheel drive and front-wheel steer.

5.2 Modeling Vehicle Dynamics and Tire Forces

This section presents the details of the models for vehicle dynamics and tire forces. The reference model consists of a general planar four-wheel vehicle dynamics model and two nonlinear brush tire force models. The controlled vehicle dynamics use a planar bicycle model and general axle forces. These models provide the foundation for developing the handling emulation control scheme.

5.2.1 Dynamics of the Reference Model

The reference model vehicle dynamics are described using the planar four-wheel vehicle model depicted in Fig. 5.2. This model has three state variables: yaw rate $\tilde{r}$, lateral velocity $\tilde{U}_{\mathrm{y}}$, and longitudinal velocity $\tilde{U}_{\mathrm{x}}$. These state variables are all referenced to the vehicle body-fixed coordinate frame at the center of gravity. For simplicity, the vehicle is rear-wheel drive and front-wheel steer, although with minor modifications both axles could be driven and steered. Note that braking is not modeled and longitudinal force comes only from acceleration on the rear axle. Summing tire forces and

moments about the center of gravity results in the total yaw moment $\tilde{\mathbf{M}}_{\mathrm{z}}$, the total lateral force $\tilde{\mathbf{F}}_{\mathrm{y}}$, and the total longitudinal force $\tilde{\mathbf{F}}_{\mathrm{x}}$.

$$\begin{aligned}\tilde{\mathbf{M}}_{\mathrm{z}} &= a(F_{\mathrm{yfl}}\cos\delta_{\mathrm{fl}} + F_{\mathrm{yfr}}\cos\delta_{\mathrm{fr}}) - b(F_{\mathrm{yrl}} + F_{\mathrm{yrr}}) \ldots \\ &\quad + d(F_{\mathrm{yfl}}\sin\delta_{\mathrm{fl}} - F_{\mathrm{yfr}}\sin\delta_{\mathrm{fr}} - F_{\mathrm{xrl}} + F_{\mathrm{xrr}}) \\ \tilde{\mathbf{F}}_{\mathrm{y}} &= F_{\mathrm{yfl}}\cos\delta_{\mathrm{fl}} + F_{\mathrm{yfr}}\cos\delta_{\mathrm{fr}} + F_{\mathrm{yrl}} + F_{\mathrm{yrr}} \\ \tilde{\mathbf{F}}_{\mathrm{x}} &= F_{\mathrm{xrl}} + F_{\mathrm{xrr}} - F_{\mathrm{yfl}}\sin\delta_{\mathrm{fl}} - F_{\mathrm{yfr}}\sin\delta_{\mathrm{fr}}\end{aligned} \tag{5.1}$$

In this description, $F_{\mathrm{y}\star}$ is the lateral tire force on a given wheel; $F_{\mathrm{x}\star}$ is the longitudinal tire force; $\delta_{\star}$ is the steer angle; $\star \in \{\mathrm{fl}, \mathrm{fr}, \mathrm{rl}, \mathrm{rr}\}$ refers to the front left, front right, rear left, and rear right wheel, respectively; a and b are the respective distances from the center of gravity to the front and rear axles; and d is the track width.

Given the total tire forces and moment, the dynamics of the vehicle are described with the equations below, where I_{z} is the yaw moment of inertia and m is the mass.

$$\begin{aligned}\dot{\tilde{r}} &= \frac{\tilde{\mathbf{M}}_{\mathrm{z}}}{I_{\mathrm{z}}} \\ \dot{\tilde{U}}_{\mathrm{y}} &= \frac{\tilde{\mathbf{F}}_{\mathrm{y}}}{m} - \tilde{r}\tilde{U}_{\mathrm{x}} \\ \dot{\tilde{U}}_{\mathrm{x}} &= \frac{\tilde{\mathbf{F}}_{\mathrm{x}}}{m} + \tilde{r}\tilde{U}_{\mathrm{y}}\end{aligned} \tag{5.2}$$

The tire slip angles α_{fl}, α_{fr}, α_{rl}, and α_{rr} are modeled as kinematic functions of the state, the steer angles, and the vehicle geometry. The slip angles are used to compute the lateral tire forces, which combine with the longitudinal tire forces to determine

the vehicle dynamics:

$$\begin{aligned}
\alpha_{\mathrm{fl}} &= \tan^{-1}\left(\frac{\tilde{U}_{\mathrm{y}} + a\tilde{r}}{\tilde{U}_{\mathrm{x}} - \frac{d}{2}\tilde{r}}\right) - \delta_{\mathrm{fl}} \\
\alpha_{\mathrm{fr}} &= \tan^{-1}\left(\frac{\tilde{U}_{\mathrm{y}} + a\tilde{r}}{\tilde{U}_{\mathrm{x}} + \frac{d}{2}\tilde{r}}\right) - \delta_{\mathrm{fr}} \\
\alpha_{\mathrm{rl}} &= \tan^{-1}\left(\frac{\tilde{U}_{\mathrm{y}} - b\tilde{r}}{\tilde{U}_{\mathrm{x}} - \frac{d}{2}\tilde{r}}\right) \\
\alpha_{\mathrm{rr}} &= \tan^{-1}\left(\frac{\tilde{U}_{\mathrm{y}} - b\tilde{r}}{\tilde{U}_{\mathrm{x}} + \frac{d}{2}\tilde{r}}\right)
\end{aligned} \tag{5.3}$$

In general, tire forces are nonlinear functions that couple lateral and longitudinal components and saturate at high values of slip angle and/or longitudinal slip. Any tire model that captures the nonlinearity of the tires and the coupling between longitudinal and lateral force can be used in this framework for handling emulation. In particular, brush tire models represent these effects with a small number of physically meaningful parameters.

Lateral Brush Tire Model

On the undriven (front) axle of the reference vehicle, there is no longitudinal force, so the tire model only needs to consider lateral forces. The Lateral Brush Tire Model is a version of the "pure side slip" model presented by Pacejka [107].

$$F_{\mathrm{y}} = \begin{cases} -C_\alpha \tan(\alpha) + \dfrac{C_\alpha^2}{3\mu F_{\mathrm{z}}} |\tan(\alpha)| \tan(\alpha) - \dfrac{C_\alpha^3}{27\mu^2 F_{\mathrm{z}}^2} \tan^3(\alpha), & |\alpha| < \alpha_{\mathrm{sl}} \\ -\mu F_{\mathrm{z}} \operatorname{sgn}(\alpha), & |\alpha| \geq \alpha_{\mathrm{sl}} \end{cases} \tag{5.4}$$

In this model, the lateral tire force F_{y} is a nonlinear function of the tire slip angle α, and is parametrized by the cornering stiffness C_α, the normal load F_{z}, and the tire-road friction coefficient μ. When the slip angle reaches the full sliding threshold $\alpha_{\mathrm{sl}} = \dfrac{3\mu F_{\mathrm{z}}}{C_\alpha}$, the lateral force saturates to a maximum magnitude determined by the friction and the normal load.

Coupled Brush Tire Model

On the driven (rear) axle of the reference vehicle, there are both lateral and longitudinal forces, so the coupling between these forces must be incorporated into the tire model. The model presented here is a slight modification of Pacejka's coupled slip brush tire model [107]. The deflection of the tire contact patch is represented by longitudinal and lateral theoretical slip quantities σ_{x} and σ_{y}, defined in terms of the practical longitudinal slip $\kappa = \dfrac{R\omega - U_{\mathrm{x}}}{U_{\mathrm{x}}}$, where R is the wheel radius and ω is the wheel speed.

$$\sigma_{\mathrm{x}} = \frac{\kappa}{1+\kappa} \qquad \sigma_{\mathrm{y}} = \frac{-\tan(\alpha)}{1+\kappa} \tag{5.5}$$

The slip can be written in vector form as $\vec{\sigma} = [\sigma_{\mathrm{x}} \quad \sigma_{\mathrm{y}}]^T$, and the magnitude of the slip vector is given by

$$\sigma = |\vec{\sigma}| = \sqrt{\sigma_{\mathrm{x}}^2 + \sigma_{\mathrm{y}}^2}. \tag{5.6}$$

Assuming isotropic tires with stiffness C, the total tire force F is given by the following, where $\sigma_{\mathrm{sl}} = \dfrac{3\mu F_z}{C}$ is the magnitude of the slip vector corresponding to total sliding of the tire.

$$F = \begin{cases} \sigma C - \dfrac{\sigma^2 C^2}{3\mu F_z} + \dfrac{\sigma^3 C^3}{27\mu^2 F_z^2}, & \sigma \le \sigma_{\mathrm{sl}} \\ \mu F_z, & \sigma \ge \sigma_{\mathrm{sl}} \end{cases} \tag{5.7}$$

The total force F is projected into longitudinal and lateral components F_{x} and F_{y} according to the slip vector $\vec{\sigma}$.

$$F_{\mathrm{x}} = \frac{\sigma_{\mathrm{x}}}{\sigma} F \qquad F_{\mathrm{y}} = \frac{\sigma_{\mathrm{y}}}{\sigma} F \tag{5.8}$$

When $\kappa = 0$ and therefore no longitudinal force exists, this model is equivalent to the Lateral Brush Tire Model presented above. The Coupled Brush Tire Model is illustrated in Fig. 5.3, which shows the decrease in lateral force capability when

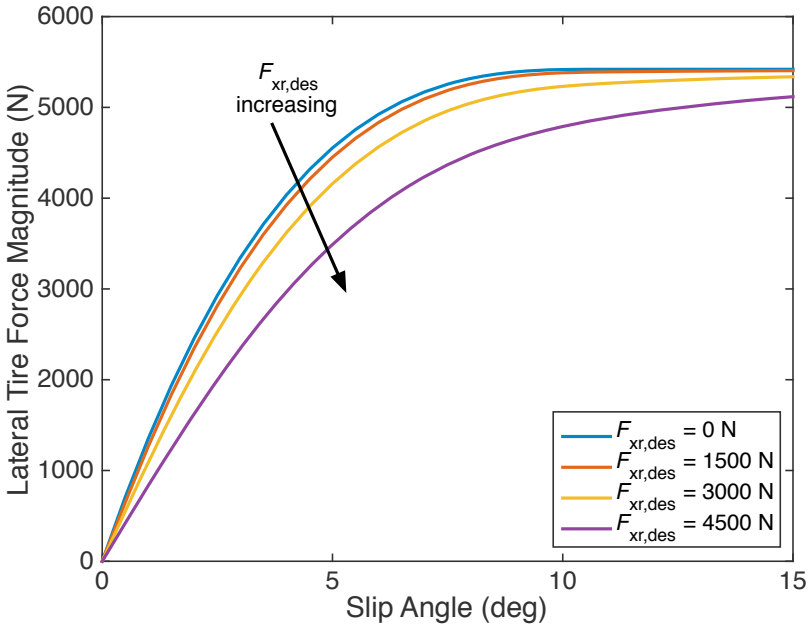

Figure 5.3: Illustration of the Coupled Brush Tire Model. As $F_{\text{xr,des}}$ increases, the available lateral tire force at a given tire slip angle is reduced.

longitudinal force demand exists.

Using the Coupled Brush Tire Model typically requires simulating wheel speed dynamics for each wheel in order to find κ and σ_{x}. Since the control strategy used in this chapter simulates the reference vehicle dynamics in real time based on the driver's inputs, the driver's desired longitudinal force $F_{\text{xr,des}}$ is used to find the corresponding κ and σ_{x}, therefore avoiding the need to simulate wheel speed states for each wheel. Given $F_{\text{xr,des}}$ divided equally between both rear wheels, the corresponding theoretical longitudinal slip σ_{x} for each wheel is found by inverting the Coupled Brush Tire Model with $\sigma_{\text{y}} = 0$. The practical slip is $\kappa = \dfrac{\sigma_{\text{x}}}{1 - \sigma_{\text{x}}}$, as found from (5.5). These values of κ and σ_{x} are then used in the Coupled Brush Tire Model with the current slip angles from the reference model simulation.

5.2.2 Dynamics of the Controlled Vehicle

The controlled vehicle requires only three inputs to track the reference vehicle dynamics – total lateral force, total longitudinal force, and total yaw moment. This can

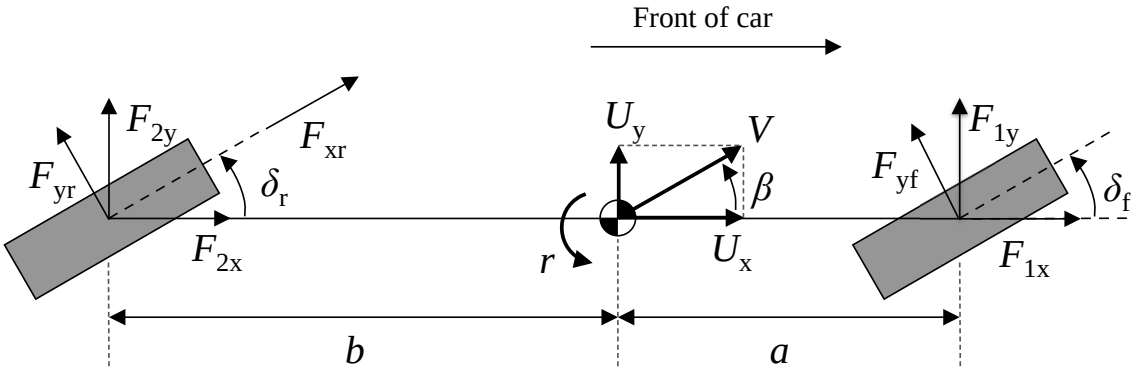

Figure 5.4: The bicycle model with tire forces and general axle forces, used to model controlled vehicle dynamics. The vehicle is rear-wheel drive and has four-wheel steering.

be achieved by actuating the front steering, rear steering, and the drivetrain. With only these three control inputs, it is convenient to use a planar "bicycle" model rather than the full four-wheel model used for the reference vehicle. Fig. 5.4 depicts the planar bicycle model, which lumps together the left and right sides of the vehicle into a single track with identical left and right steer angles. The forces on the tires can be represented either by the tire-referenced forces $\{F_{\mathrm{yf}}, F_{\mathrm{yr}}, F_{\mathrm{xr}}\}$ or the general axle forces $\{F_{1\mathrm{x}}, F_{1\mathrm{y}}, F_{2\mathrm{x}}, F_{2\mathrm{y}}\}$, which resolve the tire forces into the coordinate frame of the vehicle body. The latter is useful in a general treatment of the controlled vehicle dynamics and in proving system stability in Section 5.3.2.

With yaw rate r, lateral velocity U_{y}, and longitudinal velocity U_{x}, the vehicle dynamics for this model are

$$\begin{aligned} \dot{r} &= \frac{1}{I_{\mathrm{z}}}\left(aF_{1\mathrm{y}} - bF_{2\mathrm{y}}\right) \\ \dot{U}_{\mathrm{y}} &= \frac{1}{m}\left(F_{1\mathrm{y}} + F_{2\mathrm{y}}\right) - rU_{\mathrm{x}} \\ \dot{U}_{\mathrm{x}} &= \frac{1}{m}\left(F_{1\mathrm{x}} + F_{2\mathrm{x}}\right) + rU_{\mathrm{y}}. \end{aligned} \tag{5.9}$$

The following relationships convert between general axle forces and forces in the tire

coordinate frame.

$$\begin{aligned} F_{1\mathrm{y}} &= F_{\mathrm{yf}} \cos\delta_{\mathrm{f}} \\ F_{1\mathrm{x}} &= -F_{\mathrm{yf}} \sin\delta_{\mathrm{f}} \\ F_{2\mathrm{y}} &= F_{\mathrm{yr}} \cos\delta_{\mathrm{r}} + F_{\mathrm{xr}} \sin\delta_{\mathrm{r}} \\ F_{2\mathrm{x}} &= F_{\mathrm{xr}} \cos\delta_{\mathrm{r}} - F_{\mathrm{yr}} \sin\delta_{\mathrm{r}} \end{aligned} \tag{5.10}$$

Depending on the actuators available on the vehicle, several different methods are capable of achieving these general axle forces. The level of precision used in the conversion to actuator commands depends on the particular application. Section 5.4.1 discusses one example of solving for the steer angles and drivetrain commands.

5.3 Emulating Vehicle Dynamics Using Tire Forces

Given the reference vehicle model, the tire forces of the controlled vehicle must meet the goal of tracking the reference vehicle dynamics while maintaining the stability of the closed-loop system. The controlled vehicle tire forces consist of feedforward terms that approximate the reference vehicle tire forces, linear feedback terms for tracking and stability, and nonlinear feedback terms to correct centripetal acceleration error. For this development, the reference and controlled vehicle are assumed to have the same mass m, yaw moment of inertia I_{z}, and center of gravity location. If this is not the case for a particular application, it is straightforward to modify the controller developed here with the appropriate vehicle parameters (see Appendix C for details).

5.3.1 Choosing Tire Forces

The error state $\mathbf{e} = [e_{\mathrm{r}} \quad e_{\mathrm{y}} \quad e_{\mathrm{x}}]^T$ is defined as the difference between the reference model states and the controlled vehicle states.

$$\begin{aligned} e_{\mathrm{r}} &= \tilde{r} - r \\ e_{\mathrm{y}} &= \tilde{U}_{\mathrm{y}} - U_{\mathrm{y}} \\ e_{\mathrm{x}} &= \tilde{U}_{\mathrm{x}} - U_{\mathrm{x}} \end{aligned} \tag{5.11}$$

The error dynamics $\dot{\mathbf{e}}$ are simply the time derivative of $\mathbf{e}$.

Using the reference vehicle dynamics (5.2) and the controlled vehicle dynamics (5.9), the error dynamics can be written in terms of the general axle forces as follows.

$$\begin{aligned}
\dot{e}_{\mathrm{r}} &= \frac{1}{I_{\mathrm{z}}}\left(\tilde{\mathbf{M}}_{\mathrm{z}} - aF_{1\mathrm{y}} + bF_{2\mathrm{y}}\right) \\
\dot{e}_{\mathrm{y}} &= \frac{1}{m}\left(\tilde{\mathbf{F}}_{\mathrm{y}} - m\tilde{r}\tilde{U}_{\mathrm{x}} - F_{1\mathrm{y}} - F_{2\mathrm{y}} + mrU_{\mathrm{x}}\right) \\
\dot{e}_{\mathrm{x}} &= \frac{1}{m}\left(\tilde{\mathbf{F}}_{\mathrm{x}} + m\tilde{r}\tilde{U}_{\mathrm{y}} - F_{1\mathrm{x}} - F_{2\mathrm{x}} - mrU_{\mathrm{y}}\right)
\end{aligned} \tag{5.12}$$

Suppose the general axle forces of the controlled vehicle are the following, where K_1, K_2, K_3, K_4, and K_5 are proportional feedback gains.

$$\begin{aligned}
F_{1\mathrm{y}} &= \frac{b}{L}\tilde{\mathbf{F}}_{\mathrm{y}} + \frac{1}{L}\tilde{\mathbf{M}}_{\mathrm{z}} - \frac{mb}{L}\left(\tilde{r}\tilde{U}_{\mathrm{x}} - rU_{\mathrm{x}}\right) - \frac{(K_1 + bK_3)}{L}e_{\mathrm{r}} - \frac{(K_2 + bK_4)}{L}e_{\mathrm{y}} \\
F_{2\mathrm{y}} &= \frac{a}{L}\tilde{\mathbf{F}}_{\mathrm{y}} - \frac{1}{L}\tilde{\mathbf{M}}_{\mathrm{z}} - \frac{ma}{L}\left(\tilde{r}\tilde{U}_{\mathrm{x}} - rU_{\mathrm{x}}\right) + \frac{(K_1 - aK_3)}{L}e_{\mathrm{r}} + \frac{(K_2 - aK_4)}{L}e_{\mathrm{y}} \\
F_{\mathrm{x}} &= F_{1\mathrm{x}} + F_{2\mathrm{x}} = \tilde{\mathbf{F}}_{\mathrm{x}} + m\left(\tilde{r}\tilde{U}_{\mathrm{y}} - rU_{\mathrm{y}}\right) - K_5 e_{\mathrm{x}}
\end{aligned} \tag{5.13}$$

In these equations, the terms with $\tilde{\mathbf{M}}_{\mathrm{z}}$, $\tilde{\mathbf{F}}_{\mathrm{y}}$, and $\tilde{\mathbf{F}}_{\mathrm{x}}$ are feedforward terms that match the tire forces from the reference model. The rU_{x} and rU_{y} terms are the nonlinear feedback terms that relate to the centripetal acceleration of the vehicle. In the lateral direction, both the front and rear lateral forces help to compensate for the centripetal acceleration error, with each axle providing a force that is proportional to its share of the vehicle's mass. The terms multiplying e_{r}, e_{y}, and e_{x} are linear feedback terms that provide tracking and stability. Substituting these control forces into (5.12), the error dynamics reduce to linear functions of the error states.

$$\begin{aligned}
\dot{e}_{\mathrm{r}} &= \frac{1}{I_{\mathrm{z}}}\left(K_1 e_{\mathrm{r}} + K_2 e_{\mathrm{y}}\right) \\
\dot{e}_{\mathrm{y}} &= \frac{1}{m}\left(K_3 e_{\mathrm{r}} + K_4 e_{\mathrm{y}}\right) \\
\dot{e}_{\mathrm{x}} &= \frac{1}{m}K_5 e_{\mathrm{x}}
\end{aligned} \tag{5.14}$$

5.3.2 Stability of the Error Dynamics

Assuming the tire forces in (5.13) are exactly achieved on the controlled vehicle, the error dynamics follow (5.14), which is an LTI system, written in matrix form below.

$$\dot{\mathbf{e}} = \begin{bmatrix} \frac{K_1}{I_z} & \frac{K_2}{I_z} & 0 \\ \frac{K_3}{m} & \frac{K_4}{m} & 0 \\ 0 & 0 & \frac{K_5}{m} \end{bmatrix} \mathbf{e} = A\mathbf{e} \tag{5.15}$$

This system is asymptotically stable if all the eigenvalues of A have negative real parts; this is achieved if

$$\begin{aligned} (K_1 m + K_4 I_z) &< 0, \\ (K_1 K_4 - K_2 K_3) &> 0, \\ \text{and } K_5 &< 0. \end{aligned} \tag{5.16}$$

The model will not always perfectly match the actual performance of the vehicle; for instance, since the tire forces of the controlled vehicle are not directly measured, it is likely that these forces are not equal to the desired forces (5.13). Suppose each of the actual tire forces on the controlled vehicle is the sum of the desired force F_i and some error ΔF_i.

$$\begin{aligned} F_{1\mathrm{y,act}} &= F_{1\mathrm{y}} + \Delta F_{1\mathrm{y}} \\ F_{2\mathrm{y,act}} &= F_{2\mathrm{y}} + \Delta F_{2\mathrm{y}} \\ F_{\mathrm{x,act}} &= F_{\mathrm{x}} + \Delta F_{\mathrm{x}} \end{aligned} \tag{5.17}$$

This error could be due to uncertainty in the tire model and to unmodeled actuator dynamics. If the forces on the controlled vehicle are described by (5.17), the state error dynamics have extra terms related to the force errors. The new error dynamics can still be written as an LTI system of the form $\dot{\mathbf{e}} = A\mathbf{e} + B\Delta\mathbf{F}$, with $\Delta\mathbf{F} =$

$[\Delta F_{1\mathrm{y}} \quad \Delta F_{2\mathrm{y}} \quad \Delta F_{\mathrm{x}}]^T$ defining the force errors and A unchanged from (5.14):

$$\dot{\mathbf{e}} = \begin{bmatrix} \frac{K_1}{I_{\mathrm{z}}} & \frac{K_2}{I_{\mathrm{z}}} & 0 \\ \frac{K_3}{m} & \frac{K_4}{m} & 0 \\ 0 & 0 & \frac{K_5}{m} \end{bmatrix} \mathbf{e} + \begin{bmatrix} -\frac{a}{I_{\mathrm{z}}} & \frac{b}{I_{\mathrm{z}}} & 0 \\ -\frac{1}{m} & -\frac{1}{m} & 0 \\ 0 & 0 & -\frac{1}{m} \end{bmatrix} \Delta\mathbf{F} \tag{5.18}$$

In this case, the origin is no longer guaranteed to be an equilibrium point, nor can asymptotic stability be ensured. However, as long as all poles of $H(s) = (sI - A)^{-1}B$ have negative real parts, then the system is bounded-input, bounded-output (BIBO) stable with respect to the state error $\mathbf{e}$ (output) and the tire force uncertainty $\Delta\mathbf{F}$ (input). This means that the state error dynamics may vary but will stay within a region bounded about the origin. The size of this boundary layer depends on the magnitude of the tire force uncertainty. When the system is stable, the steady-state errors can be found from $\mathbf{e}_{\mathrm{ss}} = -A^{-1}B\Delta\mathbf{F}$, while the size of the boundary layer can be characterized by the worst-case norm of the steady-state error due to the norm of the tire force uncertainty $||\Delta\mathbf{F}||$:

$$||\mathbf{e}_{\mathrm{ss}}|| \leq || - A^{-1}B||\ ||\Delta\mathbf{F}|| \tag{5.19}$$

For the low friction emulation application described in the remainder of this chapter, realistic bounds on the tire force uncertainty can be found by computing a percentage of the maximum achievable lateral and longitudinal tire forces with the emulated friction coefficient; in this case it is reasonable to assume that the computed and measured forces are accurate to within 10%. With the vehicle parameters listed in Table 2.1, the feedback gains listed in Table 5.1, and a reference model friction coefficient of $\mu = 0.4$, all system poles have negative real parts and the tire force uncertainty is $\Delta\mathbf{F} = [340\ 433\ 774]^T$ N. This produces worst-case steady-state error norm $||\mathbf{e}_{\mathrm{ss}}|| = 0.085$, which corresponds to maximum errors of 2°/s in yaw rate, 0.03 m/s in lateral velocity, and 0.08 m/s in longitudinal velocity. Therefore, for this application the system is BIBO stable with tight bounds on the resulting tracking error.

5.3.3 Discussion

This approach to handling modification tracks a reference model within a limited error bound as long as the actuators can produce the required tire forces. It is not always possible to generate any arbitrary tire force, so the control scheme must manage actuator limitations. Section 5.4.3 discusses one way of achieving this for the application to low friction emulation.

A variety of methods exist to solve for the tire-reference forces and actuator commands from the general axle forces $\{F_{1x}, F_{1y}, F_{2x}, F_{2y}\}$. For example, Ono et al. described a hierarchical control structure that computed individual tire forces and actuator commands to achieve desired forces and moment at the vehicle center of gravity [104]. Wang et al. approached the tire force allocation problem by controlling individual tire slip angles and longitudinal slip [140]. Kasinathan et al. proposed an approach called holistic cornering control that minimized the error in the resultant force at the center of gravity by selecting optimal lateral and longitudinal tire forces [57]. Madhusudhanan et al. described the Tyre Utilization Coefficient Control method, which used measurements of tire forces to select steering angles of each individual wheel so that all tires used similar amounts of their available force, rather than allowing some tires to saturate while others were underutilized [81]. Finally, Park and Gerdes balanced force utilization among the four tires via four-wheel steering, four-wheel braking, and rear-wheel drive actuators, using a model predictive control (MPC) approach with successive quasiconvex optimization [108]. The conversion from general axle forces to individual tire actuation commands may use any of these optimal control methods. Alternatively, in some applications such as the low friction emulation controller discussed in Section 5.4, it may be appropriate to use small angle approximations to simplify the actuator command solution.

Another important part of vehicle handling is the roll dynamics. Explicit emulation of roll dynamics is not common in the handling emulation literature. One example is the work of Akar and Kalkkuhl in extending their lateral dynamics emulation platform from [4] to include active roll emulation, which required the addition

of active suspension control on all four wheels [5]. Although simulation results indicated that the platform would successfully emulate yaw, lateral, and roll dynamics, the experiments demonstrated the planar and roll dynamics separately. Another proposed method for emulation of roll dynamics is to actively control the stiffness of the vehicle's anti-roll bars, as described by Lee et al. [71]. Since the handling emulation approach presented here tracks a planar reference model, vehicle body roll is not explicitly controlled. However, roll is coupled to the other dynamic states through the vehicle suspension and can be analyzed for particular applications of handling modification. For low friction emulation, the roll dynamics of the controlled vehicle and the reference model are very similar, as discussed in Section 5.4.4.

5.4 Application to Low Friction Emulation

A compelling application of this approach to vehicle handling modification is emulation of the dynamics of a vehicle on a low friction surface, or *low friction emulation*. Driving on a low friction surface such as ice or snow is often challenging for drivers [40] due to the reduced capability of the tires to generate force and the unfamiliar, nonlinear vehicle dynamics that result. Drivers can certainly learn how to respond appropriately and safely to these conditions, in particular, countersteering (or steering out of the turn) when the vehicle starts to spin. It is less clear how they learn this skill, how long it takes them to learn at a neuromuscular level, and how well this learning is retained over long periods of time. A vehicle capable of emulating low friction conditions enables further exploration of these questions and provides a safe, repeatable training and experimental tool.

The controlled vehicle used for the emulation travels on a high friction surface such as dry asphalt, while the emulated conditions simulate ice, snow, or other low friction surfaces. This corresponds to a friction coefficient of 0.8–1.0 for the experimental 4WS vehicle, and up to 0.4 for the reference model. Fig. 5.5 shows sample lateral tire force curves for the low friction reference model and the high friction controlled vehicle. The reference lateral force $\tilde{\mathbf{F}}_{\mathrm{y}}$ is approximately the tire force that needs to be applied to the controlled vehicle (not including the feedback terms). At this force

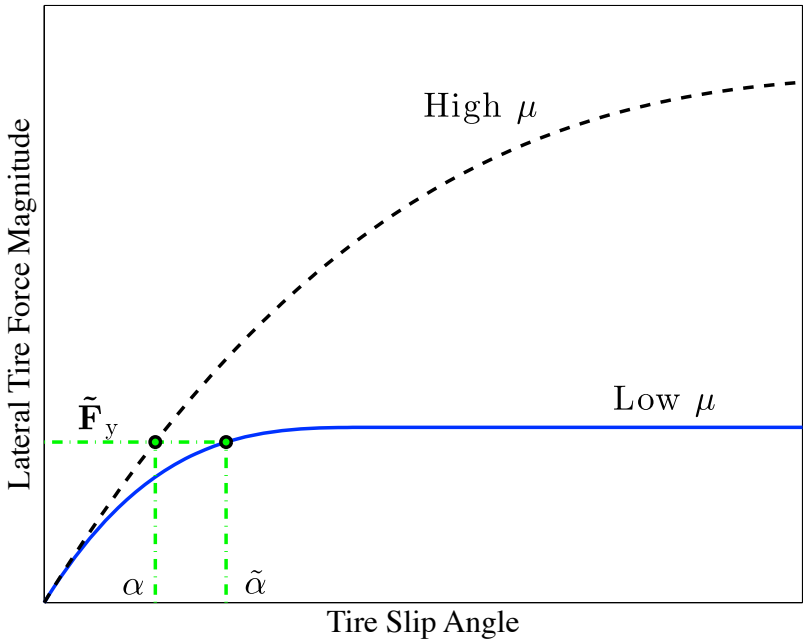

Figure 5.5: Comparison of tire force curves for high and low friction surfaces. The reference model tire force $\tilde{\mathbf{F}}_{\mathrm{y}}$ is computed from the model tire slip angle $\tilde{\alpha}$ using the nonlinear tire model. The controlled vehicle tire force is approximately equal to $\tilde{\mathbf{F}}_{\mathrm{y}}$, and occurs at a lower slip angle α, which is within the linear region of the tire curve.

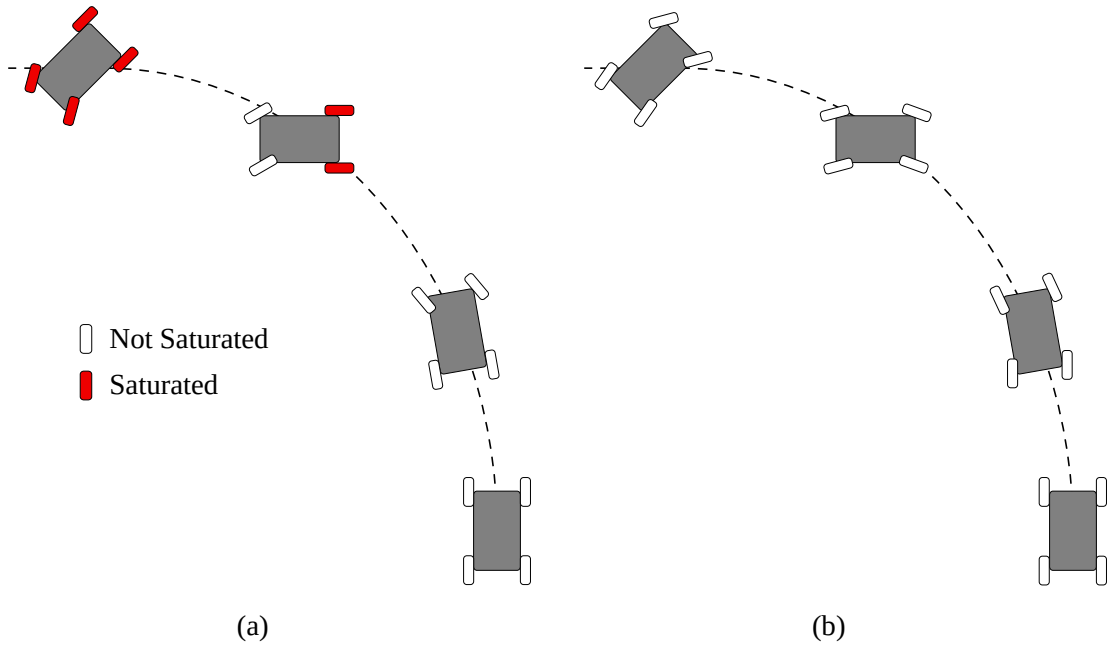

Figure 5.6: Comparison between sliding and steering. (a) Reference vehicle on a low friction surface. As the vehicle enters the turn, the tires saturate and slide, and the vehicle begins to spin. (b) Controlled vehicle on a high friction surface. The front and rear wheels steer out of the turn to reproduce the dynamics in (a), without saturating any of the tires.

value, the controlled vehicle operates at a lower tire slip angle than the reference model, which requires steering the wheels less than the driver commands.

Fig. 5.6 illustrates how the controller emulates a vehicle that starts to spin out. On the left, a reference vehicle on a low friction surface steers into a turn and ends up in a spin because all four tires saturate and therefore slide across the road. On the right, a controlled vehicle on a high friction surface experiences the same dynamics, but by steering the wheels instead of sliding. Initially, the controlled vehicle's steer angles are the same as the reference vehicle, but as the vehicle enters the turn, it steers both front and rear wheels out of the turn to reduce the force generated by the tires. This allows the vehicle to experience the same planar dynamics as the low friction reference model without losing grip on any of the tires.

The remainder of this section will develop the actuator commands for this application, address the issue of actuator limitations, and present some thoughts on unmodeled dynamics.

5.4.1 Converting Desired Force to Actuator Commands

For the low friction emulation application, the desired longitudinal force is a function of the driver's accelerator pedal position x_{p} as defined by

$$F_{\mathrm{xr,des}} = \frac{x_{\mathrm{p}} K_{\tau} K_{\mathrm{gr}}}{R_{\mathrm{w}}}, \tag{5.20}$$

where K_{τ} is the mapping from accelerator pedal position to drive motor torque, K_{gr} is the gear ratio of the transmission, and R_{w} is the wheel effective radius. The generation of the reference model dynamics through the Coupled Brush Tire Model (5.7–5.8) uses this definition of $F_{\mathrm{xr,des}}$ to compute σ_{x}.

Solving for the actuator commands requires converting the expressions for the general axle forces $\{F_{1\mathrm{x}}, F_{1\mathrm{y}}, F_{2\mathrm{x}}, F_{2\mathrm{y}}\}$ into the tire coordinate frame $\{F_{\mathrm{yf}}, F_{\mathrm{yr}}, F_{\mathrm{xr}}\}$, then finding commands for the steer angles, drive motor, and brakes that achieve these forces. The relationships between general axle forces and tire forces from (5.10) are simplified using small angle approximations on the steer angles.

$$\begin{aligned} F_{1\mathrm{y}} &= F_{\mathrm{yf}} \\ F_{1\mathrm{x}} &= 0 \\ F_{2\mathrm{y}} &= F_{\mathrm{yr}} \\ F_{2\mathrm{x}} &= F_{\mathrm{xr}} \end{aligned} \tag{5.21}$$

The small angle approximation is not required to find the tire forces from the general axle forces. If the full nonlinear expressions in (5.10) are desired, it would be straightforward to implement the solution of actuator commands with a lookup table.

Since the controlled vehicle is on a high friction surface while emulating a vehicle on a low friction surface, the actuated lateral tire force remains in the linear region of the tire force versus slip angle curve. This is evident from the force matching diagram

in Fig. 5.5. Therefore, it is reasonable to use a linear tire force model rather than a brush tire model when solving for actuator commands.

$$\begin{aligned} F_{\mathrm{yf}} &= -C_{\alpha\mathrm{f}}\alpha_{\mathrm{f}} \\ F_{\mathrm{yr}} &= -C_{\alpha\mathrm{r}}\alpha_{\mathrm{r}} \end{aligned} \tag{5.22}$$

Similarly, the tire slip angle model uses a small angle approximation for the controlled vehicle.

$$\begin{aligned} \alpha_{\mathrm{f}} &= \frac{U_{\mathrm{y}} + ar}{U_{\mathrm{x}}} - \delta_{\mathrm{f}} \\ \alpha_{\mathrm{r}} &= \frac{U_{\mathrm{y}} - br}{U_{\mathrm{x}}} - \delta_{\mathrm{r}} \end{aligned} \tag{5.23}$$

With these simplifications, the controlled steer angles become the following.

$$\delta_{\mathrm{f}} = \frac{1}{C_{\alpha\mathrm{f}}}F_{\mathrm{yf}} + \frac{1}{\tilde{U}_{\mathrm{x}}}\tilde{U}_{\mathrm{y}} + \frac{a}{\tilde{U}_{\mathrm{x}}}\tilde{r} \tag{5.24}$$

$$\delta_{\mathrm{r}} = \frac{1}{C_{\alpha\mathrm{r}}}F_{\mathrm{yr}} + \frac{1}{\tilde{U}_{\mathrm{x}}}\tilde{U}_{\mathrm{y}} - \frac{b}{\tilde{U}_{\mathrm{x}}}\tilde{r} \tag{5.25}$$

The longitudinal force F_{xr} is controlled through the drive motor torque τ_{m} and the brake force F_{b}. The drive motor applies positive (accelerating) forces on the rear axle, while the brakes apply negative (decelerating) forces split equally between the front left and front right wheels.

$$\tau_{\mathrm{m}} = \begin{cases} \dfrac{R_{\mathrm{w}}}{K_{\mathrm{gr}}}F_{\mathrm{xr}}, & F_{\mathrm{xr}} > 0 \\ 0, & F_{\mathrm{xr}} \leq 0 \end{cases} \tag{5.26}$$

$$F_{\mathrm{b}} = \begin{cases} 0, & F_{\mathrm{xr}} \geq 0 \\ F_{\mathrm{xr}}, & F_{\mathrm{xr}} < 0 \end{cases} \tag{5.27}$$

Table 5.1: Feedback gains

Gain	Value	Units
K_1	-30000	$\mathrm{N \cdot m \cdot s}$
K_2	3000	$\mathrm{N \cdot s}$
K_3	3000	$\mathrm{N \cdot s}$
K_4	-30000	$\mathrm{N \cdot s \cdot m^{-1}}$
K_5	-10000	$\mathrm{N \cdot s \cdot m^{-1}}$
K_6	-75000	$\mathrm{N \cdot m \cdot s}$

5.4.2 Feedback Gain Selection

The feedback gains $\{K_i\}$ can be chosen with any desired method that results in good tracking and stability. Table 5.1 lists the numerical values chosen for the low friction emulation application. K_1, K_2, K_3, and K_4 were selected with a linear-quadratic regulator (LQR) using a two-state bicycle model based on (5.9), then confirmed experimentally. K_5 was hand-tuned via simulation and experiment. The error dynamics can also be analyzed in terms of error time constants; for the gains chosen here, e_{r} and e_{y} have similar time constants (about 0.07 ms), while e_{x} is somewhat slower (0.2 ms). This choice of gains strikes a good balance between fast error dynamics and reasonable actuator force/torque requirements. Additionally, it is straightforward to show that these gains satisfy (5.16), so the closed loop system is stable.

5.4.3 Incorporating Actuator Range Limitations

In any vehicle there is a limit to how far the wheels can steer. This means that it may be impossible to generate a desired lateral force on a particular axle. When a wheel reaches its steering angle limit, it cannot generate additional lateral force, so it loses the ability to be an arbitrary control input. Therefore, the number of states that can be emulated is reduced. For example, if the rear wheels reach their actuation limit, the rear lateral force F_{yr} is limited, so only longitudinal force F_{xr} and front lateral force F_{yf} are available as control inputs. When this occurs, it is important that the vehicle exhibit safe and predictable behavior, so that the vehicle

dynamics continue to be as close as possible to the reference model. The following development explores how to modify the controller in the case of actuator saturation for low friction emulation.

For this application, it is indeed the rear wheels that reach their actuation limit first, which typically occurs when the reference model exhibits the large lateral velocity indicative of a spinout. The controller as formulated originally can still track the longitudinal velocity, but there is a choice to be made between lateral velocity and yaw rate as the desired state to track with the front steering actuator. Yaw rate is the logical choice because it better maintains the overall emulation performance. It is important to keep the vehicle turning in the same direction as the driver is steering, which is easily achieved by tracking the yaw rate of the reference model. If the controlled state is lateral velocity instead, the uncontrolled yaw rate can go the opposite direction as the driver's command, which is very disconcerting for the driver. In addition, the initial cues of low friction dynamics are the most important for the lane change task used in the driver adaptation studies, since the course straightens out after the lane change. Therefore yaw rate is the right choice for these studies.

It is straightforward to modify the controller to handle this situation. First, assume the rear steer angle has saturated to its maximum value. Since the rear lateral tire force is no longer equal to the desired force F_{yr}, its value $\hat{F}_{\mathrm{yr}}$ must be estimated from the measured vehicle states.

$$\delta_{\mathrm{r}} = \pm\delta_{\mathrm{r,max}} \tag{5.28}$$

$$\hat{F}_{\mathrm{yr}} = -C_{\alpha\mathrm{r}}\left(\frac{1}{U_{\mathrm{x}}}U_{\mathrm{y}} - \frac{b}{U_{\mathrm{x}}}r - \delta_{\mathrm{r}}\right) \tag{5.29}$$

With only yaw rate and longitudinal velocity to track, the desired error dynamics simplify to

$$\begin{aligned} I_{\mathrm{z}}\dot{e}_{\mathrm{r}} &= K_6 e_{\mathrm{r}} \\ m\dot{e}_{\mathrm{x}} &= K_5 e_{\mathrm{x}} \end{aligned} \tag{5.30}$$

which results in the following required forces.

$$F_{\mathrm{yf}} = \frac{1}{a}\left(\tilde{\mathbf{M}}_{\mathrm{z}} + b\hat{F}_{\mathrm{yr}} - K_6 e_{\mathrm{r}}\right) \tag{5.31}$$

$$F_{\mathrm{xr}} = \tilde{\mathbf{F}}_{\mathrm{x}} + m\left(\tilde{r}\tilde{U}_{\mathrm{y}} - rU_{\mathrm{y}}\right) - K_5 e_{\mathrm{x}} \tag{5.32}$$

Compared to the nominal controller from (5.13), the longitudinal force equation is unchanged, while the front lateral force equation is much simpler and only depends on the desired yaw moment and the measured rear lateral force. The closed loop system is still LTI and the conditions on stability are simply $K_6 < 0$ and $K_5 < 0$. Finally, the equation for the front steer angle must be modified slightly from (5.24) to reflect that the controller no longer tracks the reference lateral velocity $\tilde{U}_{\mathrm{y}}$.

$$\delta_{\mathrm{f}} = \frac{1}{C_{\alpha\mathrm{f}}}F_{\mathrm{yf}} + \frac{1}{\tilde{U}_{\mathrm{x}}}U_{\mathrm{y}} + \frac{a}{\tilde{U}_{\mathrm{x}}}\tilde{r} \tag{5.33}$$

5.4.4 Unmodeled Roll Dynamics

The reference model presented in this paper is a planar model, so it does not account for vehicle body roll angle. However, roll is an important component of vehicle handling and therefore an analysis of the success of a vehicle dynamics emulation scheme should consider it. As the vehicle maneuvers, roll is generated through the suspension due to the lateral acceleration of the vehicle, which comes from the lateral tire forces. If the tire forces are small, the roll rate and roll acceleration – the roll dynamics – are also small. When the vehicle rolls, the planar dynamics change due to their coupling with the roll dynamics, although this effect is secondary to the dynamics produced directly from tire forces. In addition, the tire forces themselves are affected by roll, which comprises one component of lateral load transfer. To account for these secondary coupling effects, the reference model can be extended out-of-plane as a yaw-roll model, which would result in slightly modified desired states, tire forces, and yaw moment. Even if the reference model is planar, the roll angle of the controlled vehicle should be nearly the same as it would be for a more complex reference model, since the tire forces applied to the controlled vehicle consist primarily of feedforward

terms that are identical to the reference model tire forces, assuming that the reference model and the controlled vehicle have the same suspension parameters. The controller structure treats changes in tire force caused by the roll dynamics as disturbances that are compensated by the feedback terms.

For the application of low friction emulation, the maximum lateral acceleration of the vehicle is small due to the limited tire force capability of the reference model. Therefore, the roll dynamics are also limited and the difference between the reference and controlled vehicle roll is particularly small. Although there will be small differences, this approach to handling modification preserves the general roll dynamics of the vehicle. In contrast, a mechanical emulation approach such as the SKIDCAR [31] drastically changes the vehicle's roll characteristics, since caster frames support most of the vehicle's mass and the tire forces do not couple with the roll dynamics in the same way they would in typical vehicle operation.

5.5 Low Friction Emulation Experimental Results

This section presents experimental results of the handling emulation controller, as applied to low friction emulation. The controller is demonstrated for reference model friction coefficient values ranging from 0.1 to 0.4. All experimental data is from open loop maneuvers in the sense that the driver does not follow a prescribed path, but steers and accelerates freely. The particular experimental maneuvers presented here were chosen to demonstrate the ability of the controller to track the reference model for a range of friction coefficients and varied dynamic maneuvers (slalom, step, etc.) and to show the performance of the controller with a steering actuator limitation (Sec. 5.5.3).

5.5.1 Experimental Setup

The X1 electric research vehicle, pictured in Fig. 2.3, implements the low friction emulation controller experimentally. The key features of the vehicle that enable the controller are independent four-wheel steer-by-wire controllers, independent four-wheel

electrohydraulic braking, rear-wheel drive-by-wire, and vehicle state measurements from a tightly coupled GPS/inertial sensor system. More details about the test vehicle are provided in Section 2.2 and the vehicle parameters used for the experiments are tabulated in Table 2.1. All experiments in this chapter were performed at Thunderhill Raceway Park in Willows, CA on an asphalt lot with friction coefficient of about 0.85 and average slope of about 2.5°; the orientation of the car with respect to the slope varied by experiment.

The reference model for these experiments follows the dynamics presented in (5.2), with the tire forces given by (5.7–5.8) for the rear axle and by (5.4) for the front axle. All four wheels have the same friction coefficient μ between 0.1 and 0.4. The cornering stiffnesses for the reference model are reduced by a factor of three from the values shown in Table 2.1 to reflect the properties of lower friction surfaces.

5.5.2 $\mu = 0.1$ – Slalom Maneuver

Fig. 5.7 shows experimental data for the controller with reference model friction coefficient $\mu = 0.1$. The experiment consists of a sequence of slalom steer maneuvers at about 1/3 Hz, the first at a longitudinal velocity of 5 m/s and the second at 6 m/s. The top three axes in the figure compare the reference and controlled vehicle states: (a) yaw rate, (b) lateral velocity, and (c) longitudinal velocity. All three controlled vehicle states track the corresponding reference states well throughout the dynamic maneuver, indicating that this controller is successful in the goal of emulating the dynamics of the low friction reference model. The increased speed in the second slalom maneuver results in larger lateral velocities, which indicate that the reference vehicle is nearing tire saturation.

Fig. 5.7(d) compares the driver's commanded front steer angle with the front and rear steer angles applied by the low friction emulation controller. The controlled front steer angle is in the same direction as the driver's command, but with lower magnitude and blunted peaks. This corresponds to the front wheels steering less in order to produce less lateral force than they would at the driver's commanded steer angle, which is consistent with the limited force capability of the low friction reference

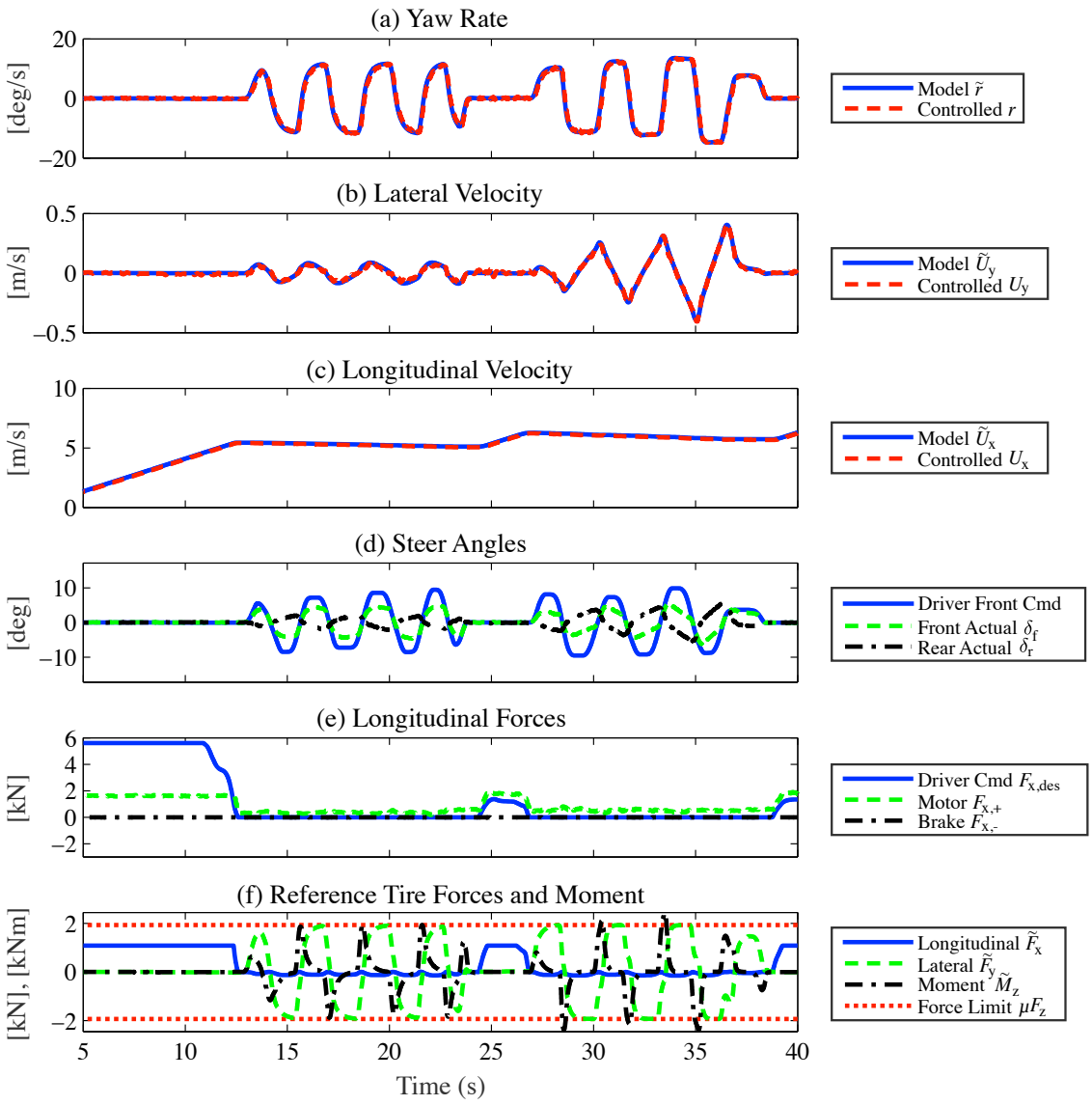

Figure 5.7: Experimental maneuver with reference model friction coefficient $\mu = 0.1$.

model. The rear wheels steer in the opposite direction as the front wheels and exhibit a phase lag.

In Fig. 5.7(e), the driver's desired longitudinal force $F_{\mathrm{x,des}}$ is compared with the longitudinal force applied to the controlled vehicle through the drive motor ($F_{\mathrm{x},+}$) and brakes ($F_{\mathrm{x},-}$). When the driver requests longitudinal force during the early part of the experiment, the controller significantly limits the force that is actually applied to the wheels. This reflects the limited force capability of the tires in the low friction reference model. For the driver of the controlled vehicle this manifests as the feeling that the vehicle is accelerating much more slowly than would be expected on a dry asphalt surface. In the sections of the experiment where the motor force exceeds the driver's command, the longitudinal control is overcoming unmodeled effects including road grade and aerodynamic drag in order to track the reference speed.

Finally, Fig. 5.7(f) shows the tire forces and yaw moment from the reference model. The total lateral force repeatedly reaches the friction-limited maximum value, which means the tires of the reference model are beginning to saturate. However, the driver steers out of the turn in time to avoid the reference model spinning out.

5.5.3 $\mu = 0.3$ – Steering Actuator Limitation

In contrast to the results in Fig. 5.7, where the controlled vehicle tracks all three reference states during the entire maneuver, Fig. 5.8 demonstrates what happens when the rear steer angle reaches its limit. When this occurs, the modified controller developed in Sec. 5.4.3 tracks yaw rate and longitudinal velocity, leaving lateral velocity uncontrolled. In the early part of the maneuver, the dynamics look similar to Fig. 5.7 with all three planar vehicle states tracking the reference model well. Just after 97 seconds, however, the reference lateral force saturates, causing the magnitude of the model's lateral velocity to increase rapidly, which corresponds to a spinout. This occurs because the driver commands a large longitudinal force (Fig. 5.8(e)) at this time, causing the rear tires of the reference model to saturate due to the coupled tire model. When the rear steer angle reaches its limit the controlled lateral velocity does not track the reference model, although the yaw rate and longitudinal velocity still

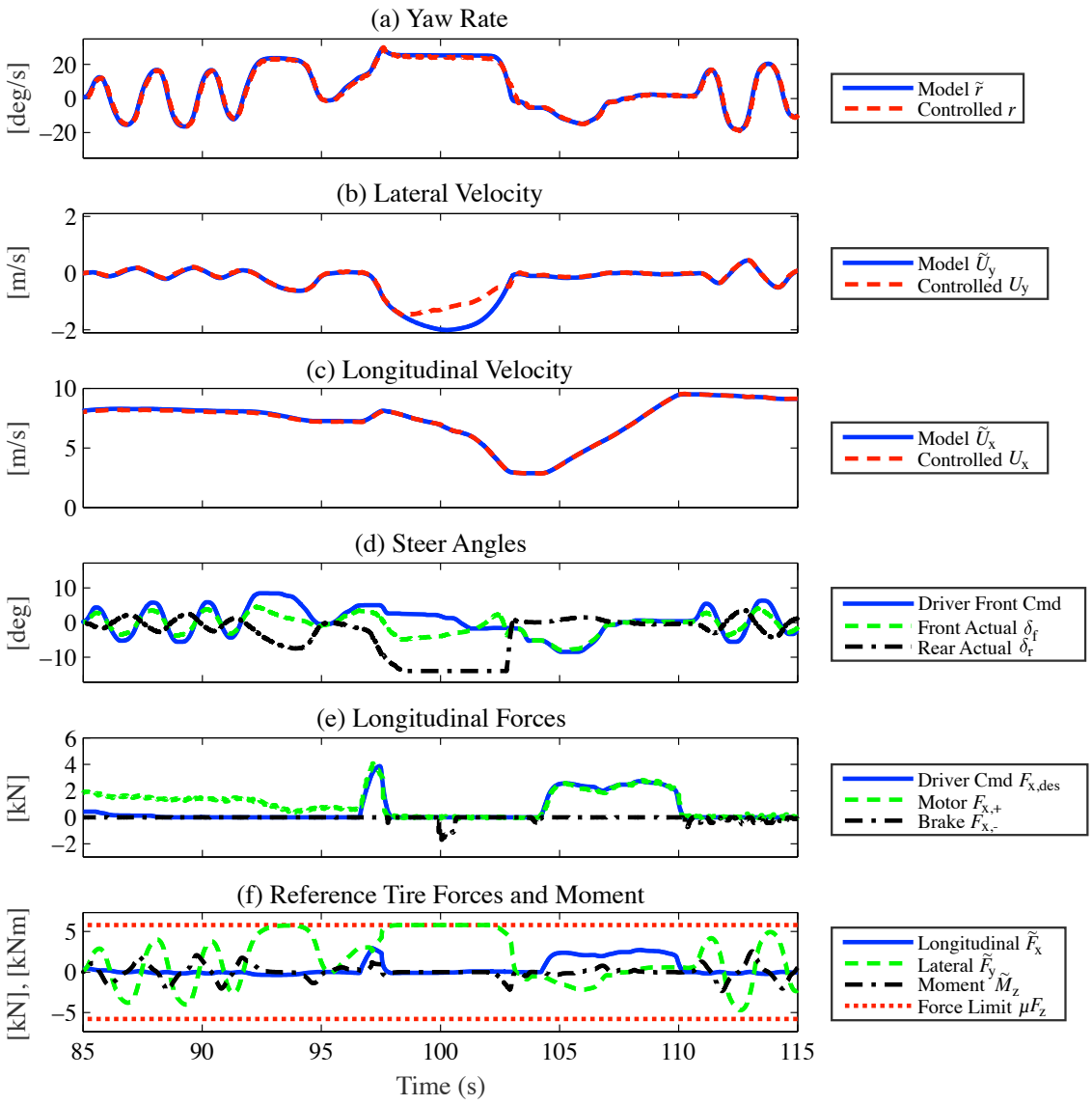

Figure 5.8: Experimental maneuver with reference model friction coefficient $\mu = 0.3$.

track closely. At about 103 seconds, the lateral velocity and yaw rate both recover to small values as the driver steers out of the turn and reduces the longitudinal velocity, resulting in all vehicle states tracking again. This steering actuator limitation can occur with any reference model friction coefficient; whether the limit is reached depends on the combination of steering wheel and accelerator pedal inputs the driver applies.

5.5.4 $\mu = 0.4$ – Step Inputs

A third experiment, shown in Fig. 5.9, demonstrates the performance of the low friction emulation controller when the driver steering command consists of a slalom maneuver followed by several approximate step inputs with the reference model friction coefficient equal to 0.4. Even when the steering command changes quickly (on the order of 30°/s), the controlled vehicle tracks all states of the reference model dynamics very well. This illustrates the value of including tire force feedforward in the control scheme: since feedback requires error to produce control forces, the response from feedback alone will lag the command regardless of the choice of feedback structure. The feedforward forces cause an immediate response to a change in steering command before error builds up. In addition, the state tracking performance of all the data sets presented in Fig. 5.7–5.9 shows that the simplified models used to compute actuator commands for low friction emulation are appropriate for a range of reference model friction coefficients.

5.6 Future Research Directions

The handling emulation controller developed in this chapter has been demonstrated experimentally for the application of low friction emulation. There are two extensions that would expand the capabilities of the controller to allow emulation of a more varied range of handling conditions.

First, the low friction emulation application is currently limited by the range of the steering actuators on the X1 vehicle so that the maximum achievable sideslip

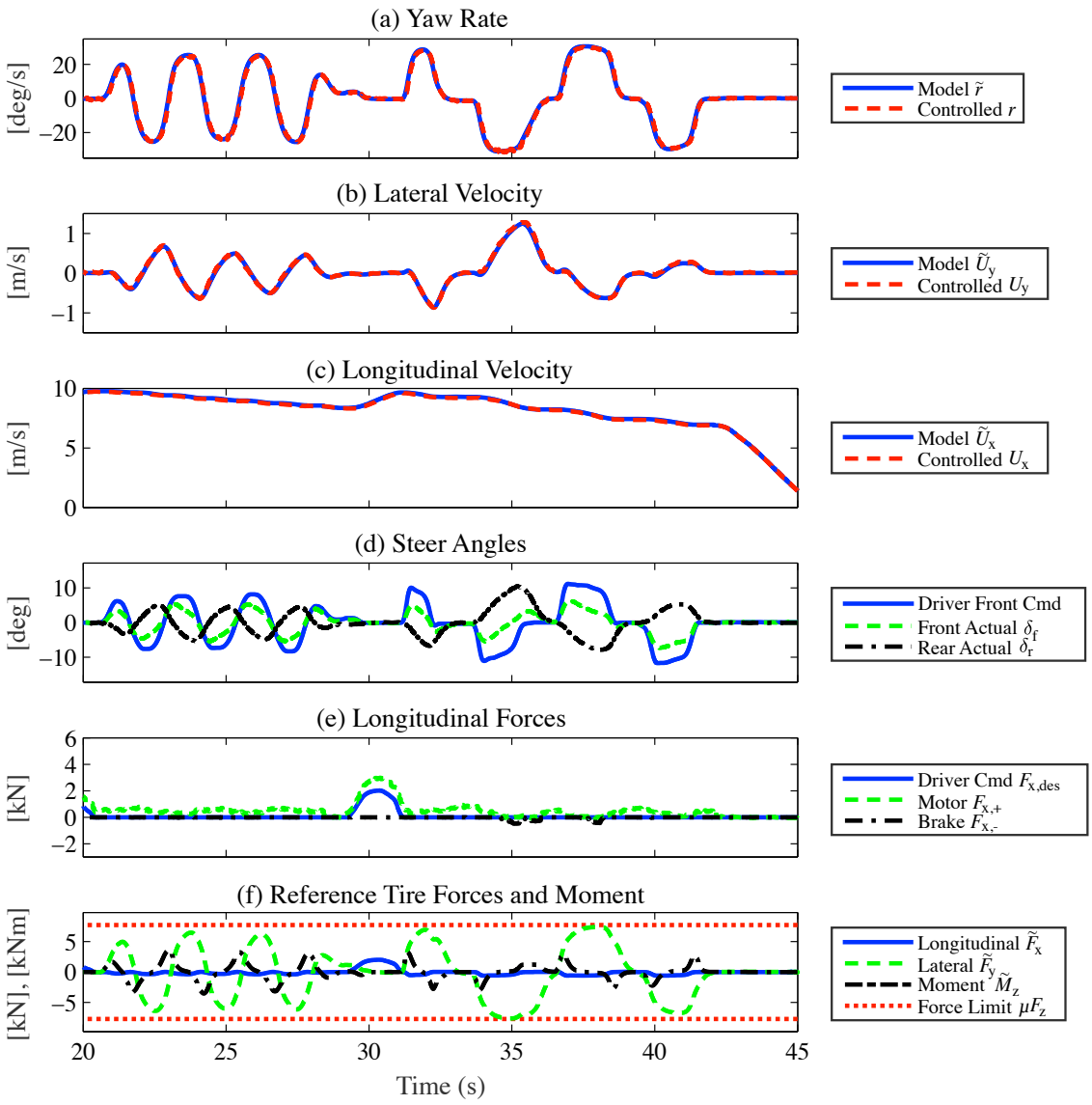

Figure 5.9: Experimental maneuver with reference model friction coefficient $\mu = 0.4$.

angle $\beta = \text{atan}(U_y/U_x)$ is approximately 10–14° depending on the reference model parameters. Large and quickly increasing sideslip angles signal to the driver that the vehicle is starting to spin; sideslip angles of at least 20° would be more realistic for this situation. Increasing the rear steering range from its current value of ±14° to ±45° would allow sideslip angles in the range of 20–30°, improving the ability of the controller to emulate extreme limit situations. Expanding the actuator range would also require a reformulation of the actuation-limited controller (Sec. 5.4.3) to ensure the desired yaw rate tracking performance is maintained in all situations.

Second, the handling emulation controller can be extended to emulate other handling changes. The formulation of the controller in Sec. 5.3 limits the handling emulation to differences in the tire forces through friction coefficient, cornering stiffness, etc. because the physical parameters (mass, length, etc.) of the experimental vehicle and the emulated vehicle are assumed to be the same. Removing this restriction enables emulation of additional handling changes. The necessary tire forces in this case are derived in Appendix C. It should be noted that the linear tire model assumption does not hold for the experimental vehicle in this case, so an alternative method should be used to convert desired tire forces to actuator commands.

5.7 Conclusion

This chapter has demonstrated a method for modifying the handling dynamics of a vehicle with a tire force-based model-following approach. This method can emulate any planar reference dynamics model up to the physical limits of the tires by controlling the front and rear steer angles, the drive torque, and the braking force. The formulation of the controller – combining feedforward, nonlinear feedback, and linear feedback – results in linear error dynamics that allow straightforward analysis of stability. The control strategy extends easily to treat other desired improvements to vehicle handling, including compensation for changes in mass distribution or cornering stiffness.

Applying this approach to the problem of emulating the dynamics of a vehicle on a low friction surface results in a safe, stable way for drivers to experience nonlinear

limit behavior of the vehicle similar to driving on an icy surface. The low friction emulation controller tracks the planar dynamics of the reference low friction vehicle and gracefully handles limitations of steering actuators. This control scheme enables the study of driver adaptation to realistic handling changes including low friction road conditions. In the following chapter, the low friction emulation controller is combined with the user study protocol to investigate driver adaptation to this critical handling situation, demonstrating that in this case adaptation is dependent on individual driving style.

Chapter 6

Adaptation to Low Friction Dynamics

The user study results presented in Chapters 3 and 4 demonstrated that drivers adapt to steering ratio scaling and steering direction reversal and are robust to steering torque increases. These results made a link between adaptation in arm reaching studies and steering a car and contributed evidence that drivers use angle rather than torque as the steering control variable.

This chapter discusses the results of the final user study to explore adaptation to another realistic driving scenario: encountering a low friction surface like an icy road. This study uses the low friction emulation controller developed in Chapter 5 to simulate changing road conditions in a controlled, repeatable manner. The protocol for this study, pictured in Fig. 6.1, follows the familiar sequence of trials, with baseline handling consisting of 15:1 steering ratio, nominal steering torque from the full steering feel emulator model (see Section 2.3.1), and the low friction emulation controller disabled so participants experience the actual friction coefficient of the parking lot (approximately 0.9). In the adaptation block, the low friction emulation controller is enabled with $\mu = 0.15$ and the steering feel emulator is modified by increasing the power assist weighting function standard deviation parameter σ from 0.03 to 0.04 to reflect the effect of the decreased friction. Only the lateral and yaw dynamics of the low friction emulation controller are modified so that the vehicle speed can still be regulated by cruise control at the target speed of 8 m/s for consistency among subjects.

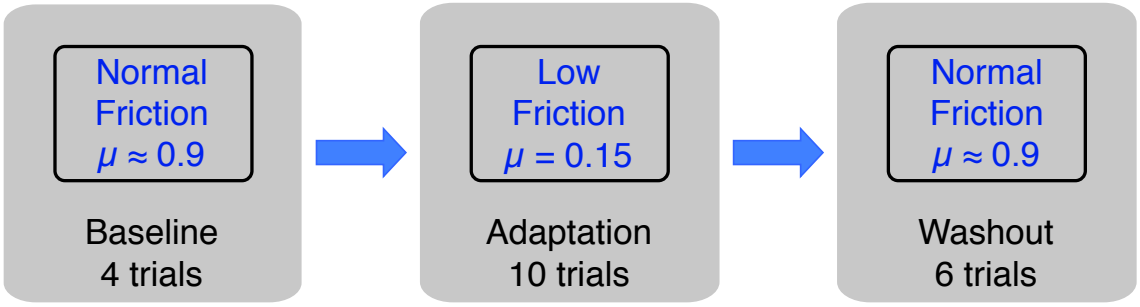

Figure 6.1: Adaptation protocol for low friction study.

The handling change in this study is more complex than the other handling changes, each of which only changed a single variable: either the steering ratio, the steering direction, or the steering torque. The low friction emulation controller makes the mapping from steering commands to vehicle dynamics a nonlinear function by steering both the front and rear wheels in a way that is different from the driver's commands. It limits the amount of lateral force at the front tires, effectively reducing the steering ratio, while at the same time steering the rear wheels. The steering torque is also modified, although based on the results from Chapter 4 this alone should not cause changes in driver steering behavior. The key question for this study, then, is do drivers adapt to this more complex handling change? If so, does the adaptation process still result in the same exponential learning curves? Are there other considerations that need to be made for this handling condition?

6.1 Study Participants

This study was conducted with fourteen participants aged 21 to 33 years with a median age of 27.5 years. Driving experience ranged from 5 to 17 years with a median of 9.5 years. There were eight men and six women; one participant was left-handed and the remainder were right-handed. The participants reported no neurological impairments. This was a distinct set of participants from the other three user studies.

6.2 Sample Participant Data

Fig. 6.2 shows the steering wheel angle traces and vehicle paths for a sample participant in this study. As before, all steering angle traces are normalized for a left turn for visualization, although participants performed an equal number of left and right turns. Note, however, that the plot shows the steering wheel angle and not the road wheel angle as in the prior studies; this is because the road wheel angle as controlled by the low friction emulation controller during the adaptation block does not directly reflect the driver's steering inputs.

As in the prior studies, the steering angles for this participant during the baseline (green) block of trials were smooth and consistent, steering first in one direction to make the lane change, then in the other direction to straighten the car relative to the gate, resulting in two clear local maximum steering angles following the signal light trigger. When the emulated friction was reduced for the first trial of the adaptation block (blue), the first steering peak was nearly twice as large as during the baseline trials, and the second steering peak was equally large and held constant for several meters along the course before returning to center. This large steering motion was not adequate to prevent the vehicle from hitting a cone (see black trace at top of Fig. 6.2B), so the trial ended a few meters before the end of the course. On subsequent trials with the reduced friction, the participant continued to make large steering motions, managing to avoid hitting cones on any other trials and gradually reducing the magnitude of the steering motions on later adaptation trials. When the friction coefficient returned to the baseline value in the washout block, the magnitude of the steering angle was reduced and the steering motion recovered its simple double-peaked characteristic. Compared to baseline, the steering motion was slower. Aside from Trial 5, the driver successfully completed all trials, but the vehicle paths (Fig. 6.2B) showed some variability, particularly during the adaptation block.

In contrast to this participant, a second sample participant made consistently smooth steering wheel angle motions throughout the entire study (Fig. 6.3). This participant made smaller steering motions that lasted longer compared to the first participant, making the lane change more gradually. The vehicle paths (Fig. 6.3B)

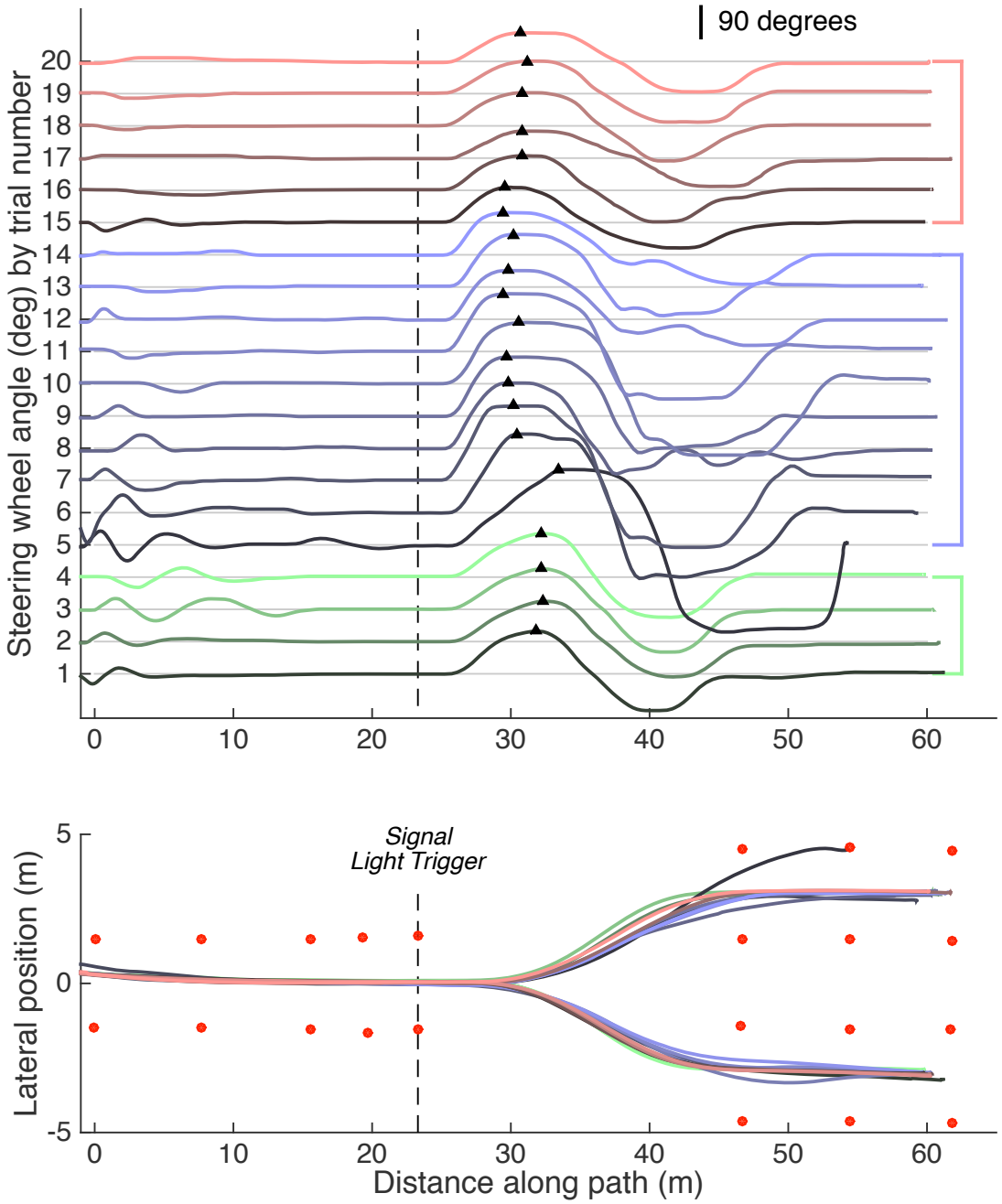

Figure 6.2: Sample data for User Study #4 (low friction dynamics), participant 1. (A) Steering wheel angle traces as a function of distance along the path for each trial, with black triangles denoting the local maximum steering angle. (B) Paths taken by the vehicle, with the vertical axis not-to-scale with the horizontal for ease of visualization.

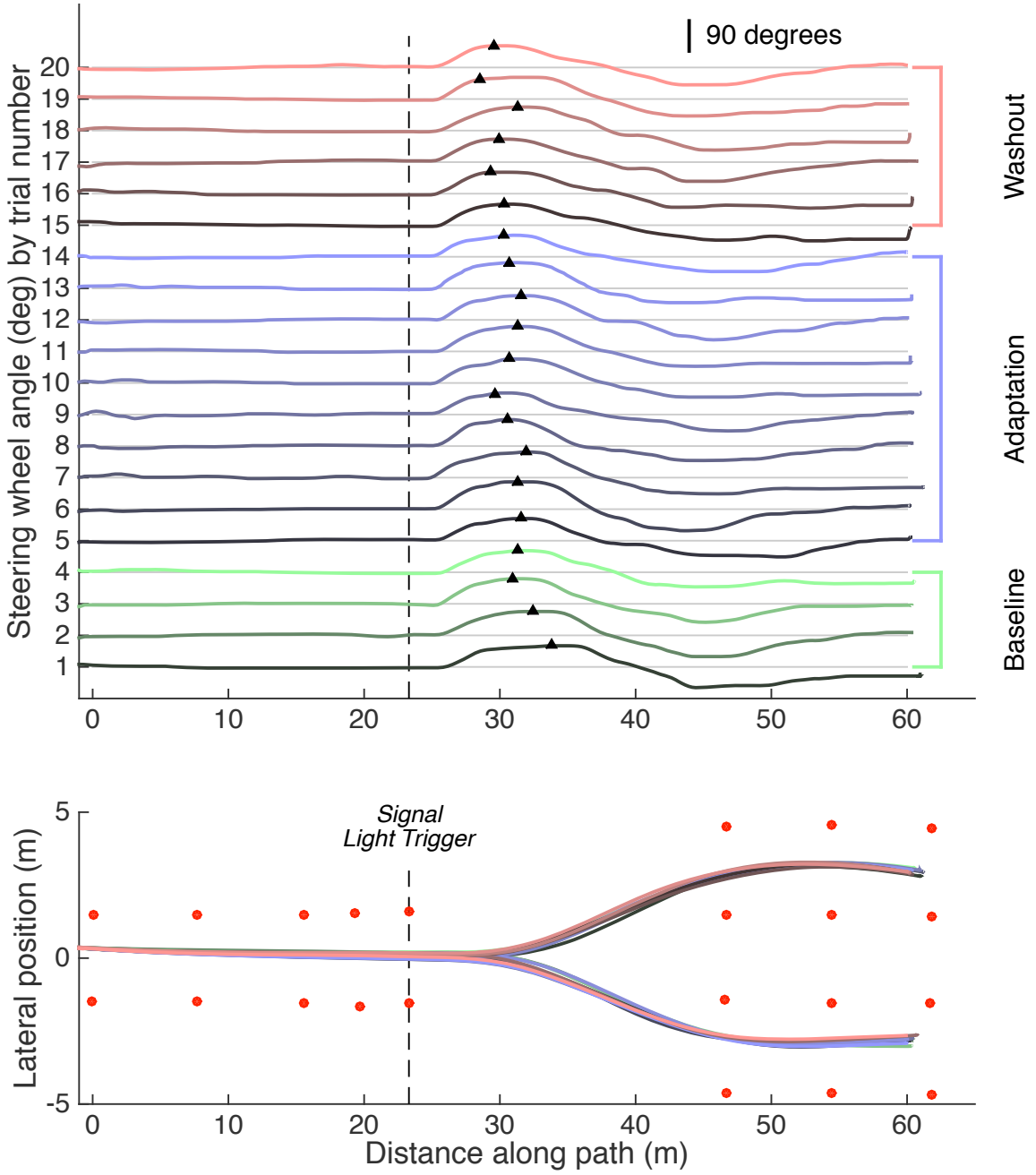

Figure 6.3: Sample data for User Study #4 (low friction dynamics), participant 2. (A) Steering wheel angle traces as a function of distance along the path for each trial, with black triangles denoting the local maximum steering angle. (B) Paths taken by the vehicle, with the vertical axis not-to-scale with the horizontal for ease of visualization.

were consistent for all trials and the lack of clear difference between the steering traces suggests that this participant did not have any trouble completing the task when the low friction emulation controller was activated during the adaptation block.

Because of the role of lateral acceleration in vehicle handling dynamics, it is likely that the diversity in steering behavior between the participants in this study reflects their experience of different levels of handling change during the adaptation block. At low levels of lateral acceleration, vehicle dynamics are consistent for road surfaces with a range of friction coefficients. As lateral acceleration increases, the vehicle dynamics become highly nonlinear for low friction surfaces as the tire forces saturate to their limits. On high friction surfaces it takes much higher levels of lateral acceleration to reach the tire limits. Attempting to reach high lateral acceleration while on a low friction surface results in a strong experience of the nonlinear vehicle dynamics. Therefore, participants who kept the lateral acceleration at lower levels by their choice of steering inputs experienced small changes in vehicle handling during the low friction adaptation block, while those who attempted to reach higher lateral acceleration experienced much greater handling changes.

6.3 Dividing Participants into Groups

Since lateral acceleration is related to the amount of low friction handling change experienced by the participants, a lateral acceleration threshold is a useful way to group the participants. The method of determining a grouping based on lateral acceleration and the precise threshold for dividing the participants is somewhat arbitrary. However, one important point is to ensure that only the baseline trials are used for the grouping; this allows classification based on the nominal driving style of each participant without the confounding effect of the handling change.

Lateral acceleration a_{y} is related to vehicle states and tire forces through the following equation for the single-track bicycle model (illustrated in Fig. 5.4).

$$a_{\mathrm{y}} = \dot{U}_{\mathrm{y}} + rU_{\mathrm{x}} = \frac{1}{m}\left(F_{\mathrm{yf}} + F_{\mathrm{yr}}\right) \tag{6.1}$$

A raw measurement of lateral acceleration is available on X1, but it includes the effects of suspension dynamics that cause oscillations at frequencies near 3 Hz, resulting in lateral acceleration spikes that are not relevant to understanding driver behavior. One way of dealing with this unwanted frequency content is to filter the acceleration signal; this is a reasonable option that requires choice of filter structure and parameters. Another method that is straightforward to achieve with readily available measurements is to approximate the lateral acceleration as $a_{\mathrm{y}} = rU_{\mathrm{x}}$, which is also the expression for lateral acceleration in a steady-state turn. Although this approximation neglects the rate of change of lateral velocity that actually occurs during the lane change, the discrepancy is minor for this application. Therefore, the approximate value of lateral acceleration is used instead of the raw measurement for the classification of participants in this study.

The threshold chosen for this study is $a_{\mathrm{y}} = 2.1$ m/s^2, which corresponds to 25% of the maximum achievable lateral acceleration on the high friction road surface. Drivers who exceeded this threshold at *any* time were assigned to Group 1, even if they stayed below the threshold for some trials, and those whose lateral acceleration *always* stayed below the threshold were assigned to Group 2, as depicted in Fig. 6.4. This resulted in nine participants in Group 1 and five participants in Group 2.

The results of the classification are demonstrated for the four adaptation metrics in Fig. 6.5 with individual data points to highlight the two groups. There is no clear difference between the groups in steering reversal rate (Fig. 6.5A) or time to steering peak (Fig. 6.5C), but the difference is notable for the the other two metrics. With few exceptions, participants in Group 1 who chose higher lateral acceleration during the baseline block had higher steering velocity (Fig. 6.5B) and yaw jerk (Fig. 6.5D) for the entire experiment than those in Group 2. Group 1 also experienced much larger changes in these two metrics when the low friction condition was applied for the adaptation block (beginning with Trial 5), indicating that they experienced a significant handling change to which they needed to adapt. Group 2 showed only small changes in these metrics during the low friction condition, suggesting that the handling change they experienced was limited. These results show that using a lateral acceleration threshold is a useful way to group participants for this handling change.

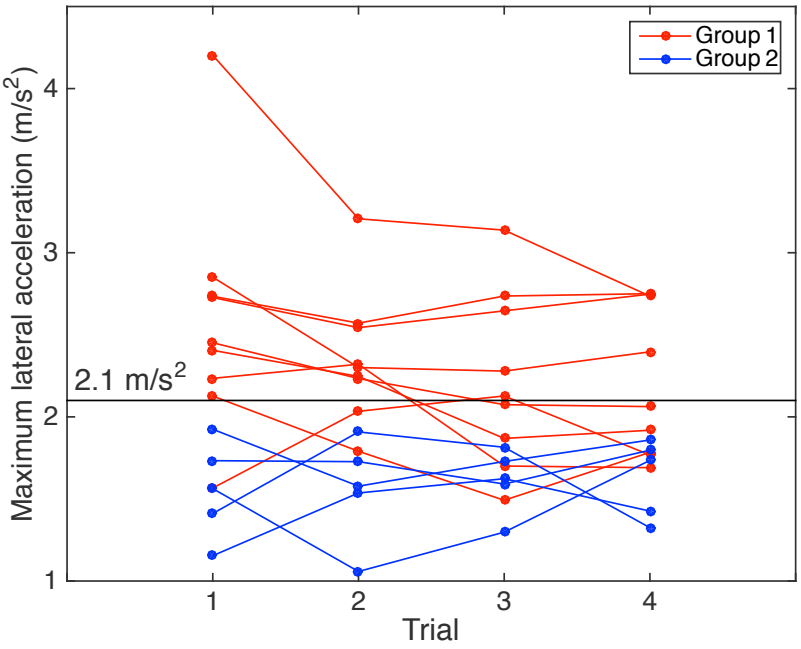

Figure 6.4: Classification of participants based on maximum lateral acceleration during the baseline block (Trials 1-4).

A one-way repeated measures ANOVA performed on the entire set of participants revealed significant differences between experimental stages (last baseline trial, first adaptation trial, etc.) for all metrics except steering reversal rate (Table D.5). There were also significant differences between participants for all metrics but time to steering peak, suggesting that there was an effect of driving style. After dividing the participants into groups with the lateral acceleration threshold, a two-way ANOVA (Table D.6) with experiment stage and driving style group as the two fixed factors revealed significant differences between groups for RMS steering velocity ($F(1,60) = 40.80$; $p = 2.75\text{e-}8$) and RMS yaw jerk ($F(1,60) = 37.38$; $p = 7.92\text{e-}8$), with no significant differences between groups for steering reversal rate ($F(1,60) = 0.17$; p=0.677) and time to steering peak ($F(1,60) = 1.95$; p=0.168). These results are consistent with Fig. 6.5 where there is clear visual separation between the two groups for the RMS metrics but not for the other metrics.

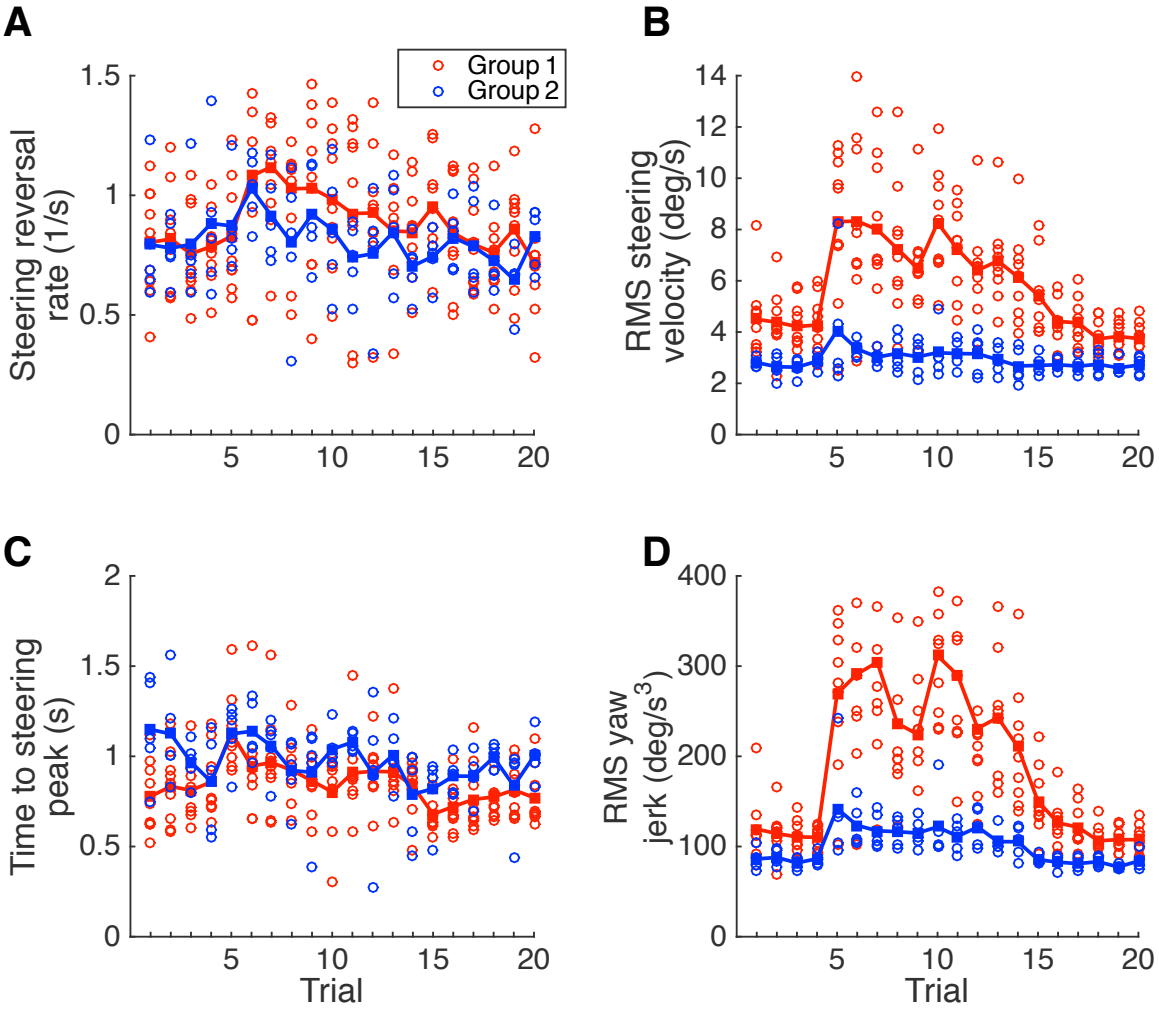

Figure 6.5: Metrics grouped by participant driving style for User Study #4 (low friction dynamics). (A) Steering reversal rate (SRR). (B) RMS steering velocity. (C) Time to steering angle peak. (D) RMS yaw jerk. Open circles are individual data points; filled squares and lines are group means based on data points of the corresponding color. $n = 9$ for Group 1, $n = 5$ for Group 2.

6.4 Group Results

Since there were statistically significant differences between the two groups for some metrics, indicating that participants experienced different levels of handling change, analysis of the adaptation process for the low friction study was performed on each group separately. One-way repeated measures ANOVA was performed for each of the four metrics on each group independently, the results of which are summarized in Table 6.1. All metrics except steering reversal rate showed significant differences between experiment stages for Group 1, while there were no statistically significant differences for Group 2. This means that participants in Group 1 changed their steering behavior in response to the low friction perturbation and those in Group 2 were robust to the change. Due to the lack of significant differences for Group 2, it was unnecessary to perform post-hoc comparisons between experiment stages for this group. Fig. 6.5 reveals only slight differences between trials in all metrics for Group 2 (blue) consistent with the ANOVA results.

The learning curves for Group 1 are depicted in Fig. 6.6, with corresponding statistical significance plots in Fig. 6.7. The steering reversal rate (Fig. 6.6A, 6.7A) did not change immediately when the low friction controller was activated in Trial 5, but increased in Trial 6, followed by an approximately linear decay over the course of the adaptation block. The lack of change on Trial 5 resulted in no statistically significant differences between the trials of interest. However, it is clear that drivers used higher steering reversal rates than baseline during subsequent trials with the low friction controller; the fact that this metric returned to baseline indicates that they adapted to the handling change.

Both the RMS steering velocity (Fig. 6.6B, 6.7B) and the RMS yaw jerk (Fig. 6.6D, 6.7D) increased significantly when the simulated friction coefficient was reduced to 0.15. For the first half of the adaptation block, participants decreased the RMS steering velocity toward baseline level, but on Trial 10 there was a sharp increase, followed by decay back toward baseline. By the end of the adaptation block, the RMS steering velocity statistically returned to baseline, so drivers had sufficiently changed their internal models of the modified vehicle dynamics that they no longer

Table 6.1: Summary of repeated measures ANOVA results for Study #4. For Group 1, the uncorrected $df_c = 4$ and $df_e = 32$; for Group 2, the uncorrected $df_c = 4$ and $df_e = 16$. Values of df_c, df_e, and p_{gg} below have been adjusted with Greenhouse-Geisser ϵ corrections for sphericity. Statistically significant p-values at the $\alpha = 0.05$ level are denoted with boldface type.

Group 1 ($n = 9$)

Metric	ϵ	df_c	df_e	$F(df_c, df_e)$	p_{gg}
Steering reversal rate	0.65	2.59	20.68	1.61	0.224
RMS steering velocity	0.51	2.03	16.26	11.43	**8.26e-4**
Time to steering peak	0.52	2.07	16.54	7.96	**3.98e-3**
RMS yaw jerk	0.54	2.15	17.21	19.70	**3.74e-5**

Group 2 ($n = 5$)

Metric	ϵ	df_c	df_e	$F(df_c, df_e)$	p_{gg}
Steering reversal rate	0.44	1.75	7.02	1.51	0.259
RMS steering velocity	0.29	1.16	4.66	1.30	0.318
Time to steering peak	0.47	1.89	7.58	2.36	0.168
RMS yaw jerk	0.29	1.16	4.64	4.12	0.112

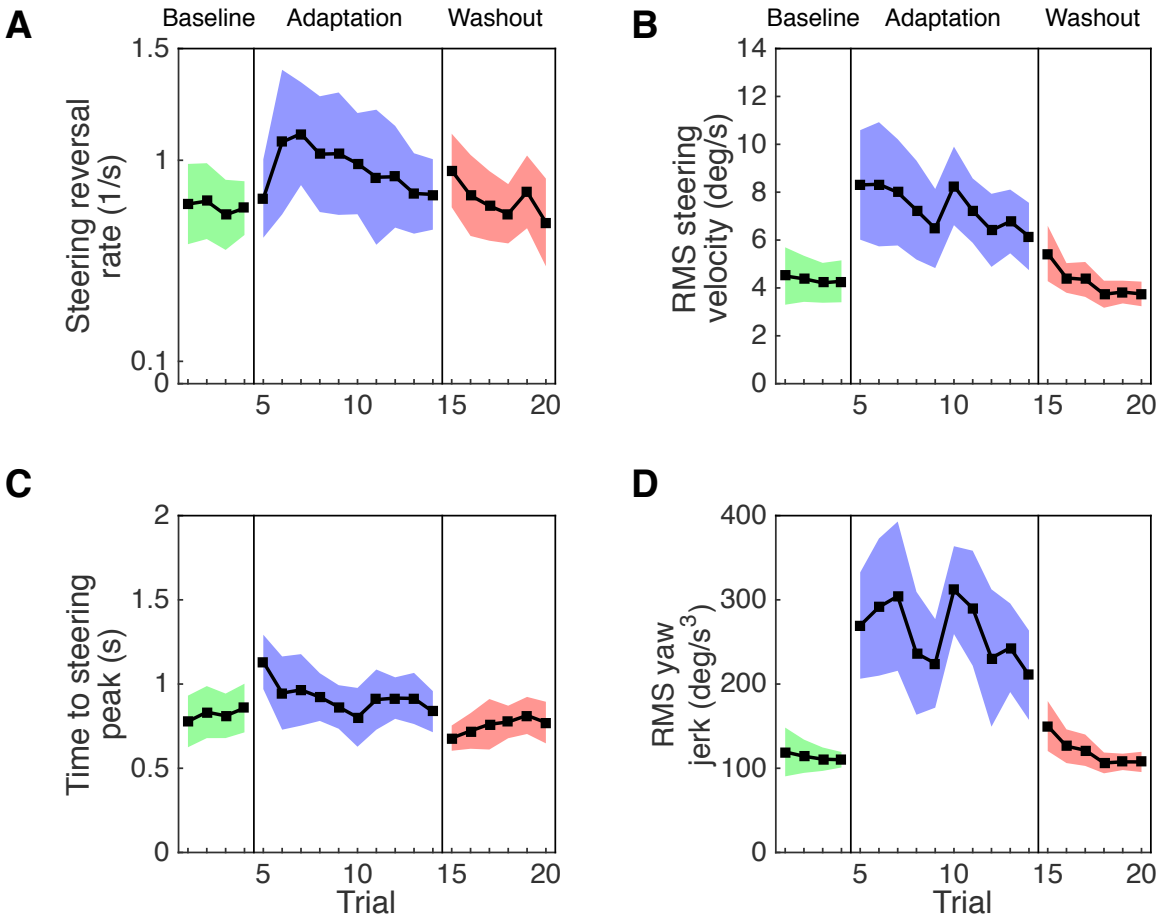

Figure 6.6: Learning curves for low friction study, Group 1 ($n = 9$). (A) Steering reversal rate (SRR). (B) RMS steering velocity. (C) Time to steering angle peak. (D) RMS yaw jerk. The friction coefficient was approximately 0.9 for the baseline and washout blocks, 0.15 for the adaptation block. Colored regions show 95% confidence intervals from a t distribution.

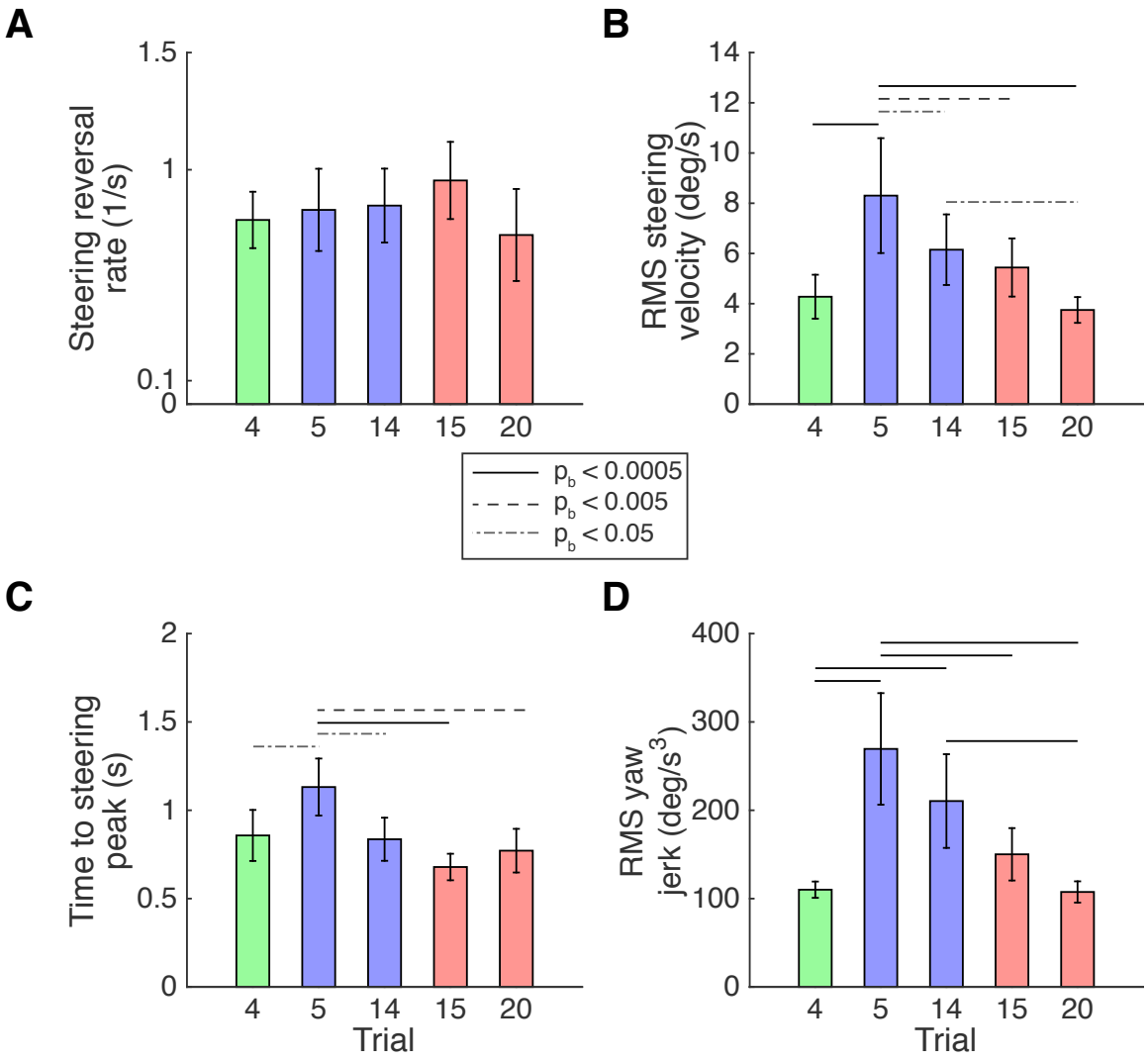

Figure 6.7: Statistical significance for low friction study, Group 1 ($n = 9$). (A) Steering reversal rate (SRR). (B) RMS steering velocity. (C) Time to steering angle peak. (D) RMS yaw jerk. In all panels, Trial 4 is the last trial of the baseline block ($\mu = 0.9$), Trials 5 and 14 are the first and last trials of the adaptation block ($\mu = 0.15$), and Trials 15 and 20 are the first and last trials of the washout block ($\mu = 0.9$). Error bars indicate 95% confidence intervals from a t distribution; horizontal lines indicate significant Bonferroni-corrected p-values between trials.

needed to make fast steering motions. The shape of the learning curve is not a simple exponential, however, which suggests that in addition to the adaptation process, there was likely another mental process involved in learning the handling change. The yaw jerk learning curve revealed a similarly interesting shape, though this metric did not return to baseline by the end of the adaptation block. Therefore, although participants recovered their steering performance, the resulting vehicle dynamics were not as smooth as baseline.

The time to steering peak (Fig. 6.6C, 6.7C) shifted later when the low friction controller was activated, resulting in an approximately exponential learning curve during the adaptation block. When the low friction perturbation was removed, the time shifted slightly earlier than baseline, indicating that there was some aftereffect, although this was not statistically significant.

For comparison, the learning curves and bar graphs for Group 2 are shown in Figs. 6.8 and 6.9, respectively. As expected from the ANOVA, the learning curves for steering reversal rate and time to steering peak were essentially constant, indicating that there was no significant change in steering behavior. The RMS steering velocity and RMS yaw jerk increased slightly (though not significantly) when the friction was reduced on Trial 5, then quickly returned toward baseline on subsequent trials. There were no statistically significant differences between trials for any of the metrics (Fig. 6.9).

6.5 Discussion

The results of this study show that participants in Group 1 adapted to the modified friction coefficient, while Group 2 did not adequately experience the handling change to have need of adaptation. The choice of driving style as characterized by maximum lateral acceleration directly influenced the vehicle dynamics that each participant experienced.

The experience of the handling perturbation in this study was more nuanced than in the other studies in this dissertation. Rather than directly changing the response of the road wheels to the steering wheel or the amount of torque felt at the steering

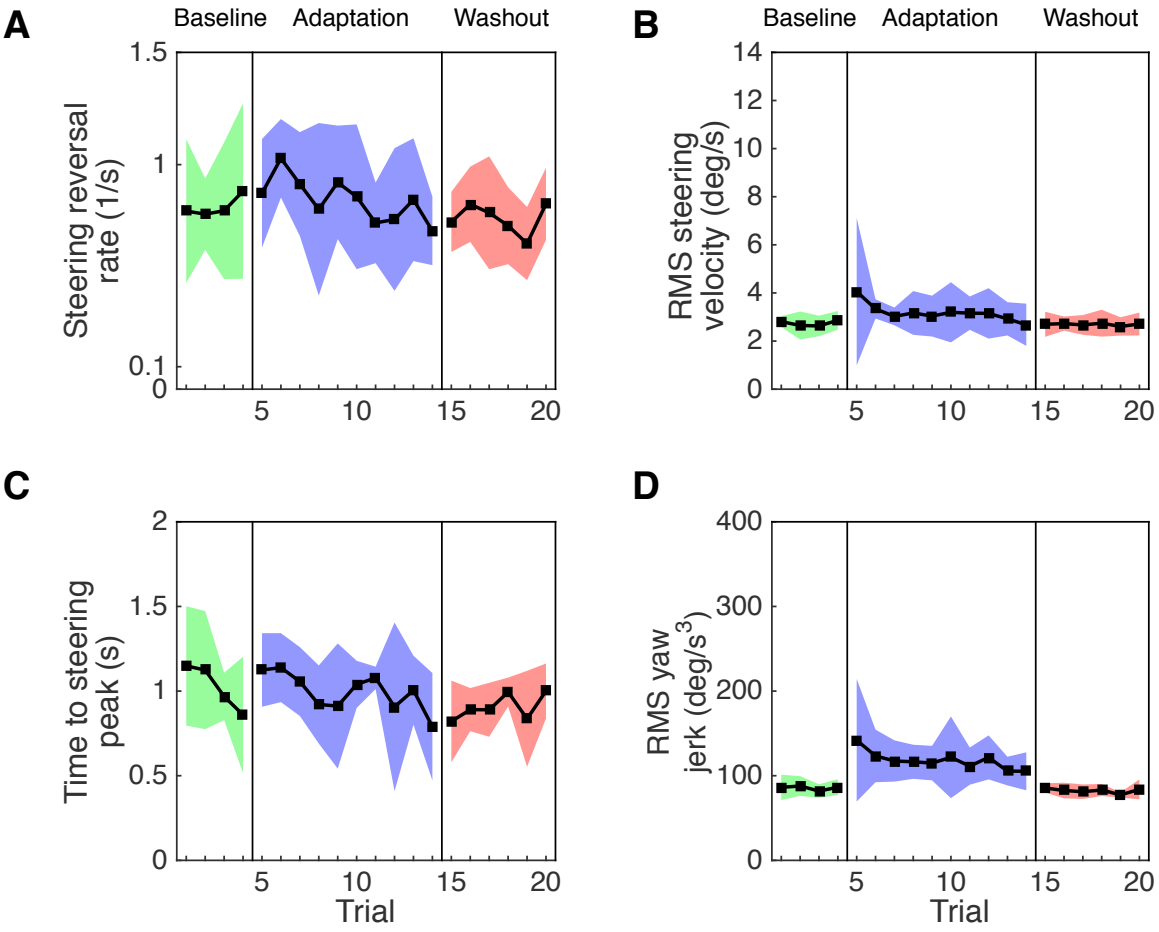

Figure 6.8: Learning curves for low friction study, Group 2 ($n = 5$). (A) Steering reversal rate (SRR). (B) RMS steering velocity. (C) Time to steering angle peak. (D) RMS yaw jerk. The friction coefficient was approximately 0.9 for the baseline and washout blocks, 0.15 for the adaptation block. Colored regions show 95% confidence intervals from a t distribution.

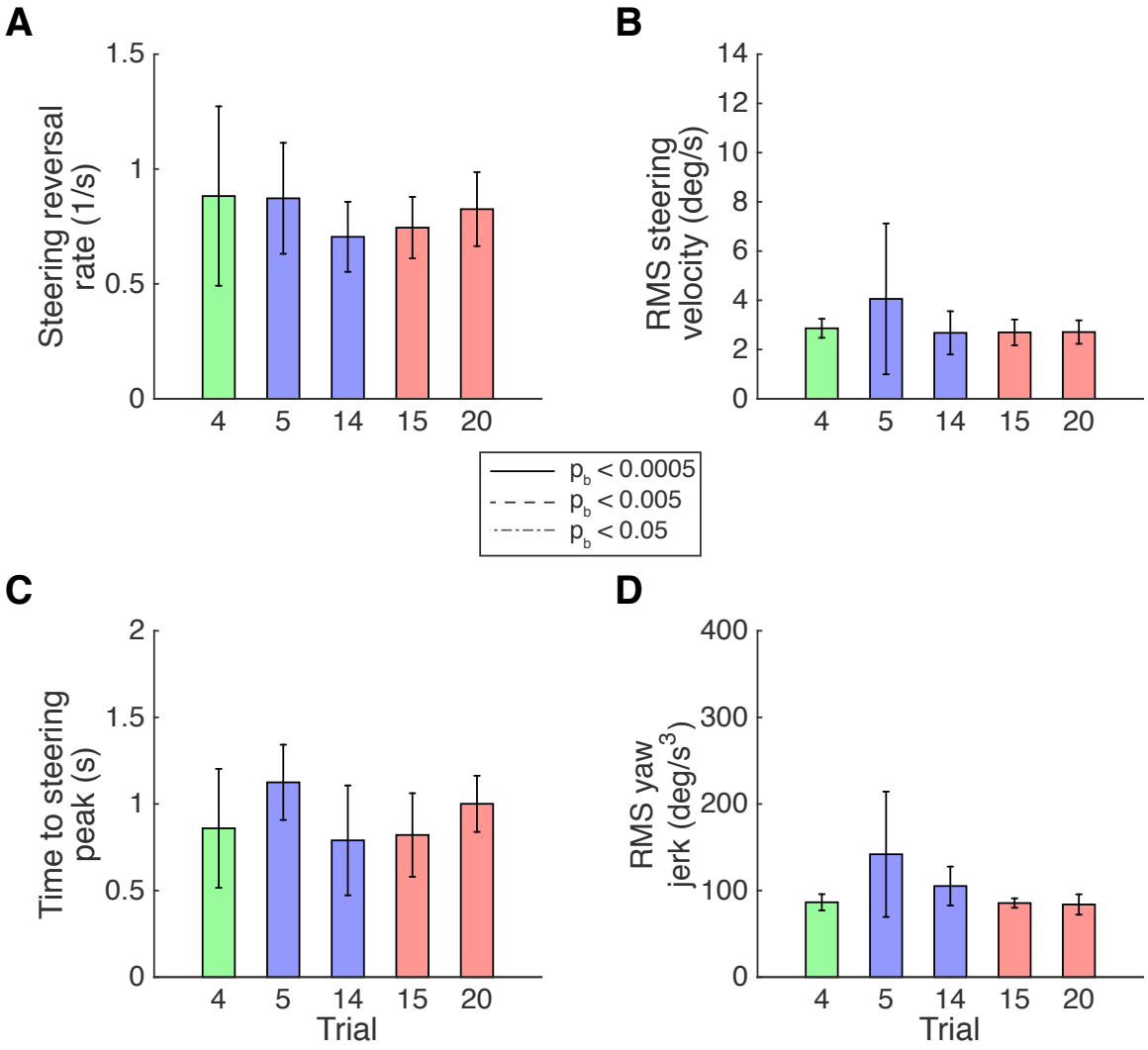

Figure 6.9: Statistical significance for low friction study, Group 2 ($n = 5$). (A) Steering reversal rate (SRR). (B) RMS steering velocity. (C) Time to steering angle peak. (D) RMS yaw jerk. In all panels, Trial 4 is the last trial of the baseline block ($\mu = 0.9$), Trials 5 and 14 are the first and last trials of the adaptation block ($\mu = 0.15$), and Trials 15 and 20 are the first and last trials of the washout block ($\mu = 0.9$). Error bars indicate 95% confidence intervals from a t distribution; horizontal lines in the legend indicate significant Bonferroni-corrected p-values between trials; there were no significant differences between trials for Group 2.

wheel, the low friction emulation controller limited the amount of tire force by steering both the front and rear wheels, and the particular vehicle dynamic states depended on the past and present steering behavior of the driver. This required drivers to learn changes to a highly nonlinear model of the mapping from steering motions to vehicle dynamics, while in the prior studies the mapping changed by directly modifying a single variable, resulting in handling changes that were guaranteed to be experienced consistently by all participants.

Participants in this study were not instructed on the nature of the handling change. They were only told immediately prior to Trial 5 that the handling would change in some way and prior to Trial 15 that it would revert to baseline handling. Therefore, they would not be expected to use any cognitive strategy specific to low friction conditions for dealing with the handling change. However, since Group 2 drivers chose to experience lower levels of lateral acceleration due to their smooth, gentle steering inputs, they implicitly used an approach that was useful for the handling change. Their natural approach limited their exposure to the low friction conditions, but it was also an effective way of maneuvering the vehicle during the low friction portion of the experiment. Group 1 participants, on the other hand, did not seem to recognize that gentler steering inputs would improve their performance in the lane change task. In fact, some of them tried very hard to maintain their desired high lateral acceleration by steering even faster and with larger magnitude during the first few low friction trials. They did adapt their steering behavior over the course of the ten perturbed trials, but if they had modified their strategy for making the lane change during this period, they may have found the handling change less challenging and required less motor adaptation.

The results of this study illuminate two key points about adaptation to this handling change. First, drivers adapted to low friction conditions by changing their steering behavior, and there was likely an additional mental process that contributed to learning the handling change. Second, drivers chose different steering behaviors to complete the lane change, and these driving styles were remarkably persistent even with fairly large changes in vehicle handling.

6.6 Comparison with Torque Increase Study

Grouping the participants using a rough measure of driving style reveals interesting differences in adaptation to low friction conditions. Does this method of partitioning the participants provide further insight into any of the earlier studies of adaptation to handling changes? When participants from the other three studies were grouped using the same lateral acceleration threshold of 2.1 m/s^2, there were no clear differences between the groups for the steering ratio scaling and steering direction reversal studies (Chapter 3). However, the steering torque increase study (Chapter 4) resulted in a distinct separation between the two groups, similar to the low friction study.

For this study, all participants were insensitive to the torque change, but each group displayed different steering behavior. A two-way ANOVA treating experiment stage and driving style group as the two factors (Table D.4) resulted in significant differences between the groups for time to steering peak ($F(1,50) = 4.59$; $p = 0.037$), RMS steering velocity ($F(1,50) = 31.13$; $p = 9.77\text{e-}7$), and RMS yaw jerk ($F(1,50) = 22.29$; $p = 1.93\text{e-}5$), with no significant difference between groups for steering reversal rate ($F(1,50) = 0.92$; $p = 0.342$). Plots of the metrics by group in Fig. 6.10 confirm the ANOVA results, with the means for the two groups appearing approximately equal for steering reversal rate and time to steering peak, and clearly separated by group for the RMS steering velocity and RMS yaw jerk. Participants in Group 1, who preferred higher lateral acceleration during baseline, maintained consistently higher RMS steering velocity throughout the study; this was the same behavior as Group 1 for the low friction study. Unlike the low friction study, however, both groups maintained essentially constant steering velocity when the torque was increased, suggesting that the desire to maintain their preferred steering behavior overshadowed the increase in arm stiffness that was required to compensate for the steering torque increase. Similarly, Group 1 experienced consistently higher levels of RMS yaw jerk than Group 2, which indicates a lower preference for smooth handling in the former.

Investigation of the results of both studies with participants classified by maximum lateral acceleration during baseline reveals a striking persistence of steering behavior in the presence of handling changes. Both studies had clear separation between

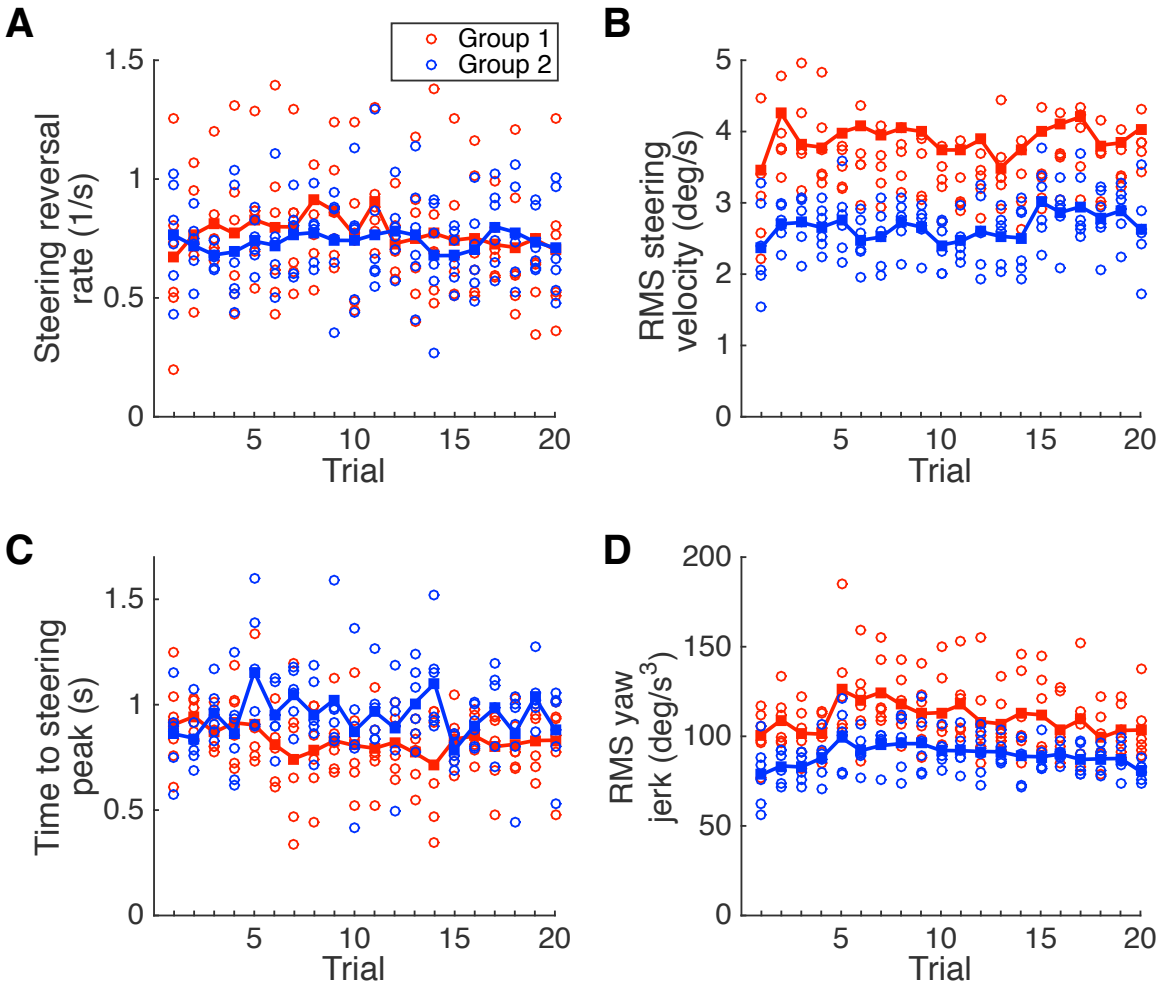

Figure 6.10: Metrics grouped by participant driving style for User Study #3 (steering torque increase). (A) Steering reversal rate (SRR). (B) RMS steering velocity. (C) Time to steering angle peak. (D) RMS yaw jerk. Open circles are individual data points; filled squares and lines are group means based on data points of the corresponding color. $n = 6$ for Group 1, $n = 6$ for Group 2.

groups in the steering velocity and yaw jerk metrics, while the steering reversal rate and time to steering peak metrics were similar between groups. The mean values for steering velocity and yaw jerk for each group during the baseline trials (1-4) were nearly the same for the two studies. For the steering torque increase study, the lateral acceleration threshold was not related to any difference in experience of the handling change, since the steering torque change did not depend on steering behavior. Using lateral acceleration to group participants in this study is interesting because it illuminates the persistent effect of driving style across handling conditions.

Group 1 can be characterized by a preference for relatively fast, high bandwidth control over their steering motions. In the steering torque study, this meant that they needed to stiffen their arms to overcome the additional steering torque during the adaptation block. In the low friction study, they made even faster steering motions during the adaptation block in an attempt to make fast, high lateral acceleration lane changes, resulting in a strong experience of the low friction conditions that required adaptation. In contrast, Group 2 used slower, gentler steering inputs to complete the lane change. They needed to stiffen their arms during the torque study, just like Group 1, but did so only enough to maintain their desired steering behavior, which remained slower than that of Group 1. In the low friction study, Group 2's gentler inputs resulted in less experience of the low friction handling change. In summary, drivers in these two studies consistently maintained their preferred driving styles even with large changes in road friction or steering wheel torque. The clear difference in driving style in two studies with independent groups of participants merits further study.

6.7 Future Research Directions

This study has demonstrated that drivers adapt their steering behavior when suddenly exposed to low friction road conditions and that preferred driving style is persistent in the face of handling changes. These observations lead to several ideas for future research to better understand the nature of human motor learning due to road friction changes.

The difference in steering behavior between the two groups of participants in Studies #3 and #4 suggests that individual driving style may be important to consider in analysis of driver adaptation to handling changes. Additional experiments could help determine whether this difference is universal or whether it is related to the particular experimental design used for these studies. Specifically, the low friction study could be modified to make the experience of the handling change more consistent between all participants. This could be achieved either by adding traffic cones to the portion of the course between the end of the straight and the target gates to guide the vehicle along a more constrained path during the lane change, or by explicitly instructing participants on how they should perform the lane change, for instance to complete the lane change as quickly as possible. It would be interesting to identify whether difference in driving style would still be observable with a more consistent experience of the low friction dynamics between all participants.

Although adaptation to low friction conditions was observed in Study #4, there are aspects of low friction driving that were not captured by this study and therefore should be investigated further. The lane change maneuver required the vehicle to reach the simulated handling limits only briefly. Maneuvers that require more time near the simulated handling limits would give drivers a fuller experience of low friction driving. These could include sharper turns, multiple lane changes, and sustained curves. Additionally, the driving task was constrained so that drivers could only control the vehicle's steering, not its speed. Allowing drivers to control both the steering and the speed would be a more realistic experience and would allow investigation of how they adapt both of these control inputs in the presence of changing road conditions. Such a study would require careful statistical analysis considerations to properly account for the effect of variable speed between participants.

There are other aspects of the overall learning process besides adaptation that are evident in low friction handling. One of these is a *countersteer*, a discrete steering motion that involves quickly steering in the opposite direction of the turn to keep the vehicle from losing grip and spinning. Although drivers may modulate that amplitude of the countersteer depending on the severity of the impending spin, countersteering does not represent a change in the internal vehicle dynamics model that would be

consistent with adaptation. Instead, it is a learned, discrete behavior that is used only in the particular situation of stabilizing the car when it reaches its handling limits. Drivers may also use explicit strategies to adjust their driving behavior in low friction conditions. Studying countersteering and explicit strategy with changing road friction conditions would complement the results on adaptation from Study #4 by illuminating the role of these other control components in steering the vehicle through large handling changes.

Chapter 7

Conclusion

7.1 Summary of Results

This dissertation has demonstrated that drivers adapt to changes in vehicle handling characteristics in just a few trials of a lane change maneuver. Chapter 2 developed a novel user study protocol using lane changes to enable experiments on driver adaptation. This protocol separated the steering and longitudinal control of the vehicle during two distinct trial phases to isolate the learning of the handling change to the lane change phase. The protocol was designed to take advantage of the unique capabilities of the X1 research vehicle and required careful engineering of subsystems including the safe stop controller, the speed limiter, and the four-wheel steering path-following controller.

In Chapter 3, two user studies demonstrated that drivers adapt to steering ratio scaling and steering direction reversal. These handling changes were designed to be similar to perturbations in arm reaching studies. The results of the steering direction reversal study indicated that this handling condition may have involved cognitive changes in addition to adaptation, perhaps in the form of an explicit steering strategy. The large change in steering behavior from baseline when the steering ratio was scaled, along with the clear adaptation to this handling change, supported the conclusion that drivers base their steering control on a model of how steering angle maps to vehicle dynamics.

This conclusion was further supported by the results of the steering torque increase study in Chapter 4. Drivers were insensitive to increased steering torque, representing a power steering failure. Therefore, their internal steering control model did not focus on the mapping from steering torque to vehicle dynamics.

Another real-world handling change of interest was a change in tire-road friction coefficient. To enable the user studies with this handling change, Chapter 5 developed a handling emulation controller that leveraged the four-wheel steering capability of X1. Using a reference model of desired vehicle dynamics and tire forces, the controller computed a set of tire forces to track the reference model. The particular choice of feedback structure allowed cancellation of nonlinear vehicle dynamics terms, resulting in linear error dynamics with strong stability properties. The handling emulation scheme was applied to low friction emulation and tracked reference models with friction coefficients between 0.1 and 0.4.

The low friction emulation controller was used with the user study protocol in Chapter 6 to explore driver adaptation to low friction conditions. Participants in this study demonstrated two distinct responses to the handling change, depending on driving style, with one group experiencing a large handling change to which they subsequently adapted, while the second group did not experience a handling change. The persistence of preferred driving style in the face of handling changes was also observed in the torque increase study and suggests an interesting component of future driver adaptation studies.

Overall, this dissertation has shown the existence of human motor adaptation in the complex task of steering an automobile, identified key ideas related to the driver's internal model of vehicle control, and laid the groundwork for several possibilities for future work, as described below.

7.2 Future Research Directions

7.2.1 Expand the Scope of Handling Emulation

Some specific ideas for extensions to the handling emulation controller were discussed in Section 5.6 to enable further driver adaptation studies. The general idea of handling emulation may be useful in additional applications beyond the study of adaptation. Handling emulation could be used in the car design process as a tool to quickly assess driver preferences of handling characteristics on a single testbed. The ability of a vehicle to emulate different handling characteristics could enable drivers to choose their own desired handling properties within a certain range, allowing for a more personalized driving experience. A car equipped with handling emulation technology could maintain desired handling performance in the face of observed changes in handling. For instance, if the front-to-rear loading of the vehicle changed drastically (say from adding a large amount of cargo to the trunk), the handling emulation controller could intervene to maintain a desired understeer gradient.

There are some technical challenges to implementing handling emulation controllers for these applications. Handling emulation is only possible within the physical limits of the controlled vehicle, including tire force limits and constraints on actuator range and slew rate. This means that there are limits to the degree of handling change that a controller can emulate or compensate for, which must be carefully considered for any specific application. Additionally, it is important to ensure that the particular implementation of a handling emulation controller is stable and therefore will not result in unsafe vehicle behavior. If the goal of the controller is to truly reproduce the dynamics of a vehicle with different physical properties, additional dynamics beyond the planar velocity states should be considered when assessing whether the emulation feels realistic. Some components that provide relevant cues to the driver are the roll dynamics and the relaxation length of the tires (which determines how quickly they generate force due to steering commands). Tracking these dynamics may require additional actuation capabilities such as active suspension control.

7.2.2 Adaptation Studies with Physiological Measurements

The studies in this dissertation used behavioral measurements (primarily of steering) to infer how drivers were modifying their internal models of the vehicle dynamics. This approach is commonly used in motor learning studies because behavioral measurements are straightforward to obtain and clearly demonstrate the outcome of an internal learning process. It would be informative to augment the behavioral metrics with physiological measurements of the drivers, particularly brain wave measurements. A promising technique is functional near infrared spectroscopy (fNIRS) [136], which measures changes in blood flow in the brain as a proxy for brain activity. Adding fNIRS measurements to the existing adaptation protocol could reveal more details about which parts of the brain are involved in adaptation to handling changes, especially for steering direction reversal, which may involve explicit strategy.

7.2.3 Generalization of Driver Adaptation

This dissertation has presented convincing evidence that drivers adapt to three different types of handling changes related to steering control. However, each type of handling change was studied for only a single modified value; for instance, the steering ratio was perturbed from 15:1 to 2:1 but no other steering ratio was used. To better understand the adaptation process for these handling changes, it would be informative to explore how adaptation to a given value of a handling characteristic influences the ability of drivers to subsequently adapt to a different value of that characteristic. This is known in the motor learning literature as **generalization** of the adaptation. For the steering ratio change, this could be explored by extending the protocol so that after the washout block, drivers would perform several more trials at a different steering ratio (e.g. 5:1). An understanding of how motor adaptation generalizes to untrained conditions could inform new approaches to training drivers by identifying training conditions that are particularly helpful in speeding up adaptation to other handling conditions.

7.2.4 Advanced Study of Adaptation to Handling Changes

The studies in this dissertation focused on adaptation of steering control to handling changes. Drivers are also responsible for controlling vehicle speed, so it is important to understand how they adapt their control of acceleration and braking under changes to vehicle handling. This is especially relevant to the case when the road friction changes: since the coupling of lateral and longitudinal tire forces is more evident near the handling limits, the way that drivers control the longitudinal dynamics influences how well they perform in low friction conditions.

The four user studies in Chapters 3, 4, and 6 demonstrated adaptation for a set of interesting and important handling changes. A straightforward next step is to repeat these studies with different parameters to characterize how the adaptation process for each handling change depends on the magnitude of the change. There are also other handling conditions in which adaptation of steering and longitudinal control may be relevant. These include changing weight distribution within the vehicle, a tire blowout, and towing a trailer. Studying adaptation to these handling changes would require modification of the handling emulation controller or design of a new controller.

Finally, a particularly important application of the study of adaptation in the automobile is the handover of control from an automated vehicle to a human driver. As discussed in Section 3.1.4, the results of the studies in this dissertation suggest that when a driver has been out of the control loop and regains control, there is a period of time when the driver's steering performance is compromised and therefore it may be challenging to steer the vehicle safely. In these studies, the vehicle was brought to a stop after each trial; a more realistic scenario would have the vehicle autonomously drive around a course and hand over control to the human driver on-the-fly. This paradigm could also incorporate analysis of drivers' situation awareness and the effect of distraction in addition to the process of motor adaptation. Characterization of the issues involved in handover of control is imperative for safe design of future automated vehicles.

Appendix A

Steering Control for the X1 Research Vehicle

To implement any of the higher level control algorithms used for this dissertation, accurate low-level steering control is essential. This appendix describes the steering controller for X1, including modeling, parameter identification, controller implementation, and special considerations for four-wheel steering.

A.1 Steering System Model

The steering system for each wheel consists of a DC motor, a harmonic drive that provides 160:1 gear reduction, a steering linkage, and a wheel and tire assembly. Each steering system is modeled as a second order dynamic system with a nonlinear friction term and an aligning moment term that represents the effect of the tire forces. The torque about the steering axis is expressed as a function of the steer angle δ as

$$\tau = J\ddot{\delta} + b\dot{\delta} + F\,\mathrm{sgn}\left(\dot{\delta}\right) + \tau_{\mathrm{a}} \tag{A.1}$$

where J is the system inertia, b is the system damping, $F\,\mathrm{sgn}\left(\dot{\delta}\right)$ is the system Coulomb friction, and τ_{a} is the aligning moment. This model includes only the most important components for steering control, neglecting effects such as jacking torque,

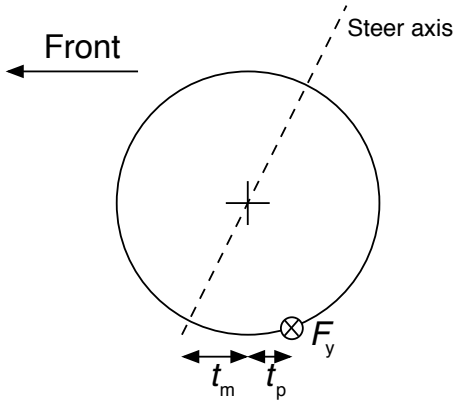

Figure A.1: Illustration of the components of aligning moment. Tire force F_y is into the page, corresponding to a force to the right as viewed by the driver.

linkage compliance, etc.

The aligning moment is the moment about the steering axis caused by lateral tire force. It is found by multiplying the lateral tire force F_y by the total trail (or moment arm), which is the sum of the mechanical trail t_m and the pneumatic trail t_p.

$$\tau_a = -(t_m + t_p)F_y \tag{A.2}$$

The relationship between these components is illustrated in Fig. A.1. The mechanical trail is the distance between the point on the ground that intersects with the steer axis and the center of the tire contact patch (directly below the wheel center). This distance can vary significantly with steer angle but is straightforward to calculate from knowledge of the suspension geometry. The pneumatic trail is the distance from the tire contact patch center to the point of application of the lateral tire force. The tire force is not truly a point load but is distributed across the entire contact patch. However, the effective point of application is the location used for determining the pneumatic trail.

The aligning moment can be estimated in real time from measurements of vehicle states; a method for this is explained in Section A.2. The inertia, damping, and Coulomb friction can be estimated through system identification techniques as described below.

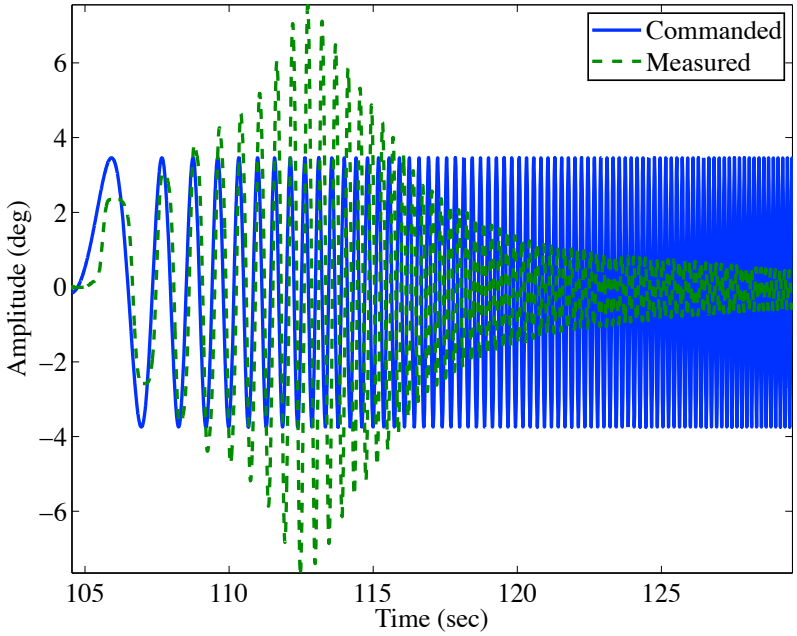

Figure A.2: Input and output steer angles used to compute ETFE for front left wheel.

A.1.1 Parameter Identification

For the identification process, the tires are placed on turn plates to allow the wheels to steer freely with essentially no lateral tire forces, making $\tau_a = 0$. The first step in identifying the model parameters in (A.1) is to find the inertia and damping using an experimental transfer function estimate (ETFE). This method applies a sinusoidal input signal that sweeps linearly through a range of frequencies and measures the resulting output steer angle, then computes the approximate frequency response model. A proportional feedback controller with gain K is applied to the steering system to provide stability during the frequency sweep, resulting in the following transfer function for the closed loop system.

$$\frac{\delta_{\text{des}}(s)}{\delta(s)} = \frac{K}{Js^2 + bs + K} \tag{A.3}$$

Fig. A.2 shows an example of the commanded and measured steer angles that are used to compute the ETFE for one wheel. The ETFE is computed using discrete

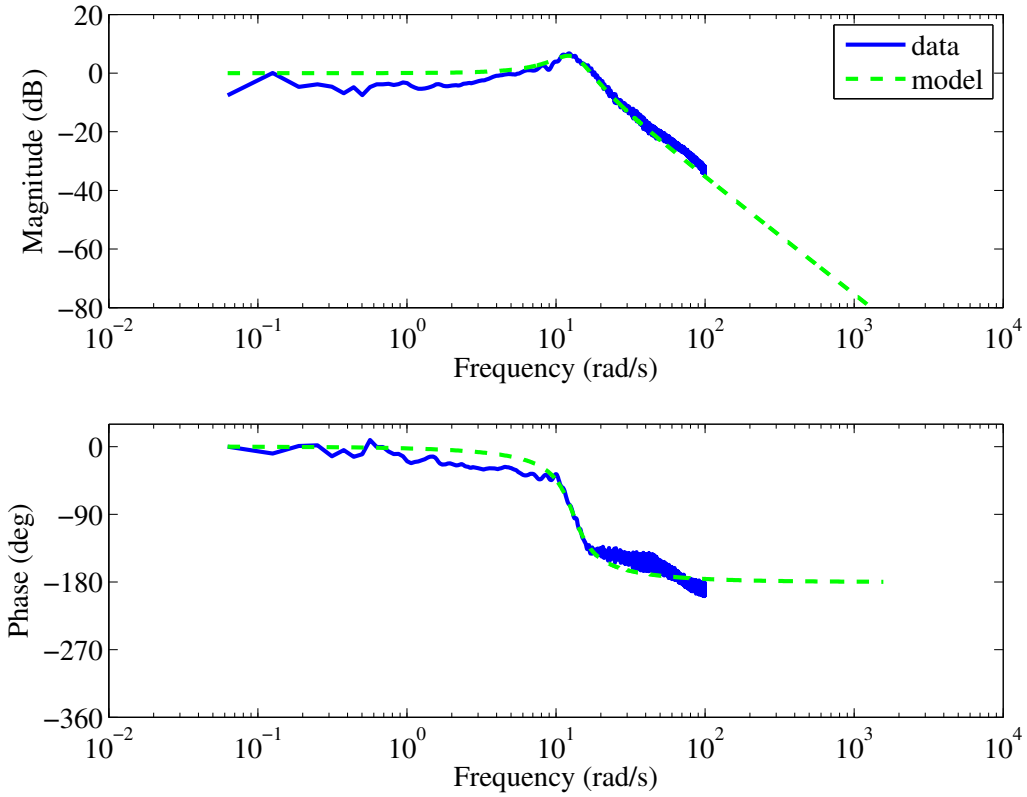

Figure A.3: ETFE for front left wheel.

Fourier transforms of the input and output signals, then the inertia and damping are estimated from a best fit of the closed loop model (A.3) to the data. The results of this fit are demonstrated for the front left wheel in Fig. A.3. Identified values of system inertia and damping are tabulated for each wheel in Table A.1. The model fits the data very well except at low frequencies; this discrepancy is due to the fact that the ETFE does not include the Coulomb friction.

The Coulomb friction for each wheel is estimated by finding the minimum amount of torque needed to start turning the wheel. This is achieved by slowly ramping the current applied to the steering motor until it starts to move. This process is repeated several times with different starting steer angles and in both directions (positive and negative current). Fig. A.4 shows the resulting data for the front left wheel. The

Table A.1: Identified steering system parameters

		FL	FR	RL	RR	units
Inertia	J	14.63	12.96	12.51	11.37	$\mathrm{N \cdot m \cdot s^2 \cdot rad^{-1}}$
Damping	b	100.1	83.2	87.0	96.9	$\mathrm{N \cdot m \cdot s \cdot rad^{-1}}$
Friction	F	0.467	0.411	0.288	0.335	$\mathrm{N \cdot m}$

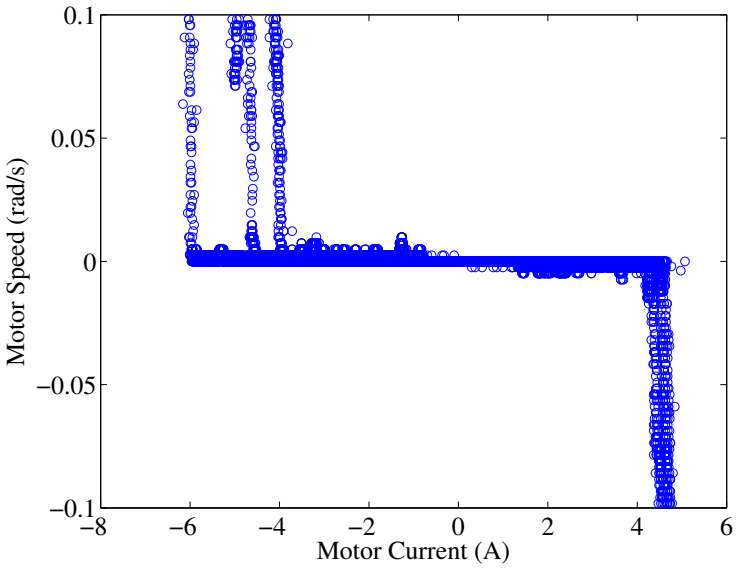

Figure A.4: Identification of Coulomb friction torque for front left wheel.

input current at which the motor speed initially becomes greater than 0.01 rad/s is taken as the minimum current. Note that this point varies with initial conditions for the data shown, indicating that the model does not perfectly capture the effect of friction. Therefore, several minimum current values are averaged for each wheel and the average current is then multiplied by the motor torque constant ($K_t = 0.1$ N·m/A) to find the Coulomb friction torque magnitude F.

A.2 Controller Implementation

Given the identified model of the steering system, the controller structure is designed to compensate for the known dynamics of the system while tracking the desired

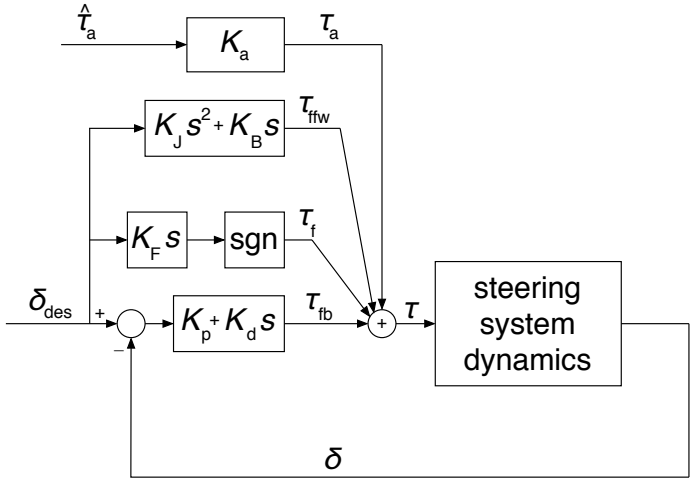

Figure A.5: Block diagram of steering controller for each wheel.

steering angle δ_{des}. The controller for each wheel is a proportional-derivative controller with feedforward, friction compensation, and aligning moment compensation, depicted in Fig. A.5. The controller takes the form

$$\tau = \tau_{\mathrm{fb}} + \tau_{\mathrm{ffw}} + \tau_{\mathrm{f}} + \tau_{\mathrm{a}} \tag{A.4}$$

$$\tau = (K_{\mathrm{p}} + K_{\mathrm{d}} s)(\delta_{\mathrm{des}} - \delta) + (K_{\mathrm{J}} s^2 + K_{\mathrm{B}} s)\delta_{\mathrm{des}} + K_{\mathrm{F}} \operatorname{sgn}\left(\dot{\delta}_{\mathrm{des}}\right) + K_{\mathrm{a}} \hat{\tau}_{\mathrm{a}} \tag{A.5}$$

with actual steer angle δ, proportional feedback gain K_{p}, derivative feedback gain K_{d}, inertia feedforward gain K_{J}, damping feedforward gain K_{B}, friction compensation gain K_{F}, estimated aligning moment $\hat{\tau}_{\mathrm{a}}$, and aligning moment compensation gain K_{a}. The controller gains currently used on X1 are $K_{\mathrm{p}} = 45000$ N·m/rad, $K_{\mathrm{d}} = 600$ N·m·s/rad, $K_{\mathrm{J}} = 0$ N·m·s^2/rad, $K_{\mathrm{B}} = 100$ N·m·s/rad, $K_{\mathrm{F}} = 0$ N·m, and $K_{\mathrm{a}} = 1.5$, for all four wheels.

To implement the controller on the X1 control computer, the continuous controller must be converted to a discrete form. This is done by replacing s by a discrete derivative plus low-pass filter equivalent

$$s \rightarrow \frac{2\pi f_c (z-1)}{z + (2\pi f_c T_s - 1)} = \frac{62.83(z-1)}{(z - 0.8743)} \tag{A.6}$$

where $f_c = 10$ Hz is the cutoff frequency for the low-pass filter and $T_s = 0.002$ s is the discrete sampling time.

The aligning moment estimate $\hat{\tau}_\mathrm{a}$ requires estimates of the lateral tire force F_y, the mechanical trail t_m, and the pneumatic trail t_p. These are found from measurements of vehicle states. First the slip angles for all four wheels are found from the following kinematic model.

$$\begin{aligned}
\alpha_\mathrm{fl} &= \tan^{-1}\left(\frac{U_\mathrm{y} + ar}{U_\mathrm{x} - \frac{d}{2}r}\right) - \delta_\mathrm{fl} \\
\alpha_\mathrm{fr} &= \tan^{-1}\left(\frac{U_\mathrm{y} + ar}{U_\mathrm{x} + \frac{d}{2}r}\right) - \delta_\mathrm{fr} \\
\alpha_\mathrm{rl} &= \tan^{-1}\left(\frac{U_\mathrm{y} - br}{U_\mathrm{x} - \frac{d}{2}r}\right) - \delta_\mathrm{rl} \\
\alpha_\mathrm{rr} &= \tan^{-1}\left(\frac{U_\mathrm{y} - br}{U_\mathrm{x} + \frac{d}{2}r}\right) - \delta_\mathrm{rr}
\end{aligned} \tag{A.7}$$

Next, the lateral tire forces are computed from the slip angles using the lateral brush tire model (5.4). The mechanical trail is found from a lookup table at the current steer angle for each wheel, although it is nearly constant for X1. The pneumatic trail is computed with the following equation, where t_p0 is the pneumatic trail at zero steer angle.

$$t_\mathrm{p} = \begin{cases} t_\mathrm{p0} - \dfrac{t_\mathrm{p0} C_\alpha}{3\mu F_\mathrm{z}} |\tan\alpha|, & |\alpha| < \alpha_\mathrm{sl} \\ 0, & |\alpha| \geq \alpha_\mathrm{sl} \end{cases} \tag{A.8}$$

Finally, the aligning moment estimate for each wheel is computed from $\hat{\tau}_\mathrm{a} = -(t_\mathrm{m} + t_\mathrm{p})F_\mathrm{y}$.

An example of the steering controller tracking performance for the front left wheel is demonstrated in Fig. A.6. The tracking error is below 0.5° throughout the entire maneuver, including during periods of rapid change in commanded steer angle, and usually stays below 0.2°. This level of tracking error is reasonable given that the

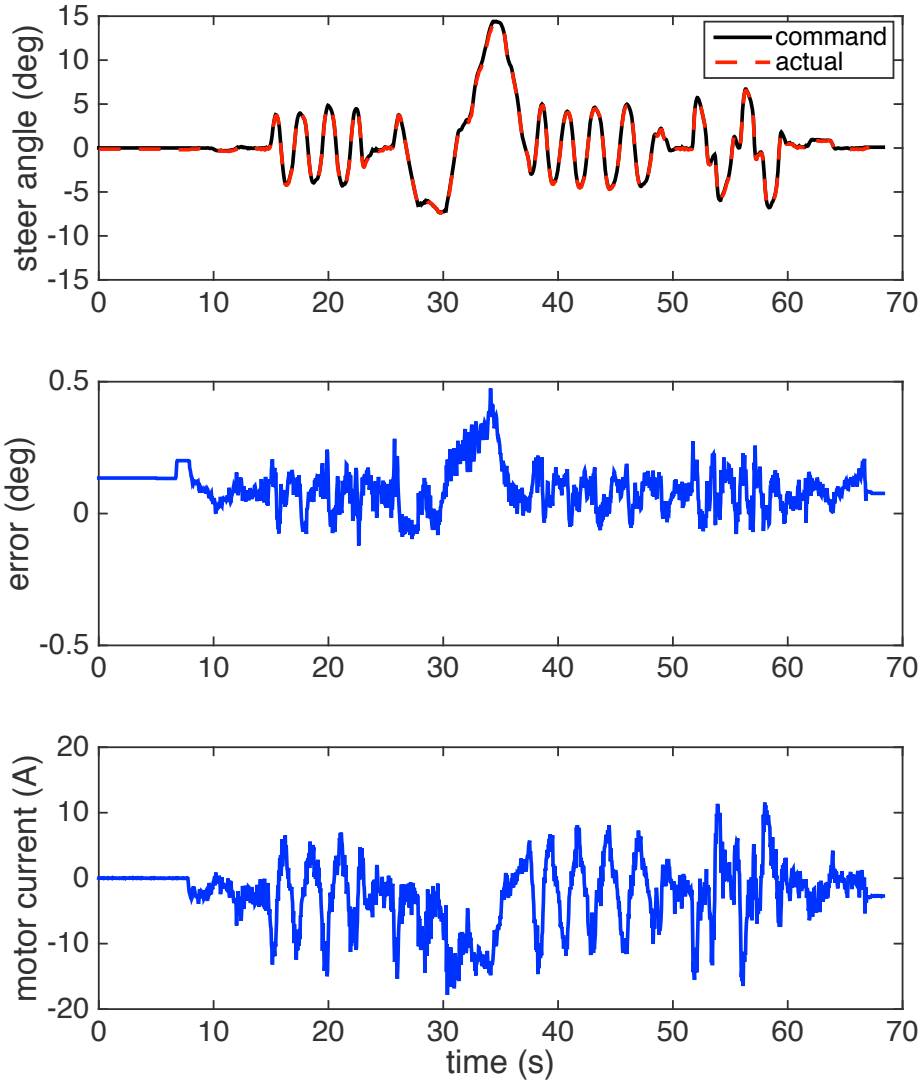

Figure A.6: Steer angle tracking for front left wheel using full steering controller.

steer angle measurement is only known within 0.2° given the uncertainty in linkage compliance.

A.3 Four-Wheel Steering Considerations

The four-wheel steering capability of X1 enables vehicle control strategies that would not be possible with only front steering, such as low friction emulation (Chapter 5). While this capability adds flexibility, it also requires additional considerations that are not necessary for front steering vehicles. Namely, the driver only controls a single input for lateral control, the steering wheel, while there are two independent actuators, front and rear steering. For nominal driving, it is necessary to choose a control algorithm for steering the wheels based on the driver's steering wheel command. This could be as simple as fixing the rear wheels straight ahead, effectively creating a front steering vehicle, or by using an algorithm such as the one described below using vehicle state measurements to choose the rear steer angle. For any 4WS implementation, steering performance is also improved by considering Ackermann geometry to maneuver in turns.

A.3.1 Speed-Varying 4WS Algorithm

In the speed-varying 4WS algorithm, the front wheels are controlled directly by the driver through the steering wheel, with $\delta_{\mathrm{f}} = \dfrac{\delta_{\mathrm{hw}}}{\mathrm{sr}}$. At a given vehicle speed, the algorithm steers the rear wheels proportionally to the front wheels; the scaling factor varies with vehicle speed so that the front and rear wheels steer in opposite directions at low speed to increase maneuverability and in the same direction at high speed to enhance vehicle stability. Given the front axle steer angle δ_{f} and the vehicle's longitudinal speed U_{x}, the rear axle steer angle δ_{r} is found from

$$\delta_{\mathrm{r}} = f(U_{\mathrm{x}})\delta_{\mathrm{f}} = \frac{C_{\alpha\mathrm{f}}\left(maU_{\mathrm{x}}^2 - bLC_{\alpha\mathrm{r}}\right)}{C_{\alpha\mathrm{r}}\left(mbU_{\mathrm{x}}^2 + aLC_{\alpha\mathrm{f}}\right)}\delta_{\mathrm{f}}. \tag{A.9}$$

This algorithm was initially proposed by Sano et al. in 1986 for the purpose of

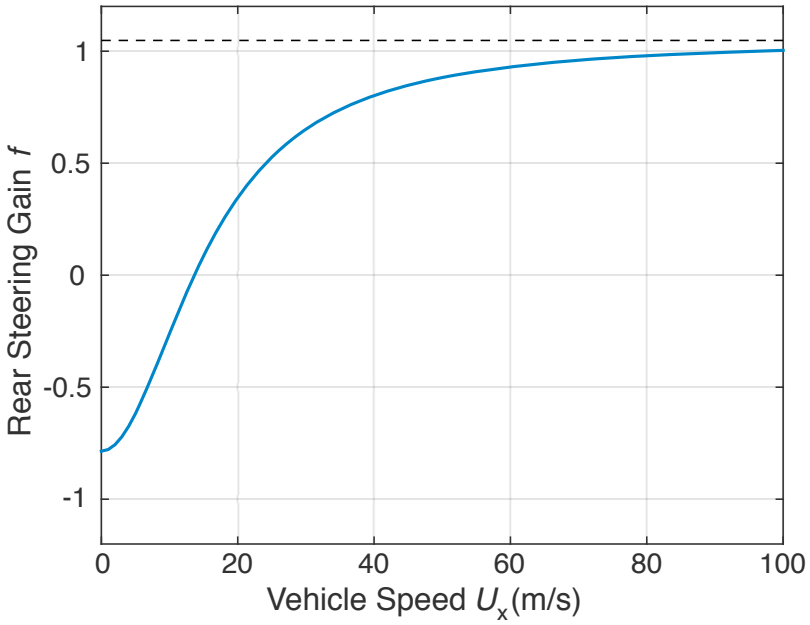

Figure A.7: Scaling factor for rear steer angle as a function of vehicle speed.

keeping the vehicle's steady-state sideslip angle $\beta = \tan^{-1}\left(\frac{U_y}{U_x}\right)$ equal to zero, which keeps the vehicle's center line along the path [120]. Fig. A.7 demonstrates how the scaling factor f varies with vehicle speed. Note that f ranges from $-\frac{b}{a}$ when $U_x = 0$ to $\frac{aC_{\alpha f}}{bC_{\alpha r}}$ as $U_x \to \infty$. At the threshold speed

$$U_x = \sqrt{\frac{C_{\alpha r} bL}{ma}} \tag{A.10}$$

the scaling factor changes sign, indicating a transition between opposite direction steering of the front and rear wheels and same direction steering.

A.3.2 Ackermann Steering Geometry for 4WS

Steering systems typically steer the front left and front right wheels to slightly different angles to account for the difference in turning radius for each of the wheels. The steering geometry is designed so that the inside wheel in a turn steers more than the

outside wheel. This reduces wear on the wheels that would occur if they were forced to steer at the same angle and is known as Ackermann steering geometry. For a front-steering vehicle, given the desired axle steering angle δ_{f}, the front left and front right steer angles (δ_{fl} and δ_{fr}, respectively) are found from the following equation, where d is the track width between the two wheels.

$$\delta_{\mathrm{fl}} = \frac{\delta_{\mathrm{f}}}{1 - \dfrac{\delta_{\mathrm{f}} d}{2L}} \qquad \delta_{\mathrm{fr}} = \frac{\delta_{\mathrm{f}}}{1 + \dfrac{\delta_{\mathrm{f}} d}{2L}} \tag{A.11}$$

When both the front and rear wheels are steered, the Ackermann geometry changes since the turning circle now depends on the nominal steer angles of both axles, as described by the following equations.

$$\delta_{\mathrm{fl}} = \frac{\delta_{\mathrm{f}}}{1 - \dfrac{(\delta_{\mathrm{f}} - \delta_{\mathrm{r}}) d}{2L}} \qquad \delta_{\mathrm{fr}} = \frac{\delta_{\mathrm{f}}}{1 + \dfrac{(\delta_{\mathrm{f}} - \delta_{\mathrm{r}}) d}{2L}} \tag{A.12}$$

$$\delta_{\mathrm{rl}} = \frac{\delta_{\mathrm{r}}}{1 - \dfrac{(\delta_{\mathrm{f}} - \delta_{\mathrm{r}}) d}{2L}} \qquad \delta_{\mathrm{rr}} = \frac{\delta_{\mathrm{r}}}{1 + \dfrac{(\delta_{\mathrm{f}} - \delta_{\mathrm{r}}) d}{2L}} \tag{A.13}$$

An example plot of the steering angles resulting from 4WS Ackermann geometry is shown in Fig. A.8, with δ_{r} fixed at 10° and δ_{f} ranging from -20° to 20°. Note that the Ackermann-corrected individual wheel steer angles are most different from the nominal axle values when $\delta_{\mathrm{f}} = 20^\circ$, which corresponds to the smallest turning radius for the range of steer angles shown in the figure.

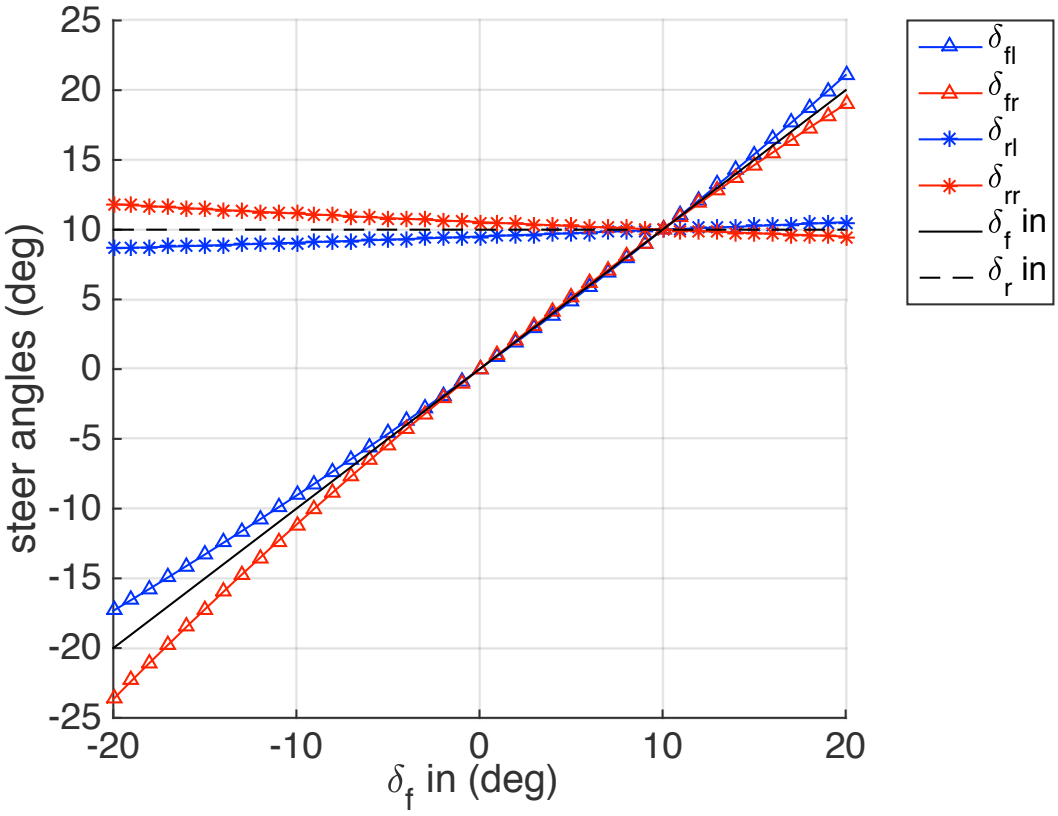

Figure A.8: Example of Ackermann geometry for 4WS. Black lines indicate the input axle steer angles, colored lines are the computed left and right steer angles.

Appendix B

Statistical Analysis Methods

This appendix describes the statistical methods used to analyze the data in this dissertation. Definitions are adapted from the text by Montgomery, Runger, and Hubele [98].

B.1 Fundamental Concepts

Suppose a given study has n participants who each perform m trials of the experiment, for a total of mn measurements of a particular metric X. Then the **sample mean** for trial i is given by

$$\bar{X}_i = \frac{1}{n}\sum_{j=1}^{n} X_{ij} \tag{B.1}$$

and the **sample variance** for trial i is given by

$$S_i^2 = \frac{1}{n-1}\sum_{j=1}^{n}(X_{ij} - \bar{X}_i)^2. \tag{B.2}$$

The sample standard deviation S is simply the square root of the variance.

B.2 Probability Distributions

Probability distributions give the likelihood that a random variable will take on particular values. For a continuous random variable X, a probability distribution is characterized by its probability density function $f(x)$. The cumulative distribution function describes the probability that X is less than or equal to each possible value, and is found from the following integral.

$$F(x) = P\{X \leq x\} = \int_{-\infty}^{x} f(t)dt \tag{B.3}$$

The probability that X falls within a given range of values is found by integrating $f(x)$ over the range, or from simply taking the difference of the cumulative distribution function at the endpoints of the range.

$$P\{a < X \leq b\} = \int_{a}^{b} f(x)dx = F(b) - F(a) \tag{B.4}$$

B.2.1 The Normal Distribution

The most commonly used probability distribution is the Gaussian or normal distribution, which is described by the following probability density function

$$f_{\mathcal{N}}(x) = \frac{1}{\sigma\sqrt{2\pi}} e^{-(x-\mu)^2/2\sigma^2}, \ -\infty < x < \infty \tag{B.5}$$

The normal distribution is characterized by the population mean μ and the population standard deviation σ. These values differ from the sample mean and standard deviation defined above in that they are assumed to be the true values for the population, not limited by the number of samples that have been measured. Fig. B.1 shows the normal probability density function with zero mean for several standard deviation values. The normal distribution is often put into a standard form that is a normal distribution with $\mu = 0$ and $\sigma = 1$. For a normal random variable X, the

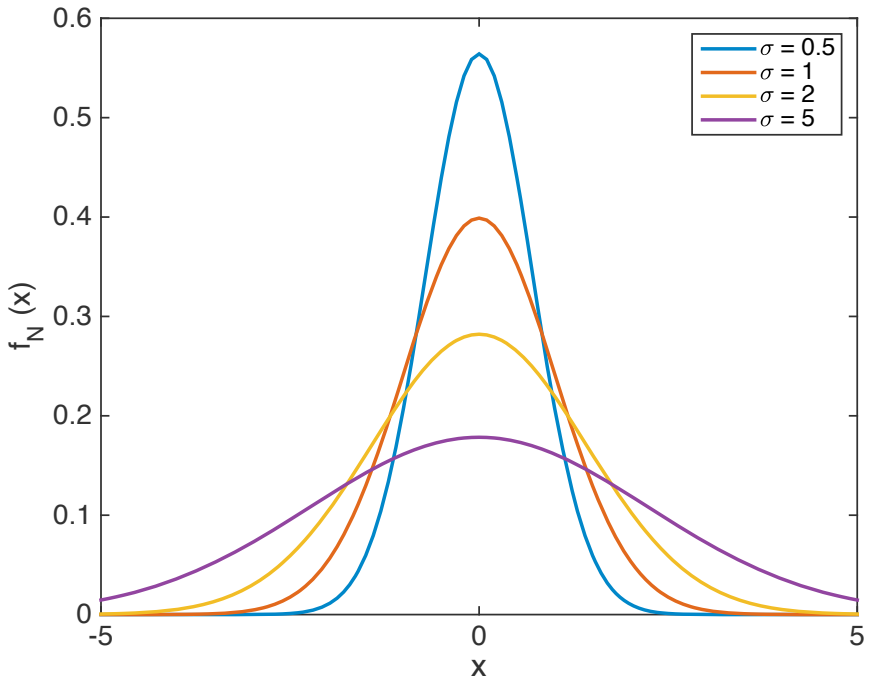

Figure B.1: The normal probability density function with $\mu = 0$ and a range of σ values.

standard normal random variable is defined as

$$Z = \frac{X - \mu}{\sigma}, \tag{B.6}$$

which has the following probability density function.

$$f_{\mathcal{N}}(z) = \frac{1}{\sqrt{2\pi}} e^{-z^2/2}, \ -\infty < x < \infty \tag{B.7}$$

The α confidence interval on the population mean is defined as the interval of possible values that is predicted to contain the population mean with probability $1 - \alpha$. For a standard normal distribution, this is written as

$$P\left\{ \frac{\sqrt{n}}{\sigma} |\bar{X} - \mu| \leq z_{\alpha/2} \right\} = 1 - \alpha \tag{B.8}$$

The most commonly used confidence level is $\alpha = 0.05$, or 95% confidence level, and the corresponding critical value is $z_{0.025} = 1.96$. The confidence interval that contains the population mean μ with 95% probability is then $\bar{X} \pm 1.96\frac{\sigma}{\sqrt{n}}$. This interval is approximately two standard deviations (2σ) on either side of the population mean μ. The confidence interval reflects the reliability of the statistical procedure, meaning that the method used to compute the interval correctly brackets the true value of the population mean $100(1-\alpha)\%$ of the time [98].

B.2.2 The t Distribution

When the population is normally distributed but the standard deviation is unknown and the sample size is small, the t distribution is used in place of the normal distribution to compute statistics on the samples. The t distribution is characterized by its degrees of freedom: if the sample consists of n measurements, the distribution has $\nu = n - 1$ degrees of freedom. The probability density function for this distribution is given by

$$f_T(x,\nu) = \frac{\Gamma\left(\frac{\nu+1}{2}\right)}{\sqrt{\nu\pi}\Gamma\left(\frac{\nu}{2}\right)}\left(1+\frac{x^2}{\nu}\right)^{-\frac{\nu+1}{2}}, \; -\infty < x < \infty \tag{B.9}$$

where

$$\Gamma(m) = \int_0^\infty e^{-x}x^{m-1}dx \tag{B.10}$$

is the gamma function. As ν increases, the t distribution approaches the normal distribution as depicted in Fig. B.2. A t random variable with $n-1$ degrees of freedom is defined in terms of the sample mean $\bar{X}$ and the sample standard deviation S as

$$T_{n-1} = \sqrt{n}\frac{\bar{X}-\mu}{S} \tag{B.11}$$

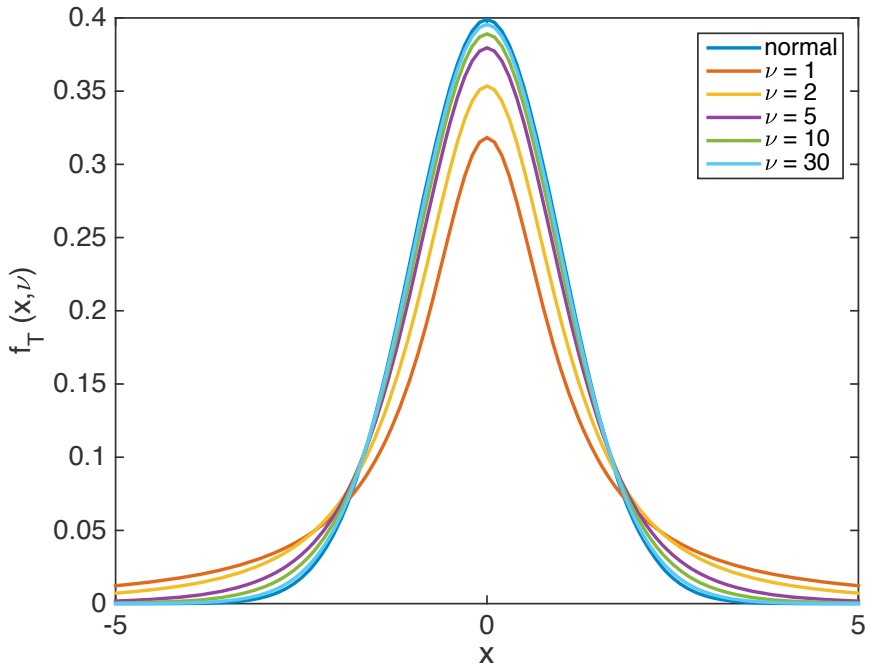

Figure B.2: Comparison of the t probability density function for several values of ν with the standard normal distribution.

The confidence interval based on the t distribution is similar to the confidence interval based on the normal distribution:

$$P\left\{|T_n| \leq t_{n,\alpha/2}\right\} = 1 - \alpha \tag{B.12}$$

For $\alpha = 0.05$, the critical value $t_{n,0.025}$ ranges from 12.706 for $n = 1$ to 1.96 as $n \to \infty$, which is exactly equal to the critical value for the normal distribution.

B.2.3 The *F* Distribution

The F distribution is used in analysis of variance (ANOVA) techniques (Section B.4) and arises from the ratio of two random variables with χ^2 distributions:

$$F = \frac{X_1/\nu_1}{X_2/\nu_2} \tag{B.13}$$

The χ^2 distribution with ν degrees of freedom arises from the sum of squares of ν standard normal random variables. Although this distribution is not used directly in computations for this dissertation, its probability density function is given below for reference.

$$f_{\chi^2}(x,\nu) = \frac{x^{\nu/2-1}e^{-x/2}}{2^{\nu/2}\Gamma\left(\frac{\nu}{2}\right)},\ 0 < x < \infty \tag{B.14}$$

The probability density function for the F distribution depends on two different degrees of freedom: the numerator degrees of freedom ν_1 and the denominator degrees of freedom ν_2.

$$f_F(x,\nu_1,\nu_2) = \frac{\Gamma\left(\frac{\nu_1+\nu_2}{2}\right)\left(\frac{\nu_1}{\nu_2}\right)^{\nu_1/2} x^{\nu_1/2-1}}{\Gamma\left(\frac{\nu_1}{2}\right)\Gamma\left(\frac{\nu_2}{2}\right)\left[\left(\frac{\nu_1}{\nu_2}\right)x+1\right]^{(\nu_1+\nu_2)/2}},\ 0 < x < \infty \tag{B.15}$$

The F probability density function is depicted in Fig. B.3 for several combinations of ν_1 and ν_2.

B.3 Hypothesis Testing

Hypothesis testing allows statistical statements to be made about the values of parameters. Of primary interest for this dissertation is whether different populations have different means. For instance, suppose we have conducted a driver adaptation study on ten participants with two trials, one with 15:1 steering ratio and the second with 2:1 steering ratio. Then we have two sets of measurements of steering reversal rates for the two trials. If we want to test whether the steering reversal rates are different between the two trials, we would state a null hypothesis H_0 that the two means are equal and an alternative hypothesis that the means are different:

$$H_0 : \mu_1 = \mu_2 \tag{B.16}$$

$$H_1 : \mu_1 \neq \mu_2. \tag{B.17}$$

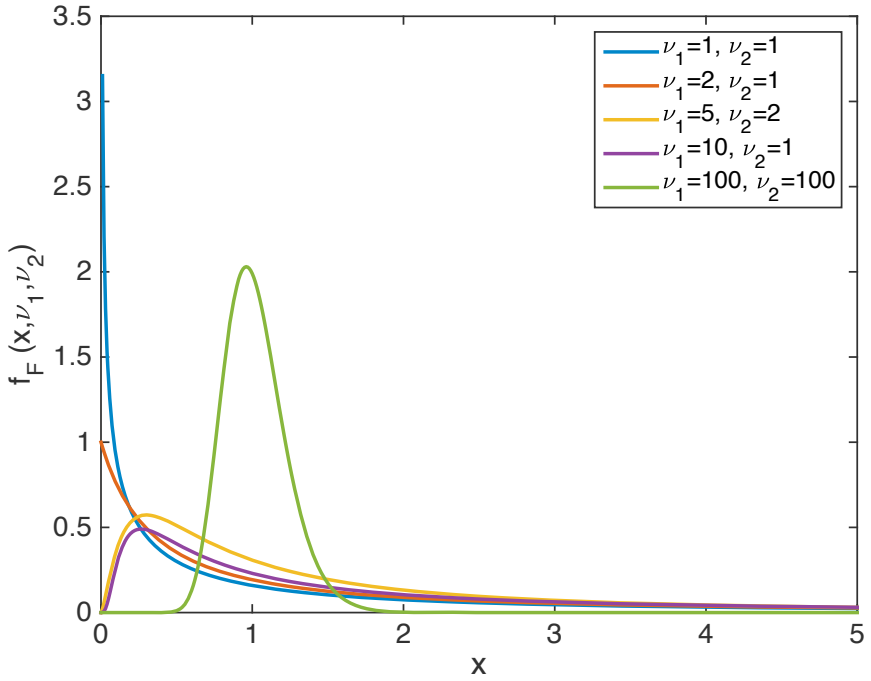

Figure B.3: The F probability density function for several values of ν_1 and ν_2.

This is equivalent to saying that the difference in means $\mu = \mu_1 - \mu_2$ is equal to zero.

$$H_0 : \mu = \mu_1 - \mu_2 = 0 \tag{B.18}$$

$$H_1 : \mu = \mu_1 - \mu_2 \neq 0 \tag{B.19}$$

We would then conduct a hypothesis test to either accept or reject the null hypothesis based on the assumed underlying probability distribution of the population.

Given this probability distribution, the test defines a critical region for the value of a test statistic (which is defined depending on the distribution), delineated by upper and lower bounds. If the test statistic falls within the critical region, the null hypothesis is accepted; otherwise, the null hypothesis is rejected and the alternative hypothesis is accepted. The bounds of the critical region are defined by a parameter α which gives the probability of rejecting the null hypothesis when it is actually true. This probability is known as the **significance level** of the hypothesis test and a level of $\alpha = 0.05$ is most commonly used.

B.3.1 The Two-Sample *t*-Test

The t-test is used when the population is assumed to be normally distributed with unknown variance. The one-sample test is used to test whether the mean of one population is different from a hypothesized mean. To compare the means of two populations, it is necessary to use a two-sample test. Given the sample means for the two trials of the experiment described above, $\bar{X}_1$ and $\bar{X}_2$, the test statistic for the two-sample t-test is

$$T = \frac{\bar{X}_1 - \bar{X}_2}{\sqrt{S_1^2/n_1 + S_2^2/n_2}}, \tag{B.20}$$

where n_1 and n_2 are the sample sizes for the two populations. After computing the test statistic, the probability that it lies within the critical region of the probability distribution is computed. This probability is called the ***p*-value** for the test. If $p < \alpha$, the null hypothesis is rejected; otherwise the null hypothesis is accepted.

B.3.2 Multiple Comparison Testing

The two-sample t-test is useful for comparing two population means, but often there are more than two populations of interest. For example, in the steering reversal rate study described above, suppose we want to compare the means of five trials with different steering ratios to make a statement on the effect of steering ratio on steering behavior. It is straightforward to compute multiple two-sample t-tests between all the pairs of populations to identify whether there are any differences in means. However, multiple comparisons increase the probability of incorrectly rejecting the null hypothesis, in other words overstating the level of statistical significance. To allow the computation of all necessary hypothesis tests without increasing the error rate, it is necessary to apply a correction factor to the computed p-values. There are several methods for correcting the p-values; the corrections used in this dissertation are called Bonferroni corrections. The corrected p-values are $p_b = Np$, where N is the total number of hypothesis tests performed. The scaled p-values are then used in place of the orignal p-values in the comparison against α to determine whether the

means are different.

B.4 Analysis of Variance

Analysis of variance (ANOVA) is a technique that allows comparison of multiple population means, rather than only comparing the means of two populations as in the t-test. This can be useful when there are multiple levels of a single factor to test or when more than one factor varies between populations. ANOVA generally assumes the measurements are drawn from a normal distribution, so it does not strictly apply to every experiment. However, it is often useful as a first analysis even when the data are not normally distributed.

ANOVA is a technique that partitions the total variability in the measured data, represented by the total sum of squares SS_T, into the variability due to each independent variable (or **treatment**), variability due to interactions between treatments, and the variability due to random processes (**error**). For each source of variability, the ratio of the sum of squares to the corresponding degrees of freedom (SS/df) gives the mean square for that source, which is an estimator for the variance of the underlying population. Given two mean square values that estimate variance due to different sources (treatments or error), the ratio of these mean squares forms a test statistic with an F distribution. The F statistic is then tested for significance at the desired α confidence level to determine whether the null hypothesis should be rejected. The null hypothesis for ANOVA is that the means for all treatments are equal to the grand mean for all the measurements, or alternatively that all measurements are drawn from the same normal distribution with mean μ and variance σ^2. The alternative hypothesis is that at least one treatment has a different mean from the other treatments. The remainder of this section describes the types of ANOVA that are useful for analyzing the results of this dissertation.

B.4.1 One-Factor ANOVA

One-factor ANOVA is useful when there is only one independent variable (or factor) of interest. The data are modeled using a linear statistical model

$$y_{ij} = \mu + \alpha_i + \epsilon_{ij} \tag{B.21}$$

which states that each measurement y_{ij} is described by the sum of the overall mean μ, the effect of level i of the treatment α_i, and some unexplained variability ϵ_{ij}. The null hypothesis for this model is

$$H0 : \alpha_i = 0 \text{ for all } i \tag{B.22}$$

For an experiment with a treatments and n measurements per treatment, the grand mean of all the measurements is found from

$$\bar{\bar{y}} = \frac{1}{an} \sum_{i=1}^{a} \sum_{j=1}^{n} y_{ij} \tag{B.23}$$

and the total sum of squares is

$$SS_T = \sum_{i=1}^{a} \sum_{j=1}^{n} \left(y_{ij} - \bar{\bar{y}}\right)^2 . \tag{B.24}$$

There are $an - 1$ degrees of freedom since there are an total measurements. In one-factor ANOVA, the total sum of squares is partitioned into only two contributions, the variability due to the treatment SS_A and the variability due to error SS_E. The corresponding sum of squares terms are

$$\begin{aligned} SS_A &= n \sum_{i=1}^{a} \left(\bar{y}_i - \bar{\bar{y}}\right)^2 \\ SS_E &= \sum_{i=1}^{a} \sum_{j=1}^{n} \left(y_{ij} - \bar{y}_i\right)^2 \end{aligned} \tag{B.25}$$

Table B.1: One-factor ANOVA table

Source of Variability	Sum of Squares	Degrees of Freedom	Mean Square	F	p
Treatments	SS_A	$a-1$	MS_A	$\frac{MS_A}{MS_E}$	p_A
Error	SS_E	$a(n-1)$	MS_E		
Total	SS_T	$an-1$			

where

$$\bar{y}_i = \frac{1}{n}\sum_{j=1}^{n} y_{ij} \tag{B.26}$$

is the mean for treatment i. The degrees of freedom are also partitioned, with $a-1$ degrees of freedom for the treatment and $a(n-1)$ degrees of freedom for the error. This leads to the following mean square values used to compute the F-statistic.

$$\begin{aligned} MS_A &= \frac{SS_A}{a-1} \\ MS_E &= \frac{SS_E}{a(n-1)} \end{aligned} \tag{B.27}$$

The results of the ANOVA are typically summarized in a table like Table B.1; each variable in this example table is replaced by its numerical value.

B.4.2 Two-Factor ANOVA

In two-factor ANOVA there are two independent variables or factors that both affect the variability of the measurements. The procedure for computing the ANOVA table is the same as in one-factor ANOVA, but now there are two additional sources of variability: the second factor and the interaction between the two factors. The linear

statistical model for two-way ANOVA is

$$y_{ijk} = \mu + \alpha_i + \beta_j + \delta_{ij} + \epsilon_{ijk}, \tag{B.28}$$

where μ is the overall mean, α_i is the effect due to level i of factor A, β_j is the effect due to level j of factor B, δ_{ij} is the effect due to the interaction between level i of factor A and level j of factor B, and ϵ_{ijk} is the unexplained variability. There are three null hypotheses corresponding to this model:

$$\begin{aligned} H_{0A} &: \alpha_i = 0 \text{ for all } i \\ H_{0B} &: \beta_j = 0 \text{ for all } j \\ H_{0AB} &: \delta_{ij} = 0 \text{ for all } i, j \end{aligned} \tag{B.29}$$

and the alternative hypotheses are that one or more of the effects are nonzero.

There are a levels of factor A, b levels of factor B, and n measurements for each combination of levels of A and B. The sum of squares terms for two-way ANOVA are the following,

$$\begin{aligned} SS_T &= \sum_{i=1}^{a}\sum_{j=1}^{b}\sum_{k=1}^{n}(y_{ijk} - \bar{\bar{y}})^2 \\ SS_A &= bn\sum_{i=1}^{a}(\bar{y}_i - \bar{\bar{y}})^2 \\ SS_B &= an\sum_{j=1}^{b}(\bar{y}_j - \bar{\bar{y}})^2 \\ SS_{AB} &= n\sum_{i=1}^{a}\sum_{j=1}^{b}(\bar{y}_{ij} - \bar{y}_i - \bar{y}_j + \bar{\bar{y}})^2 \\ SS_E &= \sum_{i=1}^{a}\sum_{j=1}^{b}\sum_{k=1}^{n}(y_{ijk} - \bar{y}_{ij})^2 \end{aligned} \tag{B.30}$$

where the means for the different treatment and interaction levels and the overall

grand mean are

$$\begin{aligned}
\bar{\bar{y}} &= \frac{1}{abn}\sum_{i=1}^{a}\sum_{j=1}^{b}\sum_{k=1}^{n} y_{ijk} \\
\bar{y}_i &= \frac{1}{bn}\sum_{j=1}^{b}\sum_{k=1}^{n} y_{ijk} \\
\bar{y}_j &= \frac{1}{an}\sum_{i=1}^{a}\sum_{k=1}^{n} y_{ijk} \\
\bar{y}_{ij} &= \frac{1}{n}\sum_{k=1}^{n} y_{ijk}.
\end{aligned} \tag{B.31}$$

As in one-factor ANOVA, the mean square values are computed for each of the sources of variability by dividing the sum of squares by the corresponding degrees of freedom. There are now three F statistics that must be computed to identify whether the null hypotheses or the alternative hypotheses are true. Each of these is computed by dividing the corresponding treatment mean square value by the error mean square. Table B.2 summarizes the values used to test the null hypotheses for two-factor ANOVA.

B.4.3 One-Factor Repeated Measures ANOVA

Repeated measures ANOVA is typically used when there are multiple measurements for each human participant in an experiment. There may be variability between participants that is separate from the effect of the treatment that is being tested, so repeated measures analysis separates this variability to improve the statistical significance of the main effect compared with one-factor ANOVA. One-factor repeated measures ANOVA is mathematically equivalent to two-factor ANOVA with only a single measurement for each combination of levels for the two factors. The linear statistical model for one-factor repeated measures ANOVA is

$$y_{ij} = \mu + \alpha_i + \beta_j + \epsilon_{ij}, \tag{B.32}$$

Table B.2: Two-factor ANOVA table

Source of Variability	Sum of Squares	Degrees of Freedom	Mean Square	F	p
A Treatments	SS_A	$a-1$	MS_A	$\frac{MS_A}{MS_E}$	p_A
B Treatments	SS_B	$b-1$	MS_B	$\frac{MS_B}{MS_E}$	p_B
A-B Interaction	SS_{AB}	$(a-1)(b-1)$	MS_{AB}	$\frac{MS_{AB}}{MS_E}$	p_{AB}
Error	SS_E	$ab(n-1)$	MS_E		
Total	SS_T	$abn-1$			

where μ is the overall mean, α_i is the effect due to level i of factor A, β_j is the effect due to level j of factor B, and ϵ_{ij} is the unexplained variability. The corresponding null hypotheses are

$$\begin{aligned} H_{0A} &: \alpha_i = 0 \text{ for all } i \\ H_{0B} &: \beta_j = 0 \text{ for all } j. \end{aligned} \tag{B.33}$$

The sum of squares terms are

$$\begin{aligned} SS_T &= \sum_{i=1}^{a}\sum_{j=1}^{b}(y_{ij}-\bar{\bar{y}})^2 \\ SS_A &= b\sum_{i=1}^{a}(\bar{y}_i-\bar{\bar{y}})^2 \\ SS_B &= a\sum_{j=1}^{b}(\bar{y}_j-\bar{\bar{y}})^2 \\ SS_E &= \sum_{i=1}^{a}\sum_{j=1}^{b}(y_{ij}-\bar{y}_i-\bar{y}_j+\bar{\bar{y}})^2 \end{aligned} \tag{B.34}$$

and the means are

$$\begin{aligned} \bar{\bar{y}} &= \frac{1}{ab}\sum_{i=1}^{a}\sum_{j=1}^{b}y_{ij} \\ \bar{y}_i &= \frac{1}{b}\sum_{j=1}^{b}y_{ij} \\ \bar{y}_j &= \frac{1}{a}\sum_{i=1}^{a}y_{ij}. \end{aligned} \tag{B.35}$$

Table B.3 details the terms used in the one-factor repeated measures ANOVA table.

B.4.4 Sphericity Corrections

The property of **sphericity** states that for every possible pairing of levels of the independent variable, the differences between these levels have equal variances. If this condition is violated, the p-values computed in the repeated measures ANOVA are inaccurate and may indicate statistical significance that is in fact not present. To account for the lack of sphericity, the degrees of freedom for each source of variability are scaled by a factor ϵ. The resulting F statistic is unchanged, since both the numerator and denominator degrees of freedom are scaled by the same ϵ, but F is compared against the distribution with the revised number of degrees of freedom

Table B.3: One-factor repeated measures ANOVA table

Source of Variability	Sum of Squares	Degrees of Freedom	Mean Square	F	p
A Treatments	SS_A	$a-1$	MS_A	$\frac{MS_A}{MS_E}$	p_A
B Subjects	SS_B	$b-1$	MS_B	$\frac{MS_B}{MS_E}$	p_B
Error	SS_E	$(a-1)(b-1)$	MS_E		
Total	SS_T	$ab-1$			

when computing the p-values.

There are several methods of computing ϵ corrections. The method used in this dissertation is the Greenhouse-Geisser approximation [41], which defines the correction as

$$\epsilon_{GG} = \frac{\left(\sum_{i=1}^{p} \lambda_i\right)^2}{(p-1)\sum_{i=1}^{p} \lambda_i^2} \tag{B.36}$$

where λ_i are the eigenvalues of the covariance matrix and p is the number of eigenvalues. The p-values for the treatments are now computed from an F distribution with $(\epsilon_{GG}(a-1), \epsilon_{GG}(a-1)(b-1))$ degrees of freedom, while for subjects it comes from an F distribution with $(\epsilon_{GG}(b-1), \epsilon_{GG}(a-1)(b-1))$ degrees of freedom.

Appendix C

Handling Emulation with Mass and Inertia Changes

The handling emulation controller formulated in Chapter 5 assumes the reference model and the controlled vehicle have the same mass m, yaw moment of inertia I_z, track width d, and front to rear mass distribution as described by the distance from the front and rear axles to the center of gravity (a and b respectively). Although not discussed in the development of the controller, differences in track width and in center of gravity location can be handled in the controller as derived by computing the reference model tire forces with the appropriate parameters. To state this explicitly, when these parameters are different between the two vehicles, the reference model tire force equations (5.1) become the following:

$$\begin{aligned}
\tilde{\mathbf{M}}_z &= \tilde{a}(F_{yfl}\cos\delta_{fl} + F_{yfr}\cos\delta_{fr}) - \tilde{b}(F_{yrl} + F_{yrr}) \ldots \\
&\quad + \tilde{d}(F_{yfl}\sin\delta_{fl} - F_{yfr}\sin\delta_{fr} - F_{xrl} + F_{xrr}) \\
\tilde{\mathbf{F}}_y &= F_{yfl}\cos\delta_{fl} + F_{yfr}\cos\delta_{fr} + F_{yrl} + F_{yrr} \\
\tilde{\mathbf{F}}_x &= F_{xrl} + F_{xrr} - F_{yfl}\sin\delta_{fl} - F_{yfr}\sin\delta_{fr}
\end{aligned} \tag{C.1}$$

Since these parameters only appear in the formulation of the tire forces, not in the reference model dynamics, there is no need to change the formulation of the handling emulation controller.

However, suppose now that the reference model and the controlled vehicle are allowed to have different mass and yaw moment of inertia. The controlled vehicle dynamics are still given by (5.9) and the reference model become

$$\begin{aligned} \dot{\tilde{r}} &= \frac{\tilde{\mathbf{M}}_{\mathrm{z}}}{\tilde{I}_{\mathrm{z}}} \\ \dot{\tilde{U}}_{\mathrm{y}} &= \frac{\tilde{\mathbf{F}}_{\mathrm{y}}}{\tilde{m}} - \tilde{r}\tilde{U}_{\mathrm{x}} \\ \dot{\tilde{U}}_{\mathrm{x}} &= \frac{\tilde{\mathbf{F}}_{\mathrm{x}}}{\tilde{m}} + \tilde{r}\tilde{U}_{\mathrm{y}}, \end{aligned} \tag{C.2}$$

which leads to the following error dynamics.

$$\begin{aligned} \dot{e}_{\mathrm{r}} &= \frac{1}{\tilde{I}_{\mathrm{z}}}\tilde{\mathbf{M}}_{\mathrm{z}} - \frac{1}{I_{\mathrm{z}}}\left(aF_{1\mathrm{y}} - bF_{2\mathrm{y}}\right) \\ \dot{e}_{\mathrm{y}} &= \frac{1}{\tilde{m}}\tilde{\mathbf{F}}_{\mathrm{y}} - \tilde{r}\tilde{U}_{\mathrm{x}} - \frac{1}{m}\left(F_{1\mathrm{y}} + F_{2\mathrm{y}}\right) + rU_{\mathrm{x}} \\ \dot{e}_{\mathrm{x}} &= \frac{1}{\tilde{m}}\tilde{\mathbf{F}}_{\mathrm{x}} + \tilde{r}\tilde{U}_{\mathrm{y}} - \frac{1}{m}\left(F_{1\mathrm{x}} + F_{2\mathrm{x}}\right) - rU_{\mathrm{y}} \end{aligned} \tag{C.3}$$

Given these error dynamics, the controlled vehicle tire forces derived in (5.13) no longer achieve the desired linear error dynamics in (5.14) since the mass and yaw inertia terms do not cancel. Instead, the controlled vehicle tire forces must be modified to account for these parameter differences:

$$\begin{aligned} F_{1\mathrm{y}} &= \frac{mb}{\tilde{m}L}\tilde{\mathbf{F}}_{\mathrm{y}} + \frac{I_{\mathrm{z}}}{\tilde{I}_{\mathrm{z}}L}\tilde{\mathbf{M}}_{\mathrm{z}} + \frac{mb}{L}\left(rU_{\mathrm{x}} - \tilde{r}\tilde{U}_{\mathrm{x}}\right) + e_{\mathrm{r}}\left(\frac{-K_1 - bK_3}{L}\right) \ldots \\ &\quad + e_{\mathrm{y}}\left(\frac{-K_2 - bK_4}{L}\right) \\ F_{2\mathrm{y}} &= \frac{ma}{\tilde{m}L}\tilde{\mathbf{F}}_{\mathrm{y}} - \frac{I_{\mathrm{z}}}{\tilde{I}_{\mathrm{z}}L}\tilde{\mathbf{M}}_{\mathrm{z}} + \frac{ma}{L}\left(rU_{\mathrm{x}} - \tilde{r}\tilde{U}_{\mathrm{x}}\right) + e_{\mathrm{r}}\left(\frac{K_1 - aK_3}{L}\right) \ldots \\ &\quad + e_{\mathrm{y}}\left(\frac{K_2 - aK_4}{L}\right) \\ F_{1\mathrm{x}} + F_{2\mathrm{x}} &= \frac{m}{\tilde{m}}\tilde{\mathbf{F}}_{\mathrm{x}} + m\left(\tilde{r}\tilde{U}_{\mathrm{y}} - rU_{\mathrm{y}}\right) - K_5 e_{\mathrm{x}} \end{aligned} \tag{C.4}$$

Note that the required tire forces are very similar to (5.13), with modifications to

the terms multiplying the reference model tire forces and moment to account for the differences in mass and yaw moment of inertia.

If the handling emulation controller is applied to the case of emulating a reference model with different physical parameters but the same tire-road friction coefficient, the linear tire model and small angle approximations used to derive actuator commands for the low friction emulation case in Section 5.4.1 will not adequately achive the required tire forces on the controlled vehicle. Instead, a different approach will be necessary to resolve actuator commands from desired tire forces. Some relevant methods are discussed in Section 5.3.3.

Appendix D

Statistical Results for Driver Adaptation Studies

Tables D.1–D.8 are ANOVA tables for all four metrics in each of the studies. Each study has a one-way repeated measures ANOVA table for the full population; Studies #3 and #4 each has a two-way ANOVA table with trial and driver group as factors; and Study #4 has one-way repeated measures ANOVA tables for each of the two driver groups. In the ANOVA tables, *SS* is the sum of squares for the given *Source* of variability, *df* is the corresponding number of degrees of freedom, *MS* is the mean squared value, F is the corresponding statistic taken from the F distribution (see Appendix B), p is the probability of the given F statistic, ϵ_{gg} is the Greenhouse-Geisser epsilon correction for lack of sphericity, $df \cdot \epsilon_{\text{gg}}$ is the modified degrees of freedom, and p_{gg} is the modified probability.

Tables D.9–D.12 contain the p-values for pairwise comparisons between trials 4, 5, 14, 15, and 20, for all four metrics in each study. The p-values were computed using a t distribution and multiplied by Bonferroni correction factors to account for multiple comparisons.

For all tables, significant differences between pairs of trials was determined at the $\alpha = 0.05$ level and denoted with boldface type.

Table D.1: One-factor repeated measures ANOVA tables for Study #1: Steering Ratio Scaling ($n = 10$). Significant values at the $\alpha = 0.05$ level are denoted with boldface type. ϵ_{gg} and p_{gg} denote the epsilon corrections and modified p-values, respectively, using the Greenhouse-Geisser method.

Metric 1: Steering reversal rate								
Source	*SS*	*df*	*MS*	*F*	*p*	ϵ_{gg}	$df \cdot \epsilon_{gg}$	p_{gg}
Stage	10.74	4	2.69	52.62	**1.50e-14**	0.64	2.54	**4.13e-9**
Subject	1.36	9	0.15	2.95	**0.010**			
Error	1.84	36	0.05				22.87	
Total	13.93	49						
Metric 2: RMS steering velocity								
Source	*SS*	*df*	*MS*	*F*	*p*	ϵ_{gg}	$df \cdot \epsilon_{gg}$	p_{gg}
Stage	711.30	4	177.83	74.97	**5.95e-17**	0.32	1.29	**3.06e-6**
Subject	64.67	9	7.19	3.03	**0.0085**			
Error	85.40	36	2.37				11.63	
Total	861.37	49						
Metric 3: Time to steering peak								
Source	*SS*	*df*	*MS*	*F*	*p*	ϵ_{gg}	$df \cdot \epsilon_{gg}$	p_{gg}
Stage	6.93	4	1.73	26.10	**3.31e-10**	0.77	3.06	**3.90e-8**
Subject	0.75	9	0.08	1.26	0.294			
Error	2.39	36	0.07				27.53	
Total	10.07	49						
Metric 4: RMS yaw jerk								
Source	*SS*	*df*	*MS*	*F*	*p*	ϵ_{gg}	$df \cdot \epsilon_{gg}$	p_{gg}
Stage	7.38e+5	4	1.85e+5	55.30	**7.00e-15**	0.29	1.17	**2.22e-5**
Subject	4.82e+4	9	5.36e+3	1.60	0.151			
Error	1.21e+5	36	3.34e+3				10.53	
Total	9.07e+5	49						

Table D.2: One-factor repeated measures ANOVA tables for Study #2: Steering Direction Reversal ($n = 11$). Significant values at the $\alpha = 0.05$ level are denoted with boldface type. ϵ_{gg} and p_{gg} denote the epsilon corrections and modified p-values, respectively, using the Greenhouse-Geisser method.

Metric 1: Steering reversal rate								
Source	*SS*	*df*	*MS*	*F*	*p*	ϵ_{gg}	$df \cdot \epsilon_{gg}$	p_{gg}
Stage	1.29	4	0.32	4.94	**0.002**	0.72	2.90	**0.015**
Subject	0.64	10	0.06	0.98	0.474			
Error	2.61	40	0.07				28.97	
Total	4.53	54						
Metric 2: RMS steering velocity								
Source	*SS*	*df*	*MS*	*F*	*p*	ϵ_{gg}	$df \cdot \epsilon_{gg}$	p_{gg}
Stage	104.27	4	26.07	10.69	**5.50e-6**	0.28	1.13	**7.48e-3**
Subject	51.39	10	5.14	2.11	**0.0468**			
Error	97.57	40	2.44				11.32	
Total	253.22	54						
Metric 3: Time to steering peak								
Source	*SS*	*df*	*MS*	*F*	*p*	ϵ_{gg}	$df \cdot \epsilon_{gg}$	p_{gg}
Stage	1.22	4	0.30	3.68	**0.012**	0.78	3.14	**0.022**
Subject	0.90	10	0.09	1.09	0.390			
Error	3.22	39	0.08				31.37	
Total	5.26	53*						
Metric 4: RMS yaw jerk								
Source	*SS*	*df*	*MS*	*F*	*p*	ϵ_{gg}	$df \cdot \epsilon_{gg}$	p_{gg}
Stage	1.63e+4	4	4.08e+3	5.33	**1.55e-3**	0.36	1.45	**0.037**
Subject	2.42e+4	10	2.42e+3	3.16	**4.55e-3**			
Error	3.06e+4	40	764.5				14.45	
Total	7.10e+4	54						

** This reflects one trial that was aborted prior to reaching the signal light trigger.*

Table D.3: One-factor repeated measures ANOVA tables for Study #3: Steering Torque Increase ($n = 12$). Significant values at the $\alpha = 0.05$ level are denoted with boldface type. ϵ_{gg} and p_{gg} denote the epsilon corrections and modified p-values, respectively, using the Greenhouse-Geisser method.

Metric 1: Steering reversal rate								
Source	*SS*	*df*	*MS*	*F*	*p*	ϵ_{gg}	$df \cdot \epsilon_{gg}$	p_{gg}
Stage	0.05	4	0.01	0.58	0.677	0.75	3.00	0.564
Subject	2.52	11	0.23	11.64	**9.43e-10**			
Error	0.87	44	0.02				32.94	
Total	3.43	59						
Metric 2: RMS steering velocity								
Source	*SS*	*df*	*MS*	*F*	*p*	ϵ_{gg}	$df \cdot \epsilon_{gg}$	p_{gg}
Stage	1.01	4	0.25	1.38	0.256	0.61	2.45	0.269
Subject	48.47	11	4.41	24.01	**4.65e-15**			
Error	8.08	44	0.18				26.96	
Total	57.56	59						
Metric 3: Time to steering peak								
Source	*SS*	*df*	*MS*	*F*	*p*	ϵ_{gg}	$df \cdot \epsilon_{gg}$	p_{gg}
Stage	0.32	4	0.08	1.89	0.130	0.73	2.93	0.168
Subject	1.05	11	0.10	2.25	**0.028**			
Error	1.87	44	0.04				32.25	
Total	3.25	59						
Metric 4: RMS yaw jerk								
Source	*SS*	*df*	*MS*	*F*	*p*	ϵ_{gg}	$df \cdot \epsilon_{gg}$	p_{gg}
Stage	3.04e+3	4	760.32	5.58	**0.001**	0.62	2.46	**0.009**
Subject	1.81e+4	11	1.65e+3	12.07	**5.43e-10**			
Error	6.00e+3	44	136.38				27.08	
Total	2.71e+4	59						

Table D.4: Two-factor ANOVA tables for Study #3: Steering Torque Increase ($n = 12$). Fixed factors are stage and group.

Metric 1: Steering reversal rate					
Source	*SS*	*df*	*MS*	*F*	*p*
Stage	0.05	4	0.01	0.17	0.951
Group	0.06	1	0.06	0.92	0.342
Interaction	0.02	4	0.005	0.08	0.989
Error	3.30	50	0.07		
Total	3.43	59			
Metric 2: RMS steering velocity					
Source	*SS*	*df*	*MS*	*F*	*p*
Stage	1.01	4	0.25	0.37	0.832
Group	21.59	1	21.59	31.13	**9.77e-7**
Interaction	0.29	4	0.07	0.11	0.980
Error	34.67	50	0.69		
Total	57.56	59			
Metric 3: Time to steering peak					
Source	*SS*	*df*	*MS*	*F*	*p*
Stage	0.32	4	0.08	1.77	0.149
Group	0.21	1	0.21	4.59	**0.037**
Interaction	0.45	4	0.11	2.49	0.055
Error	2.27	50	0.05		
Total	3.25	59			
Metric 4: RMS yaw jerk					
Source	*SS*	*df*	*MS*	*F*	*p*
Stage	3.04e+3	4	760.3	2.31	0.071
Group	7.34e+3	1	7.34e+3	22.29	**1.93e-5**
Interaction	307.2	4	76.79	0.23	0.918
Error	1.65e+4	50	329.16		
Total	2.71e+4	59			

Table D.5: One-factor repeated measures ANOVA tables for Study #4: Low Friction Dynamics, all participants. Significant values at the $\alpha = 0.05$ level are denoted with boldface type. ϵ_{gg} and p_{gg} denote the epsilon corrections and modified p-values, respectively, using the Greenhouse-Geisser method.

Metric 1: Steering reversal rate								
Source	*SS*	*df*	*MS*	*F*	*p*	ϵ_{gg}	$df \cdot \epsilon_{gg}$	p_{gg}
Stage	0.12	4	0.03	0.81	0.527	0.77	3.10	0.498
Subject	0.93	13	0.07	1.94	**0.046**			
Error	1.91	52	0.04				40.26	
Total	2.95	69						
Metric 2: RMS steering velocity								
Source	*SS*	*df*	*MS*	*F*	*p*	ϵ_{gg}	$df \cdot \epsilon_{gg}$	p_{gg}
Stage	98.85	4	24.71	10.19	**3.62e-6**	0.52	2.09	**5.04e-4**
Subject	162.42	13	12.49	5.25	**8.99e-6**			
Error	126.09	52	2.42				27.19	
Total	387.35	69						
Metric 3: Time to steering peak								
Source	*SS*	*df*	*MS*	*F*	*p*	ϵ_{gg}	$df \cdot \epsilon_{gg}$	p_{gg}
Stage	1.25	4	0.31	8.66	**1.97e-5**	0.71	2.84	**8.52e-4**
Subject	0.39	13	0.30	0.82	0.637			
Error	1.88	52	0.04				36.87	
Total	3.52	69						
Metric 4: RMS yaw jerk								
Source	*SS*	*df*	*MS*	*F*	*p*	ϵ_{gg}	$df \cdot \epsilon_{gg}$	p_{gg}
Stage	1.58e+5	4	3.96e+4	18.50	**1.66e-9**	0.50	1.98	**2.28e-4**
Subject	1.16e+5	13	8.94e+3	4.78	**1.02e-4**			
Error	1.11e+5	52	2.14e+3				25.79	
Total	3.86e+5	69						

Table D.6: Two-factor ANOVA tables for Study #4: Low Friction Dynamics ($n = 14$). Fixed factors are stage and group.

Metric 1: Steering reversal rate					
Source	*SS*	*df*	*MS*	*F*	*p*
Stage	0.12	4	0.03	0.69	0.599
Group	0.01	1	0.01	0.17	0.677
Interaction	0.27	4	0.07	1.58	0.192
Error	2.56	60	0.04		
Total	2.95	69			
Metric 2: RMS steering velocity					
Source	*SS*	*df*	*MS*	*F*	*p*
Stage	98.85	4	24.71	9.40	**5.75e-6**
Group	107.24	1	107.24	40.80	**2.75e-8**
Interaction	23.55	4	5.89	2.24	0.075
Error	151.72	60	2.63		
Total	387.35	69			
Metric 3: Time to steering peak					
Source	*SS*	*df*	*MS*	*F*	*p*
Stage	1.25	4	0.31	9.27	**6.68e-6**
Group	0.07	1	0.07	1.95	0.168
Interaction	0.18	4	0.04	1.30	0.282
Error	2.03	60	0.03		
Total	3.52	69			
Metric 4: RMS yaw jerk					
Source	*SS*	*df*	*MS*	*F*	*p*
Stage	1.58e+5	4	3.96e+4	19.37	**2.83e-10**
Group	7.64e+4	1	7.64e+4	37.38	**7.92e-8**
Interaction	2.85e+4	4	7.13e+3	3.49	**0.013**
Error	1.23e+5	60	2.04e+3		
Total	3.86e+6	69			

Table D.7: One-factor repeated measures ANOVA tables for Study #4: Low Friction Dynamics, Group 1. Significant values at the $\alpha = 0.05$ level are denoted with boldface type. ϵ_{gg} and p_{gg} denote the epsilon corrections and modified p-values, respectively, using the Greenhouse-Geisser method.

Metric 1: Steering reversal rate								
Source	*SS*	*df*	*MS*	*F*	*p*	ϵ_{gg}	$df \cdot \epsilon_{gg}$	p_{gg}
Stage	0.26	4	0.07	1.61	0.195	0.65	2.59	0.224
Subject	0.52	8	0.07	1.60	0.165			
Error	1.31	32	0.04				20.68	
Total	2.10	44						
Metric 2: RMS steering velocity								
Source	*SS*	*df*	*MS*	*F*	*p*	ϵ_{gg}	$df \cdot \epsilon_{gg}$	p_{gg}
Stage	115.3	4	28.83	11.43	**7.10e-6**	0.51	2.03	**8.26e-4**
Subject	48.98	8	6.12	2.43	**0.036**			
Error	80.69	32	2.52				16.26	
Total	244.98	44						
Metric 3: Time to steering peak								
Source	*SS*	*df*	*MS*	*F*	*p*	ϵ_{gg}	$df \cdot \epsilon_{gg}$	p_{gg}
Stage	1.03	4	0.26	7.96	**1.42e-4**	0.52	2.07	**3.98e-3**
Subject	0.08	8	0.01	0.31	0.957			
Error	1.04	32	0.03				16.54	
Total	2.15	44						
Metric 4: RMS yaw jerk								
Source	*SS*	*df*	*MS*	*F*	*p*	ϵ_{gg}	$df \cdot \epsilon_{gg}$	p_{gg}
Stage	1.75e+5	4	4.37e+4	19.70	**2.90e-8**	0.54	2.15	**3.74e-5**
Subject	3.61e+4	8	4.52e+3	2.04	0.073			
Error	7.10e+4	32					17.21	
Total	2.82e+5	44						

Table D.8: One-factor repeated measures ANOVA tables for Study #4: Low Friction Dynamics, Group 2. Significant values at the $\alpha = 0.05$ level are denoted with boldface type. ϵ_{gg} and p_{gg} denote the epsilon corrections and modified p-values, respectively, using the Greenhouse-Geisser method.

Metric 1: Steering reversal rate								
Source	*SS*	*df*	*MS*	*F*	*p*	ϵ_{gg}	$df \cdot \epsilon_{gg}$	p_{gg}
Stage	0.12	4	0.03	1.51	0.247	0.44	1.75	0.259
Subject	0.39	4	0.10	4.84	**9.46e-3**			
Error	0.33	16	0.02				7.02	
Total	0.84	24						
Metric 2: RMS steering velocity								
Source	*SS*	*df*	*MS*	*F*	*p*	ϵ_{gg}	$df \cdot \epsilon_{gg}$	p_{gg}
Stage	7.09	4	1.77	1.30	0.312	0.29	1.16	0.318
Subject	6.20	4	1.55	1.13	0.375			
Error	21.85	16	1.37				4.66	
Total	35.14	24						
Metric 3: Time to steering peak								
Source	*SS*	*df*	*MS*	*F*	*p*	ϵ_{gg}	$df \cdot \epsilon_{gg}$	p_{gg}
Stage	0.40	4	0.10	2.36	0.097	0.47	1.89	0.168
Subject	0.24	4	0.06	1.44	0.268			
Error	0.67	16	0.04				7.58	
Total	1.30	24						
Metric 4: RMS yaw jerk								
Source	*SS*	*df*	*MS*	*F*	*p*	ϵ_{gg}	$df \cdot \epsilon_{gg}$	p_{gg}
Stage	1.22e+4	4	3.04e+3	4.12	**0.018**	0.29	1.16	0.112
Subject	3.73e+3	4	932.38	1.26	0.326			
Error	1.18e+4	16	739.38				4.64	
Total	2.77e+4	24						

Table D.9: Results of pairwise comparisons for Study #1. Metric 1 is steering reversal rate, Metric 2 is RMS steering velocity, Metric 3 is time to steering peak, and Metric 4 is RMS yaw jerk. Significant differences between pairs of trials are denoted by p-values in boldface type.

Trial A	Trial B	Metric 1 p-value	Metric 2 p-value	Metric 3 p-value	Metric 4 p-value
4	5	**2.385e-11**	**2.220e-15**	**0.002**	**2.554e-13**
4	14	1.0	0.165	1.0	0.148
4	15	0.440	1.0	**8.397e-6**	1.0
4	20	1.0	1.0	1.0	1.0
5	14	**4.025e-11**	**8.771e-13**	**0.011**	**1.774e-10**
5	15	**1.310e-13**	**6.661e-15**	**5.752e-11**	**6.839e-13**
5	20	**3.642e-13**	**2.220e-15**	**1.166e-4**	**1.399e-13**
14	15	0.282	0.409	**1.655e-6**	0.382
14	20	0.712	0.122	1.0	0.079
15	20	1.0	1.0	**1.773e-4**	1.0

Table D.10: Results of pairwise comparisons for Study #2. Metric 1 is steering reversal rate, Metric 2 is RMS steering velocity, Metric 3 is time to steering peak, and Metric 4 is RMS yaw jerk. Significant differences between pairs of trials are denoted by p-values in boldface type.

Trial A	Trial B	Metric 1 p-value	Metric 2 p-value	Metric 3 p-value	Metric 4 p-value
4	5	**0.004**	**1.216e-4**	0.056	**0.012**
4	14	0.370	1.0	1.0	0.686
4	15	0.606	1.0	0.630	1.0
4	20	1.0	1.0	1.0	1.0
5	14	0.991	**0.003**	0.114	1.0
5	15	0.626	**1.542e-4**	1.0	**0.020**
5	20	**0.023**	**4.255e-5**	0.055	**0.010**
14	15	1.0	1.0	1.0	0.952
14	20	1.0	1.0	1.0	0.599
15	20	1.0	1.0	0.624	1.0

Table D.11: Results of pairwise comparisons for Study #3. Metric 1 is steering reversal rate, Metric 2 is RMS steering velocity, Metric 3 is time to steering peak, and Metric 4 is RMS yaw jerk. Significant differences between pairs of trials are denoted by p-values in boldface type.

Trial A	Trial B	Metric 1 p-value	Metric 2 p-value	Metric 3 p-value	Metric 4 p-value
4	5	1.0	1.0	1.0	**0.012**
4	14	1.0	1.0	1.0	1.0
4	15	1.0	1.0	1.0	1.0
4	20	1.0	1.0	1.0	1.0
5	14	1.0	1.0	1.0	0.297
5	15	1.0	1.0	0.222	0.232
5	20	1.0	1.0	0.680	**0.003**
14	15	1.0	0.550	1.0	1.0
14	20	1.0	1.0	1.0	0.973
15	20	1.0	1.0	1.0	1.0

Table D.12: Results of pairwise comparisons for Study #4, Group 1. Metric 1 is steering reversal rate, Metric 2 is RMS steering velocity, Metric 3 is time to steering peak, and Metric 4 is RMS yaw jerk. Significant differences between pairs of trials are denoted by p-values in boldface type.

Trial A	Trial B	Metric 1 p-value	Metric 2 p-value	Metric 3 p-value	Metric 4 p-value
4	5	1.0	**2.826e-5**	**0.018**	**1.280e-7**
4	14	1.0	0.128	1.0	**3.931e-4**
4	15	0.721	1.0	0.338	0.663
4	20	1.0	1.0	1.0	1.0
5	14	1.0	**0.048**	**0.009**	0.085
5	15	1.0	**0.003**	**3.287e-5**	**2.863e-5**
5	20	1.0	**3.301e-6**	**9.181e-4**	**9.137e-8**
14	15	1.0	1.0	0.600	0.073
14	20	1.0	**0.019**	1.0	**2.755e-4**
15	20	0.151	0.234	1.0	0.514

List of References

[1] K. J. Åström and B. Wittenmark, *Adaptive Control*, 2nd ed., Reading, MA: Addison-Wesley, 1995.

[2] W. Abend, E. Bizzi, and P. Morasso, "Human arm trajectory formation," *Brain*, vol. 105, pp. 331–348, 1982.

[3] M. Akamatsu, P. Green, and K. Bengler, "Automotive technology and human factors research: past, present, and future," *International Journal of Vehicular Technology*, vol. 2013, no. Article ID 526180, 2013.

[4] M. Akar and J. C. Kalkkuhl, "Lateral dynamics emulation via a four-wheel steering vehicle," *Vehicle System Dynamics*, vol. 46, no. 9, pp. 803–829, 2008.

[5] M. Akar and J. C. Kalkkuhl, "Design and evaluation of an integrated chassis controller for automotive vehicle emulation," *IEEE Transactions on Industrial Electronics*, vol. 56, no. 9, pp. 3571–3579, 2009.

[6] M. Asano, O. Shimoyama, and H. Hashigaya, "New approach in automotive control – an experimental variable-response vehicle," in *Proceedings of the 1991 International Conference on Industrial Electronics, Control, and Instrumentation*, pp. 123–128, 1991.

[7] C. G. Atkeson and J. M. Hollerbach, "Kinematic features of unrestrained vertical arm movements," *The Journal of Neuroscience*, vol. 5, no. 9, pp. 2318–2330, 1985.

[8] A. Balachandran and J. C. Gerdes, "Designing steering feel for steer-by-wire vehicles using objective measures," *IEEE/ASME Transactions on Mechatronics*, vol. 20, no. 1, pp. 373–383, 2015.

[9] J. Becker, M.-B. Aranda Colas, S. Nordbruch, and M. Fausten, "Bosch's vision and roadmap toward fully autonomous driving," in G. Meyer and S. Beiker, (Eds.) *Road Vehicle Automation*, pp. 49–59, Springer, 2014.

[10] O. Benderius, *Modelling driver steering and neuromuscular behaviour*, Ph.D. thesis, Chalmers University of Technology, 2014.

[11] O. Benderius and G. Markkula, "Evidence for a fundamental property of steering," in *Proceedings of the Human Factors and Ergonomics Society Annual Meeting*, vol. 58, pp. 884–888, 2014.

[12] W. Bergman, "Considerations in determining vehicle handling requirements," *SAE Technical Paper No. 690234*, 1969.

[13] W. Bergman, "Measurement and subjective evaluation of vehicle handling," *SAE Technical Paper No. 730492*, 1973.

[14] P. Bergmiller, "Design and safety analysis of a drive-by-wire vehicle," in M. Maurer and H. Winner, (Eds.) *Automotive Systems Engineering*, chap. 8, pp. 147–202, Springer Berlin Heidelberg, 2006.

[15] P. J. Bergmiller, *Towards functional safety in drive-by-wire vehicles*, Ph.D. thesis, TU Braunschweig, 2015.

[16] C. G. Bobier and J. C. Gerdes, "Steer-by-wire suspension design: geometries to enhance peak tire force estimation," in *Proceedings of the 21st International Symposium on Dynamics of Vehicles on Roads and Track*, 2009.

[17] C. G. Bobier and J. C. Gerdes, "Staying within the nullcline boundary for vehicle envelope control using a sliding surface," *Vehicle System Dynamics*, vol. 51, no. 2, pp. 199–217, 2012.

[18] O. Bock, "Adaptation of aimed arm movements to sensorimotor discordance: evidence for direction-independent gain control," *Behavioural Brain Research*, vol. 51, pp. 41–50, 1992.

[19] O. Bock and M. Burghoff, "Visuo-motor adaptation: evidence for a distributed amplitude control system," *Behavioural Brain Research*, vol. 89, no. 1-2, pp. 267–273, 1997.

[20] K. Brookhuis, D. de Waard, and W. Janssen, "Behavioural impacts of advanced driver assistance systems - an overview," *European Journal of Transport and Infrastructure Research*, vol. 1, no. 3, pp. 245–253, 2001.

[21] J. W. Brown, R. K. MacLean, S. Laws, C. Gadda, and J. C. Gerdes, "Experimental vehicle handling modification through steer-by-wire and differential drive," in *Proceedings of the 2007 American Control Conference*, pp. 2302–2307, 2007.

[22] E. Burdet, K. P. Tee, I. Mareels, T. E. Milner, C. M. Chew, D. W. Franklin, R. Osu, and M. Kawato, "Stability and motor adaptation in human arm movements," *Biological Cybernetics*, vol. 94, no. 1, pp. 20–32, 2006.

[23] P. Caselli, S. Conforto, M. Schmid, N. Accornero, and T. D'Alessio, "Difference in sensorimotor adaptation to horizontal and vertical mirror distortions during ballistic arm movements," *Human Movement Science*, vol. 25, no. 3, pp. 310–325, 2006.

[24] N. Catz, P. W. Dicke, and P. Thier, "Cerebellar-dependent motor learning is based on pruning a Purkinje cell population response," *Proceedings of the National Academy of Sciences*, vol. 105, no. 20, pp. 7309–7314, 2008.

[25] J. T. Choi and A. J. Bastian, "Adaptation reveals independent control networks for human walking," *Nature Neuroscience*, vol. 10, no. 8, pp. 1055–1062, 2007.

[26] D. J. Cole, "A path-following driver-vehicle model with neuromuscular dynamics, including measured and simulated responses to a step in steering angle overlay," *Vehicle System Dynamics*, vol. 50, no. 4, pp. 573–596, 2012.

[27] M. A. Conditt, F. Gandolfo, and F. A. Mussa-Ivaldi, "The motor system does not learn the dynamics of the arm by rote memorization of past experience," *Journal of Neurophysiology*, vol. 78, no. 1, pp. 554–560, 1997.

[28] D. A. Crolla, D. C. Chen, J. P. Whitehead, and C. J. Alstead, "Vehicle handling assessment using a combined subjective-objective approach," *SAE Technical Paper No. 980226*, 1998.

[29] D. W. Cunningham, A. Chatziastros, M. von der Heyde, and H. H. Bülthoff, "Driving in the future: temporal visuomotor adaptation and generalization," *Journal of Vision*, vol. 1, no. 2, pp. 88–98, 2001.

[30] F. W. Davis, "Power Steering for Automotive Vehicles," *SAE Technical Paper No. 450181*, 1945.

[31] M. R. Davis, "Police pursuit, dangers and liability issues," Tech. rep., Criminal Justice Institute, School of Law Enforcement Supervision, 2002.

[32] E. Donges, "A two-level model of driver steering behavior," *Human Factors*, vol. 20, no. 6, pp. 691–707, 1978.

[33] A. D. Dorey, M. C. Good, and P. N. Joubert, "A variable free control characteristic vehicle," *Vehicle System Dynamics*, vol. 9, no. 1, pp. 19–44, 1980.

[34] A. Erke, "Effects of electronic stability control (ESC) on accidents: a review of empirical evidence," *Accident Analysis and Prevention*, vol. 40, no. 1, pp. 167–173, 2008.

[35] S. M. Erlien, S. Fujita, and J. C. Gerdes, "Safe driving envelopes for shared control of ground vehicles," in *Proceedings of the 7th IFAC Symposium on Advances in Automotive Control*, pp. 831–836, 2013.

[36] S. H. Fairclough and R. Graham, "Impairment of driving performance caused by sleep deprivation or alcohol: a comparative study," *Human Factors*, vol. 41, no. 1, pp. 118–128, 1999.

[37] P. Fancher, L. Segel, J. Bernard, and R. Ervin, "Test procedures for studying vehicle dynamics in lane-change maneuvers," *SAE Technical Paper No. 760351*, 1976.

[38] J. R. Flanagan and A. K. Rao, "Trajectory adaptation to a nonlinear visuomotor transformation: evidence of motion planning in visually perceived space," *Journal of Neurophysiology*, vol. 74, no. 5, pp. 2174–2178, 1995.

[39] T. Flash and N. Hogan, "The coordination of arm movements: an experimentally confirmed mathematical model," *The Journal of Neuroscience*, vol. 5, no. 7, pp. 1688–1703, 1985.

[40] H. J. Förster, "Der Fahrzeugführer als Bindeglied zwischen Reifen, Fahrwerk und Fahrbahn," *VDI Berichte*, vol. 916, 1991.

[41] S. Geisser and S. W. Greenhouse, "An extension of box's results on the use of the f distribution in multivariate analysis," *The Annals of Mathematical Statistics*, vol. 29, no. 3, pp. 885–891, 1958.

[42] T. D. Gillespie, *Fundamentals of Vehicle Dynamics*, Society of Automotive Engineers, 1992.

[43] S. J. Goodbody and D. M. Wolpert, "Temporal and amplitude generalization in motor learning," *Journal of Neurophysiology*, vol. 79, no. 4, pp. 1825–1838, 1998.

[44] J. Gordon, M. F. Ghilardi, S. E. Cooper, and C. Ghez, "Accuracy of planar reaching movements," *Experimental Brain Research*, vol. 99, pp. 112–130, 1994.

[45] N. P. Gregersen, "Young drivers' overestimation of their own skill - an experiment on the relation between training strategy and skill," *Accident Analysis and Prevention*, vol. 28, no. 2, pp. 243–250, 1996.

[46] K. Guo, F. Pan, Y. Cheng, and H. Ding, "Driver model based on the Preview Optimal Artificial Neural Network," in *Proceedings of the 6th International Symposium on Advanced Vehicle Control (AVEC)*, 2002.

[47] C. M. Harris and D. M. Wolpert, "Signal-dependent noise determines motor planning," *Nature*, vol. 394, no. 20 August, pp. 780–784, 1998.

[48] W. Harter, W. Pfeiffer, P. Dominke, G. Ruck, and P. Blessing, "Future electrical steering systems: realizations with safety requirements," *SAE Technical Paper No. 2000-01-0822*, 2000.

[49] R. Held and S. J. Freedman, "Plasticity in human sensorimotor control," *Science*, vol. 142, no. 3591, pp. 455–462, 1963.

[50] R. A. Hess and A. Modjtahedzadeh, "A control theoretic model of driver steering behavior," *IEEE Control Systems Magazine*, vol. 10, no. 5, pp. 3–8, 1990.

[51] M. R. Hinder, L. Walk, D. G. Woolley, S. Riek, and R. G. Carson, "The interference effects of non-rotated versus counter-rotated trials in visuomotor adaptation," *Experimental Brain Research*, vol. 180, no. 4, pp. 629–640, 2007.

[52] S. Horiuchi, N. Yuhara, and A. Takei, "Two degree of freedom/H_inf controller synthesis for active four wheel steering vehicles," *Vehicle System Dynamics*, vol. 25, no. S1, pp. 275–292, 1996.

[53] Y.-H. J. Hsu, *Estimation and control of lateral tire forces using steering torque*, Ph.D. thesis, Stanford University, 2009.

[54] P. Johannessen, "SIRIUS 2001 - a university drive-by-wire project," Tech. rep., Chalmers University of Technology, 2001.

[55] I. Kageyama and H. B. Pacejka, "On a new driver model with fuzzy control," *Vehicle System Dynamics*, vol. 20, no. sup1, pp. 314–324, 1992.

[56] N. R. Kapania and J. C. Gerdes, "An autonomous lanekeeping system for vehicle path tracking and stability at the limits of handling," in *Proceedings of the 12th International Symposium on Advanced Vehicle Control (AVEC)*, pp. 720–725, 2014.

[57] D. Kasinathan, A. Khajepour, S.-K. Chen, and B. Litkouhi, "Constrained holistic cornering control," in *Proceedings of the 2014 American Control Conference*, pp. 3899–3904, 2014.

[58] M. Kawato, "Internal models for motor control and trajectory planning," *Current Opinion in Neurobiology*, vol. 9, pp. 718–727, 1999.

[59] S. D. Keen and D. J. Cole, "Steering control using model predictive control and multiple internal models," in *Proceedings of the 8th International Symposium on Advanced Vehicle Control (AVEC)*, pp. 783–788, 2006.

[60] R. H. Klein and D. T. McRuer, "Effects of automobile steering characteristics on driver/vehicle system performance in discrete manuevers," in *Proceedings of the Eleventh Annual Conference on Manual Control*, pp. 472–485, 1975.

[61] M. Kondo and A. Ajimine, "Driver's sight point and dynamics of the driver-vehicle-system related to it," *SAE Technical Paper No. 680104*, 1968.

[62] J. W. Krakauer, M. F. Ghilardi, and C. Ghez, "Independent learning of internal models for kinematic and dynamic control of reaching," *Nature Neuroscience*, vol. 2, no. 11, pp. 1026–1031, 1999.

[63] J. W. Krakauer and P. Mazzoni, "Human sensorimotor learning: adaptation, skill, and beyond," *Current Opinion in Neurobiology*, vol. 21, no. 4, pp. 636–644, 2011.

[64] J. W. Krakauer, Z. M. Pine, M.-F. Ghilardi, and C. Ghez, "Learning of visuomotor transformations for vectorial planning of reaching trajectories," *The Journal of Neuroscience*, vol. 20, no. 23, pp. 8916–8924, 2000.

[65] S. Kreft, J. Gausemeier, J. Berssenbrügge, W. Lorenz, and A. Trächtler, "Integration eines voll-aktiven X-by-wire Versuchsfahrzeugs in eine VR-basierte Simulationsumgebung," in *Proceedings of the Paderborner Workshop Augmented and Virtual Reality in der Produktentstehung*, pp. 159–171, 2010.

[66] K. Kritayakirana and J. C. Gerdes, "Autonomous vehicle control at the limits of handling," *International Journal of Vehicle Autonomous Systems*, vol. 10, no. 4, pp. 271–296, 2012.

[67] J. R. Lackner and P. DiZio, "Rapid adaptation to Coriolis force perturbations of arm trajectory," *Journal of Neurophysiology*, vol. 72, no. 1, pp. 299–313, 1994.

[68] S. Laws, C. Gadda, S. Kohn, P. Yih, J. C. Gerdes, and J. C. Milroy, "Steer-by-wire suspension and steering design for controllability and observability," in *Proceedings of the 16th IFAC World Congress*, 2005.

[69] A. Y. Lee, "Emulating the lateral dynamics of a range of vehicles using a four-wheel-steering vehicle," *SAE Technical Paper No. 950304*, 1995.

[70] A. Y. Lee, "Matching vehicle responses using the model-following control method," *SAE Technical Paper No. 970561*, 1997.

[71] A. Y. Lee, A. T. Marriott, and N. T. Le, "Variable dynamic testbed vehicle: dynamics analysis," *SAE Technical Paper No. 970560*, 1997.

[72] J.-Y. Lee and N. Schweighofer, "Dual adaptation supports a parallel architecture of motor memory," *The Journal of Neuroscience*, vol. 29, no. 33, pp. 10396–10404, 2009.

[73] E. K. Liebemann, K. Meder, J. Schuh, and G. Nenninger, "Safety and performance enhancement: the Bosch electronic stability control (ESP)," *SAE Technical Paper No. 2004-21-0060*, 2004.

[74] A. Liu and S. Chang, "Force feedback in a stationary driving simulator," in *Proccedings of the IEEE International Conference on Systems, Man, and Cybernetics*, vol. 2, pp. 1711–1716, Vancouver, 1995.

[75] C. C. MacAdam, "Application of an optimal preview control for simulation of closed-loop automobile driving," *IEEE Transactions on Systems, Man, and Cybernetics*, vol. SMC-11, no. 6, pp. 393–399, 1981.

[76] C. C. MacAdam, "Development of driver/vehicle steering interaction models for dynamic analysis – final technical report No. UMTRI-88-53," Tech. rep., University of Michigan Transportation Research Institute, 1988.

[77] C. C. MacAdam, "Development of a driver model for near/at-limit vehicle handling – final technical report No. UMTRI-2001-43," Tech. rep., University of Michigan Transportation Research Institute, 2001.

[78] C. C. MacAdam, "Understanding and modeling the human driver," *Vehicle System Dynamics*, vol. 40, no. 1-3, pp. 101–134, 2003.

[79] C. C. MacAdam and G. E. Johnson, "Application of elementary neural networks and preview sensors for representing driver steering control behaviour," *Vehicle System Dynamics*, vol. 25, no. 1, pp. 3–30, 1996.

[80] W. A. MacDonald and E. R. Hoffmann, "Review of relationships between steering wheel reversal rate and driving task demand," *Human Factors*, vol. 22, no. 6, pp. 733–739, 1980.

[81] A. K. Madhusudhanan, M. Como, and E. Holweg, "Lateral vehicle dynamics control based on tyre utilization coefficients and tyre force measurements," in *Proceedings of the 52nd IEEE Conference on Decision and Control*, pp. 2816–2821, 2013.

[82] T. Maeda, N. Irie, and K. Hidaka, "Performance of driver-vehicle system in emergency avoidance," *SAE Technical Paper No. 770130*, 1978.

[83] R. E. Magdaleno and D. T. Mc Ruer, "Experimental validation and analytical elaboration for models of the pilot's neuromuscular subsystem in tracking tasks," Tech. Rep. CR-1757, National Aeronautics and Space Administration, 1971.

[84] L. Marchal-Crespo, S. McHughen, S. C. Cramer, and D. J. Reinkensmeyer, "The effect of haptic guidance, aging, and initial skill level on motor learning of a steering task," *Experimental Brain Research*, vol. 201, no. 2, pp. 209–220, 2010.

[85] R. Marino and S. Scalzi, "Asymptotic sideslip angle and yaw rate decoupling control in four-wheel steering vehicles," *Vehicle System Dynamics*, vol. 48, no. 9, pp. 999–1019, 2010.

[86] T. A. Martin, J. G. Keating, H. P. Goodkin, A. J. Bastian, and W. T. Thach, "Throwing while looking through prisms – I . Focal olivocerebellar lesions impair adaptation," *Brain*, vol. 119, no. 4, pp. 1183–1198, 1996.

[87] P. Mazzoni and J. W. Krakauer, "An implicit plan overrides an explicit strategy during visuomotor adaptation," *The Journal of Neuroscience*, vol. 26, no. 14, pp. 3642–3645, 2006.

[88] K. J. McKenna, "A variable response vehicle – description and applications," in *Proceedings of the Joint Automatic Control Conference*, 1974.

[89] J. R. McLean and E. R. Hoffmann, "Steering reversals as a measure of driver performance and steering task difficulty," *Human Factors*, vol. 17, no. 3, pp. 248–256, 1975.

[90] D. McRuer, "Human dynamics in man-machine systems," *Automatica*, vol. 16, pp. 237–253, 1980.

[91] D. McRuer and R. Klein, "Effects of automobile steering characteristics on driver/vehicle performance for regulation tasks," *SAE Technical Paper No. 760778*, 1976.

[92] D. McRuer and D. H. Weir, "Theory of manual vehicular control," *IEEE Transactions on Man-Machine Systems*, vol. 10, no. 4, pp. 257–291, 1969.

[93] D. T. McRuer, R. W. Allen, D. H. Weir, and R. H. Klein, "New results in driver steering control models," *Human Factors*, vol. 19, no. 4, pp. 381–397, 1977.

[94] D. T. McRuer and R. Klein, "Effects of automobile steering characteristics on driver vehicle system dynamics in regulation tasks," in *Proceedings of the Eleventh Annual Conference on Manual Control*, 1975.

[95] D. T. McRuer and E. S. Krendel, "Mathematical Models of Human Pilot Behavior," Tech. rep., Advisory Group for Aerospace Research and Development, 1974.

[96] D. T. McRuer, D. H. Weir, H. R. Jex, R. E. Magdaleno, and R. W. Allen, "Measurement of driver-vehicle multiloop response properties with a single disturbance input," *IEEE Transactions on Systems, Man, and Cybernetics*, vol. SMC-5, no. 5, pp. 490–497, 1975.

[97] A. Modjtahedzadeh and R. A. Hess, "A model of driver steering control behavior for use in assessing vehicle handling qualities," *Journal of Dynamic Systems, Measurement, and Control*, vol. 115, no. 3, p. 456, 1993.

[98] D. C. Montgomery, G. C. Runger, and N. F. Hubele, *Engineering Statistics*, 5th ed., John Wiley and Sons, 2011.

[99] P. Morasso, "Spatial control of arm movements," *Experimental Brain Research*, vol. 42, no. 2, pp. 223–227, 1981.

[100] S. M. Morton and A. J. Bastian, "Cerebellar contributions to locomotor adaptations during splitbelt treadmill walking," *The Journal of Neuroscience*, vol. 26, no. 36, pp. 9107–9116, 2006.

[101] I. Nisky, A. M. Okamura, and M. H. Hsieh, "Effects of robotic manipulators on movements of novices and surgeons," *Surgical Endoscopy*, vol. 28, pp. 2145–2158, 2014.

[102] C. T. Noto and F. R. Robinson, "Visual error is the stimulus for saccade gain adaptation," *Cognitive Brain Research*, vol. 12, no. 2, pp. 301–305, 2001.

[103] M. Nötzli, "Porsche-forschungsauto P. E. P." *Automobil Revue: Erste schweizerische Automobilzeitung*, vol. 18, no. 21, 1987.

[104] E. Ono, Y. Hattori, Y. Muragishi, and K. Koibuchi, "Vehicle dynamics integrated control for four-wheel-distributed steering and four-wheel-distributed traction/braking systems," *Vehicle System Dynamics*, vol. 44, no. 2, pp. 139–151, 2006.

[105] E. Ono, S. Hosoe, H. D. Tuan, and S. Doi, "Bifurcation in vehicle dynamics and robust front wheel steering control," *IEEE Transactions on Control Systems Technology*, vol. 6, no. 3, pp. 412–420, 1998.

[106] J. M. Owens, S. B. McLaughlin, and J. Sudweeks, "Driver performance while text messaging using handheld and in-vehicle systems," *Accident Analysis and Prevention*, vol. 43, no. 3, pp. 939–947, 2011.

[107] H. B. Pacejka, *Tire and Vehicle Dynamics*, 3rd ed., Butterworth-Heinemann, 2012.

[108] H. Park and J. C. Gerdes, "Optimal tire force allocation for trajectory tracking with an over-actuated vehicle," in *Proceedings of the 2015 IEEE Intelligent Vehicles Symposium*, 2015.

[109] A. J. Pick and D. J. Cole, "Neuromuscular dynamics in the driver-vehicle system," *Vehicle System Dynamics*, vol. 44, no. sup1, pp. 624–631, 2006.

[110] A. J. Pick and D. J. Cole, "Driver steering and muscle activity during a lane-change manoeuvre," *Vehicle System Dynamics*, vol. 45, no. 9, pp. 781–805, 2007.

[111] A. J. Pick and D. J. Cole, "A mathematical model of driver steering control including neuromuscular dynamics," *Journal of Dynamic Systems, Measurement, and Control*, vol. 130, p. 031004, 2008.

[112] M. Plöchl and J. Edelmann, "Driver models in automobile dynamics application," *Vehicle System Dynamics*, vol. 45, no. 7-8, pp. 699–741, 2007.

[113] W. Reichelt, "Correlation analysis of open/closed loop data for objective assessment of handling characteristics of cars," *SAE Technical Paper No. 910238*, 1991.

[114] P. I. Ro and H. Kim, "Four wheel steering system for vehicle handling improvement: a robust model reference control using the sliding mode," *Proceedings of the Institution of Mechanical Engineers, Part D: Journal of Automobile Engineering*, vol. 210, no. 4, pp. 335–346, 1996.

[115] E. J. Rossetter and J. C. Gerdes, "A study of lateral vehicle control under a 'virtual' force framework," in *Proceedings of the 6th International Symposium on Advanced Vehicle Control (AVEC)*, 2002.

[116] M. F. Rotella, I. Nisky, M. Koehler, M. D. Rinderknecht, A. J. Bastian, and A. M. Okamura, "Learning and generalization in an isometric visuomotor task," *Journal of Neurophysiology*, vol. 113, no. 6, 2015.

[117] H. E. B. Russell and J. C. Gerdes, "Low friction emulation of lateral vehicle dynamics using four-wheel steer-by-wire," in *Proceedings of the 2014 American Control Conference*, pp. 3924–3929, 2014.

[118] R. L. Sainburg, C. Ghez, and D. Kalakanis, "Intersegmental dynamics are controlled by sequential anticipatory, error correction, and postural mechanisms." *Journal of Neurophysiology*, vol. 81, no. 3, pp. 1045–1056, 1999.

[119] S. Sano, "Evaluation of motor vehicle handling," *International Journal of Vehicle Design*, vol. 3, no. 2, pp. 171–189, 1982.

[120] S. Sano, Y. Furukawa, and S. Shiraishi, "Four wheel steering system with rear wheel steer angle controlled as a function of steering wheel angle," *SAE Technical Paper No. 860625*, 1986.

[121] R. A. Scheidt and C. Ghez, "Separate adaptive mechanisms for controlling trajectory and final position in reaching," *Journal of Neurophysiology*, vol. 98, no. 6, pp. 3600–3613, 2007.

[122] G. Schmidt, K. L. R. Talvala, J. P. Switkes, M. Kiss, and J. C. Gerdes, "Changing lanes with active lanekeeping assistance: a simulator study," in D. de Waard, F. Flemisch, B. Lorenz, H. Oberheid, and K. Brookhuis, (Eds.) *Human Factors for Assistance and Automation*, pp. 49–61, Maastricht, The Netherlands: Shaker Publishing, 2008.

[123] R. D. Seidler, J. Bo, and J. A. Anguera, "Neurocognitive contributions to motor skill learning: the role of working memory," *Journal of Motor Behavior*, vol. 44, no. 6, pp. 445–453, 2012.

[124] R. Shadmehr and F. A. Mussa-Ivaldi, "Adaptive representation of dynamics during learning of a motor task," *The Journal of Neuroscience*, vol. 14, no. 5, pp. 3208–3224, 1994.

[125] R. Shadmehr, M. A. Smith, and J. W. Krakauer, "Error correction, sensory prediction, and adaptation in motor control," *Annual Review of Neuroscience*, vol. 33, pp. 89–108, 2010.

[126] R. S. Sharp, D. Casanova, and P. Symonds, "A mathematical model for driver steering control, with design, tuning and performance results," *Vehicle System Dynamics*, vol. 33, no. 5, pp. 289–326, 2000.

[127] T. B. Sheridan, "Three models of preview control," *IEEE Transactions on Human Factors in Electronics*, vol. HFE-7, no. 2, 1966.

[128] N. E. Shoemaker, F. Dell'Amico, and R. J. Chwaiek, "A pilot experiment on driver task performance with fixed and variable steering ratio," *SAE Technical Paper No. 670508*, 1967.

[129] S. Singh, "Critical reasons for crashes investigated in the National Motor Vehicle Crash Causation Survey," Tech. rep., National Highway Traffic Safety Administration, 2015.

[130] M. A. Smith, A. Ghazizadeh, and R. Shadmehr, "Interacting adaptive processes with different timescales underlie short-term motor learning," *PLoS Biology*, vol. 4, no. 6, pp. 1035–1043, 2006.

[131] J. P. Switkes, J. C. Gerdes, G. F. Schmidt, and M. Kiss, "Driver response to steering torque disturbances: a user study on assisted lanekeeping," in *Proceedings of the 5th IFAC Symposium on Advances in Automotive Control*, pp. 243–250, 2007.

[132] J. A. Taylor and R. B. Ivry, "Flexible cognitive strategies during motor learning," *PLoS Computational Biology*, vol. 7, no. 3, p. e1001096, 2011.

[133] S. Telgen, D. Parvin, and J. Diedrichsen, "Mirror reversal and visual rotation are learned and consolidated via separate mechanisms: recalibrating or learning de novo?" *The Journal of Neuroscience*, vol. 34, no. 41, pp. 13768–13779, 2014.

[134] P. A. Theodosis and J. C. Gerdes, "Generating a racing line for an autonomous racecar using professional driving techniques," in *Proceedings of the ASME 2011 Dynamic Systems and Control Conference*, pp. 853–860, 2011.

[135] D. Toffin, G. Reymond, A. Kemeny, and J. Droulez, "Influence of steering wheel torque feedback in a dynamic driving simulator," in *Proceedings of the 2003 Driving Simulator Conference – North America*, 2003.

[136] H. Tsunashima and K. Yanagisawa, "Measurement of brain function of car driver using functional near-infrared spectroscopy (fNIRS)," *Computational Intelligence and Neuroscience*, vol. 2009, no. Article ID 164958, 2009.

[137] A. Ungoren and H. Peng, "An adaptive lateral preview driver model," *Vehicle System Dynamics*, vol. 43, no. 4, pp. 245–259, 2005.

[138] P. Vindras and P. Viviani, "Altering the visuomotor gain: evidence that motor plans deal with vector quantities," *Experimental Brain Research*, vol. 147, no. 3, pp. 280–295, 2002.

[139] H. von Helmholtz, *Handbuch der physiologischen Optik: mit 213 in den Text eingedruckten Holzschnitten und 11 Tafeln*, vol. 9, Voss, 1866.

[140] J. Wang and R. G. Longoria, "Coordinated and reconfigurable vehicle dynamics control," *IEEE Transactions on Control Systems Technology*, vol. 17, no. 3, pp. 723–732, 2009.

[141] D. H. Weir and R. J. DiMarco, "Correlation and evaluation of driver/vehicle directional handling data," *SAE Technical Paper No. 780010*, 1978.

[142] S. Werner and O. Bock, "Mechanisms for visuomotor adaptation to left-right reversed vision," *Human Movement Science*, vol. 29, no. 2, pp. 172–178, 2010.

[143] J. R. Wessel, "Performance monitoring in realistic environments: can translating neuroscientific insights augment real-world behavioral adaptation?" *The Journal of Neuroscience*, vol. 34, no. 27, pp. 8934–6, 2014.

[144] D. M. Wolpert, J. Diedrichsen, and J. R. Flanagan, "Principles of sensorimotor learning," *Nature Reviews Neuroscience*, vol. 12, no. 12, pp. 739–751, 2011.

[145] D. M. Wolpert, Z. Ghahramani, and M. I. Jordan, "Are arm trajectories planned in kinematic or dynamic coordinates? An adaptation study," *Experimental Brain Research*, vol. 103, no. 3, pp. 460–470, 1995.

[146] D. M. Wolpert, R. C. Miall, and M. Kawato, "Internal models in the cerebellum," *Trends in Cognitive Sciences*, vol. 2, no. 9, pp. 338–347, 1998.

[147] D. G. Woolley, A. De Rugy, R. G. Carson, and S. Riek, "Visual target separation determines the extent of generalisation between opposing visuomotor rotations," *Experimental Brain Research*, vol. 212, no. 2, pp. 213–224, 2011.

[148] Y. Yamaguchi and T. Murakami, "Adaptive control for virtual steering characteristics on electric vehicle using steer-by-wire system," *IEEE Transactions on Industrial Electronics*, vol. 56, no. 5, pp. 1585–1594, 2009.

[149] P. Yih and J. C. Gerdes, "Modification of vehicle handling characteristics via steer-by-wire," *IEEE Transactions on Control Systems Technology*, vol. 13, no. 6, pp. 965–976, 2005.